R-10-03

Site investigation SFR

Hydrogeological modelling of SFR

Model version 0.2

Johan Öhman, Golder Associates AB

Sven Follin, SF GeoLogic

January 2010

Svensk Kärnbränslehantering AB
Swedish Nuclear Fuel
and Waste Management Co

Box 250, SE-101 24 Stockholm
Phone +46 8 459 84 00

ISSN 1402-3091
SKB R-10-03

Site investigation SFR

Hydrogeological modelling of SFR

Model version 0.2

Johan Öhman, Golder Associates AB

Sven Follin, SF GeoLogic

January 2010

Keywords: DFN, Fracture network, PFL, Modelling, Parameterisation, SKBDoc id 1245181.

Abstract

The Swedish Nuclear Fuel and Waste Management Company (SKB) has conducted site investigations for a planned extension of the existing final repository for short-lived radioactive waste (SFR). A hydrogeological model is developed in three model versions, which will be used for safety assessment and design analyses.

This report presents a data analysis of the currently available hydrogeological data from the ongoing Site Investigation SFR (KFR27, KFR101, KFR102A, KFR102B, KFR103, KFR104, and KFR105). The purpose of this work is to develop a preliminary hydrogeological Discrete Fracture Network model (hydro-DFN) parameterisation that can be applied in regional-scale modelling. During this work, the Geologic model had not yet been updated for the new data set. Therefore, all analyses were made to the rockmass outside Possible Deformation Zones, according to Single Hole Interpretation. Owing to this circumstance, it was decided not to perform a complete hydro-DFN calibration at this stage. Instead focus was re-directed to preparatory test cases and conceptual questions with the aim to provide a sound strategy for developing the hydrogeological model SFR v. 1.0.

The presented preliminary hydro-DFN consists of five fracture sets and three depth domains. A statistical/geometrical approach (connectivity analysis /Follin et al. 2005/) was performed to estimate the size (i.e. fracture radius) distribution of fractures that are interpreted as Open in geologic mapping of core data. Transmissivity relations were established based on an assumption of a correlation between the size and evaluated specific capacity of geologic features coupled to inflows measured by the Posiva Flow Log device (PFL-f data).

The preliminary hydro-DFN was applied in flow simulations in order to test its performance and to explore the role of PFL-f data. Several insights were gained and a few model technical issues were raised. These are summarised in Table 5-1.

Sammanfattning

Svensk Kärnbränslehantering AB (SKB) har genomfört platsundersökningar för en planerad utbyggnad av den befintliga anläggningen för slutförvaring av låg- och medelaktivt radioaktivt avfall, Slutförvar för kortlivat radioaktivt avfall (SFR). En hydrogeologisk modell utvecklas i tre versioner i syfte att användas för säkerhets- och konstruktionsanalyser.

Denna rapport presenterar en dataanalys av tillgängliga hydrogeologiska data från den pågående platsundersökningen för utbyggnad SFR (KFR27, KFR101, KFR102A, KFR102B, KFR103, KFR104, and KFR105). Målet med detta arbete är att utveckla och parameterisera en preliminär hydrogeologisk spricknätverksmodell (hydro-DFN). Under arbetet hade den Geologiska modellen ännu inte uppdaterats med avseende på nya data. Av denna anledning gjordes analyserna på bergmassan utanför potentiella deformationszoner (PDZ; Possible Deformation Zones) enligt enhålstolkningar (SHI; Single Hole Interpretation). Mot bakgrund av detta beslutades det att i detta skede inte utveckla en fullständigt kalibrerad hydro-DFN, utan att istället fokusera på förberedande konceptuella frågeställningar i syfte att ta fram en lämplig strategi för utvecklingen av den hydrogeologiska modellen SFR v. 1.0.

Den preliminära hydro-DFN består av fem sprickset och tre djupdomäner. En statistisk/geometrisk metod (konnektivitetsanalys /Follin et al. 2005/) användes för att skatta storleksfördelningen av de sprickor som tolkats som öppna vid kartering av borrkärnor (dvs fördelningen i sprickors radie). Transmissivitetssamband togs fram baserat på ett antagande om en direkt koppling mellan sprickstorlek och utvärderad specifik kapacitet för i PFL-f data (geologiska strukturer kopplade till inflöden som uppmätts med flödesloggning med Posiva Flow Log).

Den preliminära hydro-DFN tillämpades i flödessimuleringar för att kontrollera modellens duglighet, samt att undersöka PFL-f datans roll i modellen. Detta ledde till ett flertal insikter samt att vissa modelltekniska frågeställningar kunde identifieras. Dessa sammanfattas i Table 5-1.

Contents

1 Introduction

1.1 Background

In 1987, the first stage of a final repository for short-lived radioactive waste (SFR) was constructed and taken into operation. An investigation programme for its future extension was initiated in 2008 by the Swedish Nuclear Fuel and Waste Management Company (SKB). This extension of SFR is necessitated by the pending decommissioning of the closed reactors Barsebäck, Studsvik and Ågesta, the additional amounts of operational waste associated with the extended operating time of the remaining nuclear power plants, as well as the future decommission of running nuclear power plants Oskarshamn, Forsmark and Ringhals /SKB 2008a/.

This report provides an analysis of the hydrogeologic data from the ongoing site investigation programme at SFR and the preliminary hydro-DFN parameterization for the rockmass between deformation zones. The work reported here was carried out in accordance with activity plan AP SFR-09-007. The controlling documents for performing this activity are listed in Table 1-1. Both the activity plan and the method descriptions are SKB's internal controlling documents.

Table 1-1. Controlling documents for the performance of the activity reported here.

Activity plan	**Number**	**Version**
Platsmodellering Hydrogeologi 0.2	AP SFR-09-007	1.0
Method descriptions	**Number**	**Version**
Hantering av data och modeller inom SFR – utbyggnad	SKB MD SDU-203	1.0
Hantering av primärdata vid platsundersökningar	SKB MD SDK-508	

1.2 General objectives of the hydrogeological programme

This section presents the essential issues in the overall hydrogeological investigations and modelling of SFR. The specific scope of this report, SFR hydrogeological model v. 0.2, is specified in Section 1.5.

The primary objective of the ongoing hydrogeological investigations at SFR is to develop a description of the hydrogeological system inside the SFR regional domain (Figure 1-1). The descriptive model should provide parameter values to a *groundwater flow model,* which will be used by Safety Assessment and Design for predictions. In addition to the new data gathered from the ongoing hydrogeological investigations at SFR, the hydrogeological description should also comprise hydrogeological information available from the constructions of the Forsmark nuclear power plant and the existing SFR, as well as from the nearby Site Investigation Forsmark for a deep repository for high level spent nuclear fuel /Follin et al. 2007c/.

A second objective is to provide feedback to the overall SFR field investigation programme /SKB 2008a/ and to bring attention to important conceptual uncertainties that need to be resolved in time due. It is imperative that the contributing disciplines (geology, rock mechanics, hydrogeology, and hydrogeo-chemistry) iteratively exchange feedback during the sequential development of model versions in order to improve and/or reinforce the characterisation of the hydrogeological system, but also to attain interdisciplinary conceptual model consistency and creditability.

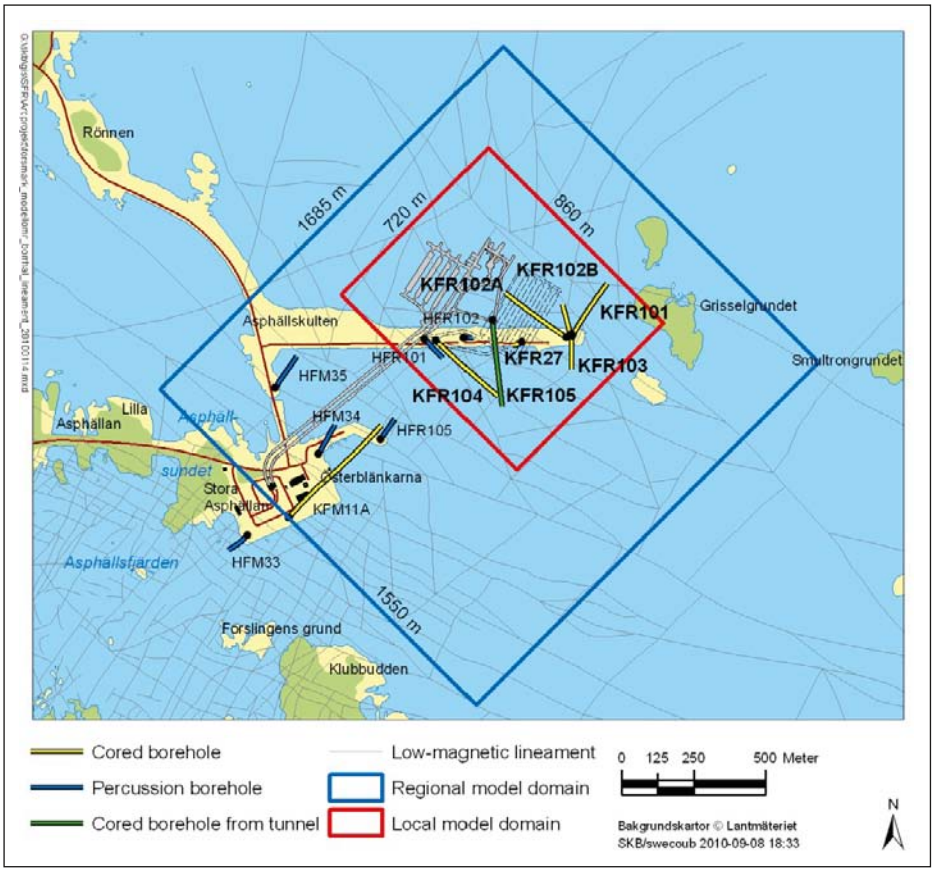

Figure 1-1. *Location map of the SFR facility, model domains and boreholes studied. The regional model domain boundaries are shown in blue and the local model domain is shown with red lines.*

Four key issues have been specified for the hydrogeological modelling at SFR /SKB 2008a/:

1) Hydraulic properties of deformation zones interpreted from low-magnetic lineaments (i.e. HCDs).
2) Hydraulic properties of the bedrock between the deformation zones within target model volume (i.e. HRD).
3) The extent and character of hydraulic connectivity within the target volume as well as the hydraulic connectivity to the surrounding bedrock.
4) Spatial extent and hydraulic properties of sheet joints and gently dipping deformation zones.

Other important issues in conceptual hydrogeological modelling have been raised by /Follin et al. 2007a/:

5) Is there a general observation that deformation zones are more conductive than the surrounding bedrock?
6) Is there any data support for dividing the bedrock between the deformation zones into different sub domains?
7) What is the statistical significance of a potential depth dependence in the fracture transmissivity?

These issues have been setup for the overall SFR hydrogeologic programme. The work is developed in sequential model versions (Section 1.3). As explained in sections 1.3, 1.4, and 1.5, it is not possible to address all these issues at this modelling stage. The specific scope of this report, SFR hydrogeological model v. 0.2, is specified in Section 1.5.

1.3 Model versions

The ongoing investigation programme at SFR involves field investigations inside the target area (Figure 1-1) as well as modelling. The hydrogeological modelling is to be developed in three model versions, 0.1, 0.2 and 1.0, that successively incorporate data from the ongoing SFR field investigations and the feedback from the other modelling disciplines. The work follows SKB's established methodology for modelling /Rhén et al. 2003/ and /Follin et al. 2007a/ and is described in Chapter 2.

Flow model version v. 0.0 of SFR /Odén 2008/ was an implementation of the flow model developed by /Holmén and Stigsson 2001/ in DarcyTools v. 3.1. The objective of flow model version v.0.0 was to reproduce the modelling results from the previous state-of-the-art model of SFR using a different computer code (software) than /Holmén and Stigsson 2001/. The DarcyTools program package is comprehensively described in /Svensson et al. 2007, Svensson and Ferry 2004, Svensson 2004/.

The SFR hydrogeological model v.0.1 /Öhman and Follin 2010/ reviewed the historic hydraulic data of SFR with respect to the preliminary SFR geological model v.0.1 /Curtis et al. 2009/. In other words, hydrogeological model v.0.1, was based on hydraulic data available prior to the initiation of the current SFR investigation programme, the same hydraulic data as /Holmén and Stigsson 2001/, but used an updated model of the geological structures /Curtis et al. 2009/. The associated flow modelling is reported in /Öhman 2010/.

At the onset of the SFR project, it was intended that a Geologic model v. 0.2 should form the backbone of this hydrogeologic model (v. 0.2). According to SKB's established methodology /Rhén et al. 2003/, the geological model has the essential role of classifying data into deterministic geologic structures or rockmass between deformation zones (see Section 1.4). However, at a later stage it was decided to omit the intermediate geological model version, and instead focus on the final Geologic model (v. 1.0). Consequently, a hydrogeological model v. 0.2 could not be developed according to the SKB methodology. Instead, the focus in this study was shifted to analyse the available data and to examine the hydro-DFN concept.

This model version, SFR hydrogeological model v.0.2, presents an analysis of new core borehole data (KFR27, KFR101-105; Figure 1-1) and a preliminary hydro-DFN parameterisation of the rockmass between zones. However, the important step of parameterising zones had to be omitted in this model version (c.f. /Follin et al. 2007b, Öhman and Follin 2010/).

The final SFR geologic model v.1.0 is currently in progress and will be available for the final hydraulic parameterisation of both zones and the rockmass between zones in the final SFR hydrogeologic model v.1.0. The Site Descriptive Model intended to provide the foundation for the long-term safety assessment and the detailed design for the extension of SFR.

1.4 Hydraulic domains

The hydrogeological system is conceptually divided into three hydraulic units: Hydraulic Soil Domain (HSD), Hydraulic Conductor Domain (HCD), and Hydraulic Rock Domain (HRD) /Rhén et al. 2003/, see Figure 1-2. The hydrogeological model consists of geometrical definitions and hydraulic parameterisation of these hydraulic domains. Each of the three hydraulic domains can be split into subdomains, e.g. soil layers, fracture domains, and individual zones /Follin et al. 2007c/. The HCD is defined by structures of the prevailing geological model, whereas the HRD is the rockmass between deformation zones.

The methodology to parameterise the units (HCD and HRD) has been developed and applied in the Site Investigation programme /Follin et al. 2007b, c/. The HCD is parameterised by effective transmissivity values, while the HRD is parameterised by means of a stochastic hydro-DFN. Hydraulic borehole data are analysed and classified as belonging to either HCD or HRD; this should normally be based on the geometrical definitions of the prevailing structural model. Characterised trends or local deviations within HCD or HRD data subpopulations may provide grounds for splitting the hydraulic units into different subdomains. In a second step, effective HCD and HRD parameters are calculated from its different populations (types) of hydraulic data.

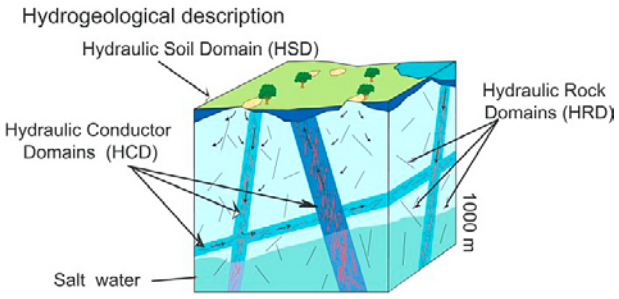

Figure 1-2. *The hydraulic subdomains of a hydrogeological model /Rhén et al. 2003/.*

The SFR geologic model v.0.1 /Curtis et al. 2009/ is based on extrapolated lineaments, conditioned to borehole and tunnel data in the vicinity of SFR available prior to the initiation of the SFR Site Investigation. The geologic model is currently being updated for the new data set (KFR27, KFR101-105) and will result in a model version 1.0. Thus, at present there exists no structural model that is applicable to the current data set. Nevertheless, the classification of data into HRD/HCD is a fundamental step in the hydrogeological modelling.

In absence of an applicable geologic model, it was decided to tentatively classify data based on Single Hole Interpretation (SHI) definitions of Possible Deformation Zones (PDZ). However, the SHI definitions should not be taken as definite boundaries; the final definitions of HCDs are expected to change in the SFR geological model v.1.0, at least to some extent. This imposes additional uncertainty in the current analysis.

Furthermore, the PDZ in SHI have not been associated to individual deterministic structures of the geological model. Obviously, different HCD parameterisation alternatives could have been explored, by testing hypothetical associations of the SHI definitions to the HCDs in the structural model v. 0.1. This was not considered meaningful, as the final geologic model, v. 1.0, is currently under development in parallel by the geological team. Therefore, it was decided that the HCD parameterisation is beyond the scope of the hydrogeological modelling v. 0.2, and instead, the focus of this report was turned to the characterisation of HRD. The latest version of the HCD parameterisation is based on historic data and reported in /Öhman and Follin 2010/.

1.5 Scope of model version v.0.2

A complete hydrogeological model could not be developed, according to SKB's established methodology, owing to the absence of an updated geologic model (see sections 1.2 and 1.3). Instead, the focus in this study has been redirected to:

- Analysis of new borehole data (KFR27, KFR101-105) outside possible deformation zones.
- Preliminary hydro-DFN parameterisation for the HRD.
- Examining the hydro-DFN methodology and the role of geologic features coupled to inflow measured by the Posiva Flow Logging device (PFL-f data).

These analyses target cored borehole data in HRD (Open fractures and PFL-f data). PFL-f data are briefly described in Appendix C. In this study, HRD is defined as the rockmass between Possible Deformation Zones, according to SHI /Petersson et al. 2009a–d, 2010/. The analysis includes the new core borehole data from the ongoing SFR site investigations: KFR27, KFR101-105; all percussion data were excluded. It was also decided to exclude the cored borehole KFM11A , which is located outside the SFR Local model domain, but inside the Regional domain (Figure 1-1). The reason is that KFM11A data exhibits deviating characteristics, possibly influenced by the Singö zone. The model domain extends down to -1,100 m RHB70, and its areal extent is shown in Figure 1-1.

1.6 Data used

The data studied in this report was delivered from SKB's database Sicada (Table 1-2). The hydro-DFN parameterisation is based on the currently available core data from the ongoing SFR site investigation programme, KFR27 and KFR101-105. Based on a cursorily review, it was decided to exclude percussion data, HFR101-105 and core data from the nearby Site Investigation Forsmark, KFM11A. The upper part of KFR27 (down to 147.49 m) was drilled during the construction of SFR. Within the ongoing Site investigations, KFR27 was extended down to 501.64 m borehole length. No core is available for this upper part of KFR27 (0 to 147.49 m) and therefore these data were also excluded from this analysis. These boreholes are considered to be highly influenced by the Singö zone, and less representative of the general SFR characteristics. The geometrical data used to classify the rockmass in terms of HRD/HCD is *not* based on the geological model, according to SKB's established methodology /Rhén et al. 2003/, but instead on Possible Deformation Zones, according to SHI. In this study, the geological model /Curtis et al. 2009/ was only used to calculate the intensity of deformation zones ($P_{32,\ HCD}$). For traceability, geological model was transferred from the geological modelling team via SKBdoc (Table 1-2).

Table 1-2. Summary of data.

Type/table/file	IDcodes	Source
Hydraulic data		
plu_impeller_anomaly.xls	HFR101, HFR105	Sicada_2009_103
plu_pfl_diff_seq_flo.xls plu_pfl_inferr_anom.xls	KFR101–104, KFR27	Sicada_2009_103
p_transmissivity.xls plu_impeller_anomaly.xls	HFM33–35	Sicada_2009_104
plu_pfl_diff_seq_flo.xls	KFM11A	Sicada_2009_141
plu_pfl_inferr_anom.xls	KFM11A	Sicada_2009_157
plu_pfl_inferr_anom.xls	KFR105	Sicada_2009_159
Geological data[1)]		
p_core_loss.xls p_fract_core.xls p_fract_percussion.xls p_fract_crush.xls p_fract_sealed_nw.xls p_rock_struct_feat.xls p_rock.xls p_rock_alter.xls p_rock_occur.xls	HFM33–35, HFR101,HFR105, KFM11A, KFR101–104, KFR27, KFR04,KFR08,KFR09,KFR13, KFR35,KFR36,KFR54,KFR55, KFR7A, KFR7C	Sicada_2009_101
p_fract_core.xls p_fract_crush.xls p_fract_sealed_nw.xls p_rock_struct_feat.xls (Not created: p_core_loss.xls) p_rock.xls p_rock_alter.xls p_rock_occur.xls	KFR105	Sicada_2009_127
BIPS imagery		
92222_KFR101_KFR101_Geosigma_2__.bdt 96914_KFR102A_KFR102A_Geosigma_2__.bdt 93845_KFR102B_KFR102B_Geosigma_2__.bdt 93855_KFR103_KFR103_Geosigma_2__.bdt 94624_KFR104_KFR104_Geosigma1__.bdt 94644_KFR27_KFR27_Geosigma_2__.bdt KFR27_11-147m_20080709.bdt KFR27_140_500m_20081104.bdt	KFR101–104, KFR27	Sicada_2009_110

Type/table/file	IDcodes	Source
KFR101_13-335m_20080710.BIP KFR102A_71-598m_20090114.BIP KFR102B_13-179m_20080910.BIP KFR103_13-199m_20080911.BIP KFR104_8-440m_20081014.BIP KFR27_11-147m_20080709.BIP KFR27_140_500m.BIP		
97779_KFR105_No_BIPS2__.bdt 97780_KFR105_No_BIPS1__.bdt 97781_KFR105_Geosigma__.bdt KFR105_4-303m_20090616.BDT KFR105_4-303m_20090616.BIP	KFR105	Sicada_2009_127
Geometrical data		
p_SHI.xls object_location.xls	HFM33–35, HFR101–105, KFM11A, KFR101–105, KFR27, KFR04,KFR08,KFR09,KFR13, KFR35,KFR36,KFR54,KFR55, KFR7A, KFR7C	Sicada_2009_180
Deformation zone geometry[2)]	RVS model file defining deformation zone geometry in the Geological model SFR v.0.1	See footnote

[1)] p_fract_core.xls applies to core-drilled boreholes, with IDcodes starting with letter “K”, while p_fract_percussion.xls applies to percussion-drilled boreholes, with IDcodes starting with letter “H”.

[2)] SKBdoc 1224857 – DZ_SFR_REG_v0.1, Version 1.0, 2010-06-08.

1.7 This report

This report is organised as follows:

Chapter 1 summarizes the context of this report: the purpose, scope and data used for the SFR hydrogeological model v. 0.2.

Chapter 2 describes the modelling principles in detail: the assumptions made, the methodologies, and the equations used in calculations. Some assumptions are of a more general and conceptual nature. These were mainly based on previous modelling work performed for the nearby Site Investigation Forsmark, e.g. /Follin et al. 2005, 2007a–c, 2008/. Other assumptions were adapted to observations in site-specific data, e.g. appropriate cut-off limit for PFL-f data and the calibration criterion for the size scaling exponent, k_r.

Chapter 3 presents all results in sequential order, starting with a visualisation of orientation and intensity patterns in data (Section 3.1). Based on these findings, a preliminary hydro-DFN is developed. An orientation model is defined and is used to divide the hydraulic data into fracture sets. The model domain is divided into three depth domains, based on observations in vertical trends. Fracture size is estimated by means of a simplified statistical/geometrical approach (connectivity analysis). Empirical relations are established for fracture transmissivity, defined per fracture set and per depth domain.

Chapter 4 presents an evaluation of the approach taken. The preliminary hydro-DFN is applied in flow simulations to test its performance, as well as different conceptual assumptions. Several insights are gained, which are summarized in Chapter 5.

Chapter 5 summarizes the main findings of Chapters 3 and 4.

The details of analyses are reported in the Appendices B–J.

Conventions used in presentation of data:

Most data analyses are presented in terms of *elevation* to facilitate data comparison between boreholes. Elevation specifications are consistently denoted by its reference system "*m RHB70"*. This convention may seem tedious and unfavourable for text readability. However, it was considered necessary to avoid confusion with other commonly used location references, such as borehole length, or vertical depth.

Several analyses are presented in histograms, showing the frequency of data falling into different bins (i.e. predefined intervals). Where bins are numerous, it is difficult to fit in all necessary information on binning intervals to make the figures completely unambiguous. The following convention was used: values specified *at* tick-marks refer to bin *boundaries*, while values specified *between* tick-marks refer to bin *mid-values*.

During the time of analysis, the orientation uncertainty parameter Ω was not yet available. Instead, this uncertainty was preliminary judged by visibility in BIPS. Fractures visible in BIPS have higher accuracy in orientation measurement. Analysis of fracture *orientation* includes fractures *visible in BIPS only*, while analysis of fracture *intensity* include *all fractures*.

This report frequently uses acronyms, abbreviations, and parameter notations that in some cases are rarely used outside SKB-related work. To facilitate the readability of this report, they are listed in Appendix K.

2 Data analysis and modelling approach

2.1 Approach

The hydrogeological modelling methodology was developed during the Site Investigation Forsmark /Follin et al. 2005, 2007a–c, 2008/. Most of the assumptions and concepts described in this section are taken from, or modified from, the work of /Follin et al. 2005, 2007b/. The hydro-DFN for Site Investigation Forsmark was developed in two stages: 1) an initial statistical/geometrical method, which is approximate but computationally efficient for estimating reasonable size distributions, followed by 2) a hydraulic method, which is considerably more computationally demanding (Table 2-1). The purpose of the latter step is to ensure that the DFN honours borehole data in terms of flow. This modelling methodology was developed in context with the introduction of PFL-f data, which was a pioneering type of hydraulic data with high precision measurements of discrete, continuously flowing flow paths. Consequently, the outlook on what PFL-f data represents has had a central role in the development of the established modelling methodology. Therefore, the role of PFL-f data in DFN parameterisation has been given much attention in this study (Section 2.2.4 and Appendix C).

Due to the fact that no updated geological model was available for the current data set, it was not considered meaningful to complete both stages of the calibration process at this stage. Instead the focus was redirected to data analysis, evaluation of methodology, and test cases. Only the first calibration stage, connectivity analysis (Table 2-1), was completed in full. The result is a preliminary hydro-DFN parameterization, which is conditioned to geometry and statistics alone. The significance of the latter stage, the hydraulic method (Table 2-1), could then be evaluated by applying the preliminary hydro-DFN directly to flow simulations and comparing to borehole data.

The purpose of this reverse approach was to evaluate the effects of hydraulic chokes (Figure 2-1) in the calibration. The degree to which the flow system is controlled by chokes depends on 1) how well-connected the network of Open fractures is (i.e. largely determined by size and intensity), and 2) the variability in fracture transmissivity over flow paths. Note that in this study Open fractures are conceptually perceived as planar structures with constant hydraulic properties (i.e. the complexity of within-plane heterogeneity is not considered). The hydro-DFN is intended as input for application in DarcyTools modelling, which implies a step of translating fracture hydraulics into Equivalent Continuous Porous Medium (ECPM) properties. The hydro-DFN controls the magnitude of ECPM conductivity, anisotropy, and correlation lengths. The translation is done in the DarcyTools module GEHYCO, using an algorithm based on volumetric fractions of intersections between fractures and computational cells /Svensson et al. 2007/. At the level of practical discretisation limitation in regional-scale modelling (say 10 m), GEHYCO does not take hydraulic chokes into account.

Table 2-1. Overview of the hydro-DFN methodology, established by SKB.

1) Statistical/geometrical method: connectivity analysis /Follin et al. 2005/		**Performed in this study**
Orientation	Fracture sets identified and parameterized by Open fractures in Boremap	Appendix E
Intensity	Terzaghi weighted frequency of Open fractures in Boremap	Section 2.2.7
Size	Calibrated to match a defined Connected Open Fracture intensity.	Section 2.2.10
	Bounded by intensity of Open fractures and PFL-f records	Section 2.2.11
		Section 2.3
Transmissivity	Values assigned directly from PFL-f data, correlated to size.	Section 2.2.9
		Section 2.3.3
2) Hydraulic method: inverse flow modelling /Follin et al. 2007b/		**Performed in this study**
Orientation	Identical to the Statistical/Geometrical method	
Intensity	Identical to the Statistical/Geometrical method	
Size	Calibrated to reproduce the frequency of PFL-f inflow.	Not performed
Transmissivity	Calibrated to reproduce the magnitude of simulated PFL-f inflows	Not performed

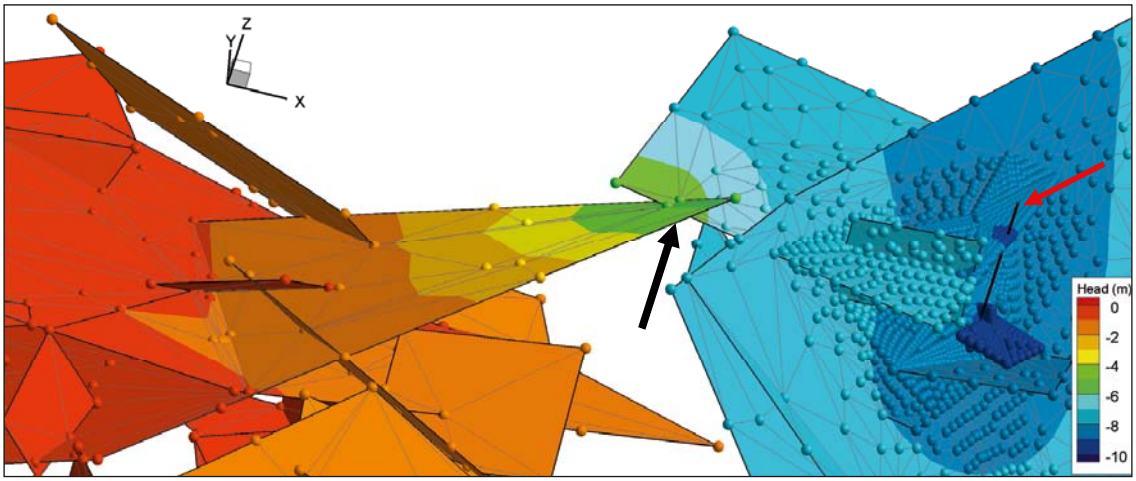

Figure 2-1. *Example of a hydraulic choke (black arrow) controlling inflow to borehole (red arrow). The borehole inflow may depend more on the transmissivity and amount of contact at this bottleneck, than on the transmissivity of borehole-intercepted fractures.*

Therefore, there is a clear risk that a flow system predominantly constrained by hydraulic chokes cannot be well-represented in the subsequent DarcyTools application. This risk is conceptually illustrated for a hypothetical case in Figure 2-2.

A hypothetical and highly simplified case is considered, where the modelling is executed in the following three sequential steps (Figure 2-2):

Step 1. The preliminary connectivity analysis renders two possible solutions for fracture size:
a) an interconnected network of small fractures, mainly controlled by hydraulic chokes, or
b) large autonomous fractures that are mainly independent on chokes.

In this step, fracture transmissivity is assigned directly from PFL-f data (without consideration to chokes). At this stage, both solutions (a) and (b) are expected to translate rather well into ECPM properties, as assigned fracture transmissivity represents the average flow-channel transmissivity of PFL-f data (illustrated by brown colour in Figure 2-2).

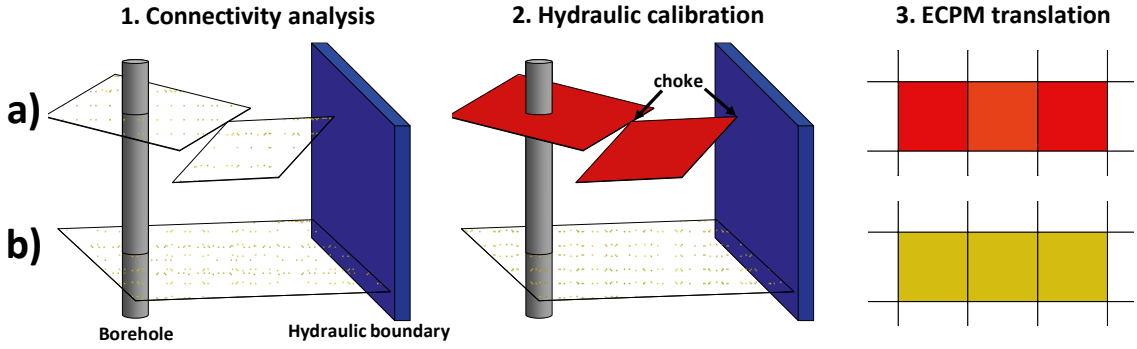

Figure 2-2. *Conceptual illustration of the potential risk in calibrating a hydro-DFN primarily controlled by hydraulic chokes for later application in a coarsely discretised regional-scale model. Model steps 1-3 are illustrated for two fracture network cases: a) and b). The difference in absolute values between the different entities transmissivity and conductivity is not shown; brown colour represents hydraulic properties in line with PFL-f data, red represents parameter values exceeding actual field measurements.*

Step 2. In the hydraulic calibration fracture transmissivities are adjusted to honour the measured borehole inflow in PFL-f data. Within the DFN modelling framework flow is governed by transmissivity, as well as, the fine-detailed geometric intersection at fracture contacts. In case a) the transmissivity must therefore be increased to compensate chokes (possibly, several order of magnitude, illustrated by red colour in Figure 2-2). However, case b) is largely unadjusted.

Step 3. The calibrated DFN is applied in a regional-scale model by means of ECPM translation, which does not take these choking effects into account. Consequently, in this hypothetical case, a) may result in overestimated ECPM conductivity in relation to measured hydraulic data. The middle cell contains the choke, and may be translated into a somewhat lower conductivity, owing to lesser volumetric fraction (shown with pink colour). However, this will be on a different order of magnitude, as compared to the DFN modelling framework.

Obviously, the simplified hypothetical case in Figure 2-2 demonstrates an exceptional, extreme case. This scenario is not based on actual numerical calculations; it currently only exists as a speculation. A real application is shown in Figure 4-4, where even decimetre-scale discretisation in DarcyTools overestimates the connectivity. However, this pin-points the dilemma that fine-tuning fracture transmissivity within a high resolution DFN framework does not necessarily imply that the final application in a regional-scale model has improved. The question also relates to the conceptual definition of fractures, flow paths, the role of PFL-f data, and what type of input that is most consistent for application in DarcyTools. In fact, a key question is what the primary objective is: to develop a hydro-DFN that accurately reproduces borehole data in a DFN modelling tool, or to establish reasonable input data for the ECPM-concept. Consequently, it is important to evaluate the significance of hydraulic chokes at an early modelling stage (i.e. before completing the complete DFN calibration). Furthermore, the significance of using the true borehole radius (r_w= 0.038 m), versus using a zero-radius scanline, is evaluated.

2.2 Model principles

2.2.1 Borehole data used

This model version is based on the new core data available inside the local SFR model domain: KFR27, KFR101, KFR102A, KFR102B, KFR103, KFR104, and the underground sub-horizontal KFR105 (Figure 1-1). Data coverage with depth is shown in Figure 2-3 and the hydraulic data are summarized in Table 2-2. A more detailed presentation of data is given in Section 3.1 and Appendix C.

The excluded data are percussion-drilled boreholes HFR101, HFR102, and HFR105, inside the local SFR model domain, and: HFM34, HFM35, and KFM11A, inside the regional domain, but outside the local model domain (Appendix B). Data from percussion-drilled boreholes have a lower confidence in the interpretation of fractures as Open or Sealed. Dark mineral filling can easily be mistaken for an open aperture in BIPS imagery, and therefore it is difficult to make this fracture interpretation without actual support from the core. The use of percussion data therefore implies a risk of including Sealed fractures in the analysis, which would overestimate the intensity of Open fractures. Furthermore, the Sealed fractures have different orientation characteristics, which may introduce errors in the orientation model. Moreover, it is difficult to combine hydraulic data from percussion-drilled, respectively, cored boreholes. The reason is that impeller flow loggings in percussion boreholes have a much higher detection limit compared to the PFL-f data and its correlation to fracture data is more uncertain. KFM11A also exhibits deviating characteristics which are assumed to relate to influence of the Singö zone; since an updated geological model is currently unavailable, it is currently difficult to clearly state if these characteristics should be interpreted as general signs of a separate fracture domain, or if it relates to uncertainty in the definitions of HRD (see Appendix B).

Due to these circumstances it was decided to exclude all percussion data, as well as KFM11A, from the SFR hydro-DFN v.0.2.

2.2.2 Borehole information with depth

Several analysis and calculations relate to borehole length. A region with little available core length implies local low confidence in the parameterization of the hydro-DFN. In terms of depth trends, the total amount of borehole information varies with depth — a fact that must be taken into account in borehole-to-borehole comparisons, depth trend analysis, and the evaluation of fracture domains. The hydro-DFN targets the HRD, which is here defined as the rock mass between the PDZ according to the SHI. Consequently, all data and borehole lengths falling inside the PDZ are excluded from further analysis.

The variability in available core length with depth is shown as a stacked histogram in Figure 2-3, where the core lengths of each borehole are added over 10-m elevation bins, and normalised by the bin size. The corresponding histogram for PFL-f logged borehole sections is not shown, as is virtually identical to that for core data; the exceptions are found at the 0 to –10 m bin, owing to borehole casing, and the last couple of meters at the end of the boreholes, which cannot be measured due to technical difficulties. The data gaps, for example between –420 to –450 m RHB70, indicate data exclusion owing to possible deformations zones. The target volume, i.e. repository depth between –100 and –150 m RHB70, is the most extensively examined interval. In this interval approximately 10 m core length are available per vertical meter. As can be seen in Figure 2-3, the highest contribution in this interval comes from the sub-horizontal borehole KFR105. Below –350 m RHB70 the only data sources are KFR102A and KFR27.

There is also a data gap in the shallow HRD for several boreholes: KFR101, KFR102A, KFR105, and KFR27. KFR102A was telescope drilled down to 70 m borehole length (–63 m RHB70), while in KFR101 a possible deformation zone has been interpreted down to 88 m borehole length (–70 m RHB70). The upper 146 m of KFR27 was drilled during the construction of SFR (down to –143 m RHB70), and as no core is available today this part was excluded. KFR105 is an underground borehole, which starts at –107 m RHB70. KFR104 provides the most continuous information, extending from the surface and down to greater depths (–337 m RHB70). The discontinuity and "depth trend" in sampled core length with depth (Figure 2-3) must be carefully considered in all analysis steps, as it can easily be mistaken for local heterogeneity, respectively, depth trend in parameters estimated.

For example, the maximum transmissivity at different depths is a practical estimate of depth trends, as done in the Site Investigation Forsmark /e.g. Follin et al. 2007b/. However, transmissivity is known to be highly skewed (e.g. log-normally or power-law), which implies that the larger the sample size, the larger is the expected maximum transmissivity. Thus, a "depth trend" in sample size is likely to exaggerate the depth trend in maximum transmissivity.

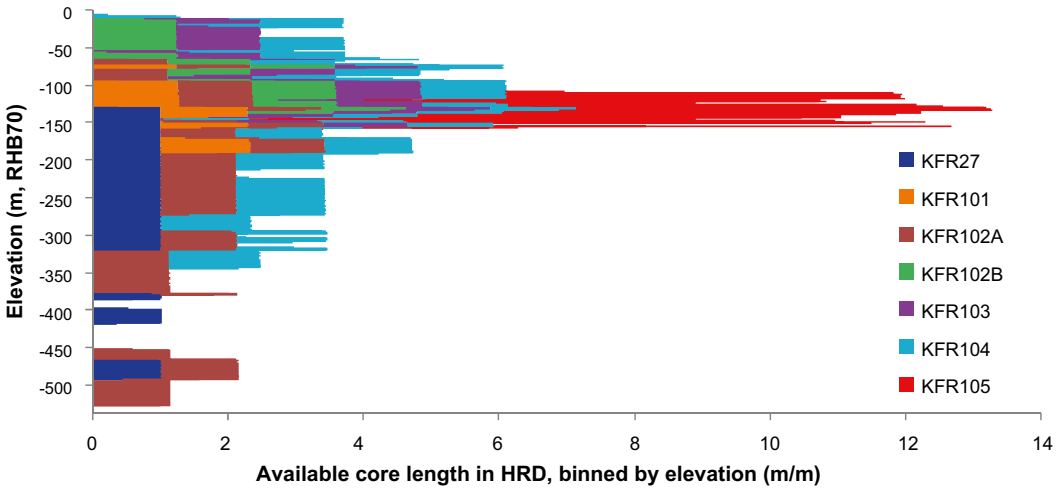

Figure 2-3. *Available borehole information for HRD with depth, shown for boreholes KFR101–105 and KFR27. Stacked bars reflect total available core length per elevation interval. Binning interval = 1 m.*

The discontinuity in sampled core length with depth causes complications in the analysis of deterministic heterogeneity and fracture domains. For example, KFR102B and KFR27 completely lack vertical overlap (Figure 2-3). If the fracture characteristics should prove to differ significantly between these two boreholes, it is difficult to infer if this relates to a depth trend or a lateral trend.

2.2.3 Conceptual perception of modelled fractures

All fractures are modelled as squared, planar surfaces with equivalent homogeneous hydraulic properties. Open and Partly open fractures are considered as potential features for flow, while Sealed fractures are assumed to be impervious, and therefore excluded in the analysis. In reality, the geometry of fractures is known to be complex and highly irregular, which channels flow into preferential paths of low resistance. These flow channels tend to be concentrated to only a minor part of the total fracture volume, whereas the remaining fracture volume may contain gauge material and pools of more or less stagnant water. Thus, it is important to consider that the "binary" fracture interpretation at a borehole intercept (Sealed, Open, or Partly open) is based only on the information available at the cross-sectional area of the borehole. In other words, a fracture that is clearly Sealed at a borehole intercept will be mapped as "Sealed" and treated as such, although it may very well carry channelized flow at some distance away from the borehole intercept.

The Partly open fractures constitute 10% of the population of Open and Partly open fractures in the rock between possible deformation zones. In later analyses, it is found that the Partly open fractures are predominantly NE-NW striking and sub-vertical. In the PFL-f data set, the corresponding fraction of Partly open fractures is 8%.

2.2.4 PFL-f data

PFL-f data has a fundamental role in the hydro-DFN. These are hydraulic data for continuously flowing paths, determined at a high spatial resolution in the borehole. The PFL-f data set is presented and discussed in more detail in Appendix C. In summary, the Posiva Flow Logging (PFL) device is used to identify discrete borehole inflow over 0.1 m sections with a accuracy of ±0.2 m borehole length, see /Hurmerinta and Väisäsvaara 2009a, b, Kristiansson and Väisäsvaara2008, Pekkanen et al. 2008/. Borehole logging is initially performed under undisturbed conditions and repeated after c. one week of pumping, which implies that inferred flowing features are persistent and presumably in contact with a constant head boundary. These discrete inflows (i.e. PFL-f records) have also been coupled to Boremap features /Öhman et al. 2010/, providing the orientation and geologic interpretation of features that are associated to PFL-f data.

Using a relation for measured inflow under pumped conditions, respectively, undisturbed conditions, a transmissivity value is evaluated for each PFL-f record, see e.g. /Hurmerinta and Väisäsvaara 2009a/. This evaluation is based on an assumption of cylindrical flow regime and a constant radius of influence (i.e. independent of the magnitude of the measured specific capacity). More precisely, this evaluated transmissivity is an apparent value reflecting the network of Open fractures that connects the tested borehole section (0.1 m) to the surrounding hydraulic boundary. In reality, the flow dimension depends on the geometry and connectivity of the fracture network studied; it does not necessarily have to be cylindrical (Figure 2-1). In fact, it may be more appropriate to refer to this apparent hydraulic property as specific capacity (Q/s; inflow per unit drawdown). Moreover, the PFL-f data are censored by a practical detection limit which varies locally (Appendix C). In order to simplify the data analysis and DFN parameterisation, it was decided to assume a constant truncation threshold, T_{lim}, excluding all records $Q/s < 2.5\times10^{-9}$ m^2/s. It should be emphasised that the detection limit varies in reality; this assumed constant truncation limit is a simplification for the purpose of comparing PFL-f data from different boreholes and from different depths. The evaluated transmissivity of PFL-f data is summarized in Table 2-2; details are given in Appendix C.

Table 2-2. Summary of PFL-f data.

Borehole	Unit	Borehole length (m) From	To	PFL-logged length[1] (m)	Elevation (m, RHB70) From	To	No. PFL	NA[2]	ΣPFL T [3] (m²/s)
KFR101	DZ1	13.72	88.00	74.28	–8.85	–69.55	19		1.6E–5
	HRD	88.00	97.00	9.00	–69.55	–76.87	0		–
	DZ2	97.00	116.00	19.00	–76.87	–92.22	1		8.3E–6
	HRD	116.00	179.00	63.00	–92.22	–142.04	5		5.1E–7
	DZ3	179.00	186.00	7.00	–142.04	–147.47	1		1.3E–5
	HRD	186.00	197.00	11.00	–147.47	–155.96	0		–
	DZ4	197.00	213.00	16.00	–155.96	–168.22	0		–
	HRD	213.00	242.00	29.00	–168.22	–190.11	1		1.8E–8
	DZ5	242.00	341.76	90.20	–190.11	–262.03	25		6.1E–6
KFR102A	HRD	71.95	149.00	77.05	–63.01	–133.29	28		1.2E–6
	DZ1	149.00	161.00	12.00	–133.29	–144.21	2		9.5E–9
	HRD	161.00	302.00	141.00	–144.21	–271.89	50		1.3E–5
	DZ2	302.00	325.00	23.00	–271.89	–292.56	1		1.9E–8
	HRD	325.00	422.00	97.00	–292.56	–379.2	0		–
	DZ3	422.00	503.00	81.00	–379.2	–450.99	21		1.7E–6
	HRD	503.00	589.51	86.51	–450.99	–527.38	2		9.6E–9
KFR102B	HRD	13.95	70.00	56.05	–8.89	–54.34	37		3.9E–6
	DZ1	67.00	70.00	3.00	–51.91	–54.34	3		8.8E–7
	HRD	70.00	109.00	39.00	–54.34	–85.81	23		4.3E–7
	DZ2	109.00	114.00	5.00	–85.81	–89.83	5		1.4E–7
	HRD	114.00	149.50	35.50	–89.83	–118.39	10		2.5E–6
	DZ3	149.50	150.50	1.00	–118.39	–119.19	1		5.0E–6
	HRD	150.50	173.00	22.50	–119.19	–137.21	8		1.1E–6
	DZ4	173.00	180.00	1.77	–137.21	–142.81	2		5.9E–7
KFR103	HRD	13.33	24.50	11.17	–8.46	–17.5	5		1.0E–4
	DZ1	24.50	26.50	2.00	–17.5	–19.12	1		2.5E–7
	HRD	26.50	84.00	57.50	–19.12	–65.61	24		5.2E–6
	DZ2	84.00	91.00	7.00	–65.61	–71.24	5		1.6E–5
	HRD	91.00	180.00	89.00	–71.24	–142.53	5		1.9E–7
	DZ3	180.00	182.50	2.50	–142.53	–144.52	3		5.1E–6
	HRD	182.50	195.03	12.53	–144.52	–154.52	1		2.2E–8
KFR104	HRD	8.73	30.00	21.27	–4.32	–21.72	4		1.6E–7
	DZ1	30.00	45.50	15.50	–21.72	–34.36	9		1.8E–7
	HRD	45.50	149.00	103.50	–34.36	–117.66	55		4.6E–6
	DZ2	149.00	154.00	5.00	–117.66	–121.63	1		3.9E–9
	HRD	154.00	268.00	114.00	–121.63	–210.79	16		4.6E–7
	DZ3	268.00	283.00	15.00	–210.79	–222.34	2		1.1E–7
	HRD	283.00	382.00	99.00	–222.34	–297.64	4	1	7.6E–8
	DZ4	382.00	387.00	5.00	–297.64	–301.39	0		–
	HRD	387.00	396.00	9.00	–301.39	–308.13	0		–
	DZ5	396.00	405.00	9.00	–308.13	–314.86	1		1.1E–8
	HRD	405.00	443.18	38.18	–314.86	–343.28	0		–
	DZ6	447.00	454.57	–	–346.11	–351.71	0		NA
KFR105	HRD	2.97	45.00	42.03	–107.34	–114.61	15		1.5E–7
	DZ1	45.00	52.00	7.00	–114.61	–115.8	2		6.1E–9
	HRD	52.00	88.50	36.50	–115.8	–122	18		3.8E–8
	DZ2	88.50	96.50	8.00	–122	–123.33	3		2.3E–9
	HRD	96.50	170.80	74.30	–123.33	–135.53	40		8.8E–7
	DZ3	170.80	176.00	5.20	–135.53	–136.36	5		2.7E–7
	HRD	176.00	258.00	82.00	–136.36	–149.36	42		7.8E–8
	DZ4	258.00	283.00	25.00	–149.36	–153.16	11		4.1E–8
	HRD	283.00	293.60	10.60	–153.16	–154.73	5		5.7E–9
	DZ5	293.60	304.00	10.40	–154.73	–156.23	9		1.4E–8
	HRD	304.00	305.88	1.88	–156.23	–156.5	0		–
KFR27	HRD	12	108.00	Excluded[4]	–9.13	–105.12	3	3	NA
	DZ1	108.00	120.00	Excluded[4]	–105.12	–117.12	5	5	NA
	HRD	120.00	143.00	Excluded[4]	–117.12	–140.12	1	1	NA
	HRD	143.00	323.00	180.00	–140.12	–319.49	22	2	7.2E–6
	DZ2	323.00	379.50	56.50	–319.49	–375.63	29		1.2E–6
	HRD	379.50	389.00	9.50	–375.63	–385.07	0		–
	DZ3	389.00	401.00	12.00	–385.07	–396.99	1		1.2E–9
	HRD	401.00	421.00	20.00	–396.99	–416.85	6		5.4E–8
	DZ4	421.00	469.00	48.00	–416.85	–464.53	8		2.0E–6
	HRD	469.00	496.61	27.61	–464.53	–491.93	1		1.1E–7

[1] Excluding non-PFL logged interval length.

[2] Transmissivity not evaluated for PFL record.

[3] Coloured by log(Σ T/PFL-logged length); red = high values, yellow = median, blue = low values.

[4] Excluded owing to low confidence data; lacking core (12–147.49 m), coarse measurement scale (0.5 m) for reference PFL measurements, several non-evaluated transmissivity values (99–135 m).

Role of PFL-f data in the hydro-DFN

In essence, PFL-f data reflects hydraulic properties of Connected Open Fractures above the practical detection limit. PFL-f data provide the following crucial properties for the parameterisation of the hydro-DFN:

1) Spatial location of flowing features (accuracy of ±0.2 m borehole length).
2) Orientation of intercepted flowing features (confidence in orientation subjective to coupling to Boremap data).
3) Frequency of flowing 0.1 m test sections (censored by the detection limit; note that test sections may contain more than one fracture).
4) Specific capacity defined over 0.1 m test sections (censored by practical detection limit).

The main difference between the two calibration stages (Table 2-1) is the perspective on what PFL-f data represents and how the data are applied in the calibration process. In the connectivity analysis, the evaluated hydraulic property for a PFL-f record is assumed to constitute the explicit transmissivity of the most likely candidate of fractures that intersects the test section. Based on this assumption the evaluated PFL-f transmissivities are directly assigned to a Connected network of Open fractures. This is a reasonable assumption for a fracture that, in its entire extent, is in direct contact with a constant head boundary (or extends to the radius of influence).

However, in sparsely fractured rock, the amount of contact between fractures, as well as upstream fracture transmissivity, may equally well be the constraining factor for borehole inflow, referred to as hydraulic bottlenecks or hydraulic chokes (Figure 2-1). In other words, the evaluated PFL-f transmissivities is an apparent value, representing the total specific capacity for the flow paths between the tested borehole section and surrounding constant head boundary. PFL-f data is of pseudo-stationary type, and so the distance to the hydraulic choke/head boundary cannot be deduced directly from data. Therefore, it is preferable to use inverse flow simulations (Table 2-1) where fracture transmissivity is treated as a fitting parameter and the calibration criterion is that specific capacity is reproduced in simulated inflow. The benefit of this method is that it circumvents relying on assumptions of flow dimension, yet honours borehole data in terms of flow.

2.2.5 Fracture domains

Fracture domains /Olofsson et al. 2007/ can be used to represent local deviations in characteristics of the Hydraulic Rock Domain (i.e. rockmass between deformation zones) /e.g. Follin et al. 2007b/. The fracture domain concept is used to delineate components in heterogeneity that are interpreted as deterministic (i.e, as opposed to stochastic heterogeneity). Without support from a geological inference, the spatial extent of a fracture domain can, for example be extrapolated by statistical methods (krieging, nearest neighbour, etc). For example in work by /Follin et al. 2005/, each borehole in the early Site Investigation Forsmark was assumed to reflect a separate fracture domain and the spatial definition of each fracture domain was assumed to be a prism volume surrounding the borehole. However, the model confidence improves, if its spatial extrapolation of deviant characteristics can be associated to hydrogeological inference to support its spatial definition. For example, a fracture domain can be associated to a particular geologic setting, influence of major deformation zones, stress-regime, rock types, etc. Depth trends in hydraulic properties can be accounted for by subdividing fracture domains into vertical domains, e.g. /Follin et al. 2007b/.

There currently does not exist a fracture domain model for the SFR domain. There is also little support available from the geological modelling. The Geologic model v.0.1 /Curtis et al. 2009/ was based on data from the construction of SFR and a more recent interpretation of surface lineaments. It was conditioned to the near field of the existing SFR, but does not include the more recent borehole data used in this study. A rock domain model is currently under development and will become available in the SFR Geologic model v. 1.0. To some extent, the preliminary definitions of the rock domain model appear to support the observed variation in fracture characteristics. Furthermore, the final definitions of deformation zones have not yet been established, which causes uncertainty in the parameterisation of the HRD. In other words, it is quite possible that deviating hydraulic properties in fact is the result of uncertainty in the PDZ/HRD classification.

Thus, at the onset of this analysis, it is not known whether the SFR modelling domain should be treated as a single entity, or if the domain needs to be divided into several sub-units. The characteristics considered important for motivating the formulation of fracture domains include:

1) Conceptual support from the hydrogeological context.
2) Deviating transmissivity.
3) Deviating intensity (Open fractures and PFL-f data).
4) Deviations in orientation distribution.

At this stage, prior expectations are that the Singö deformation zone ZFMWNW0001, and its splay ZFMNW0805a,b (formerly known as zone 8) may constitute fracture domain boundaries. ZFM871 (formerly known as SFR zone H2) is also considered a possible divide between fracture domains.

As the goal of the SFR hydrogeological model v. 0.2 is to parameterise a hydro-DFN, both the PFL-f data and Open and Partly open fractures inside HRD are regarded as indicators for fracture domain definitions. However, the PFL-f data are considered to be the primary indicator, while the Open and Partly open fractures are considered to be of subordinate importance. The decision on if the model domain should be divided into fracture domain, or not, must be taken early in the modelling workflow, as all hydro-DFN parameter estimations require that the sub-populations of data are properly defined.

This dilemma was approached in the following steps:

1) A preliminary visual inspection of data was undertaken to decide if one global orientation model, or if different local orientation models should be used. This step largely depends on visual inspection of data and subjective judgment.
   a. The orientation, depth, and transmissivity of PFL-f data were compared visually, in terms of stereograms on borehole-to-borehole basis
   b. The orientation of Open and Partly open fractures were compared visually, in terms of Kamb-contoured stereograms on borehole-to-borehole basis, and for different depth intervals
   c. The intensity of Open and Partly open fractures were binned by orientation and elevation and compared visually borehole-to-borehole basis
2) Based on the preliminary analysis, it was considered reasonable to use one global orientation model for the entire SFR Regional domain.
3) All Open and Partly open fractures and the PFL-f data were divided into sets according to the global orientation model, which allows the heterogeneity in fracture characteristics to be analysed in terms of set-intensity with depth. The orientation model statistics (mean pole and Fisher κ) were then updated according to each identified data sub-population (i.e. depth intervals).

There is a clear risk in breaking the data into too many subsets based on deviating statistics alone (i.e. without geological inference). The confidence in small data sets decreases with smaller underlying sample size and the extrapolation of deviant hydraulic properties over sub-volumes without the support of a conceptual model may in fact overrepresent heterogeneity. With respect to the current situation, it was decided to be restrictive with fracture domain definitions at this stage. However, it is expected that the SFR Hydrogeological model v. 1.0 will provide better insight into the existence and spatial definition of fracture domains. Instead, more attention was paid to vertical variation, as depth trends in hydraulic data are of more general character /e.g. Gustafson 2009/ and less dependent on site-specific geological conditions.

2.2.6 Orientation model

Fracture sets are assumed to follow the Univariate Fisher distribution, defined by a mean pole (trend and plunge) and a concentration parameter, Fisher κ. As a first step, the identification of fracture sets is made by visual inspection of contoured plots of cluster significance /Kamb 1959/ and /Robin and Jowett 1986/. These initial hard sectors are defined by a mean pole and a confining hard-sector solid angle. The hard sectors are primarily used for visualisation purposes, i.e. reference for illustrating local variation in borehole data. For modelling purposes, the hard sectors are only used as initial estimates of a soft-sector parameterisation (see Figure E-1). All modelling is based on soft-sector

divided data, which is necessary to obtain consistency between data and simulations. This is explained in more detail in Appendix E.

The Fisher distributed sets will overlap to various degrees. During analysis of PFL-f data it was found that transmissivity is highly anisotropic (i.e. different expectation for different sets). Therefore, special care was taken for the set-assignment of PFL-f data. In sectors of high Fisher distribution overlap, it was decided that the set-assignment of PFL-f data should not be based on geometry alone, but also weighted by transmissivity. This procedure was considered necessary in order to preserve the hydraulic contrast between sets, yet preserving the geometric expectation value of the Fisher distribution.

2.2.7 Fracture intensity

The three-dimensional fracture intensity P_{32} [m^2/m^3] is estimated from one-dimensional borehole fracture frequency P_{10} [1/m]. There exist several methods to compensate for geometrical sampling bias in cases where fractures are sub-parallel to the borehole. The more advanced methods take the relation between borehole radius and fracture size distribution into account /e.g. Mauldon and Mauldon 1997/, or the continuity in fracture orientation, by assuming Fisher distributed sets /Wang 2005/. In this analysis it was decided practical to use the Terzaghi method to estimate P_{32} from P_{10}.

$$w = \frac{1}{\sin(\max(\alpha, \alpha_{\min})} \tag{2-1}$$

where α is the solid angle between the borehole and the fracture plane. The Terzaghi method treats the borehole as a scan-line (i.e. no borehole radius) and does not take fracture size into account. Therefore it is considered less reliable for very small α and consequently a minimum bias angle, α_{min}, must be used, in order to avoid infinite weights at α = 0°. A standard practise is to use a maximum Terzaghi weight of 10, corresponding to a minimum bias angle α_{min} = 5.7° /Yow 1987, Priest 1993/. In this analysis, the minimum bias angle was set to α_{min} =1° (in practise the smallest measured bias angle is 2° for Open fractures, and 6° for PFL-f data).

The reason for selecting the Terzaghi method is that it is convenient to apply consistently to both fracture data and the simulated exploration of DFN realisations. The small minimum bias angle is necessary to reflect the sub-vertical sets with a simulated vertical borehole in the later DarcyTools calibration of $P_{32, COF}$. Moreover, the fracture size is highly uncertain, and with respect to other uncertainties the method is considered adequate for these modelling purposes. For example, increasing minimum bias angle to 10° would decrease the total $P_{32, Open}$ by 4%. The uncertainty in the calibration target $P_{32, COF}$ is much larger than that (Section 2.2.11).

The intensity of a power-law size distributed fracture network can be calculated over any radius interval [r_{min} and r_{max}] by

$$P_{32}[r_{\min}, r_{\max}] = \frac{r_{\min}^{2-k_r} - r_{\max}^{2-k_r}}{r_0^{2-k_r}} P_{32}[r_0, \infty] \tag{2-2}$$

where r_0 is the minimum fracture radius, k_r is the power-law scaling exponent of the radius distribution, and P_{32} [r_0,∞] is total fracture intensity. The intensity of Open and Partly open fractures recorded in borehole data is assumed to reflect fractures equal to, or larger than, borehole radius, but smaller than the equivalent radius of deterministically modelled deformation zones (since PDZ is excluded from borehole analysis). The borehole data are located within the local SFR model domain, which has a lineament cut-off of 300 m, corresponding to an equivalent radius of 169 m. In other words the HRD intensity of Open and Partly open fractures is assumed to be equal to P_{32}[0.038 m, 169 m], eq. (2-2).

2.2.8 Spatial distribution of Open and Connected fractures

The spatial pattern of all Open and Partly open fractures in the rock mass between deformation zones is assumed to follow a Poissonian distribution. This has also been assumed in the Site Investigation Forsmark programme /Follin et al. 2007b/. The assumption is convenient, as the software DarcyTools only generates Poissonian fracture networks. Using in-built sorting algorithms,

non-connected fractures can then be removed prior to flow simulations. The end product, after the removal of isolated fractures, is a network of Connected Open Fractures. This connected fracture network is non-Poissonian (also referred to as Poissonian clusters, which implies fracture clusters that are Poissonien distributed).

2.2.9 Transmissivity of Connected fractures

Two types of distributions are commonly used to parameterise transmissivity data: the log-normal distribution and the power-law distribution. These two types of distributions are fairly similar in shape at their upper tails, the region where data are more certain. The discrepancy between the two distributions grows larger at lower transmissivity, which is a region where data are more uncertain and truncated by the detection limit of the measurement device. Owing to the nature of data, it is difficult to infer if the PFL-f data should be fitted to a log-normal distribution, or a power-law distribution.

Three assumptions have been suggested for the relation between transmissivity and fracture size /e.g. in Follin et al. 2005/:

1. Uncorrelated transmissivity, T, following a log-normal distribution, defined by a mean, μ_{logT}, and standard deviation, σ_{logT}:

$$T = 10^{N(\mu\sigma)} \tag{2-3}$$

2. Correlated transmissivity, T, to fracture radius, r, with a factor, a, and an exponent, b:

$$T(r) = a\, r^b \tag{2-4}$$

3. Semi-correlated transmissivity, T, to fracture radius, r, similarly to eq. (2-4), but with a log-normal random component, defined by standard deviation, σ_{logT}:

$$T(r) = a\, r^b \times 10^{N(0,\sigma)} = 10^{\left[\log(a\, r^b) + N(0,\sigma)\right]} \tag{2-5}$$

Several arguments exist for assuming the correlated model, eq. (2-4). One such argument is the support-scale for hydraulic tests. A high transmissivity value implies a large influence radius, and vice-versa. In other words, unless the conductive feature indeed has a spatial persistence that exceeds the radius of influence, the hydraulic test would have been censored by the hydraulic bound at the fracture perimeter (that is, unless should it be well-connected to a fracture with even higher transmissivity). Another argument is that there exist geologic observations on weak correlation between trace length and maximum visible aperture. In general, the width of deformation zones is also larger for large zones /Stephens et al. 2007/, and it seems reasonable that the same should hold for large fractures.

The uncorrelated model, eq. (2-3), is considered to be unrealistic, based on the arguments above. The most realistic model is perhaps some kind of semi-correlated model, eq. (2-5), but it is not straightforward exactly how that should be pursued and parameterised. For example, to what extent should the magnitude of the random component be assumed to be dependent on size? It was therefore decided to pursue the directly correlated model, eq. (2-4), as a base case. The reason for doing so is both simplicity, i.e. the principle of Ockham's razor, but also because it is considered to be the most conservative assumption, i.e. high transmissivity implies long spatial persistence. Different transmissivity models are evaluated in Section 4.2.2.

2.2.10 Fracture size

For a given fracture intensity and orientation model, the size distribution controls the connectivity of the hydraulic network. If the fracture intensity is low, it can be a critical parameter for percolation of the system. In the ECPM approach, fracture size relates (indirectly) to correlation lengths of hydraulic properties. A widely used assumption is that a tectonic continuum spans across all measurement scales (i.e. meter scale to kilometre scale), which allows the relation between fracture intensity and size to be described by a single power-law distribution. As mentioned in Section 2.2.7, stochastic Open and Partly open fractures in HRD are assumed to be bounded by r_{min} = 0.038 m and r_{max} = 169 m. It should be noted that although r_{min} is a key parameter for the connectivity of the

fracture network, it cannot be deduced from data. /Follin et al. 2005/ evaluated the impact of r_{min}, and assumed r_{min} = 0.038 m based on a match in intensity between Connected fractures and PFL-f data.

One possibility to estimate approximate fracture size could be using the statistics on fracture intersection type (borehole central axis, or only borehole wall; Appendix H). Results of such an analysis suggest a considerable larger r_{min}, particularly for horizontal fractures. However, these results must be interpreted with caution. The confidence in the estimation method relies on an assumption that Boremap data reflects an unbiased mapping of fractures. Obviously, tiny fractures with partial borehole intercepts must be much more difficult to detect during the geologic mapping and thereby possibly causing an unintentional, systematic underrepresentation of tiny fractures (i.e. a bias in the mapped data set). Thus, the estimated sizes in Appendix H relate to the *mapped* fracture system, which may be a biased subset of the *real* fracture system. According to observations in the core data, the bias in Open fractures at SFR is judged to be small or even negligible, while it is more frequent for Sealed fractures (particularly when included in Sealed Networks). As stated in Section 2.2.3, this study includes only Open and Partly open fractures. The main finding of Appendix H is that horizontal fractures seem to be longer than sub-vertical or gently dipping fractures.

The size of fractures cannot be directly measured from borehole data. Fracture size distributions can be estimated from two-dimensional trace data from outcrops, tunnels, and lineaments. However, the objective of this study is to derive size distributions for Open and Partly open fractures, exclusively, and in trace data the distinction between Open or Sealed is often difficult to make. Sealed and Open fractures have distinctively different orientation patterns (Appendix B), and it can be suspected that they also have different size distributions. Therefore trace data may be inadequate for estimating size distributions of Open fractures.

Water-bearing fractures were mapped during the construction of SFR /Christiansson and Bolvede 1987/. The data is not available in a digital format and thus not readily applicable. It is also questionable if mapped tunnel inflow is representative for the *in situ* rockmass. The tunnel construction is known to affect the rockmass in the tunnel wall (e.g. stress re-distribution and blasting damage), which alters the flow pattern of fractures. For example, owing to stress re-distribution, horizontal fractures were found to be more water-bearing in the tunnel ceiling than in the tunnel walls. Dripping water is also easier to detect in the ceiling, than it is in tunnel walls and tunnel invert. Additionally, there is an aspect of geometric sampling bias, which may provide a biased picture of fracture flow. For example, the tunnel walls have a larger area exposed to horizontal fractures, with decreased flow that is more difficult to detect. Furthermore, large extents of the construction tunnel were grouted (in the first 600 m tunnel length), which censors the largest tunnel inflows, and thereby provides an unrepresentative pattern of flowing, respectively, non-flowing fractures. Horizontal traces are reported have a maximum length of 10 m and sometimes appear interconnected. Steep traces are reported to have a maximum length of 10–15 m, and may appear in vertical structures extending over 100 m. The storage facilities (including the Silo) were relatively dry and therefore only grouted in a few locations. The non-grouted Silo has an exposed area of 8,000 m^2 and is located close to two highly conductive deformation zones (10 m above ZFM871 and 60 m from ZFMWNW805), but nevertheless only has an inflow of 2 l/min. From a site characterisation viewpoint, it should be considered that the storage facilities were located in rock that is favourable from a hydraulic viewpoint, and therefore may exhibit characteristics that are unrepresentative for the SFR modelling domain. Today, only parts of the lower construction tunnel (Nedre ByggTunneln, NBT) is exposed, as most of the tunnel walls were shotcreted for rock stability /Berglund 2008/. Within the currently ongoing SFR investigation programme, 482 fractures were re-mapped in NBT, although it was found too difficult to make the distinction between Open and Sealed fractures /Berglund 2008/.

Fracture size has been evaluated from outcrop data for the nearby Forsmark Site, suggesting a larger r_{min} /Fox et al. 2007/. The distinction between Open and Sealed fractures is also difficult to make in outcrops. Furthermore, outcrop data provide very local and shallow information that may be unrepresentative of the general deep rock, i.e. with consideration to spatial heterogeneity, shallow geologic and chemical processes. Consequently, it was decided not to use trace data for the estimation of size. Instead, two different approaches are considered to estimate fracture size scaling exponent, k_r, the connectivity analysis or the Tectonic continuum.

Connectivity analysis

One method to estimate the size distribution is to perform Connectivity analyses /Follin et al. 2005/ that is based on the difference in intensity between mapped Open fractures and measured PFL-f data (see Sections 2.2.11 and 2.3). At shallow depth about 10% of the Open and Partly open fractures are registered as flowing fractures (i.e. coupled to PFL-f data), while at greater depth this ratio is about 1%. In the connectivity analysis this is inferred as a difference in connectivity to constant hydraulic boundaries. For example, the higher connectivity in the shallow bedrock is explained by larger fractures that interconnect to, either the Seafloor, or a deformation zone, while in deeper rock the poorer connectivity is due to shorter fractures that can only interconnect to deformation zones. Fractures are assumed to be power-law distributed, defined by its three-dimensional scaling exponent, k_r, and the minimum fracture radius, r_0. The minimum fracture radius is assumed equal to borehole radius 0.038 m, based on the approach taken by /Follin et al. 2005/. The maximum radius for stochastic fractures was set to 169 m, which corresponds to a side-length (of a square fracture) of 300 m, which was the general cut-off trace length for deterministically modelled deformation zones within the SFR local domain /Curtis et al. 2009/. The scaling exponent k_r is determined by calibration to intensity of Connected fractures (Section 2.3.2). Analyses of k_r for Open fractures in Site Investigation Forsmark rendered a range from 2.38 to 3.4 /Follin et al. 2007b/, including all fracture domains. For all fracture domains, k_r was found to be higher than 3.0 for the sets EW and NW, while it was lower than 3.0 for the other sets. The horizontal sets had the lowest k_r. The SFR domain is not expected to exhibit the same characteristics as the tectonic lens of Forsmark. However, both domains have a common tectonic history, in terms of stress regime, loading/unloading cycles, and rock types. There are also similarities in geologic setting; both sites are enclosed by ductile WNW-striking deformation zones (i.e. Eckarfjärden and Singö deformation zones, respectively, ZFMWNW805, formerly known as zone 8). The a priori assumption is that k_r for the SFR domain will fall in a similar range as found in Forsmark.

Tectonic continuum

The calibration of k_r proves to be difficult for the vertical sets (Section 3.4). Therefore, an alternative approach is also considered (see Appendix J.3), where the assumption of Tectonic Continuum is used to fit k_r between the two reference points: borehole radius and a cut-off radius of deterministically modelled deformation zones. If $P_{32,\,HCD}$ is the deformation zone intensity at a cut-off radius of r_{HCD}, then eq. (2-2) can be used to estimate the exponent k_r by setting $P_{32,\,Open+HCD} = P_{32}\,[r_0, r_{max}]$ and $P_{32,\,HCD} = P_{32}\,[r_{HCD}, r_{max}]$. Here, $r_0 = 0.038$ m and r_{max} is a large reference size (e.g. 10^{25} m). This concept is also illustrated in Figure J-8, Appendix J.3.

It was decided to calculate $P_{32,\,HCD}$ as the intensity of zones inside the regional SFR domain, with a lineament length exceeding 1,000 m (i.e. a cut-off radius of 564 m). In these calculations, the regional SFR domain was chosen in preference of the local SFR domain for two reasons:

1) it covers the full vertical extent of the SFR hydrogeological domain down to –1,100 m RHB70, while the local SFR domain extends only down to –300 m RHB70, and
2) the deformation zones are clipped against the regional domain boundaries, which is a necessity for its P_{32} calculations (i.e. the deformation zones inside the local SFR domain does not terminate against its domain boundaries).

Tectonic Continuum is a convenient, widely used, modelling hypothesis to interpolate unavailable intermediate-scale data. However, there exists little evidence that borehole-scale fractures should follow the same size pattern as kilometre-scale deformation zones. It is therefore difficult to conclude if the Tectonic Continuum-based approach should be more realistic than the calibration method; the purpose is to demonstrate that different conceptual approaches provide alternative possible solutions.

2.2.11 Intensity of Connected Open Fractures, $P_{32,\,COF}$

The fracture network modelled in the hydro-DFN consists of Connected Open Fractures (COF). Isolated fractures are excluded from the hydro-DFN, as they do not contribute to flow (which

becomes important in the later translation into ECPM). Furthermore, isolated fractures must be excluded from the model, as PFL-f data only reflects Connected Open Fractures. The COF is a subset of all Open and Partly open fractures that, unfortunately, cannot be fully measured in the field. Fractures mapped in Boremap include isolated fractures, while on the other hand, PFL-f data are censored by the detection limit (Figure 2-4). To be more precise, a PFL-f record reflects a borehole section with inflow above detection limit; and may thus reflect the total inflow of several intercepted fractures. In this study this fact was not considered, but its implications on the calibration process are discussed in Appendix G.1. Thus, the intensity of Connected Open Fractures is therefore unknown, but it is known to be bounded by $P_{32,\,Open}$ and $P_{32,\,PFL}$, according to eq. (2-6) (after /Follin et al. 2007b/).

$$P_{32,\,All} \geq P_{32,\,Open} \geq P_{32,\,COF} \geq P_{32,\,PFL} \qquad (2\text{-}6)$$

Calibration target for $P_{32,\,COF}$

The lack of a well-defined conditioning target, $P_{32,\,COF}$, in combination with the unknown size distribution parameter, k_r, implies a major source of uncertainty in the hydro-DFN. The bounds established in eq. (2-6) renders an ensemble of non-unique solutions of different combinations of $P_{32,\,COF}$ and k_r. In theory, this ensemble of possible solutions could perhaps be evaluated by inverse modelling, and the range of estimated parameter values would then demonstrate the uncertainty in the estimation of $P_{32,\,COF}$ and k_r. However, such a rigorous analysis would be time consuming to perform and its benefit is considered to be relatively small, as the equifinality of $P_{32,\,COF}$ and k_r is already known to be large. This hydro-DFN is based on the methodology developed during Site Investigation Forsmark /Follin et al. 2005, 2007b/ for the purpose of practical implementation in downstream modelling. The model requisites are that its parameterisation should be realistic, with respect to current understanding of the SFR/Site Investigation Forsmark domains, and that it honours borehole data.

Different methods to estimate a reasonable calibration target for $P_{32,\,COF}$ are explored in Appendix F. As a tentative calibration target it was decided that $P_{32,\,COF}$ shall exceed $P_{32,\,PFL}$ by a factor ranging from 2 to 4.

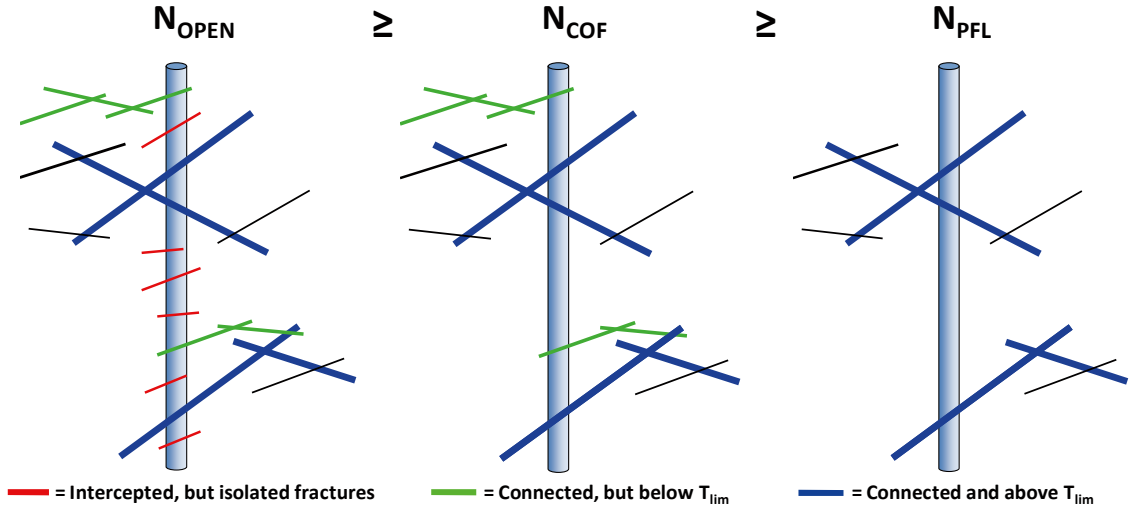

Figure 2-4. *Illustration of the relation between the number of Open and Partly open fractures mapped in a borehole, N_{OPEN}, the number of Connected Open Fractures, N_{COF}, and the number of fractures included in the PFL-f data, N_{PFL}. Modified after /Follin et al. 2007b/.*

2.3 DFN simulations

The Connected fracture network is calibrated by means of connectivity analyses of DFN realisations and simulated borehole exploration using a vertical scan-line (Figure 2-5). The vertical extent of the total fracture generation domain is from +40 m down to –600 m RHB70, while extent of the simulated borehole is defined by the range of available data, from –10 m down to –525 m RHB70. The horizontal extent of the domain was 100 m, which is defined by the typical distance between vertical deformation zones in the SFR local domain. In other words, the deformation zones are considered to act as hydraulic boundaries.

This is a highly idealised representation of reality, in order to simplify the model setup. A more realistic model setup, honouring both borehole orientation and deformation zone geometry would probably improve reproducing the spatial patterns in PFL-f data. The horizontal extent of fracture generation domain was also set equal to the typical separation distance between zones. The centre point of fractures is generated within the defined volume and hence there is an underestimation of fracture intensity close to the boundaries. The smaller the fracture, the smaller the effect is. For the purposes of the current study, the implication of this error has not been evaluated, but it is assumed to be of minor significance in relation to other simplifications made (e.g. borehole orientation and true deformation zone geometry). However, the model domain setup should be improved considerably in the hydrogeological model SFR v. 1.0 (Table 5-1).

Based on analysis of depth dependency in fracture data (Section 3.3.2), the fracture generation domain is subdivided into three depth domains, with different parameterizations in each domain.

2.3.1 Fracture generation

Small fractures (i.e. close to borehole radius) are only considered to be important for the connectivity analysis if they are located in the vicinity of the sampling borehole. Owing to power-law relations, the number of fractures grows extensively with small radii and therefore small fractures are computationally demanding to generate for large volumes and multiple realisations. Therefore, the smallest fractures are only included in the fracture generation process at the distances from the sampling

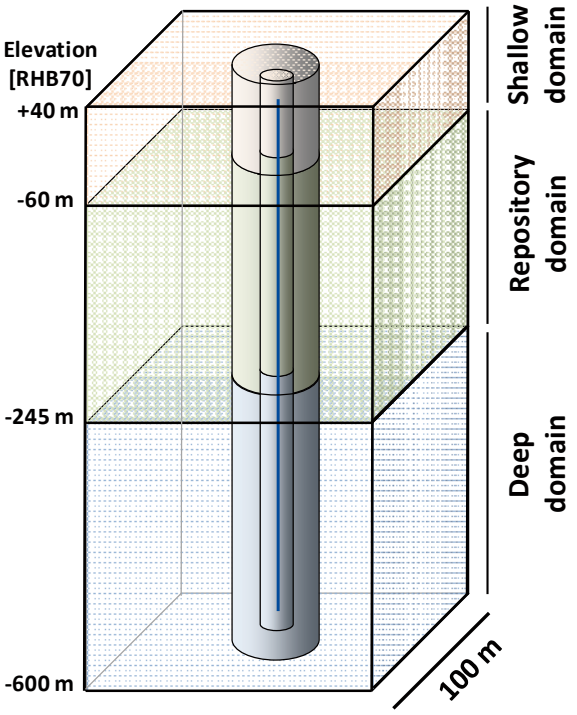

Figure 2-5. *DFN calibration model setup divided into three depth domains. Computational demand is reduced by use of fracture generation volumes (cylinders), which includes small fractures only in the vicinity of the sampling scan-line (blue).*

borehole where their contribution to the connectivity analysis is assumed relevant. This was accomplished by subdividing the fracture generation into three volumes (Table 2-3). Fracture radii in the range between 2.62 m and 169 m were generated over the entire domain. A fraction of smaller fractures (0.564 m < r < 2.26 m) were superimposed within an outer cylinder, which was defined by a 2.83 m radius around the sampling scanline (true borehole radius neglected). The smallest fraction of fractures (0.038 m < r < 0.564 m) were only generated inside an inner cylinder, defined by a 1.42 m radius around the sampling scanline. In other words, the entire size distribution, ranging from 0.038 m to 169 m, is represented in the vicinity of the borehole. Note that the smallest fractures are likely to have an insignificant role for connectivity at the larger scale. However, at borehole scale they have the important conceptual role in explaining the ratio between mapped Open fractures and PFL-f data. The fracture generation cylinders were also divided with respect to depth domains, resulting in a total of 3×3 = 9 fracture generation volumes. The maximum fracture radius for stochastic fractures was set to 169 m, which corresponds to the minimum size of deterministic deformation zones (side length, L = 300 m). That is, the threshold between stochastic and deterministic features is assumed to be a radius of 169 m. It should be noted that if the characteristic horizontal distance between vertical deformation zones is 100 m, horizontal fractures with a radii larger than 50 m can short-circuit flow between zones (particularly since transmissivity is assumed correlated to size).

Table 2-3. Fracture sizes generated depending on distance from sampling borehole.

Fracture generation volume	Radial distance from borehole (m)	Minimum radius (m)	Maximum radius (m)
Inner cylinder	1.42	0.038	0.564
Outer cylinder	2.83	0.564	2.26
Entire horizontal extent	–	2.26	169

2.3.2 Simulated exploration and calibration of size scaling exponent, k_r

Two methods are considered for defining set-wise k_r of each depth-domain. The first method is to calibrate k_r according to an iterative trial-and-error scheme, listed below, with the objective to match the criterion set up in Section 2.2.11. The alternative method is to define k_r for vertical sets based on the assumption of Tectonic Continuum. In this latter case k_r is defined by data, which only requires Steps 1–4 to be executed once.

1) Realisations of Open fractures are generated, as described above (50 or 100 realisations)
   – Known set-wise parameters: $P_{32,\,Open}$, mean pole, Fisher κ, calculated from data
   – Fitted parameters: set-wise k_r (allowed to range from 2.5 to 3.45, Section 2.2.10)
2) Borehole exploration simulated by vertical scanline
   – Intensity of Open fractures, $P_{10,\,Open}$ and $P_{32,\,Open}$, verified versus data
3) Isolated fractures, unconnected to the hydraulic bounds (vertical sides in Figure 2-5) are removed
4) Simulated borehole exploration is repeated for Connected Open Fractures
   – Intensity of Connected Open Fractures, $P_{10,\,COF}$ and $P_{32,\,COF}$, are related to PFL-f data
5) Based on the ratio between $P_{32,\,COF}$ and $P_{32,\,PFL}$, the set-wise k_r are updated for each depth domain and steps 1–4 are iterated until the calibration criteria are met (i.e. the ratio between $P_{32,\,COF}$ and $P_{32,\,PFL}$ should be in the range 2 to 4).

The three-dimensional intensities $P_{32,\,Open}$ and $P_{32,\,COF}$ are estimated by Terzaghi-weighting (Section 2.2.7). It should be noted that the variability in $P_{32,\,COF}$ is large between realisations, and that therefore a better estimate of k_r could have been achieved by increasing the number of realisations. It should also be noted that the connectivity analysis is a multi-dimensional problem: the connectivity of one fracture set depends on the connectivity of the other fracture sets. In other words, the parameter adjustment of one fracture set affects the connectivity of all other sets and therefore the connectivity analysis must be made simultaneously for all sets.

2.3.3 Relation between transmissivity and size

Transmissivity is assumed to be correlated to fracture radius (Section 2.2.9). The correlation between transmissivity and radius is defined by empirical exponential relations, by determining the coefficients *a* and *b* in eq. (2-4). Here, *a* is the transmissivity of a fracture with 1.0 m radius, while *b* is the exponent by which transmissivity scales with radius. These transmissivity-radius relations are determined per set and per depth domain.

The following approach was used to establish an empirical relation between transmissivity and radius for a given fracture set and a given depth domain:

1) The size distribution of Connected fractures that are intercepted by the simulated borehole was plotted as an experimental complementary cumulative distribution of fracture intensity for a large number of realisations (Figure 2-6a)
2) The transmissivity distribution of PFL-f data above T_{lim} was likewise plotted in an experimental complementary cumulative distribution of fracture intensity (Figure 2-6b).
3) The Connected fracture intensity is expected to exceed the intensity of PFL-f data above T_{lim} by a factor of 2–4 (Appendix F). This fraction of $P_{32, COF}$ exceeding $P_{32, PFL}$ is assumed to reflect transmissivity below T_{lim}. Consequently, the highest percentile of the PFL-f data above T_{lim} will be equal to $([P_{32, COF}–P_{32, PFL}]/P_{32, COF})$, as shown by purple line in Figure 2-6.
4) Under the assumption of a 1:1 correlation between transmissivity and fracture radius distributions, the PFL-f data can be linked to simulated Connected fractures, by matching the two CCDFs, percentile-by-percentile. Each PFL-f record can then be associated to a fracture radius, and vice-versa, each simulated Connected fracture can be associated to a transmissivity value (cf. Figure 2-6a and b).
5) Finally, an empirical relation can be evaluated between PFL-f transmissivity and its percentile-matched fracture radius, either by means of least root-mean-square, or by a visual fit (e.g. $a = 2.06\times10^{-9}$ m²/s and $b = 1.85$, in Figure 2-6b)

It should be noted that the upper tail of the simulated Connected fractures extends further (to lower percentiles) than the PFL-f data set. The reason for this is that simulations represent several realisations (i.e. a larger data population).

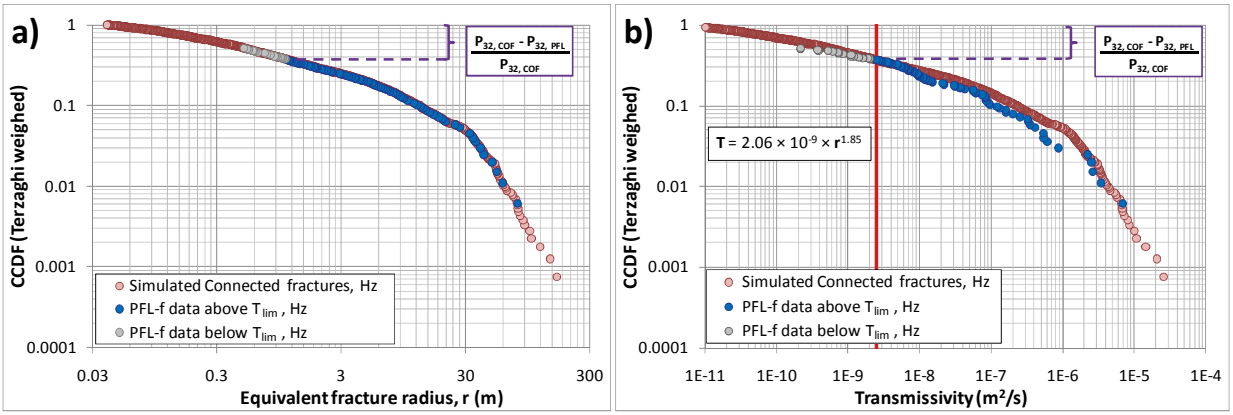

Figure 2-6. *Example of simulated Connected fractures matched by percentiles to PFL-f data in terms of complementary cumulative fracture intensity; a) assigning fracture radius to PFL-f data from the simulated size distribution, and b) assigning transmissivity to the simulated Connected fracture network using an empirical relation.*

3 Results

3.1 Visual inspection of data

3.1.1 Borehole orientation bias

In order to minimize effects of sampling bias in borehole data for vertical fractures, the boreholes have been drilled with different bearings and an inclination generally in the range 50° to 60° (Figure 3-1). The two exceptions are the almost vertical KFR27, and the sub-horizontal, underground KFR105. All intensity calculations in this report are Terzaghi compensated (Section 2.2.7) to further reduce artefacts of sampling bias. Terzaghi compensation reduces the geometrical bias, but it cannot be completely eliminated. The Terzaghi-compensated orientation distribution of Open fractures in KFR105 (inside HRD and visible in BIPS) is compared to the data from the other boreholes within the same elevation interval (Figure 3-1). Note that the two samples compared are of similar size. Suggested fracture clusters are shown by grey, respectively, pink lines as reference (see Section 3.1.2). The great circle to KFR105 shows the blind region, where fracture planes are parallel to the borehole (Figure 3-1a). The Terzaghi weight is equal to infinity, or equal to the maximum allowed value along this great circle, although the probability of detecting a fracture parallel to the borehole is exceptionally small. The combined data set (Figure 3-1b) is less exposed to sampling bias, as the different borehole orientations cover up the blind sampling regions. As can be seen in Figure 3-1, the horizontal fractures appears underrepresented in KFR105, in comparison to the combined data set. It can also be noted that the NW-striking sub-vertical fractures seem underrepresented in the combined data set. It must therefore be kept in mind that full agreement between KFR105 and the combined data set cannot be expected due to lateral heterogeneity.

3.1.2 Orientation of Open fractures

The orientation of Open and Partly open fractures and PFL-f data (i.e. features coupled to detected flow) are analysed in terms of Kamb cluster analysis (Figure 3-2). Kamb contours are the result of a statistical test on cluster significance and useful for identification of potential fracture sets. Visual inspection suggests four sets of Open and Partly open fractures (Table 3-1). Three sets are sub-vertical and referred to by their strike: EW, NW, and NE. The fourth set is sub-horizontal, and referred to as Hz. The PFL-f data are clearly dominated by the horizontal set and a subordinate NW set (Figure 3-2), although there is no evidence of the EW and NE sets. However, it should be noted that the Kamb analysis reflects the sum of Terzaghi weights (i.e. it is not weighted by transmissivity).

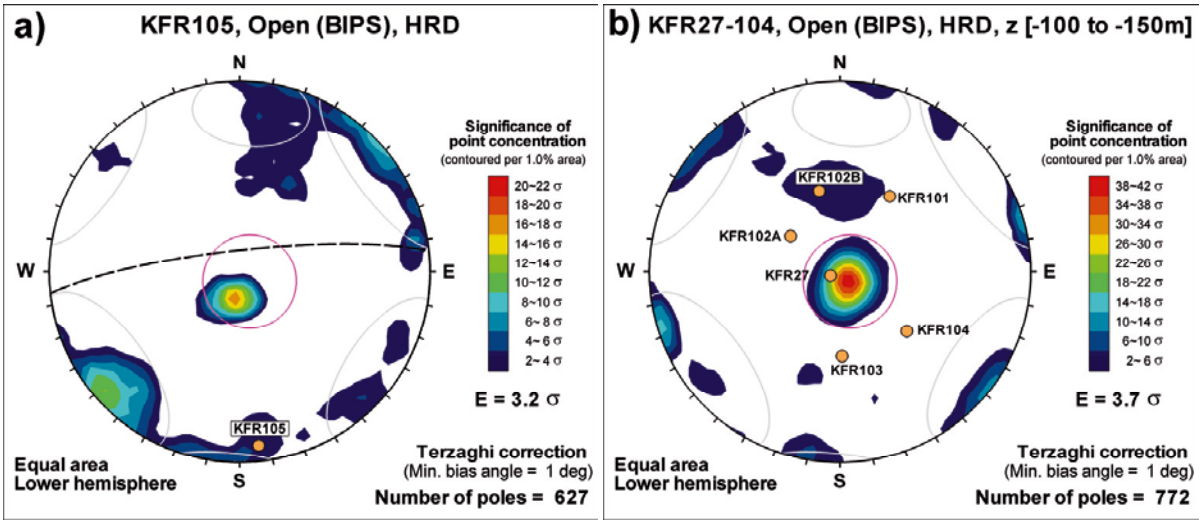

Figure 3-1. *Evaluation of sampling bias a) KFR105 compared to b) other core data within the same elevation range. Kamb-contoured orientation of Open and Partly open fractures in HRD, visible in BIPS. The fracture set hard sectors (Figure 3-2) and the blind great circle to KFR105 are shown for reference.*

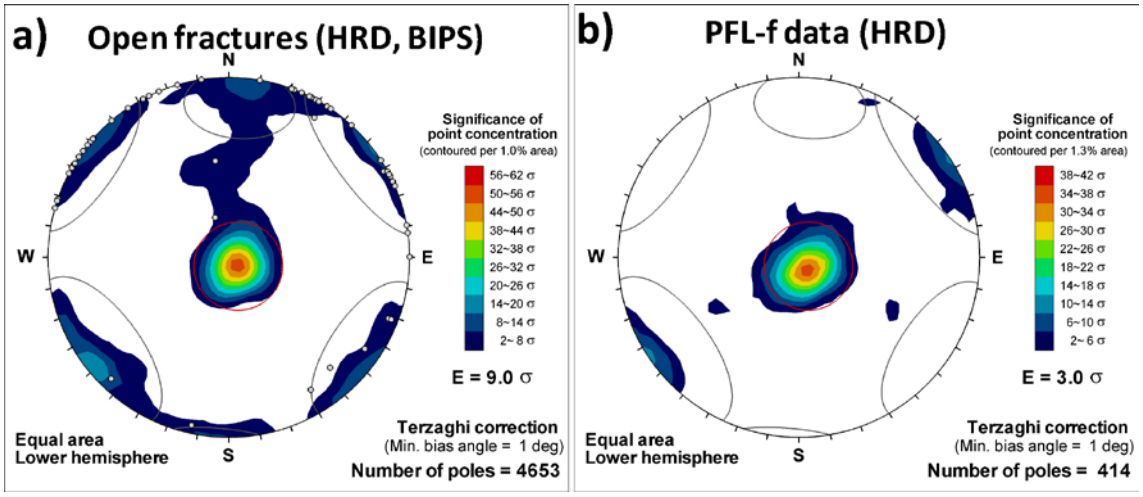

Figure 3-2. *Kamb-contoured orientation of Open and Partly open fractures in KFR101–105, KFR27 (HRD); a) Open and Partly open fractures visible in BIPS and b) PFL-f data. The deformation zones of the regional SFR domain /Curtis et al. 2009/ are shown as poles and suggested fracture set hard sectors are shown as circles (grey lines are sub-vertical sets EW, NE, and NW, and red line for the sub-horizontal set).*

A closer analysis of hydraulic data indicates deviating transmissivity in the dip range 40° to 50°, suggesting the possible presence of a fifth wide-spread Gently dipping set (see Sections 3.1.5 and 3.2.2). These fracture sets were approximated by hard sectors that will be used as initial estimations in the orientation model (Section 3.2). The hard sectors are also used for visual reference in the presentation of Open fracture orientation (grey and red lines in Figure 3-2). The hard sectors shown reflect the final mean poles (Table 3-2), although for visualization purposes set Gd is omitted.

In several aspects the SFR data is different from findings from the nearby Site Investigation Forsmark, /Follin et al. 2007a–c/. The set Hz is more pronounced in SFR, both in terms of Open fractures and in PFL-f data. However, in this comparison it should be noted that the SFR data set covers shallower rock. In the Site Investigation Forsmark, the strongest sub-vertical set was NE, and particularly so for PFL-f data, while in the SFR data it is the weakest set. In fact, SFR has insignificant clusters of PFL-f data for both sets EW and NE. Furthermore, there is no evidence of the set NS that was identified in Forsmark. It is expected that the hydraulic anisotropy in SFR will be dominated by Hz and NW.

The borehole-to-borehole variability in orientation of Open and Partly open fractures in HRD is shown in Figure 3-3). The overall orientation pattern is that the sub-horizontal set shows little variability and tends to be the dominating set (note that KFR105 is a sub-horizontal borehole, Figure 3-3f), while the variability between boreholes is larger for the sub-vertical sets. Which of the sub-vertical sets is the strongest differs from borehole to borehole, and in most cases one or two of the sub-vertical sets is insignificant. It should be noted that the orientation data in Figure 3-3 have been sampled by different borehole orientations and over different elevation ranges. The Kamb contours are very useful for reflecting the orientation distribution of a data sample, but it is impractical for analysing vertical trends and variation intensity. A more thorough analysis of lateral and vertical variability of fracture set intensity is shown in Section 3.3, however, it depends on fracture set assignment and therefore it must first be established if a global orientation model is applicable.

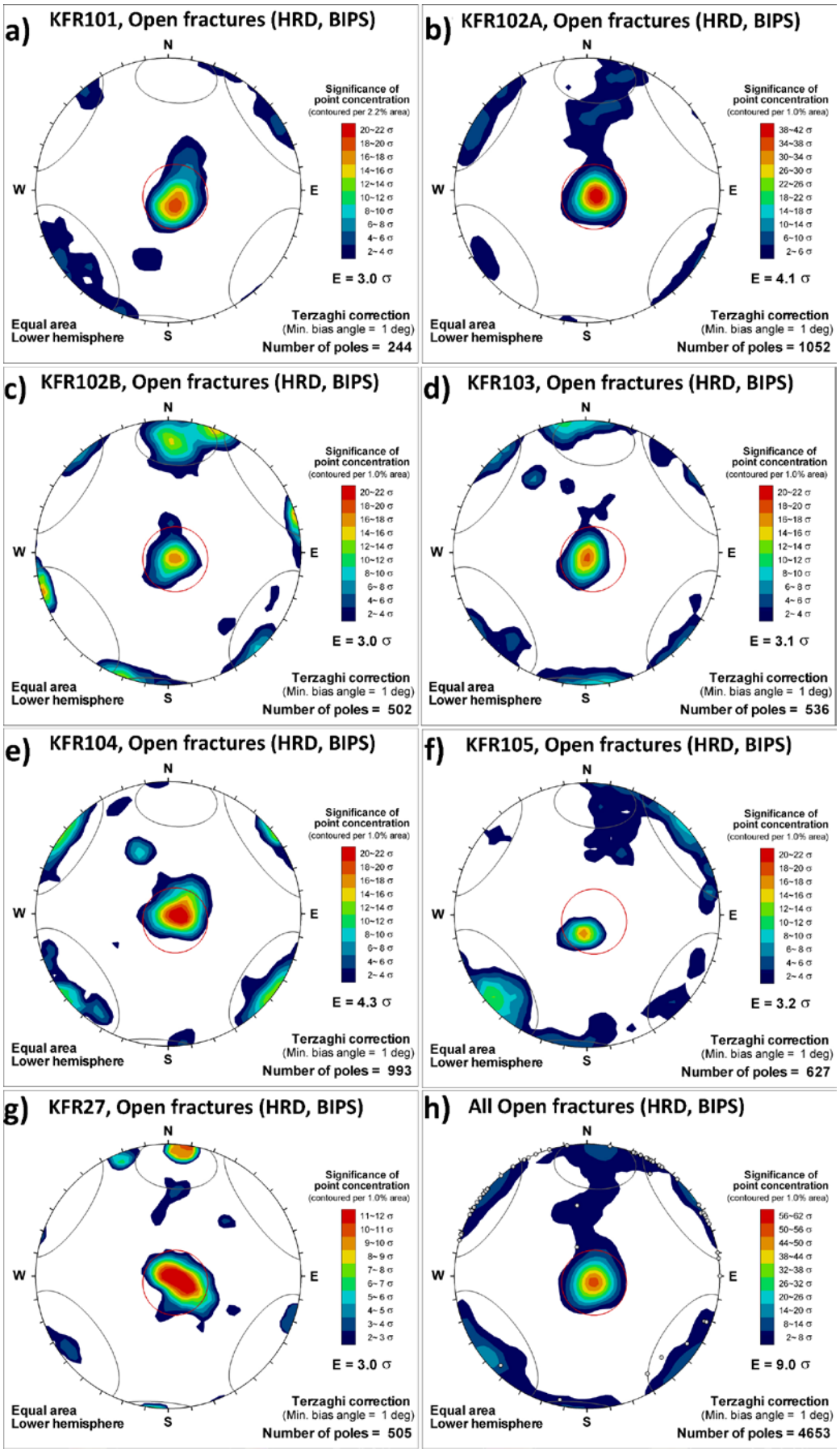

Figure 3-3. *Kamb-contoured orientation of Open and Partly open fractures in KFR101–105, KFR27 (excluding upper part with core missing). The fracture set hard sectors (Figure 3-2) shown for reference.*

3.1.3 Lateral trend in orientation of Open fractures

The largest contrast in orientation pattern of Open fractures is found if the borehole data are divided into two groups: a South-western group with KFR104, KFR105, and a North-eastern group with KFR101–103 and KFR27 (cf. Figure 1-1 and Figure 3-4). The North-eastern group is dominated by set Hz and seems connected to the set EW, which is also strong. In comparison, the sets Hz and EW are weaker in the South-western boreholes, while the sets NW and NE are stronger. A resemblance in orientation pattern can be noted between the South-western boreholes and KFM11A (i.e. domination by Hz and NW). In fact, the orientation pattern of Open fractures and PFL-f data changes with borehole length in KFR105, from a Hz domination at the beginning of the borehole to a NW/EW domination further down the borehole. One may speculate if the South-western boreholes may be influenced by WNW-oriented lineaments (Figure 1-1).

3.1.4 Vertical trends in orientation and intensity of Open fractures

Spatial trends in orientation and intensity are most conveniently analysed based on set-divided data. However, prior to the definition of an orientation model, histograms are useful for examining possible trends by visual inspection. The borehole data was therefore binned by strike, dip and elevation and examined in terms of trends in fracture intensity (Appendix I).

In summary, the observed orientation characteristics in Figure 3-2, which is dominated by Hz and NW, appear to be relatively constant with depth, particularly within the elevation range –80 to –350 m RHB70. At shallower depths 0 to –60 m RHB70 the sub-vertical sets are instead dominated by set EW, mainly based on data from KFR102B and KFR103 (drilled in different orientations from the same starting location; Figure 1-1). Data are also scarce for depths below –350 m (only available from KFR102A and KFR27), although it seems that set NE dominates over Hz at greater depths. Figure I-1 and Figure I-2 do not only show the variability in intensity of fracture orientations with depth and between boreholes, but also illustrates the discontinuity in data after the removal of PDZ. This fact complicates the inference of observed deviating fracture patterns. However, at this modelling stage, the general impression is that the suggested fracture sets can be assumed global for application to the entire data set. If the orientation model is assumed to be global, the observed variability must be interpreted as heterogeneity in fracture set intensity (in contrast to a locally rotated orientation model). Note that excluded data in the vicinity of the Singö deformation zone has different characteristics (Appendix B).

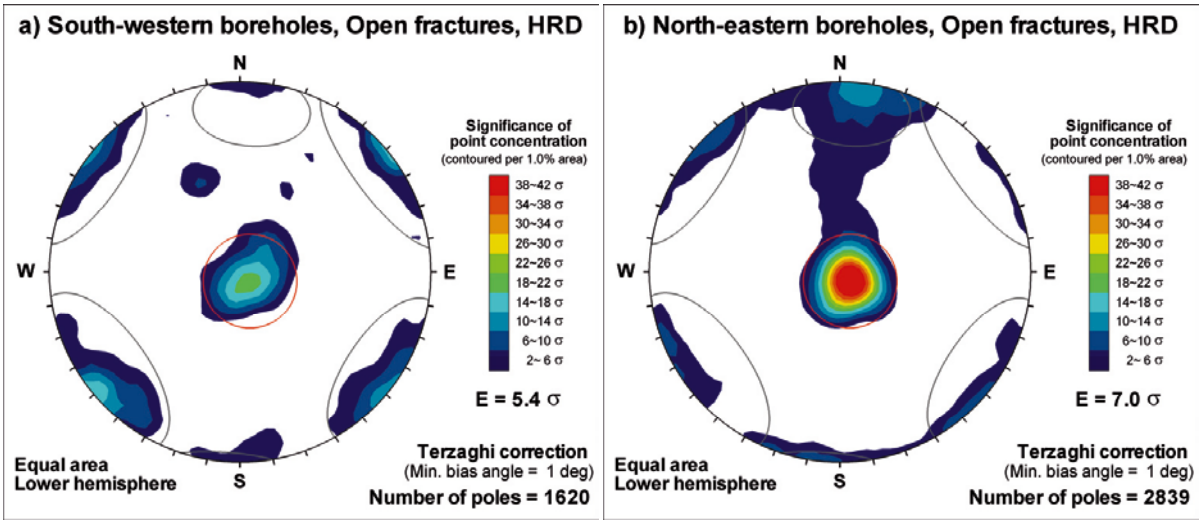

Figure 3-4. *Kamb-contoured orientations of Open fractures in HRD visible in BIPS; a) South-western boreholes KFR104 and KFR105 compared to North-eastern boreholes KFR101-KFR103, and cored part of KFR27. For reference, the fracture set hard sectors identified in the SFR data set (Figure 3-2) are shown as circles.*

3.1.5 Orientation of PFL-f data

Visual inspection suggests a dependency between PFL-f data in HRD and dip (Figure 3-5; note also its dependency to depth, Figure 3-9). In terms of relative frequency of PFL-f data as a function of dip, there appears to be two modes: one sub-horizontal (dip = 15°) and one at dip = 85°, which reflects the three sub-vertical sets, EW, NE, and NW. The highest transmissivity (> 10^{-6} m^2/s) is constrained to sub-horizontal fractures, dip < 30°. High transmissivity (between 10^{-6} and 10^{-8} m^2/s) do exist for all orientations, but in terms of relative frequency, only the steepest fractures (dip > 60°) are dominated by transmissivity lower than 10^{-8} m^2/s. This anisotropic hydraulic pattern, with high horizontal transmissivity relative to the sub-vertical transmissivity, is similar to findings made during the Site Investigation Forsmark. This finding is in line with prior expectations, and it also seems compatible with the tentative fracture sets for Open fractures (Figure 3-2).

However, a closer inspection of Figure 3-5b suggests a possible third mode in the dip range between 40° and 50°, which is dominated by an approximate transmissivity of 10^{-7} m^2/s. This subpopulation appears to be detached from both the sub-horizontal and the sub-vertical data populations (Figure 3-5b). It also seems fairly symmetrically distributed in strike, although its centre is somewhat concentrated towards a trend of 320° (green poles dipping 40° to 50° in Figure 3-6a). This subpopulation is largely insignificant in the Kamb cluster analysis of pole concentration (Figure 3-2b), in comparison to the Open fractures dipping 40° to 50°, which has a significant cluster mode at a trend of 350° (Figure 3-2a). However, it should be pointed out that transmissivity was not considered in the Kamb analysis.

The objective of the hydro-DFN is to reproduce the hydraulic observed hydraulic characteristics of data in a realistic way. This requires that the transmissivity distribution within a fracture set represents a homogeneous, randomly distributed, population. This implies that the orientation model set up (i.e. definition of fracture sets) cannot be based on geometry alone, but must also reflect any deviating transmissivity characteristics. Now, with only one exception, the PFL-f transmissivity inside the hard sectors of sets EW and NE, as defined from Open fractures, is low (< 10^{-8} m^2/s, Figure 3-6a). It would seem reasonable that the low transmissivity in the vicinity of the cluster centre is representative of the fracture set. It would therefore be inappropriate to include the higher transmissivity in the dip range 40° to 50° to sets EW and NE. Likewise, the sub-horizontal set cannot be extended up to a dip of 50°, as both its intensity and transmissivity seems constrained to a dip of approximately 30°.

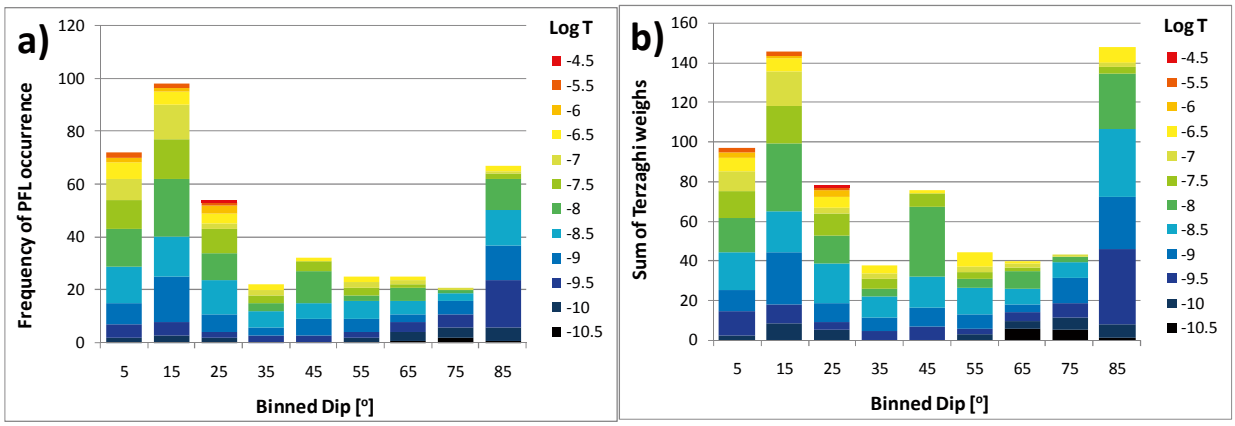

Figure 3-5. *PFL-f transmissivity data in HRD binned by dip; a) frequency of occurrence, and b) Terzaghi-weighted frequency of occurrence. The legend of the transmissivity colour scale is labelled by the mid-value of each bin, e.g. the mid-value –6.5 represents the interval of logarithmic transmissivity between –6.25 and –6.75.*

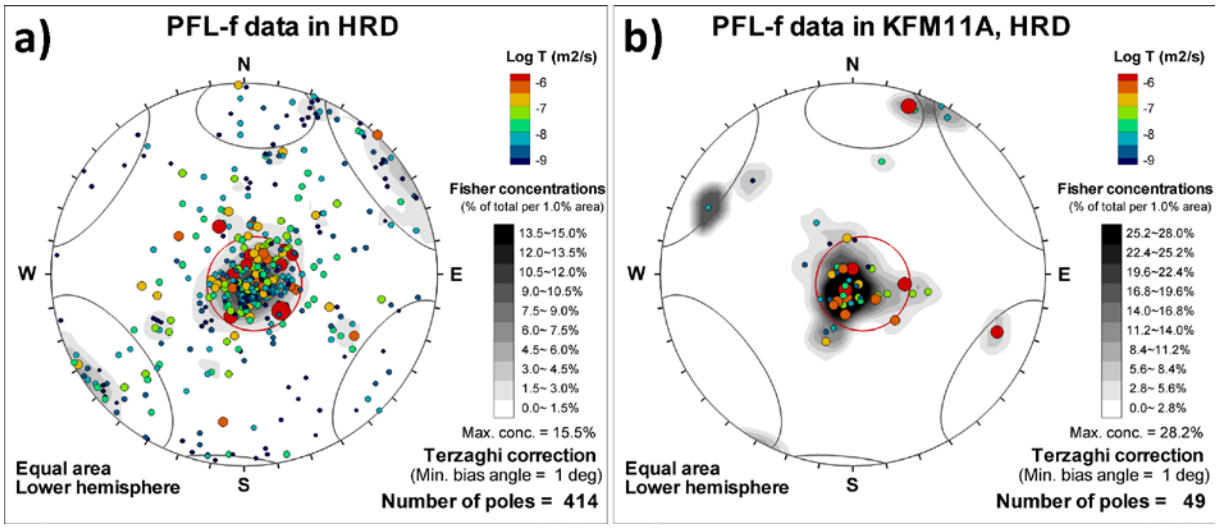

Figure 3-6. *Fisher-contoured orientation of PFL-f data in HRD and transmissivity-scaled poles; a) KFR101–105 and KFR27 and b) KFM11A. For reference, the fracture set hard sectors identified in the SFR data set (Figure 3-2) are shown as circles.*

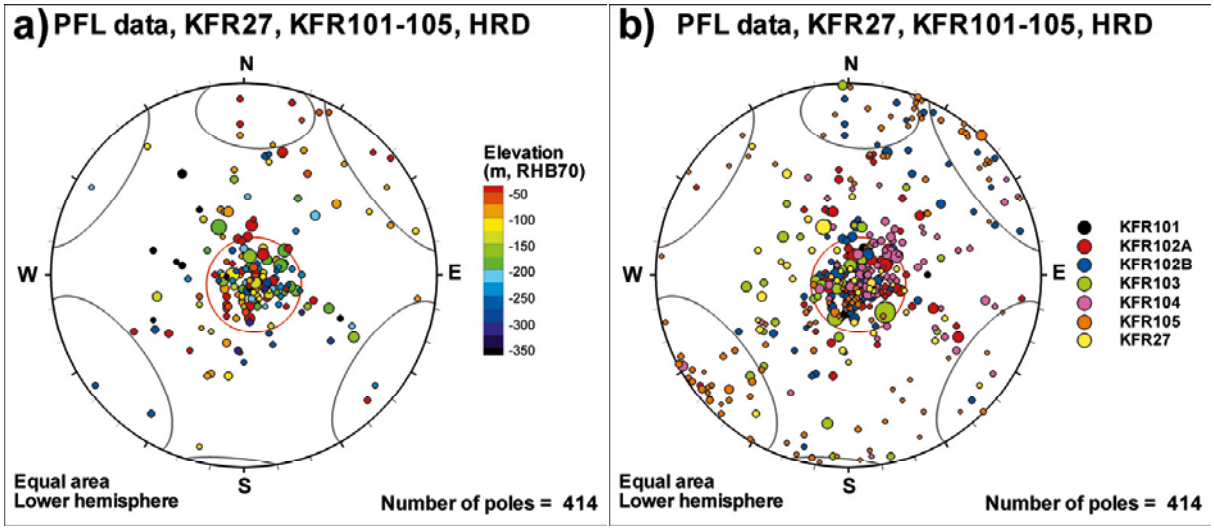

Figure 3-7. *PFL-f data orientation in HRD KFR101–105 and KFR27; a) coloured by elevation and b) coloured by borehole. The size of poles is scaled by transmissivity. For reference, the fracture set hard sectors identified in the SFR data set (Figure 3-2) are shown as circles.*

The observations made therefore suggest the inclusion of a fifth, Gently dipping set. This Gently dipping set should be defined so as to dominate in the dip range 40° to 50°, and such that its transmissivity distribution is homogenous (i.e. independent of dip). The Gently dipping set will completely overlap the horizontal set, but also partially overlap the subvertical sets (see Figure 3-15). The geometric definition of the Gently dipping set is described in Section 3.2.2, while its transmissivity-based definition is described in Appendix E.

3.1.6 Transmissivity and intensity patterns in PFL-f data

The transmissivity and intensity patterns of PFL-f data were examined by visual inspection of histograms, binned by transmissivity and by elevation (Figure 3-8). After the exclusion of possible deformation zones, the information from KFR101 is limited, but indicates a low transmissivity with few large transmissivity values. The intensity and transmissivity in KFR102A is relatively high down to an elevation of –250 m RHB70, after which it drops drastically. There are particularly high transmissivity values within the range –170 to –190 m RHB70 (see Section 3.1.7). KFR102B has

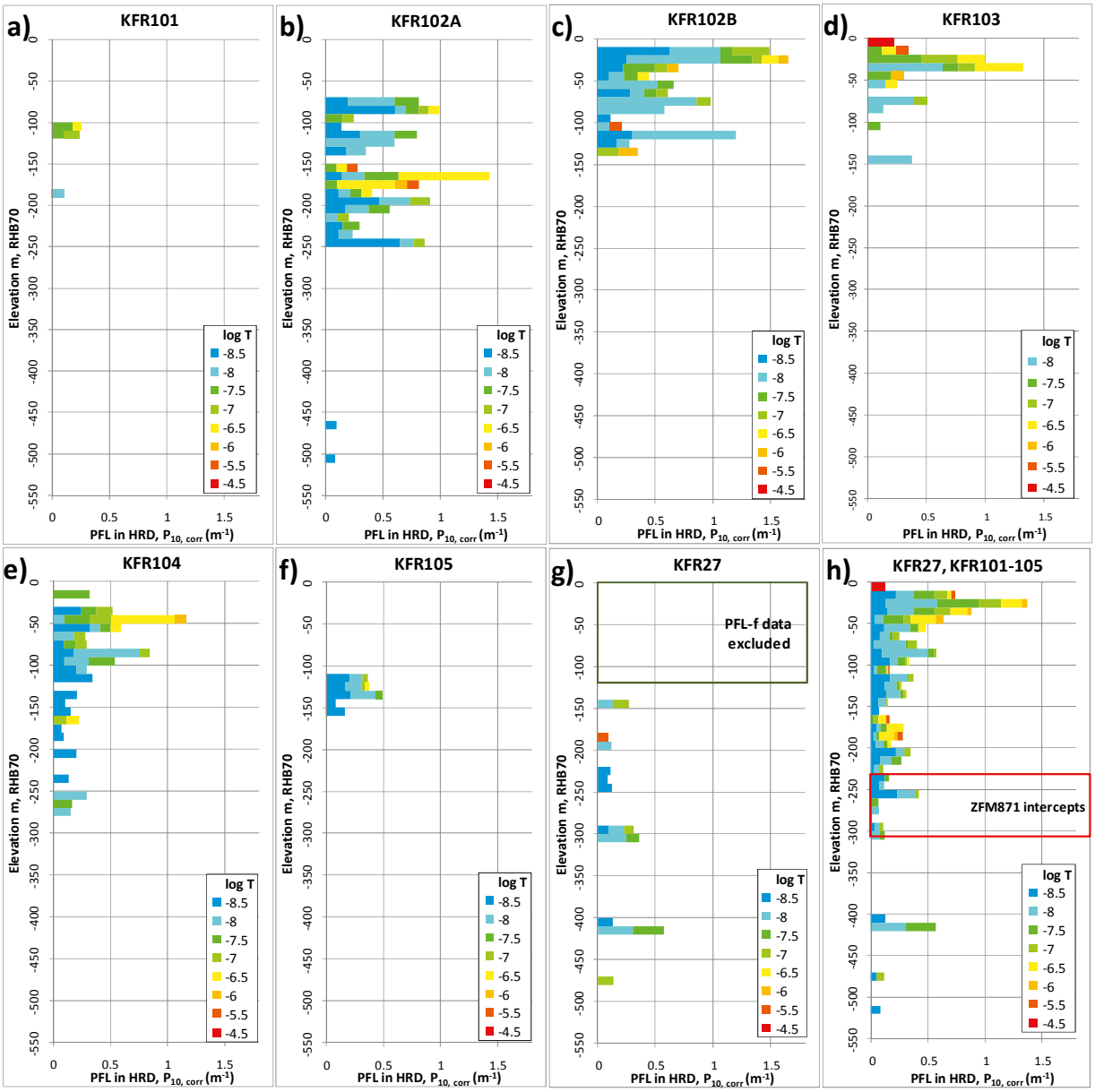

Figure 3-8. *PFL-f intensity ($T > T_{lim}$) in HRD binned by transmissivity and elevation, shown for boreholes KFR101–105 and KFR27. The PFL-f data are unavailable/excluded in the upper part of KFR27 (see Appendix C; also excluded in h). Grey area indicates elevation bins outside the HRD (i.e. either classed as possible deformation zone, according to SHI, or beyond the borehole extent.*

a high intensity in PFL-f data, dominated by transmissivity around 10^{-8} m²/s, which decreases at the borehole end at an elevation of –140 m RHB70. KFR103 has higher shallow transmissivity, but shows a stronger decline with depth. KFR104 has a continuous decrease in both transmissivity and intensity down to –350 m RHB70. The sub-horizontal borehole KFR105 provides little information on the variation with depth, but has an average intensity and transmissivity (relative to other boreholes). KFR27 has an overall low intensity, but relatively large transmissivity at depth (Figure 3-8g).

In summary, both intensity and transmissivity is high within the elevation range 0 to –60 m RHB70 (Figure 3-8c–e). This is consistent with the observations made in the hydraulic data available prior to the initiation of Site Investigation programme for the extension of SFR /Öhman and Follin 2010/. The elevation range –60 to –200 m RHB70 has a considerably lower intensity of PFL-f data (Figure 3-8h). However, the pattern is relatively scattered, with high intensity and transmissivity in KFR102A and KFR102B, relatively to KFR101, KFR103 and KFR27. In KFR102A the PFL-f intensity is above average in the elevation range –150 to –250 m RHB70. Exceptional high transmis-

sivity is observed in KFR102A and KFR27 at elevations –160 to –190 m (see Section 3.1.7). Below –250 m RHB70, data are only available from KFR102A, KFR104, and KFR27. At these depths, the intensity is generally low, but the few, scattered, PFL-f records can have high transmissivity (e.g. 10^{-7} m^2/s in KFR104 and KFR27, even as deep as –470 m RHB70). Possibly, the observed break in PFL-f intensity at –250 m RHB70 can be associated to the intercepts of ZFM871, as modelled in the SFR Geological model v.0.1 (Figure 3-8h).

3.1.7 Possible PFL-f outliers

In absence of an updated Geological model, the HRD in this study is tentatively defined as outside possible deformation zones, according to the SHI. The definitions in SHI are not definitive, which implies uncertainty in the HRD classification of data. Therefore the PFL-f data set was screened for high transmissivity data that possibly should belong to the HCD, as the inclusion of HCD data risks overestimating the transmissivity parameterisation in the DFN. It is well-known that transmissivity generally decreases with depth. In order to identify exceptionally high transmissivity, the general pattern of maximum transmissivity was estimated as a function of depth, based on visual inspection (Figure 3-9). This estimation was not based on the actual maximum transmissivity at each elevation, but on judgment with respect to the overall intensity pattern of PFL-f data with depth. Note that the PFL-f intensity of KFR105 appears high, since it is a sub-vertical borehole. It must also be taken into account that the decreasing core length at depth may exaggerate the appearance of the transmissivity depth trend (Section 2.2.2).

In the previous analysis of hydraulic data available prior to the initiation of the Site Investigation for extension of SFR /Öhman and Follin 2010/, the fitted depth trends in the elevation range 0 to –250 m RHB70 were very similar to Figure 3-9. The data in /Öhman and Follin 2010/ was better covered in terms of tested borehole length with elevation; however, it was centred on a different target volume (the existing SFR) and were of poorer quality.

Bearing this in mind, two possible anomalies are identified:

1) In the elevation range –170 to –190 m RHB70 there are three exceptionally high values in KFR102A and one in KFR27 (red oval in Figure 3-9). During the field investigations, hydraulic connections were detected, not only between KFR27 and KFR102A, but also to packed-off borehole sections associated to ZFM871 that were drilled during the construction of the existing SFR (Appendix D). The orientations of the PFL-f data within this interval are shown in Figure 3-10. PFL No. 38 has a dip of 55°; it is assigned to set NE (Section 3.2.2) and proves to have a particularly strong influence on its hydraulic parameterisation (Appendix J.2.1 and J.3.1). The intensity of Open fractures in KFR102A is larger than average within this interval; three Open fractures have an aperture > 1 mm and there is one crush zone (18 mm). In KFR27 the crush zone is 0.2 m (Figure 3-10b). It is speculated if these data belong to ZFM871, or to some other feature indirectly connected to ZFM871.
2) at –470 m RHB70 in KFR27 there is a single PFL-f record with transmissivity of 10^{-7} m^2/s (Figure 3-9). This PFL-f record is relatively close to the possible deformation zone 4 (See Appendix C). It has an aperture of 5 mm and a dip of 52° and is assigned to set EW (Section 3.2.2).

The general pattern is that high transmissivity data are horizontal or gently dipping (Figure 3-6). To some extent, this could be a sampling bias effect resulting from borehole orientation, or relate to the stress-regime which tends to open sub-horizontal fractures, and thereby increasing its mapped confidence (which is an important Boremap parameter considered during the manual coupling of PFL-f data to Boremap /Öhman et al. 2010/). However, with the exception of KFR105, there is a distinct domination of Hz/Gd fractures within the geometric coupling interval for PFL-f data (L_A ±0.2 m). It is therefore somewhat surprising that anomalously transmissive fractures dip more than 50°. It was decided to notify these observations to the Geologic modelling team, but to include these PFL-f data in the hydraulic parameterisation in the current modelling stage. PFL-f No. 38 in KFR102A has a strong influence on the hydraulic parameterisation of the DFN model, and therefore transmissivity relations are presented both with and without this record.

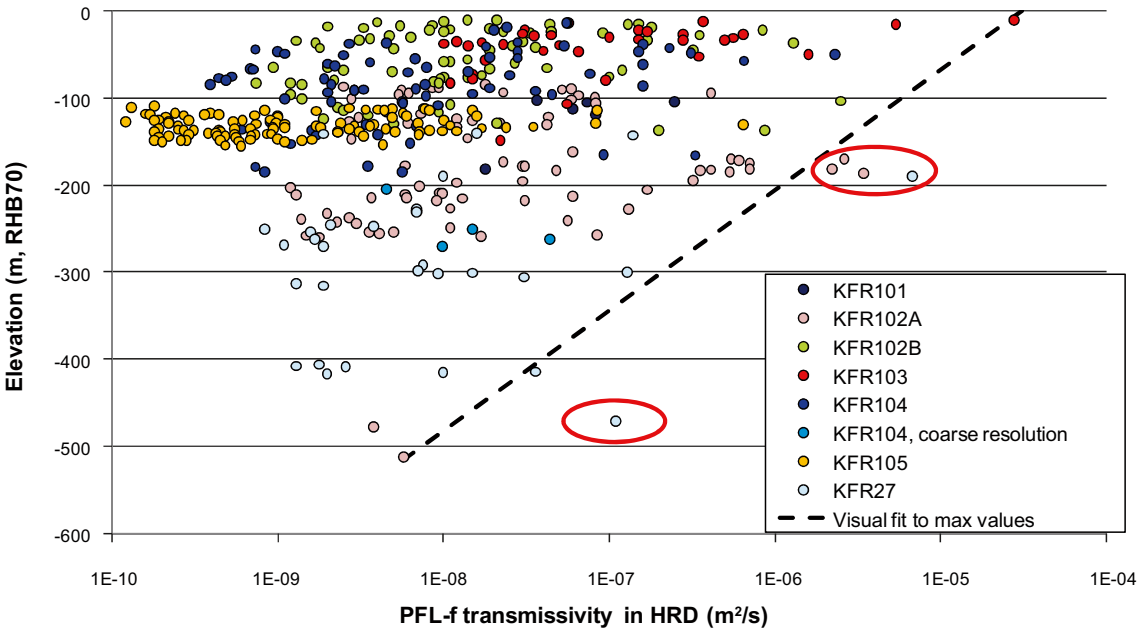

Figure 3-9. *PFL-f data transmissivity with depth in HRD, shown for boreholes KFR101–105 and KFR27. High transmissivity records, with respect to depth, are marked by red ovals.*

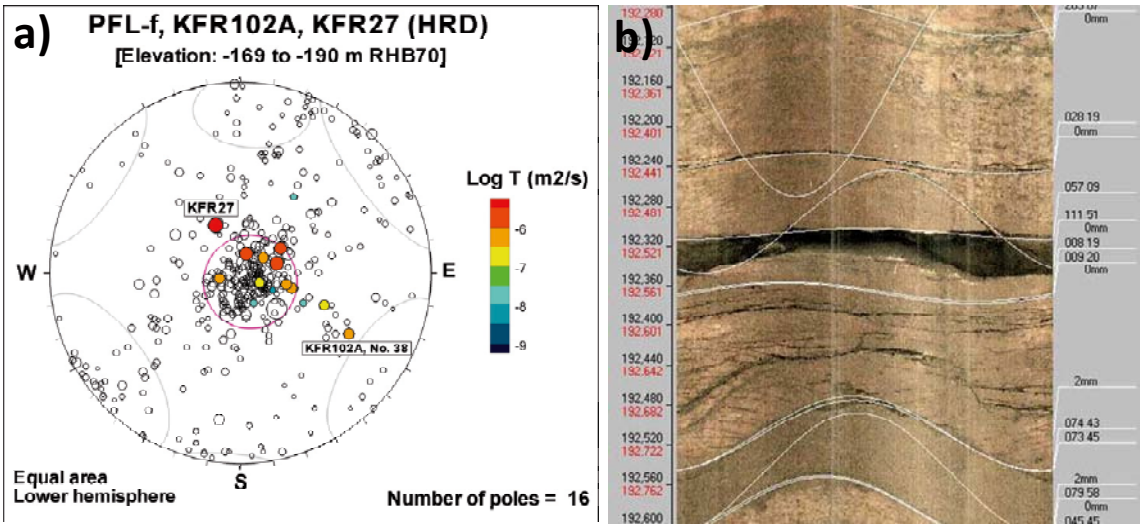

Figure 3-10. *Anomalous PFL-f data within the elevation range –169 m to –190 m; a) PFL-f orientation and b) BIPS imagery of the PFL-f record in KFR27. The PFL-f record in KFR27 has the highest transmissivity and is hydraulically connected to several boreholes drilled during the construction of SFR, KFR101, and indirectly to KFR102A (Appendix D).*

3.1.8 Comparison of PFL-f data in HRD and PDZ

There were no final HCD definitions available during this analysis. Instead, the hydraulic properties inside possible deformation zones (PDZ) were compared to characteristics outside possible deformation zones (here tentatively referred to as HRD). The total PFL-f intensity in PDZ is approximately equal to that in HRD; however, the PDZ transmissivities tend to be half an order of magnitude higher (Figure 3-11a). The PFL-f orientations in PDZ (Figure 3-11b) are fairly similar to that in HRD (Figure 3-6): dominated by sets Hz, Gd and NW. Similarly to observations in HRD, the transmissivity in PDZ also seems to be larger at lower dip (cf Figure 3-5). However, some differences can also be noted. The NW transmissivities are much larger in PDZ. The mean pole of the Gently dipping PFL-f data is also steeper, at an approximate dip of 40°, and appears to be EW-striking.

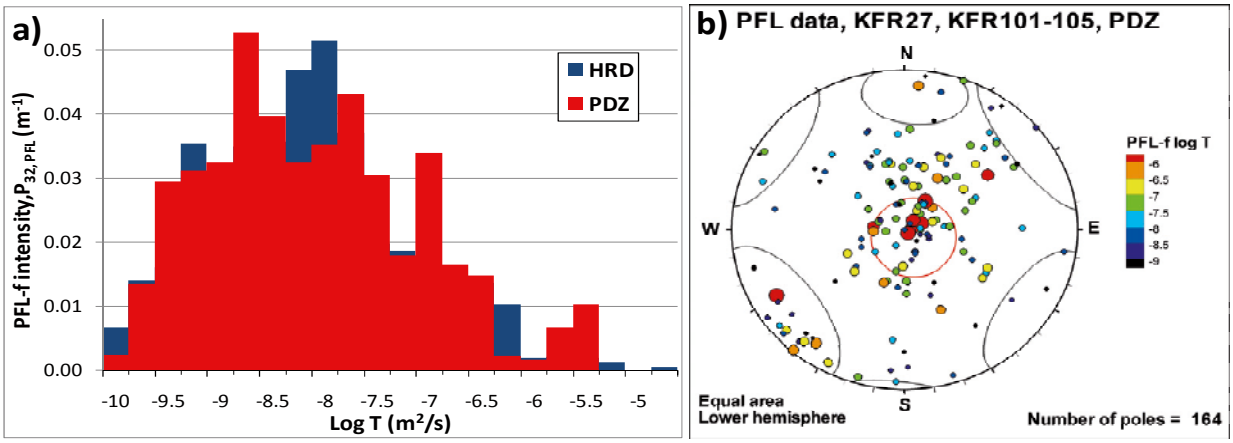

Figure 3-11. *PDZ transmissivity; a) comparison between PDZ and HRD transmissivity distributions, and b) orientation of PDZ PFL-f data. The histogram in a) is translucent, such that dark red indicate the overlap of distributions, while light red and grey indicate excessive intensity of PDZ, respectively, HRD.*

3.2 Orientation model for Open fractures

3.2.1 Four set model

Four sets of Open fractures were suggested by Kamb contoured stereoplots (Figure 3-2). As a first step, these were approximated in terms of hard sectors: a set mean pole and its enclosing solid angle (Table 3-1). In the second step, these hard sectors were used as initial values for translation into a soft-sector parameterisation, as described in Appendix E. A trial-and-error based iteration was used with three calibration targets:

1) to find a reasonably geometrically stable parameterisation (from iteration to iteration),
2) maximise Fisher concentration κ for all sets, and
3) to set-divide PFL-f transmissivity into homogeneous transmissivity populations, with particular emphasis to the dip range 40° to 50° (Figure E-3). In other words, PFL-f data far from a set mean pole (bin 45°) should follow the same distribution as PFL-f data near its mean pole (e.g. bin 85°).

Only Open and Partly open fractures in HRD, which are visible in BIPS and have a mapped orientation, were used to determine the probability of belonging for each set (Appendix E). Once the set-wise probability fields had been defined, all oriented Open fractures (both visible and not visible in BIPS) were randomly assigned to a fracture set (Table 3-1). In the final step, the non-oriented Open fractures (52 fractures) were set-assigned based on the relative Terzaghi-sums of the different sets.

Table 3-1. Open fracture sets, identified by visual inspection .

Set Acronym	EW-striking EW	NW-striking NW	NE-striking NE	Sub-Horizontal Hz
Hard sector input, applied to all oriented Open fractures visible in BIPS				
Trend	3	234	125	153
Plunge	15	6	3	88
Hard sector angle [°]	27	24	25	25
Soft sector results, all Open and Partly open fractures				
Trend	3	237	124	212
Plunge	11	8	1	86
Fisher k	8.2	13.8	9.7	10.3
No. fractures	1,500	626	970	2,462
Terzaghi sum	2,653.1	1,608.1	1,886.4	3,192.7

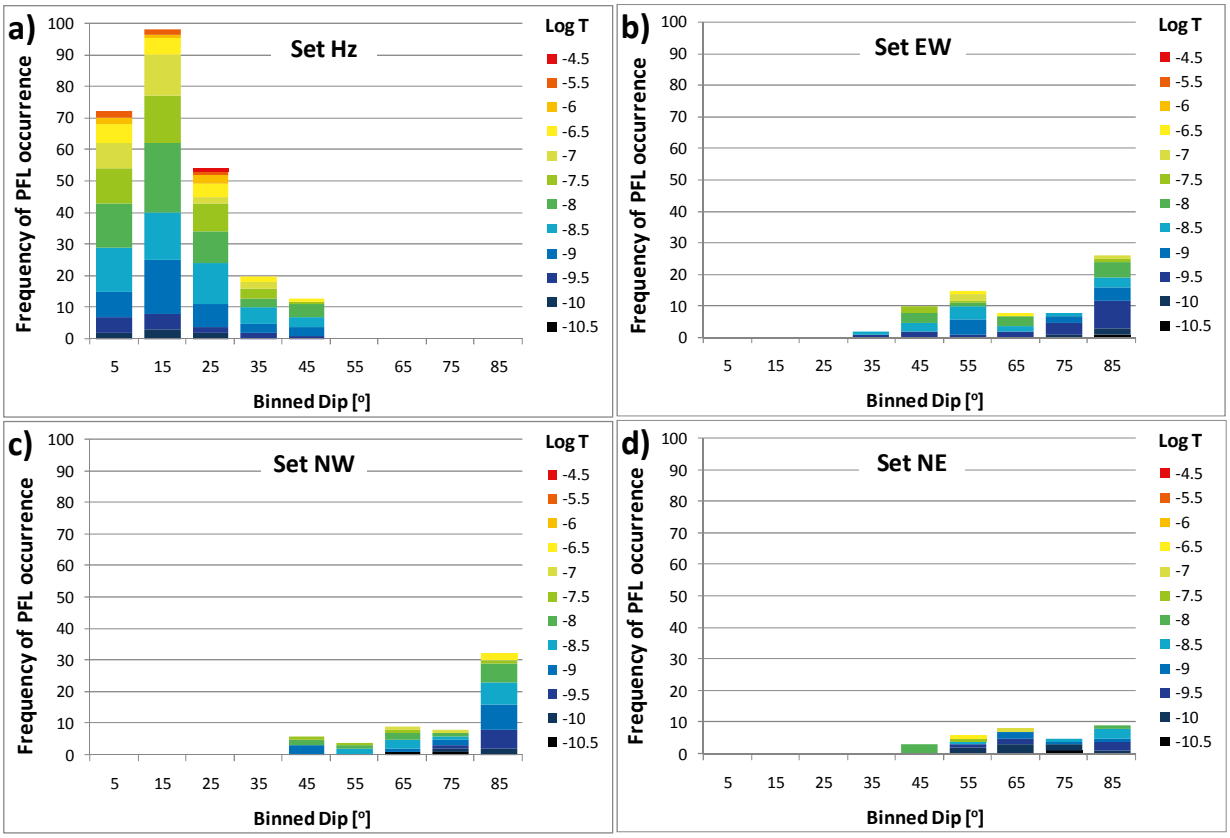

Figure 3-12. *Set-wise transmissivity distributions binned by dip angle (bin size = 10°). A calibration target was to set-divide the PFL-f data into homogenous transmissivity populations, with emphasis to the dip bin 45° (cf Figure 3-5).*

Evaluation

The set division is evaluated by visual inspection of frequency distributions of set-assigned Open fractures as a function of dip (Figure 3-13). Two aspects of should be noted concerning the projection of three-dimensional orientation to dip in Figure 3-13:

1) the fracture orientation is not radial symmetric (in particular for higher dips, see Figure 3-2).
2) The dip bins do not reflect equal areas of the orientation hemisphere (i.e. the figure does not account for the jacobian, sin φ in eq. (E-6)). Therefore the clustering of the sub-horizontal set may appear underrepresented in visual inspection relatively to the sub-vertical sets (i.e. there are few fractures at exactly dip = 0° (Figure 3-13), although the fracture clustering reaches its maximum value (Figure 3-2).

The expectation value of the fitted Fisher distributions (Table 3-1) takes on its minimum value at the overlap between the sub-horizontal fracture set and the sub-vertical sets (in the dip range 40° to 50°). In this dip range, the frequency of data is higher than expected by the fitted parameterisation. Also, the Fisher distributions appear to have been fitted unnecessarily wide (low Fisher κ) in order to minimize the mismatch in the dip range 40° to 50°. For example, the mode of the Fisher distribution for the sub-horizontal set is 17°, while the data suggests a mode at 10–12°, depending on bin-size (Figure 3-13).

Visual inspection of contoured stereograms demonstrates that the Open fractures assigned to set Hz are asymmetric. In a comparison to simulations of the fitted Fisher distribution, a cluster peak can be identified in the data at an approximate trend of 130°, while its dispersion of lower Fisher concentrations extend slightly further at a trend of 320° (Figure 3-14). Note also that the maximum concentration of data is 20%, while it is only 10% in the simulations. This would further support sub-dividing the data below a dip of 50° into one horizontal set (tightly clustered) and a more dispersed Gently dipping set. This notion is pursued in the following section.

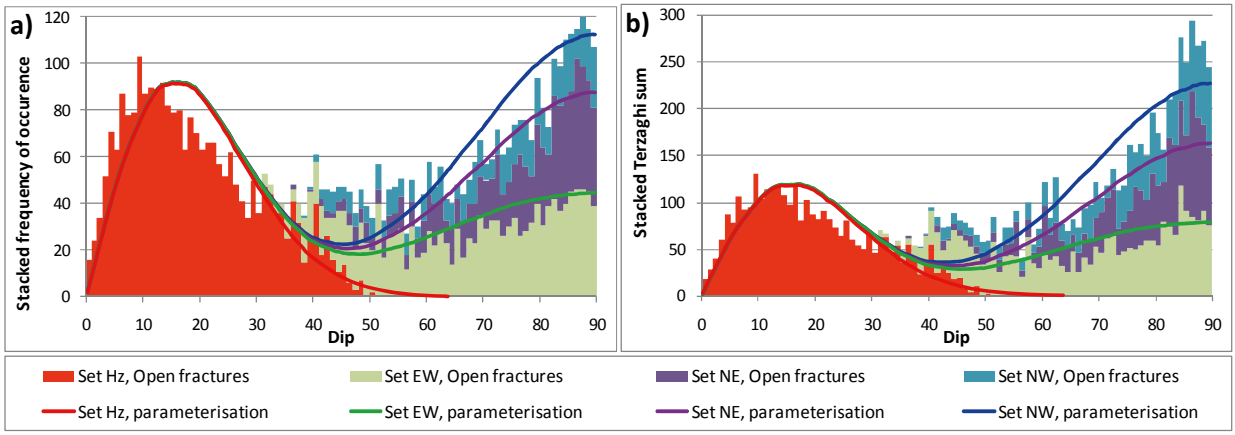

Figure 3-13. *Stacked histograms of Open fractures binned by dip angle; a) frequency of occurrence and b) Terzaghi sum. The Open fractures are divided into 4 sets and compared to the expectation values from fitted theoretical Fisher distributions.*

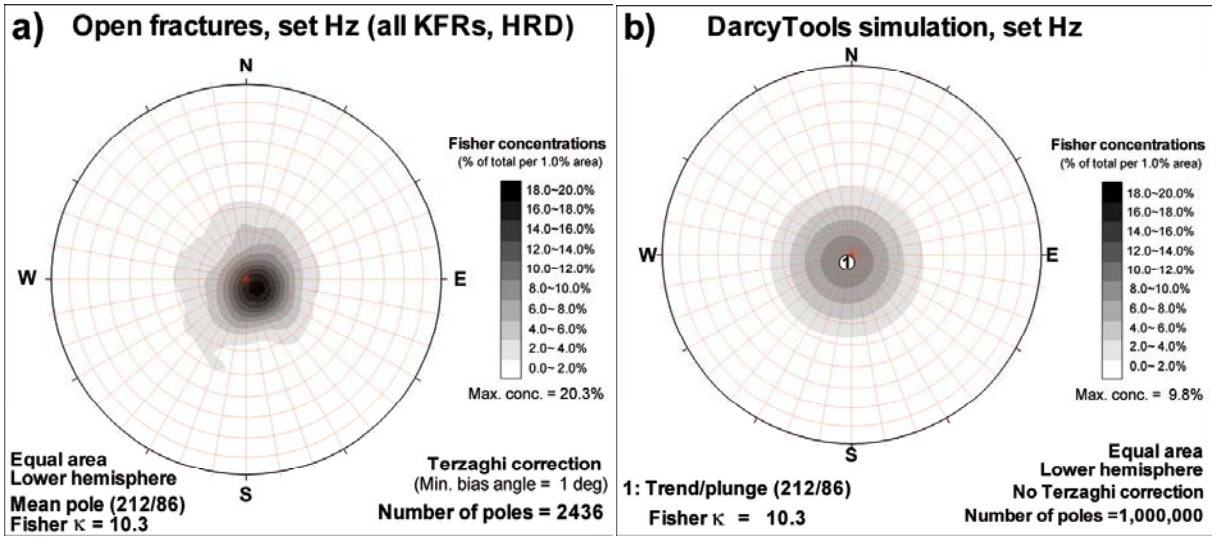

Figure 3-14. *Evaluation of contoured stereograms of set Hz; a) Open fractures in HRD compared to b) simulated orientations. Note that Terzaghi compensation does not apply for DarcyTools simulation, as it does not involve borehole sampling.*

3.2.2 Five set model

Most high transmissivity values, $T > 10^{-7}$ m²/s, are found to be gently dipping (dip < 55°). However, a sub group of particularly transmissive fractures, $T > 10^{-6}$ m²/s, can be identified as sub-horizontal (dip < 30°; Figure 3-5). Analytical estimation of fracture size suggests that horizontal fractures are considerably larger than other fractures (Appendix H). In the Forsmark area, horizontal sheet joints of extraordinary transmissivity and persistence have been observed in shallow bedrock, which is the result of glacial loading/unloading history and the current stress-regime. One of the key issues for the investigations of SFR is to been to elucidate if sheet joints occur also in the SFR domain /SKB 2008a/. In this context, it may be suspected that sub-horizontal fractures are different from the gently dipping and therefore a fifth, Gently dipping set (Gd) was introduced to the orientation model. This Gently dipping set is conceptualised as relatively dispersed in comparison to set Hz. It overlaps set Hz completely and partially overlaps the sub-vertical sets. The introduction of set Gd is expected to tighten the other sets (increase their Fisher concentration κ; see Section 3.2.1) and to capture the deviating subpopulation of fractures in the dip range 40° to 50°, which proved difficult with the 4-set approach (Section 3.1.5).

The four-set orientation model was used as a starting point. As initial values, set Gd was assigned the same mean pole as set Hz, with half its intensity (Terzaghi sum = 3,140.7/2) and half its Fisher concentration. Set Hz was reduced to half its intensity (Terzaghi sum = 3,140.7/2), while its Fisher concentration was doubled. The five-set parameterisation was then determined by trial-and-error based iteration, with the objective to find a stable solution with maximised Fisher concentrations κ. Probability fields are then calculated based on the iterated solution (Appendix E; Figure 3-17a), after which all Open fractures are randomly assigned to fracture sets. The result is that all Fisher κ increase and set Gd grows in intensity at the expense of other sets (Table 3-2).

Table 3-2. Five sets; soft sector parameterisation by iteration.

Set	Acronym	Trend	Plunge	Fisher κ	No. fractures	Terzaghi sum
EW-striking	EW	4	14	9.05	1,350	2,385.3
NW-striking	NW	234	6	14.17	570	1,528.9
NE-striking	NE	124	3	11.98	947	1,827.4
Horizontal	Hz	133	84	41.87	1,102	1,383.0
Gently dipping	Gd	315	84	7.39	1,589	2,215.8

Evaluation

The set division is evaluated by visual inspection of frequency distributions of set-assigned Open fractures as a function of dip (Figure 3-15). The overall impression is that the five-set parameterisation provides a better fit to data. Set Gd (and set EW) dominate the dip range 40° to 50°. The combined sets Hz and Gd improve the representation of the asymmetry in data (cf Figure 3-16 and Figure 3-14) and also in terms of maximum concentration (Figure 3-16). Note also that the parameterization of set Hz has improved considerably (Figure 3-15). Only moderate changes are observed in terms of mean poles for sub-vertical sets. The mean pole of set Hz moves towards a trend of 133°, and appears to coincide with the centre of high PFL-f transmissivity (> 10^{-6} m^2/s, see Figure 3-16).The mean pole of set Gd moves in the opposite direction, towards a trend of 315° and provides means to capture most of intermediate transmissivity data (10^{-7} m^2/s). The set-assignment of PFL-f data is not made with respect to geometric expectation values alone (e.g. Figure 3-17), but also with respect to transmissivity, as explained in (Appendix E).

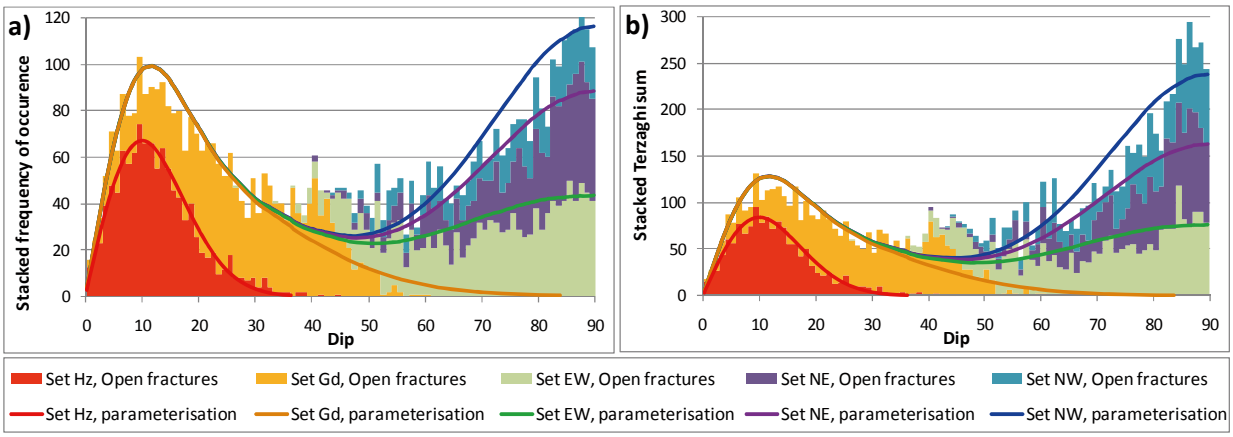

Figure 3-15. *Stacked histograms of Open fractures binned by dip angle; a) frequency of occurrence and b) Terzaghi sum. The Open fractures are divided into 5 sets and compared to the expectation values from fitted theoretical Fisher distributions (cf. Figure 3-13). A hemispherical projection of the probability fields is shown in (Figure 3-17).*

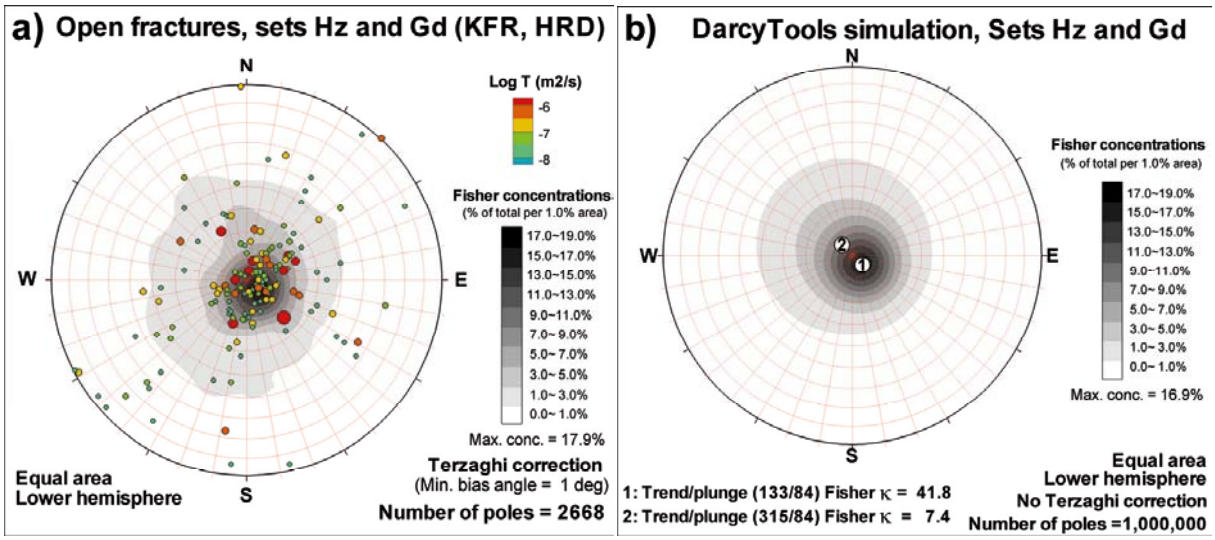

Figure 3-16. *Evaluation of contoured stereograms of set Hz and Gd; a) Open fractures in HRD compared to b) simulated orientations. All PFL-f data with transmissivity > 10^{-8} m^2/s are included as poles to demonstrate that the majority, but not all, are covered by Gd and Hz. Note that Terzaghi compensation does not apply for DarcyTools simulation, as it does not involve borehole sampling.*

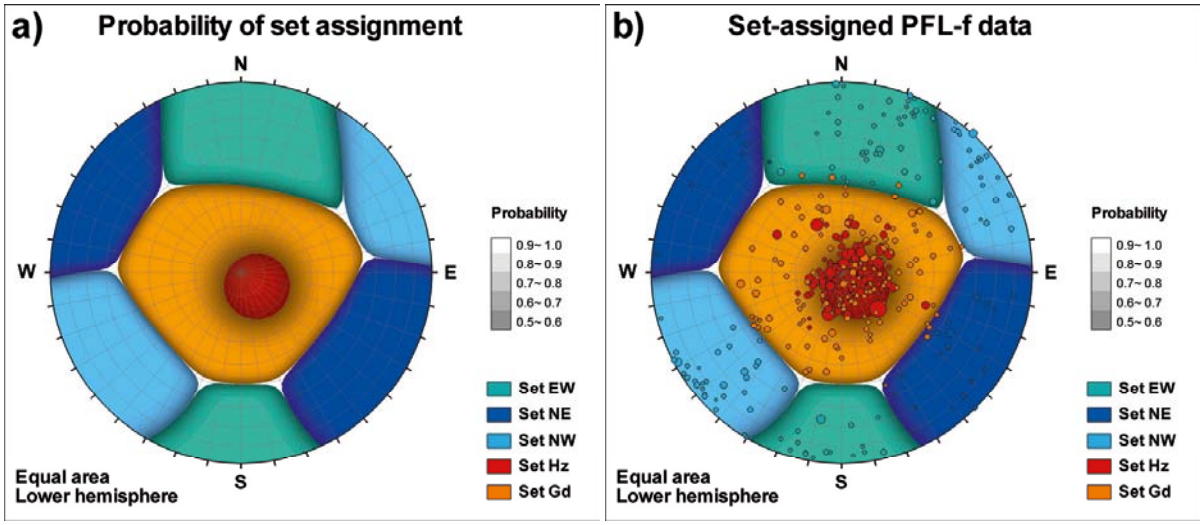

Figure 3-17. *Hemispherical projection of probability fields for set assignment (a), and set-assigned PFL-f data (b). For clarity, only the dominant set is shown (i.e. probability values > 0.5). The PFL-f poles are scaled by transmissivity.*

3.3 Fracture domains

3.3.1 Vertical trends in fracture set intensity

Once the data has been set-assigned, the vertical variability in intensity of Open fractures and PFL-f data can be analysed in terms of fracture sets (Figure 3-18 and Figure 3-19). Note that the exclusion of PDZ reduces the data in some elevation bins (both borehole length and fracture data); partial coverage implies higher variability, and may appear as intensity spikes in incompletely covered elevation bins. For example, the possible deformation zone DZ1 in KFR102A (from 149 to 161 m borehole length) reduces the available core length in elevation bin –130 to –140 m RHB70 to 3.6 m, compared to its average 11 m core length per elevation bin. Anomalous intensities are calculated over this interval (Figure 3-18 and Figure 3-19), in spite of removing fracture and PFL-f

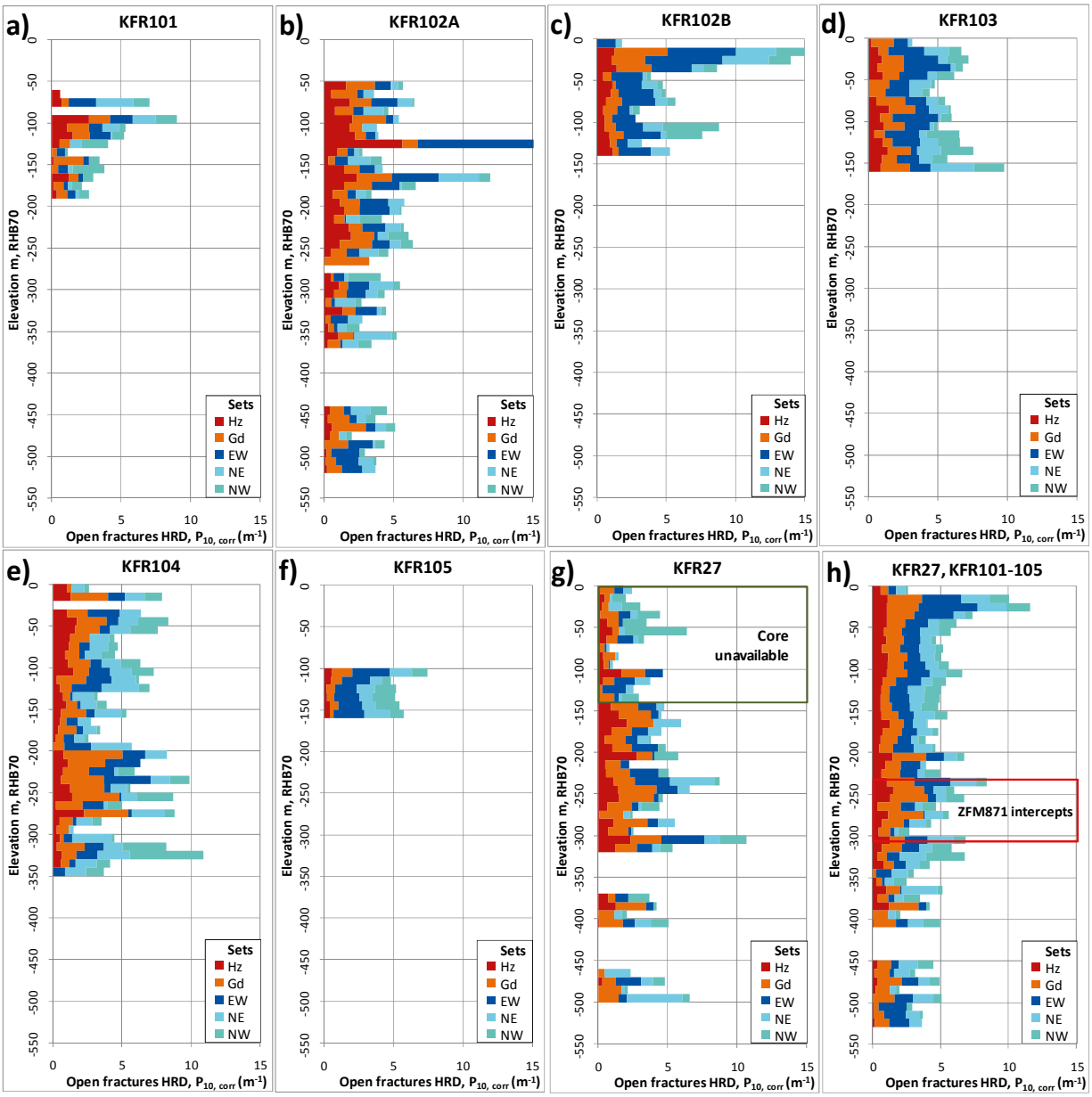

Figure 3-18. *Intensity of Open fractures in HRD binned by set and elevation, shown for boreholes KFR101–105 and KFR27. Core is unavailable in upper part of KFR27 (data excluded in h). Grey area indicates elevation bins outside the HRD (i.e. either classed as possible deformation zone, according to SHI, or beyond the borehole extent.*

data over the same borehole length intensity, which simply reflects the effects of a smaller sample size. It should therefore be emphasised that the intention with Figure 3-18 and Figure 3-19 is not to identify local deviations, but to compile a representation of the overall intensity patterns with depth.

The depth trend in total intensity is much stronger for PFL-f data, than it is for Open fractures (cf. Figure 3-18h and Figure 3-19h). As stated earlier, the high intensity in shallow bedrock 0 to –60 m RHB70 are dominated by data from KFR102B and KFR103. It can be noted that the PFL-f intensity is not set-wise proportional to the Open fracture intensity; instead they are clearly dominated by sets Hz and Gd (even in the sub-horizontal KFR105). For example, in spite of the domination of sub-vertical Open fractures in KFR102B (Figure 3-18), its PFL-f data are nonetheless dominated by sets Gd and Hz (Figure 3-19). Other examples include KFR27 and KFR102A below –250 m RHB70, where Open fracture intensity is about average, whereas the PFL-f intensity is very low.

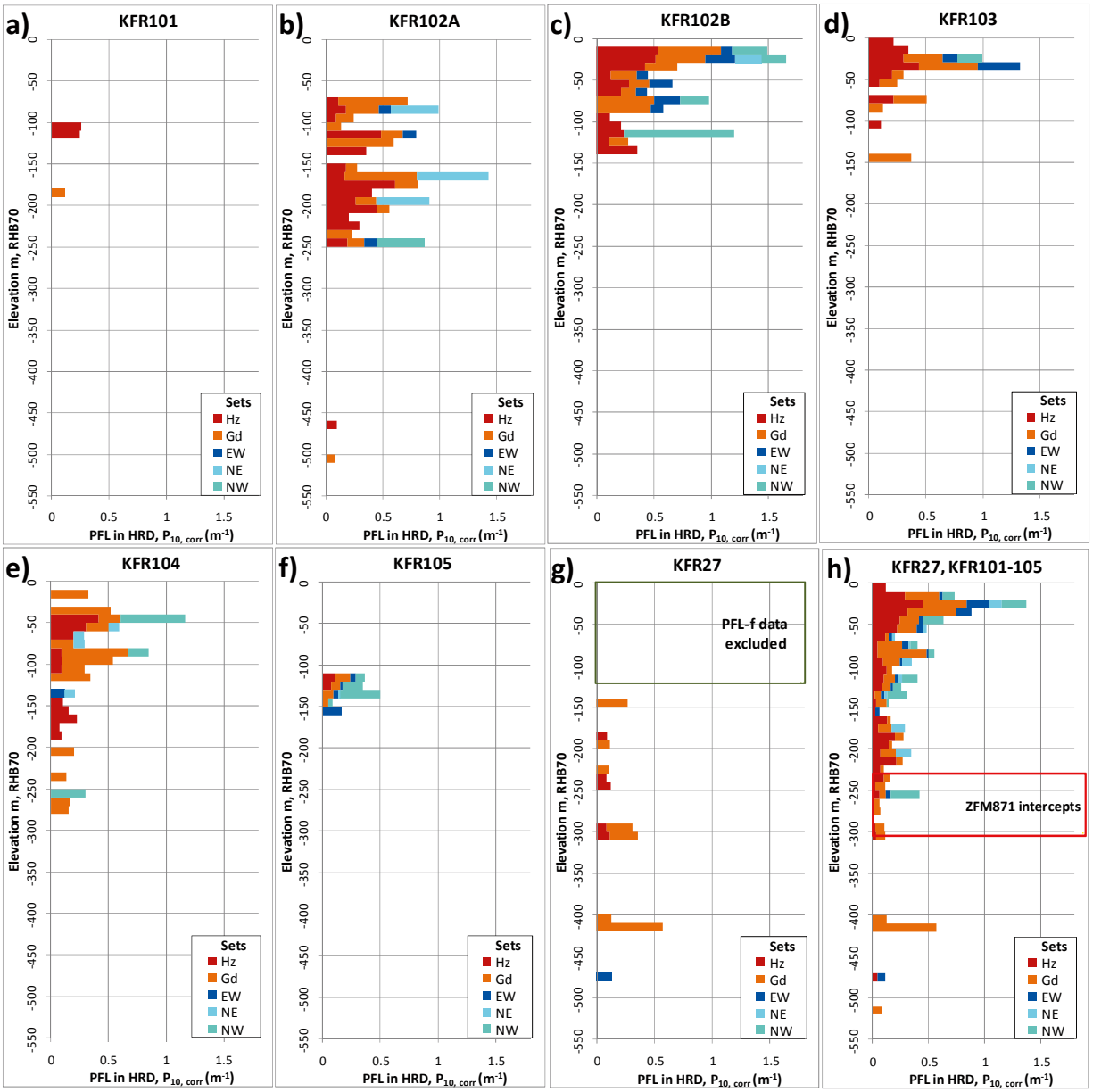

Figure 3-19. *Intensity of PFL-f data ($T > T_{lim}$) in HRD binned by set and elevation, shown for boreholes KFR101–105 and KFR27. The PFL-f data are unavailable/excluded for in the upper part of KFR27 (see Appendix C; also excluded in h). Grey area indicates elevation bins outside the HRD (i.e. either classed as possible deformation zone, according to SHI, or beyond the borehole extent.*

It can be noted that the coarsely resolved PFL-f data in KFR104, below –190 m RHB70 has a very low intensity, whereas its Open fracture intensity is high. Owing to its similarity to the other deep boreholes, KFR102A and KFR27, it is assumed that the low PFL-f intensity in KFR104 is not an artefact of its coarse resolution.

Note that the high PFL-f record at elevation of –470 RHB70 with a transmissivity of 10^{-7} m^2/s (Figure 3-9) is not horizontal, but belongs to set EW (Figure 3-19) even though set EW Open fractures are scarce in KFR27 (Figure 3-18).

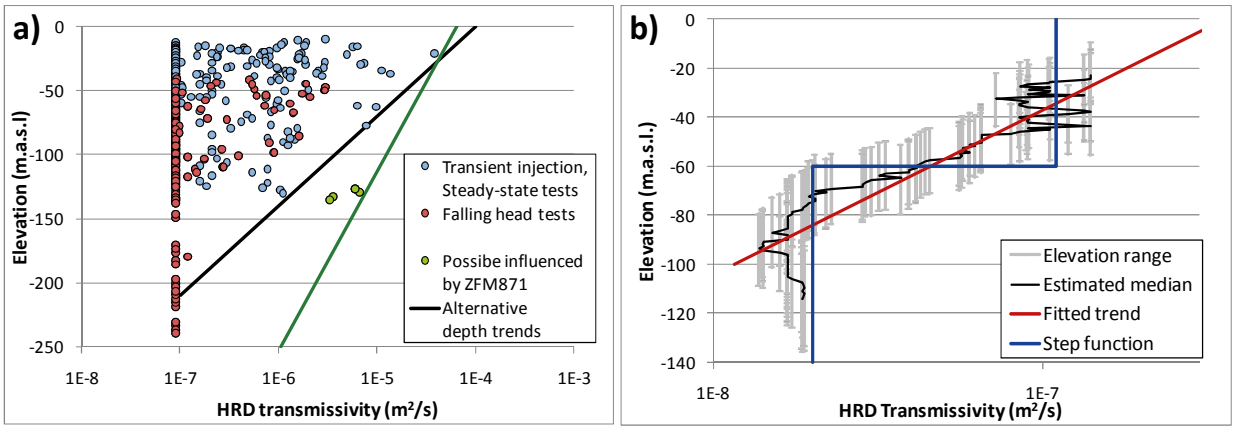

Figure 3-20. *Depth trend analysis of transmissivity data available prior to the initiation of the Site Investigation program for the SFR extension; a) depth trend fitted to transmissivity data and b) estimated trend of the median, based on a rolling set of 100 data. Modified from /Öhman and Follin 2010/.*

3.3.2 Depth domains and calculated intensity

Without the supporting information from an updated Geological model, it is difficult to infer if the observed deviating patterns in the patched borehole information should be linked to lateral or vertical variability. Lateral spatial patterns are more site-specific, as they are closely related to geologic structures (Section 2.2.5). Vertical trends in hydraulic data, on the other hand, are of a more general nature, as they relate to increasing stress with depth, shallow geologic processes, and its connectivity to the surface boundary. Therefore it was decided to formulate the fracture domains at the current modelling stage in terms of elevation intervals. Based on the observations made in Chapter 3 (e.g. Figure 3-18 and Figure 3-19), the modelling domain is divided into three elevation intervals: the Shallow domain, the Repository domain, and the Deep domain (Table 3-3). Although data is only available down to –530 m RHB70, the properties of the Deep domain is assumed to extend down to –1,100 m RHB70.

Table 3-3. Definition of DFN model domains and calculated intensity.

Domain	Shallow domain	Repository domain	Deep domain
Elevation interval (m, RHB70)	**0 > z ≥ –60**	**–60> z ≥ –245***	**–245*) > z ≥ –1,100**
Fracture set	**Open fracture intensity in HRD, $P_{32,\ Open}$**		
EW	2.60	1.41	0.92
NW	1.15	0.86	0.87
NE	1.34	1.03	1.02
Hz	1.06	0.85	0.59
Gd	1.87	1.20	1.28
Fracture set	**PFL-f intensity in HRD ($T \geq T_{lim}$), $P_{32,\ PFL}$**		
EW	0.10	0.02	0.01
NW	0.11	0.05	0.01
NE	0.03	0.02	0
Hz	0.36	0.08	0.01
Gd	0.34	0.09	0.03

* Alternatively, the boundary between the Repository domain and the Deep domain can be associated to ZFM871.

Once the Depth domains have been defined, their respective geometric DFN-parameterisations can be calculated from data. One possible option here *could have been* to: 1) review the orientation model in the light of the depth domains, 2) define separate orientation models for each depth domain, and 3) set-assign data according to the separate orientation models. This complex refinement step was *not* undertaken; instead domain-wise fracture set mean poles and Fisher κ were calculated based on the existing set-assignment, done in Section 3.2.2. The set-wise $P_{32,\ Open}$ and $P_{32,\ PFL}$ for each depth domain are reported in Table 3-3, while the corresponding mean poles and Fisher κ are reported in the summarized Table 3-4 and Table 3-5. Two properties cannot be determined directly from data: a) the size scaling exponent, k_r, and b) fracture transmissivity. These are determined by means of statistical DFN analysis using the computational code DarcyTools. Two alternative approaches are explored for doing so, the connectivity analysis (Appendix J.2) and a Tectonic Continuum approach (Appendix J.3).

3.4 DFN calibration

The calibration of size and transmissivity was performed by multiple DFN realisations of Connected fracture networks, as described in Section 2.3. The scaling exponent was calibrated by trial and error with the target to achieve an intensity of Connected Open Fractures, *as seen by a vertical borehole*, in the range 2 to 4 times larger than the intensity of PFL-f data above T_{lim}. For sets Gd and Hz, the fitted k_r is within the range 2.55 to 2.79 (Table 3-4), while it is generally above 3.0 for the sub-vertical sets. This is in line with observations from Site Investigation Forsmark, see Section 2.2.10 /Follin et al. 2007b/. It was found difficult to meet the calibration target for the sub-vertical sets, even for high k_r. The exponent k_r was not allowed to exceed 3.45, as higher values were considered unrealistic and were not found to further improve the connectivity analysis. This can be expected, as for example, the influence of k_r on connectivity ceases below the percolation threshold. Therefore, it seems reasonable that in the presence of a well-connected Hz/Gd network, the dependency of k_r on the connectivity of subvertical fractures will deteriorate above a certain threshold. In other words, beyond some point (above a certain k_r for vertical sets), the presence of sub-vertical fractures in the Connected network do not necessarily mean sub-vertical connectivity; the sub-vertical fractures may simply appear as single dead ends on the Connected Hz/Gd network. Thus, increasing k_r further beyond this point may have little effect on the overall Connectivity.

This is more a conceptual problem of equi-finality, than it is a practical problem. Firstly, the calibration criterion is not based on solid evidence, but rather a working hypothesis formed out of necessity (Appendix F). In reality, little is known about the intensity of the Connected fracture network below T_{lim}. Secondly, the hydraulic data are nevertheless conditioned to the upper tails of distributions (Figure 2-6), as remaining data are censored by the detection limit, T_{lim}. The excess sub-vertical intensity of Connected fractures are associated to large population of short fractures, with unknown fracture transmissivity below T_{lim}. Fine-tuning the size-transmissivity relations demonstrate that the hydro-DFN is still capable of honouring the intensity in PFL-f records above T_{lim} (see Section 4.1.3). The details of the applied connectivity analysis are given in Appendix J. The resulting hydro-DFN parameterisation is summarized in Table 3-4.

As discussed above, the calibration of k_r with the connectivity analysis proved to be difficult for the vertical sets (NE and EW in particular, Appendix J). The calibration criterion could not be met, even for high scaling exponents ($k_r = 3.45$). A high k_r results in a strong dependency between size and transmissivity, which may result unrealistically high maximum transmissivity (e.g. Figure J-4e). Also, the assumed calibration target of a ratio $P_{32,\ COF}/P_{32,\ PFL}$ within a range 2 to 4 is hardly indisputable (Appendix F). It was set up by practical necessity rather than based on solid evidence. Furthermore, for a $k_r = 3.45$, the intensity of fractures with a radius larger than 30 m is negligible, which means that power-law scaling between fractures and deformation zones does not apply (Figure J-8).

Table 3-4. Hydro-DFN model parameterisation, k_r calibrated by connectivity analysis.

Domain	Set	Intensity [4] $P_{32\ (r0,\ 169\ m)}$	$P_{32\ Tot}$	Size r_0	k_r	Orientation Tr	Pl	Fisher κ	Transmissivity ($T = a\ r^b$) a	b
Shallow										
0 to –60 m	EW	2.60	2.60	0.038	3.45	2.7	7.4	12.6	NA[2]	NA[2]
(RHB70)	NW	1.15	1.15	0.038	3.1	232.7	11.9	13.2	NA[2]	NA[2]
	NE	1.34	1.34	0.038	3.45	128.3	8.2	11.7	NA[2]	NA[2]
	HZ	1.06	1.06	0.038	2.6	115.9	84.5	27.6	1.41E–7	1.43
	Gd	1.87	1.87	0.038	2.79	232.2	85.1	6.5	2.11E–8	1.09
Repository										
–60 to –245[1] m	EW	1.41	1.41	0.038	3.45	5	12.7	8.5	6.00E–9	1.29
(RHB70)	NW	0.86	0.86	0.038	2.95	234	6	12.3	8.00E–9	1.13
	NE	1.03	1.03	0.038	3.45	128.2	5.5	11.5	1.70E–7	3.19
	NE[3]	1.03	1.03	0.038	3.45	128.2	5.5	11.5	1.00E–8	1.25
	HZ	0.85	0.85	0.038	2.55	137	84.3	42.9	2.06E–9	1.85
	Gd	1.20	1.21	0.038	2.72	354.2	85.4	7.1	4.00E–9	1.05
Deep										
–245[1] to –525 m	EW	0.92	0.92	0.038	3.45	2.5	19.6	9.7	NA[2]	NA[2]
(RHB70)	NW	0.87	0.87	0.038	3.1	233.3	7	14.9	NA[2]	NA[2]
	NE	1.02	1.02	0.038	3.45	304.7	0.1	11.2	NA[2]	NA[2]
	HZ	0.59	0.60	0.038	2.75	127.7	80.9	27.9	1.34E–9	1.32
	Gd	1.28	1.29	0.038	2.7	269.8	84.5	6.6	9.80E–10	0.93

[1] Approximate average borehole intercepts with ZFM871 (KFR102A and KFR27) based on SFR geologic model v.0.1.

[2] Not evaluated because of scarce data. Must be extrapolated set-wise from the repository level (e.g. Section 4.1.3).

[3] Based on exclusion of PFL No. 38 in KFR102A. The final SFR Geo model v. 1.0 is not complete, and thus the HRD of the hydro-DFN v 0.2 is strictly based on SHI interpretation. However, this PFL record is an outlier with respect to the complete data set, and therefore it is hypothesised that it may be assigned to HCD in the final SFR Geo-model.

[4] The smallest modelled deterministic zones are on the order 300 m (SFR Geo. v.0.1), corresponding to a radius of 169 m. Stochastic fractures are therefore assumed to have a maximum radius of 169 m.

Therefore, an alternative approach is demonstrated, which is based on the assumption of Tectonic Continuum. This is only performed for the sub-vertical sets EW, NE, and NW, as the deformation zone model is primarily based on extrapolation of sub-vertical lineaments /Curtis et al. 2009/ and only contains two sub-horizontal zones. Furthermore, k_r for sets Hz and Gd could be calibrated satisfactorily using the connectivity analysis (Appendix J). The scaling exponent k_r is fit between the borehole intensity of Open fractures (more specifically $P_{32,\ Open+HCD}$) and that of modelled deterministic deformation zones, $P_{32,\ HCD}$. As a result, k_r drops from 3.45 to approximately 2.6, which is similar to that of sets Hz and Gd. Consequently, the fitting parameter *a* in the size-transmissivity relation (the transmissivity of a fracture with a radius of 1.0 m; Table 3-5) drops by more than one order of magnitude. By visual inspection, the general impression is that the fits (Figure J-10) are comparable to those of the connectivity analysis, which again demonstrates the dilemma of non-unique solutions when calibration is made to the upper tail of distributions.

The details of the applied assumption of Tectonic continuum are given in Appendix J. The resulting hydro-DFN parameterisation based on the assumption of Tectonic Continuum is summarized in Table 3-5.

Table 3-5. Hydro-DFN model parameterisation, assuming Tectonic Continuum.

Domain	Set	Intensity [4] $P_{32\ (r0,\ 169\ m)}$	$P_{32\ Tot}$	Size r_0	k_r	Orientation Tr	Pl	Fisher κ	Transmissivity ($T = a\ r^b$) a	b
Shallow										
0 to –60 m	EW	2.6	2.6	0.038	2.694	2.7	7.4	12.6	NA[2]	NA[2]
(RHB70)	NW	1.15	1.15	0.038	2.778	232.7	11.9	13.2	NA[2]	NA[2]
	NE	1.34	1.34	0.038	2.626	128.3	8.2	11.7	NA[2]	NA[2]
	HZ	1.06	1.06	0.038	2.6	115.9	84.5	27.6	3.20E–7	1.53
	Gd	1.87	1.87	0.038	2.79	232.2	85.1	6.5	3.40E–8	1.20
Repository										
–60 to –245[1] m	EW	1.41	1.41	0.038	2.63	5	12.7	8.5	4.0E–12	2.22
(RHB70)	NW	0.86	0.86	0.038	2.752	234	6	12.3	6.0E–10	1.31
	NE	1.03	1.03	0.038	2.596	128.2	5.5	11.5	1.8E–11	2.83
	NE[3]	1.03	1.03	0.038	2.596	128.2	5.5	11.5	3.0E–10	1.25
	HZ	0.85	0.85	0.038	2.55	137	84.3	42.9	4.1E–10	2.18
	Gd	1.2	1.21	0.038	2.72	354.2	85.4	7.1	3.0E–9	1.08
Deep										
–245[1] to –525 m	EW	0.92	0.92	0.038	2.585	2.5	19.6	9.7	NA[2]	NA[2]
(RHB70)	NW	0.87	0.87	0.038	2.75	233.3	7	14.9	NA[2]	NA[2]
	NE	1.02	1.02	0.038	2.597	304.7	0.1	11.2	NA[2]	NA[2]
	HZ	0.59	0.6	0.038	2.75	127.7	80.9	27.9	6.1E–10	2.20
	Gd	1.28	1.29	0.038	2.7	269.8	84.5	6.6	4.2E–10	1.22

[1] Approximate average borehole intercepts with ZFM871 (KFR102A and KFR27) based on SFR geologic model v.0.1

[2] Not evaluated because of scarce data. Must be extrapolated set-wise from the repository level (e.g. Section 4.1.3).

[3] Based on exclusion of PFL No. 38 in KFR102A. The final SFR Geo model v. 1.0 is not complete, and thus the HRD of the hydro-DFN v 0.2 is strictly based on SHI interpretation. However, this PFL record is an outlier with respect to the complete data set, and therefore it is hypothesised that it may be assigned to HCD in the final SFR Geo-model.

[4] The smallest modelled deterministic zones are on the order 300 m (SFR Geo. v.0.1), corresponding to a radius of 169 m. Stochastic fractures are therefore assumed to have a maximum radius of 169 m.

4 Evaluation

4.1 Geometrical evaluation

4.1.1 Open fracture orientation

The simulated borehole exploration of Open fractures renders the type of orientation distributions that can be expected from the DFN-parameterisation: the global orientation model is fairly well reproduced (Figure 4-1), although the lateral borehole-to-borehole variability (Figure 3-3) cannot be reproduced. Note that the simulated orientation pattern is independent on whether scaling exponents are calibrated with respect to intensity of Connected fractures, or by the assumption of Tectonic Continuum. More precisely, Figure 4-1b and c involve several realisations with respect to the set-up shown in Figure 2-5; however the total simulated borehole exploration length is equal to the cored borehole length in HRD, and therefore it is referred to as "one full realisation of the SFR data set". A corresponding depth domain-wise comparison between data and simulated borehole exploration is shown in Figure 4-2.

The general impression is that the 5-set orientation model fairly well reproduces the orientation pattern of Open fractures in the SFR data set. Since a vertical borehole was used in simulations the number of simulated intercepts is somewhat lower, however, the Terzaghi weight sums are in similar range. It can be noted that the deviating pattern of EW-striking fractures dipping 50°–60° (at –200 m RHB70 in KFR102A) are not captured in simulations. It can also be noted that simulated sub-vertical sets occasionally has a higher significance of point concentration. This is an artefact of the vertical simulated borehole, which has strong Terzaghi-weighting at high dips, whereas the data are more balanced represented in terms of sampling bias, with boreholes generally inclined 50°–60° (Section 3.1.1).

4.1.2 Connected fracture orientation above T_{lim}

The PFL-f data of the three depth domains were compared to simulated borehole exploration in terms of transmissivity and orientation (Figure 4-3). The purpose of this verification is to demonstrate if the 5-set approach reasonably well can reproduce the transmissivity-orientation patterns observed in data. A single realisation (defined as total simulated borehole exploration length equal to the cored borehole length in HRD) was examined for both alternative strategies to define the scaling exponent k_r (parameterisation set up taken from Table 3-4, respectively, Table 3-5). Transmissivity was calculated by the established empirical relations to fracture radius, eq. (2-4), and transmissivity below T_{lim} is excluded. For the Shallow and Deep domains no empirical relations were established for the sub-vertical sets; therefore their coefficients, *a* and *b*, were taken set-wise from the Repository domain. Only one realisation is analysed, and therefore the stochastic variability must be accounted for in the comparison to data. Note also that this comparison is made in terms of poles to illustrate the transmissivity values. Therefore Terzaghi compensation is inapplicable, and in particular, the sub-vertical sets will be underrepresented by the vertical simulated borehole exploration.

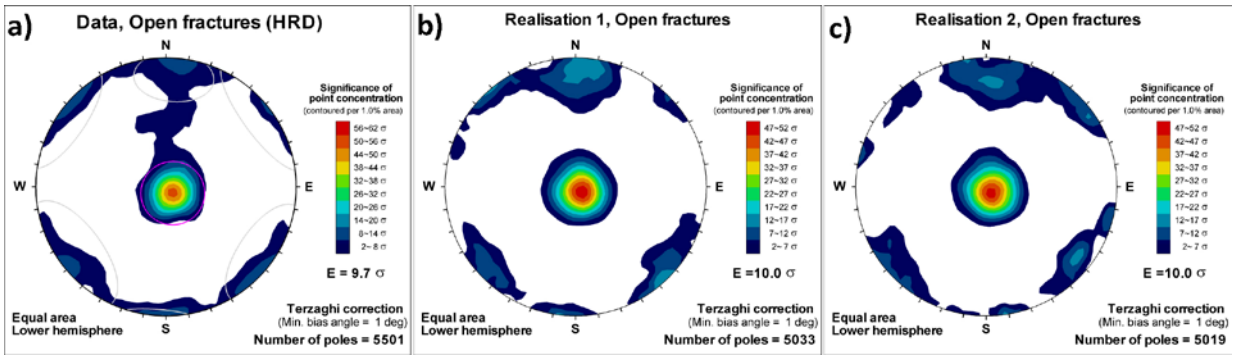

Figure 4-1. *Open and Partly open fracture data a), compared to simulated borehole exploration for two realisations b) and c).*

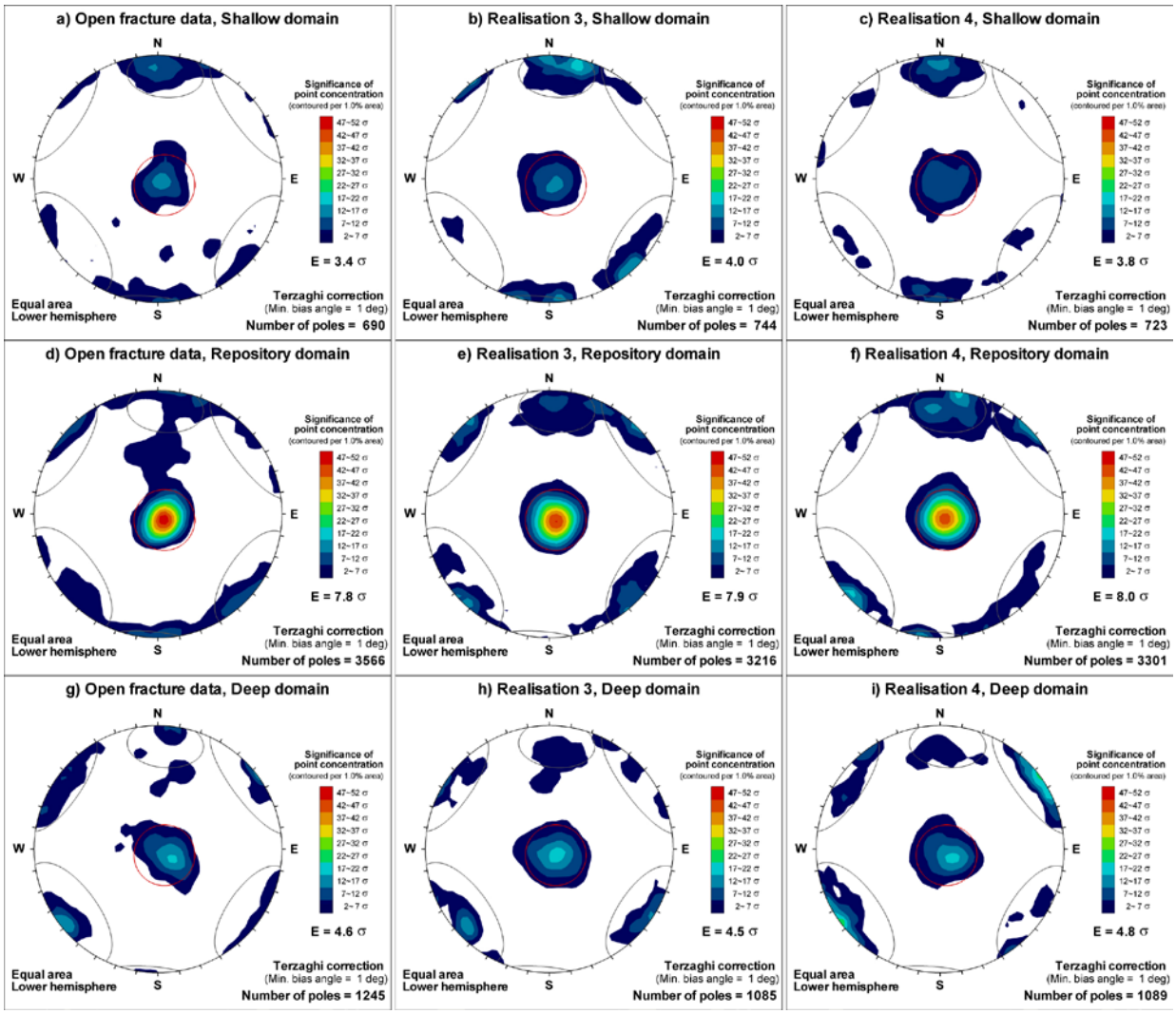

Figure 4-2. *Domain-wise comparison between Open and Partly open fracture data and simulated borehole exploration for two realisations.*

In the light of stochastic heterogeneity and the simplified modelled borehole geometry, it is difficult to clearly state if the hydraulic orientation patterns are well reproduced. However, the Tectonic Continuum-based approach overestimates transmissivity in both the Shallow and Deep domains. It can also be noted that the simulated number of poles exceed data in the Shallow domain. The reason for this is that the empirical transmissivity relations were fitted to PFL-f data above a transmissivity of 10^{-8} m^2/s (as opposed to the general cut-off at 2.5×10^{-9} m^2/s; see Appendix C). Although the $P_{32,\,COF}/P_{32,\,PFL}$-ratio for the sub-vertical sets exceeded the defined calibration target (typically 10 to 60; Table J-1 and Table J-2), the simulated sub-vertical sets with transmissivity above T_{lim} appear underrepresented (except Figure 4-3i). In fact, the simulated intensity of sub-vertical sets ($T > T_{lim}$) agree very well with data, if studied over a larger number of realizations (Section 4.1.3). The under-representation of sub-vertical sets in Figure 4-3 is merely an artefact of the simulated borehole being vertical.

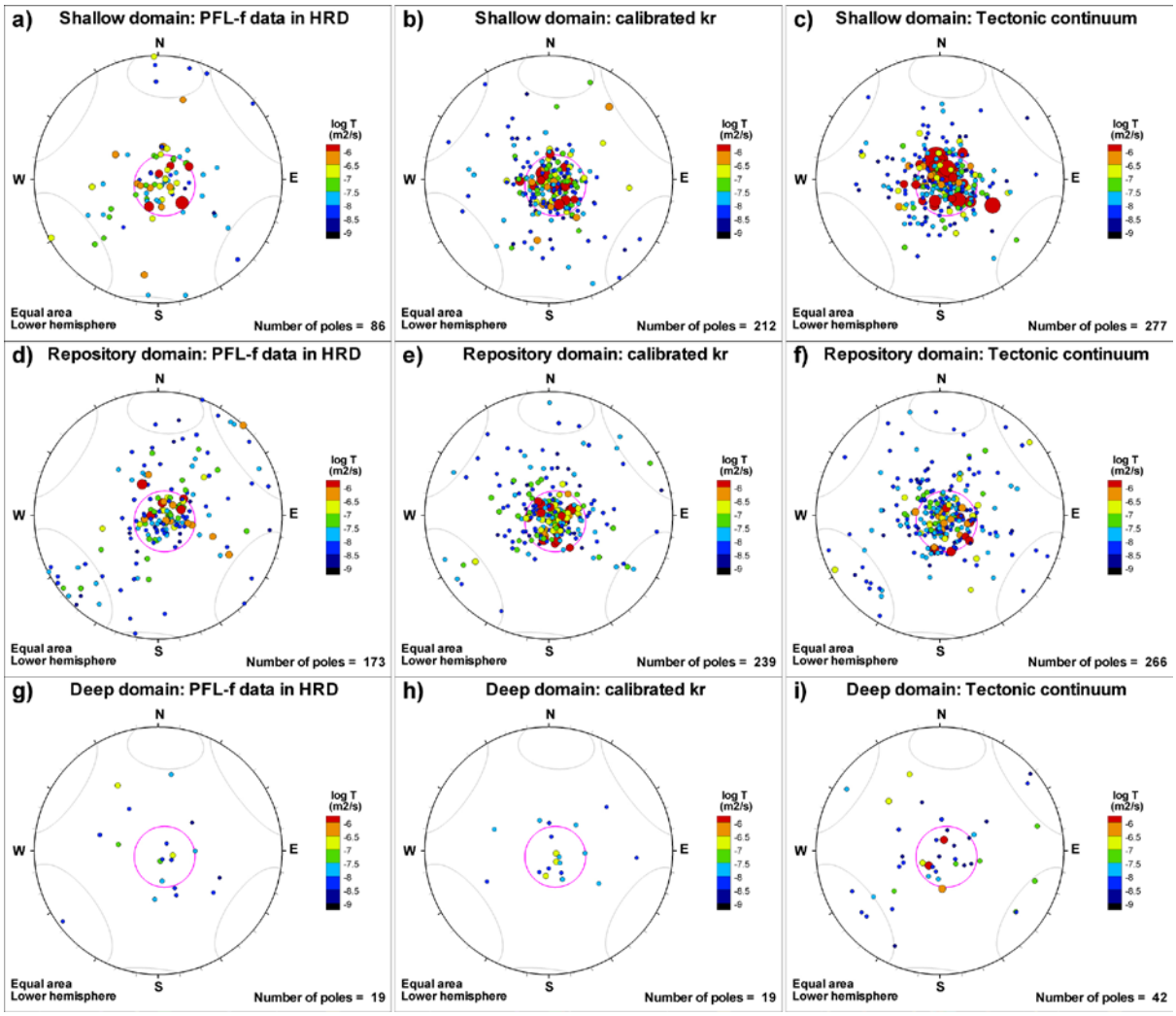

Figure 4-3. *PFL-f data for the three depth domains compared simulated borehole exploration of a single realisation of with the two alternative strategies to define the scaling exponent k_r. Transmissivity below T_{lim} is excluded. The transmissivity of the sub-vertical sets in the Shallow and Deep domains were calculated by the empirical transmissivity coefficients, a and b, defined for the Repository domain.*

4.1.3 Connected fracture intensity above T_{lim}

The connectivity analysis was performed in terms of the ratio $P_{32,\,COF}/P_{32,\,PFL}$ for PFL-f data above T_{lim}. Once the empirical transmissivity relations have been established, they can be verified by calculating the $P_{32,\,COF}/P_{32,\,PFL}$-ratio for a common cut-off of T_{lim} (i.e. $P_{32,\,COF,\,T>Tlim}/P_{32,\,PFL,\,T>Tlim}$; Table 4-1). This ratio should be close to 1.0. The intesity ratio above T_{lim} can also be used to suggest the coefficients, a and b for the sub-vertical sets in the Shallow and Deep domains, as no empirical relations could be established in Table 3-4 and Table 3-5. Based on observations for sets Hz and Gd (Table 3-4 and Table 3-5), it appears that the exponent b changes less with depth than the coefficient a does. The set-wise exponents b for sub-vertical sets were therefore assumed to be constant and equal to the values determined for the Repository domain. The coefficient *a* could then determined by requiring that $P_{32,\,COF,\,T>Tlim} = P_{32,\,PFL,\,T>Tlim}$ (Table 4-1). In this analysis, it was decided to exclude the possible outlier, PFL-f record No. 38 in KFR102A, from data.

Table 4-1. Intensity of Connected fractures above T_{lim} compared to PFL-f data.

	Factor ($P_{32, COF}/P_{32, PFL}$) for $T > T_{lim}$ (calibrated coefficient a within parenthesis)				
Calibrated k_r approach	**EW**	**NW**	**NE**	**Hz**	**Gd**
Shallow domain	(a =1.2E–8 m^2/s)	(a =1.2E–8 m^2/s)	(a =5.5E–9 m^2/s)	1.7	1.6
Repository domain	1.0	1.0	0.8	1.0	1.1
Deep domain	(a =7.0E–9 m^2/s)	(a =6.0E–9 m^2/s)	(a =3.0E–11 m^2/s)	1.2	1.0
Tectonic Continuum approach	**EW**	**NW**	**NE**	**Hz**	**Gd**
Shallow domain	(a =1.2E–10 m^2/s)	(a =1.5E–9 m^2/s)	(a =4.3E–10 m^2/s)	2.3	2.2
Repository domain	1.0	1.2	1.2	1.0	1.3
Deep domain	(a =9E–13 m^2/s)	(a =5.7E–11 m^2/s)	(a =4.0E–12 m^2/s)	2.2	1.2

As can be expected, the simulated fracture transmissivity above T_{lim} agrees well with PFL-f data, particularly for the Repository domain. It can be noted that the simulated transmissivity in the Shallow domain is somewhat larger, especially for the Tectonic Continuum approach. This is due to the observed break-points in PFL-f data at 10^{-8} m^2/s, which has may indicate a higher practical detection limit in the Shallow domain that censors PFL-f data below 10^{-8} m^2/s. In other words, if the ratio is recalculated for a transmissivity cut-off equal to the lower fitting point in Figure J-6a and b, it would conform to 1.0.

4.2 Flow simulations

The hydro-DFN SFR model v.0.2 was calibrated to PFL-f data by means of a geometrical/statistical approach (Table 2-1). The calibration was based on geometry alone; actual flow simulations were not used during the calibration phase. The size distributions were varied, set-wise, until the intensity of Connected fractures, as seen by a vertical borehole, was equal to a specified criterion (Appendix J). This criterion was set equal to the intensity of PFL-f records, scaled by a factor (Appendix F). The Connected fractures intercepted by a simulated borehole (scan-line) were assigned size-transmissivity relations taken directly from measured PFL-f apparent transmissivity values in order to match borehole data (Section 2.3.3 and Appendix J). The outcome was two alternative parameterisations of a preliminary hydro-DFN, one based on the connectivity analysis, and one based on the assumption of Tectonic continuum; both were assigned measured properties directly to intersected fractures, without use of flow simulations.

The hydro-DFN calibrated with the connectivity analysis was applied in flow simulations (Appendix G), without further fine-tuning the parameterization. The purpose was to improve the understanding of the current data set, the obtained parameterisation, identify critical pitfalls, and test assumptions to further develop the modelling approach. Two computational softwares were applied in parallel: FracMan and DarcyTools. In FracMan, the flow is solved explicitly inside discrete fracture planes (assuming an impervious rock matrix), while DarcyTools the connected fracture network is translated into an Equivalent Continuous Porous Medium (ECPM). This ECPM translation enhances the connectivity of the fracture network depending on cell size used, as gaps between fractures that are smaller than the applied cell size are not fully represented (see examples in /Svensson et al. 2007/).

4.2.1 Summary of findings

The geometrically conditioned hydro-DFN has systematically lower the specific capacity than the PFL-f data (Figure 4-4). This underestimation is size-dependent (as high as a factor 10 for small fractures). The choking phenomenon is higher in the Shallow domain, probably due to its geometric connectivity dominated by low-transmissive fractures connecting to ground surface. However, these results depend on assumptions and simplifications made in the model setup and can therefore

not be taken as definite. Also, the results depend on the fitted scaling exponents, k_r, and cannot be generalized. It is quite possible that a more well-connected fracture network would suffer less from the effects of hydraulic chokes. Nevertheless, the results from Appendix G clearly demonstrate the necessity of completing the second calibration stage of hydro-DFN parameterisation (the hydraulic method; Table 2-1), in order to fully honour borehole data, at least for model validity within a DFN framework.

Firstly, an inconsistency was found in the calibration target relating $P_{32,\,COF}$ to $P_{32,\,PFL}$ (Appendix G.1. Simulated networks of Connected Open Fractures are Poissonian clusters (Section 2.2.8). This implies that fractures intercepted by a simulated borehole appear as clusters (e.g. Figure G-14). The PFL-f data reflects effective transmissivity over a 0.1 m borehole section. In practise, it is even unrealistic to expect that two neighbouring inflows less than 0.2 m apart can be resolved as two separate features. The distribution of distance to the nearest PFL-f record is shown in Figure G-1. For PFL-f data in HRD there are no records with separation distance 0.2 m, and only 3 records separated 0.3 m. The most common separation distance range from 0.5 to 2 m (Figure G-1). In the interpretation of PFL-f data /Öhman et al. 2010/, all features within 0.1 m (or effectively 0.2 m) sections were not regarded as Connected fractures, but instead as Alternative Best Choices. Out of these alternative candidates, only one is finally selected as "the flowing PFL-f feature". In other words, according to the PFL-f interpretation methodology, the fracture count in PFL-f data over a 0.1 m bin can never exceed 1. In practise, the PFL-f fracture count over a 0.2 m bin never exceeds 1 in the SFR data set.

Thus, the only consistent way to apply the frequency of PFL-f data in the calibration process is in relation to the number of frequency of borehole sections (at 0.1 or 0.2 m scale) that provides a net flow exceeding the detection limit.

Secondly, the effects of hydraulic chokes were demonstrated by comparing geometrically sampled fracture transmissivity to simulated specific capacity for a simulated borehole (details given in Appendix G.2). Geometric borehole sampling is performed by a scan-line (zero-radius), while the true radius was used in flow simulations. The motivation for using a scan-line in geometric sampling is that the vast majority of fractures are reported to intersect the central axis of the borehole. There are two reasons for using the true radius in flow simulations: 1) to accurately represent the non-linear gradient in draw-down close to the borehole perimeter, and 2) all flowing features intersecting the borehole wall will contribute to measured PFL-f inflow, regardless to whether the borehole central axis is intersected or not. The use of different borehole radii provided surprisingly large discrepancies in number of intercepted fractures (cf. total count in flow simulations versus geometric sampling in Figure 4-4). This finding was examined further in Appendix H.

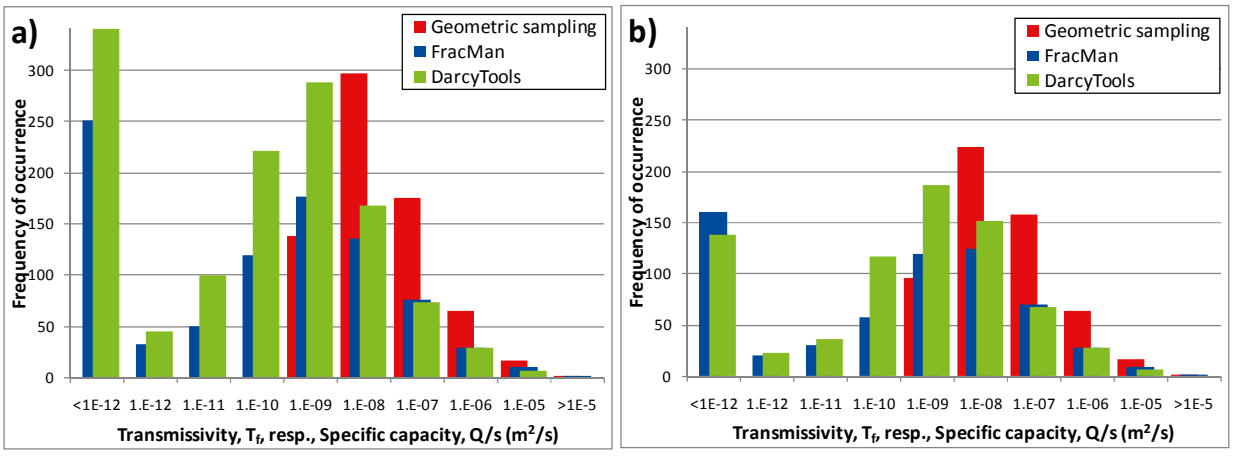

Figure 4-4. *Transmissivity of the connectivity analysis compared to simulated specific capacity over different borehole interval bins; a) bin size = 0.3 m, and b) bin size = 1.0 m. Note that flow simulations involve borehole radius that provide a larger total number of intercepts, as compared to the connectivity analysis, which reflects geometric intercepts with a scan-line. The bin "< 1E–12" reflects non-zero values lower than* $10^{-12.5}$ *m²/s.*

The results of 10 realisations are shown in Figure 4-4. Note that the geometrically sampled fracture transmissivity are directly comparable to PFL-f data (a result of the assumptions made in the connectivity analysis, Appendix J.2.1). However, the simulated specific capacity (Q/s) is systematically lower than the sampled fracture transmissivity, T_f. The discrepancy has a strong dependency to fracture size. Detailed analyses reveal that large fractures tend to be autonomously well-connected to the hydraulic boundary, and so, the difference between T_f and Q/s tends to be small. Small fractures depend on their geometric contact to the Connected fracture network and its upstream transmissivity (subject to hydraulic chokes). In essence, this implies that the PFL-f transmissivity has been inappropriately used in the calibration process, at least for small fractures. The fracture transmissivity for small fractures should be increased about an order of magnitude, in order for the hydro-DFN to be consistent with PFL-f data. Thus, an important conclusion from this evaluation is that the evaluated apparent PFL-f transmissivity does not represent explicit properties of mapped fractures, but rather averaged transmissivity over entire flow paths between the tested borehole section and the hydraulic boundary. In other words, the measured inflow in PFL-f data is also subject to hydraulic chokes. However, the extent, to which these flow simulations accurately demonstrate the hydraulic chokes in PFL-f data, obviously depends on how realistic the hydro-DFN parameterisation is. As stated in Section 2.3, the model can be setup in a considerably more realistic way.

It can also be noted that the FracMan results exhibit a higher control of hydraulic chokes in comparison to results from DarcyTools (cf. Figure 2-2). This discrepancy occurs in spite of the fine discretisation in DarcyTools (decimetre-scale), which is unrealistic for regional-scale modelling, owing to practical limitations (c. 10 m scale).

4.2.2 Hydraulic chokes and different transmissivity models

The hydro-DFN was calibrated with the correlated transmissivity model (Section 2.2.9), which is based on the assumption that there exists a deterministic relation between fracture size and transmissivity. This hydro-DFN was directly applied in flow simulations (Appendix G.2); consequently, those results were also based on the Correlated model, eq. (2-4). Flow simulations demonstrate that hydraulic chokes primarily affect small fractures, while larger fractures are better connected to the hydraulic boundary, and thus there is little difference between assigned fracture transmissivity and simulated specific capacity for larger fractures (Figure 4-5b). Evidently, hydraulic chokes contribute to a size-dependent variability component in the PFL-f data. However, these findings relate to the Correlated model, eq. (2-4). Hydraulic chokes relate to the combined effects of: 1) amount of geometric contact between fractures, as well as, 2) upstream fracture transmissivity. In order to evaluate the interplay between hydraulic chokes and the variability in assigned fracture transmissivity, other transmissivity models were explored in flow simulations.

Ten realizations of Connected Open Fractures were selected from the previous study (Appendix G.2). Thus, the results for the correlated model were already at hand (Figure 4-5b). The fracture geometry and model setup for these 10 realizations was maintained intact (details given in Appendix G.2), only the fracture transmissivity, T_f, was modified according to different test cases (the differences between these cases are conceptually illustrated in Figure 4-5f):

b) Constant T: $T_f = 10^{-6}$ m^2/s, without stochastic variability or dependency to size.

c) Correlated model: this is the base case, eq. (2-4), T_f is assumed deterministically dependent on size, determined by the coefficients *a* and *b*. Results are known from Appendix G.2.

d) Cone model: this is a variant of the semi-correlated model, eq. (2-5), where the mean T_f is assumed dependent on size by the coefficients *a* and *b*. It also has a stochastic component that increases with size, such that the standard deviation σ_{logT}, is assumed equal to 0.0 at $r = r_0$ and equal to 1.0 at $r = r_{max}$.

e) Semi-correlated model: the mean T_f is assumed size- dependent by the coefficients, *a* and *b*, and the stochastic component σ_{logT}, which is constantly assumed equal to 1.0, eq. (2-5).

f) Uncorrelated model: T_f is assigned stochastic variability, independently of size, eq. (2-3). In order to preserve the statistical moments from case b), the random values were not drawn from a lognormal distribution. Instead, the random values were randomly taken from bore-hole sampled fractures in case b), with transmissivity exceeding 10^{-10} m^2/s. The random values were drawn separately by fracture set and depth domain, but without respect to the actual fracture size.

Cases a) and b) were only run once per DFN geometry, as they do not contain a random component, whereas cases c), d), and e) were run for 10 different random seeds. All simulations are compared to a "Target range", which is sampled fracture transmissivity in the connectivity analysis, and corresponds to the expected distribution of PFL-f transmissivity for a vertical borehole of equal length. Note also, that the results presented here represent the total samples of borehole inflow (not presented per fracture set and depth domain).

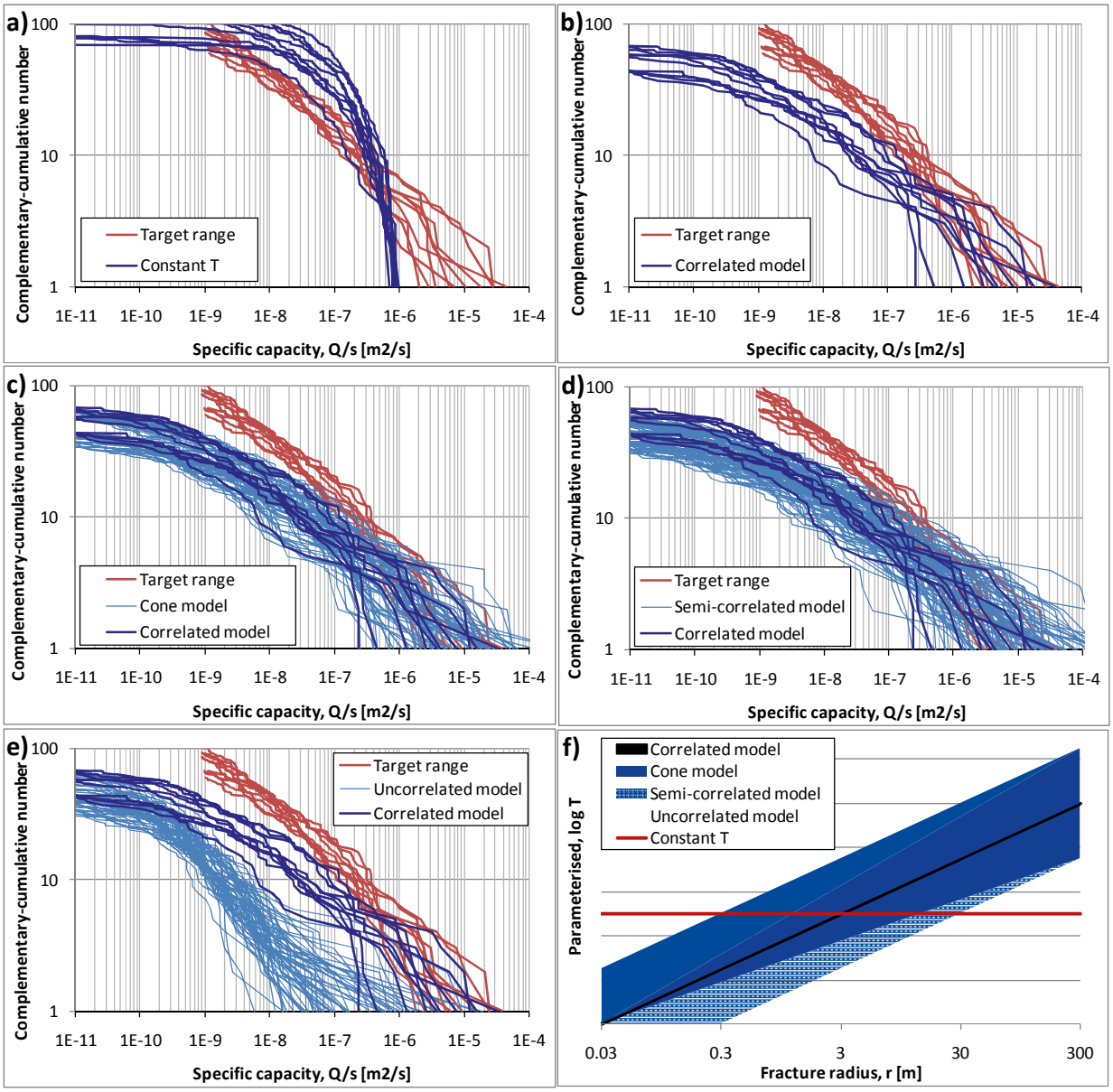

Figure 4-5. *Simulated distributions of specific capacity for tested size-transmissivity relations; a) constant fracture transmissivity, b) Correlated model, c) Cone model, d) semi-correlated model, e) uncorrelated model, and f)conceptual illustration of the different transmissivity models. Note that figure f) has no scale on the y-axis, as the actual values depend on fracture set and depth domain.*

The constant T case (a) demonstrates the explicit variability in simulated flow owing to hydraulic chokes (i.e. without the presence of hydraulic chokes, the simulated specific capacity is expected to be constantly equal to 10^{-6} m^2/s). This means that the variability in assigned fracture transmissivity cannot be evaluated directly from PFL-f data, without information on the variability arising from hydraulic chokes. The Cone model demonstrates that the stochastic variability (primarily) assigned to larger fractures, as a net effect, enhances the choking effect on fractures with initially low specific capacity (cf. light blue and dark blue lines in Figure 4-5c). This net effect is accentuated in the Semi-correlated model (Figure 4-5d). The Uncorrelated model results in simulated specific capacity about two orders of magnitude below the "Target range", although a similarity in slopes can be noted. In this case, hydraulic chokes are predominantly determined by upstream fracture transmissivity. For example: in this case, a 100 m fracture, may serve as the geometric connection for an entire fracture cluster, yet it can be randomly assigned a low transmissivity value (say, 10^{-9} m^2/s), and thus choking the entire downstream cluster.

5 Conclusions

This report has presented a data analysis, a preliminary hydro-DFN parameterisation, and preparatory investigations for the development of the final hydrogeologic model SFR v. 1.0. The currently available hydrogeologic data from the ongoing Site Investigations SFR are applied. However, during the course of this study, no updated Geological model was available. Therefore, all analyses were based on data from the rockmass outside Possible Deformation zones, according to the Single Hole Interpretation. In absence of an updated Geological model, it was decided not to perform the complete DFN calibration, but instead to use a simplified approach and re-direct the focus towards developing a strategy for the final model version. Much attention has been given to understanding the role of PFL-f data in the hydro-DFN calibration, as well as exploring the consistency in methodology concepts, in order to avoid potential pitfalls.

The main issues raised for the overall hydrogeological modelling programme of SFR are numbered 1–7 in section 1.2. Some, but not all, of these issues have been addressed at this modelling stage:

1) **Hydraulic properties of HCDs:** No updated Geological model was available during this work. Consequently, it was not considered meaningful to evaluate hydraulic properties of Possible Deformation Zones (PDZs).
2) **Hydraulic properties of HRD:** Hydraulic data have been analysed and parameterised by means of a hydro-DFN. The hydraulic data are clearly anisotropic, dominated by horizontal, gently dipping, and North-west striking sub-vertical fractures. Depth trends have been observed in Open fractures and PFL-f data, with decreasing intensity and transmissivity with depth. The depth trend in PFL-f data is stronger than that in Open fractures (cf. Figure 3-18h and Figure 3-19h), implying that there is also a depth trend in connectivity. It can be noted that the PFL-f intensity is not set-wise proportional to the Open fracture intensity; instead they are clearly dominated by horizontal and gently dipping fractures (even in upper parts of the sub-horizontal borehole KFR105). The indications of high intensity and transmissivity in shallow bedrock 0 to –60 m RHB70 is dominated by data from KFR102B and KFR103, but is also supported by the evaluation of historic data /Öhman and Follin 2010/. The intensity of Connected fractures above the transmissivity detection limit is low below an elevation of –250 m RHB70.
3) **Hydraulic connectivity:** Unfortunately, the degree of compartmentalization cannot be evaluated by a comparison between PFL-f data and injection test data, as the latter data type is unavailable. However, much attention has been given to the relation between connectivity and PFL-f data in the hydro-DFN parameterisation (Appendix J and F) and the subsequent DFN flow simulations (Appendix G). Methodological issues are specified in Table 5-1.
4) **Indication of Sheet joints:** This important issue cannot be adequately resolved at this modelling stage. The largest observed transmissivities are on the order 10^{-5} m^2/s, which is considerably lower than observations in shallow rock in the Forsmark Site (Appendix D). Anomalous PFL-f data have been suggested in the elevation interval –169 to –190 m RHB70 in boreholes KFR102A and KFR27 (Section 3.1.7). During the field investigations a hydraulic connection was found between the two boreholes within this interval; this interval also hosts crush zones in both boreholes. Most notably, PFL No. 38 in KFR102A has a drastic influence on the maximum simulated transmissivity for set NE (two orders of magnitude). It is speculated if this interval reflects a potentially missed deformation zone connected to ZFM871, or possibly even an unusually deep sheet joint.
5) **Difference between HCD and HRD:** At this modelling stage, only PDZ can be compared to HRD. No general differences in hydraulic character can be inferred between PDZ and HRD; some PDZs do reflect anomalously high transmissivity, while others have lower transmissivity than the surrounding HRD (see Section 3.1.8 and figures in Appendix C). It is suspected that PDZs cannot be compared to the HRD as a uniform population, but that HCDs comprise a heterogeneous population with different characteristics, depending on orientation.

6) **Support for fracture domains:** Indications of possible lateral trends have been observed (Section 3.1.3), with increasing dominance of the NW-striking set towards the Singö-zone (KFR104 and KFR105), while the North-eastern part of the domain (KFR101, KFR102A, KFR102B, and KFR103) is more dominated by horizontal Open fractures at depth, and EW-striking fractures at the shallow depth. The difference is larger in terms of PFL-f transmissivity, with higher transmissivity in the North-eastern than the South-western part. In the absence of an updated Geological model, it is premature to state to what extent these observations should be taken as true evidence for fracture domains, or as artefacts of data scarcity, sampling bias, local heterogeneity, and borehole location with respect to deformation zones.

7) **Depth trend:** Based on visual inspection, it is judged that a depth trend does exist in PFL-f transmissivity (Sections 3.1.6 and 3.3.1, also Figure 3-9). This is difficult to support by statistical tests, owing to a "depth trend" in data coverage (Section 2.2.2) and uncertainties related to the absence of an updated Geologic model. In spite of data gaps, the shallow rock, i.e. the upper 60 m, seems to be more transmissive in general. This finding is also supported by older hydraulic data that was obtained during the construction of SFR (Figure 3-20). Below 245 m depth borehole data outside deformation zones are scarce, but transmissivity appears to be lower and the intensity in PFL-f data is considerably lower.

To summarize the findings of the DFN parameterisation, visual inspection of Kamb-contoured stereoplots suggests three sub-vertical sets: EW-striking, NW-striking, and NE-striking, as well as one sub-horizontal set. The hydraulic DFN representation improves with the inclusion of a fifth, Gently dipping set. This Gently dipping set is wide spread, completely overlaps the horizontal set and partly overlaps the sub-vertical sets, and has intermediate transmissivity. In general, the hydraulic anisotropy seems dominated by sets Hz, Gd, and NW.

A preliminary hydro-DFN parameterisation was calibrated by a simplified statistical/geometrical method. The size distribution of Connected fractures was calibrated by an iterative connectivity analysis for multiple DFN realisations, after which set-specific transmissivity-size relations were established by statistical matching to PFL-f data. From a conceptual viewpoint, this is an appealing and highly consistent approach; however owing to the limitations in data it suffers severely from non-uniqueness (i.e. for a wide range of fitted size distributions, a transmissivity-size relation can be fine-tuned so as to match the PFL-f data above T_{lim}). In other words, the calibrated size distribution of Connected fractures is highly uncertain. A Tectonic Continuum-based approach is suggested as an alternative for the sub-vertical sets. It cannot be concluded which of the two approaches is the more realistic; its purpose is to demonstrate that the uncertainty in the characterisation of rock require different conceptual approaches, which render alternative possible solutions.

The preliminary hydro-DFN was applied in flow simulations to test its performance and different test cases. A number of insights were achieved, which are useful for setting up a strategy for developing the final hydrogeological model SFR v. 1.0 (Table 5-1). An interesting speculation is that the significance of hydraulic chokes must be considered in modelling context (Figure 2-2); the negligence in accounting for chokes in the calibration stage (bullet 4 in Table 5-1) may very well be compensated by a negligence in accounting for chokes in a subsequent translation into ECPM properties in a regional-scale model (bullet 9 in Table 5-1). In other words, if the simplifications in the connectivity analysis are compatible with those in the downstream application, it may well provide a realistic description of the rockmass at the large scale, even if discrepancies can be identified at the local scale.

Table 5-1. Methodological aspects for consideration in the hydrogeological model SFR v. 1.0.

1.	Model setup	The DFN calibration was made with a simplified model configuration (Section 2.3). Considerable improvement must be made to geometric representation of borehole orientation and deformation zone geometry. The fracture generation domain must be expanded to avoid boundary effects in intensity. Perhaps, the variation in PFL-f data can be better reproduced, if the variable censoring detection limit of PFL-f data is applied to flow simulations in a realistic way (as opposed to using a constant T_{lim}).
2.	Geometric calibration target	The applied calibration target: $P_{32,\,COF} = [2 \ldots 4] \times P_{32,PFL}$ was formed out of necessity, rather than based on solid evidence (Appendix F). It could not be satisfied for all sets, but this failure was found to be irrelevant in the subsequent transmissivity calibration, given the additional degrees of freedom in constants *a* and *b* of the transmissivity parameterisation (Appendix J). Unless the fitted size scaling parameters k_r are unrealistic, this inconsistency is expected to be obsolete after completion of the second stage of calibration (hydraulic method; Table 2-1).
3.	Intensity of PFL-f data	A PFL-f record is a borehole section where **apparent transmissivity** (interpreted transmissivity) exceeds the practical detection limit; it may well reflect the total inflow of several fractures. In the current study, the intensity calculations of simulated Connected fracture networks did not properly account for the spatial resolution of PFL-f data. By definition, the number of PFL-records over a 0.1 m borehole section cannot exceed 1, whereas there may be several simulated fractures over the same interval. The model will underestimate the true intensity (Appendix G.1). Recommendation: consistency requires that simulation results must also be binned over borehole sections, before comparison to PFL-f data.
4.	Role of PFL-f transmissivity	In this study, the apparent PFL-f transmissivity was assumed to reflect the explicit transmissivity of the fractures intercepted by the borehole. This assumption relies on cylindrical flow regime that is well-connected to the hydraulic bounds. This assumption appears to be inconsistent for the current hydro-DFN approach, due to presence of upstream hydraulic bottle-necks (Figure 2-1; Appendix G.2). The geometry-based calibration approach does not guarantee that PFL-f data is honoured in terms of flow. Unless the fitted size scaling parameters k_r are unrealistic, this inconsistency is expected to be overcome in the second calibration stage (hydraulic method; Table 2-1).
5.	Variability in apparent PFL-f transmissivity	Hydraulic chokes may constitute large component of the variability in evaluated apparent transmissivity of PFL-f data. Likewise, the variable distance to the surrounding deformation zones (head boundaries), and the locally variable censoring detection limit may contribute to spatial trends in PFL-f variability. This is expected to be accounted for by applying the hydraulic method and a more realistic model set up (see item 1.), although it raises concerns regarding non-unique solutions.
6.	Discretisation at borehole intercepts	In a numerical application of the hydro-DFN model, the true borehole must be exhaustively discretised in order to reproduce expected inflow with high precision (elements below centimetre scale; Appendix G). However, this was found to be of lesser importance; using a considerable coarser discretisation flow can be reasonably well solved with a correction factor (decimetre-scale elements).
7.	Fracture size	Borehole radius is not accounted for in the scan-line sampling. The vast majority of Open fractures mapped in Boremap intersect the borehole centre (CENTRUM_COVERED = 99%). This would imply that only 1% of the intensity is neglected if simulated borehole exploration is approximated by a scan-line. However, flow simulations where the true borehole radius is applied, suggests that, either the proportion of neglected fractures is considerably higher (implying that such intercepts are difficult to detect), or the modelled minimum fracture size, r_0, is larger than 0.038 m (Appendix H). Increasing r_0 is expected to have a drastic effect on connectivity. The most interesting finding in Appendix H is that horizontal fractures may be considerably larger than other sets.
8.	Tectonic continuum	Tectonic continuum is a convenient working hypothesis in DFN simulations, arising from absence of intermediate scale data. The size scaling parameter k_r fitted by the connectivity analysis do not conform to the intensity of deformation zones (Appendix J). Two alternative size parameterisations are presented; both conditioned to transmissivity (see item 2.), in terms of geometrical sampling. This demonstrates the difficulty in non-unique solutions resulting from calibration to the upper tail of distributions (Appendix F), but also uncertainty in the applicability of the assumed Tectonic continuum.
9.	DFN application in Regional-scale modelling	Application in DarcyTools regional-scale modelling entails a step of upscaling of the Connected fracture network (GEHYCO), where the normal cell size is tens of meters. This upscaling scheme is not flow-based, which implies that hydraulic chokes are not accounted for, i.e. cell conductivities may become too large. If indeed the flowing fracture network is predominantly controlled by the fine-detailed geometry at fracture contacts, then there is a clear risk that the GEHYCO upscaling method is inappropriate, unless a very detailed discretisation can be applied at fracture contacts (Section 2.1).

References

SKB's (Svensk Kärnbränslehantering AB) publications can be found at www.skb.se/publications.

Berglund J, 2008. Site investigation SFR. Geological mapping and laser scanning of the lower construction tunnel. SKB P-09-74, Svensk Kärnbränslehantering AB.

Carlsson A, Christiansson R, 2007. Construction experiences from underground works at Forsmark. Compilation Report. SKB R-07-10, Svensk Kärnbränslehantering AB.

Christiansson R, Bolvede P, 1987. Byggnadsgeologisk uppföljning. Slutrapport. SKB SFR 87-03, Svensk Kärnbränslehantering AB (in Swedish).

Curtis P, Petersson J, Triumph C-A, Isaksson H, 2009. Site investigation SFR. Deformation zone modelling. Model version 0.1. SKB P-09-48, Svensk Kärnbränslehantering AB.

Davis J C, 2002. Statistics and data analysis in geology. 3rd ed. New York: Wiley.

Fisher R, 1953. Dispersion on a sphere. Proceedings of the Royal Society of London. Series A, Mathematical and Physical Sciences, 217, pp 295–305.

Follin S, Stigsson M, Svensson U, 2005. Regional hydrogeological simulations for Forsmark – numerical modelling using DarcyTools. Preliminary site description. Forsmark area – version 1.2. SKB R-05-60, Svensk Kärnbränslehantering AB.

Follin S, Johansson P-O, Levén J, Hartley L, Holton D, McCarthy R, Roberts D, 2007a. Updated strategy and test of new concepts for groundwater flow modelling in Forsmark in preparation of site descriptive modelling stage 2.2. SKB R-07-20, Svensk Kärnbränslehantering AB.

Follin S, Levén J, Hartley L, Jackson P, Joyce S, Roberts D, Swift B, 2007b. Hydrogeological characterisation and modelling of deformation zones and fracture domains, Forsmark modelling stage 2.2. SKB R-07-48, Svensk Kärnbränslehantering AB.

Follin S, Johansson P-O, Hartley L, Jackson P, Roberts D, Marsic N, 2007c. Hydrogeological conceptual model development and numerical modelling using CONNECTFLOW, Forsmark modelling stage 2.2. SKB R-07-49, Svensk Kärnbränslehantering AB.

Follin S, Hartley L, Jackson P, Roberts D, Marsic N, 2008. Hydrogeological conceptual model development and numerical modeling using CONNECTFLOW, Forsmark modeling stage 2.3. SKB R-08-23, Svensk Kärnbränslehantering AB.

Fox A, La Pointe P, Hermanson J, Öhman J, 2007. Statistical geological discrete fracture network model. Forsmark modeling stage 2.2. SKB R-07-46, Svensk Kärnbränslehantering AB.

Gustafson G, 2009. Hydrogeologi för bergbyggare. Stockholm: Formas (in Swedish).

Holmén J G, Outters N, 2002. Theoretical study of rock mass investigation efficiency. SKB TR-02-21, Svensk Kärnbränslehantering AB.

Holmén J G, Stigsson M, 2001. Modelling of future hydrogeological conditions at SFR. SKB R-01-02, Svensk Kärnbränslehantering AB.

Hurmerinta E, Väisäsvaara J, 2009a. Site investigation SFR. Difference flow logging in boreholes KFR104 and KFR27 (extension). SKB P-09-20, Svensk Kärnbränslehantering AB.

Hurmerinta E, Väisäsvaara J, 2009b. Site investigation SFR. Difference flow logging in borehole KFR102A. SKB P-09-21, Svensk Kärnbränslehantering AB.

Kamb W B, 1959. Ice petrofabric observations from Blue Glacier, Washington, in relation to theory and experiments. Journal of Geophysical Research, 64, pp 1891–1919.

Kristiansson S, Väisäsvaara J, 2008. Site investigation SFR. Difference flow logging in boreholes KFR102B and KFR103. SKB P-08-99, Svensk Kärnbränslehantering AB.

Mauldon M, Mauldon J G, 1997. Fracture sampling on a cylinder: From scanlines to boreholes and tunnels. Rock Mechanics and Rock Engineering, 30, pp 129–144.

Munier R, 2004. Statistical analysis of fracture data, adapted for modelling Discrete Fracture Networks – Version 2. SKB R-04-66, Svensk Kärnbränslehantering AB.

Odén M, 2008. Site investigation SFR. Hydrogeological modelling at SFR using DarcyTools. Site description SFR version 0.0. SKB P-08-94, Svensk Kärnbränslehantering AB.

Olofsson I, Simeonov A, Stephens M, Follin S, Nilsson A-C, Röshoff K, Lindberg U, Lanaro F, Fredriksson L, 2007. Site descriptive modelling Forsmark, stage 2.2. A fracture domain concept as a basis for the statistical modelling of fractures and minor deformation zones, and interdisciplinary coordination. SKB R-07-15, Svensk Kärnbränslehantering AB.

Pekkanen J, Pöllänen J, Väisäsvaara, J, 2008. Site investigation SFR. Difference flow logging in boreholes KFR101 and KFR27. SKB P-08-98, Svensk Kärnbränslehantering AB.

Petersson J, Curtis P, Bockgård N, Simeonov A, Mattsson H, Döse C, Stråhle A, Winell S, 2009a. Site investigation SFR. Geological single-hole interpretation of KFR102B and KFR103. SKB P-09-33, Svensk Kärnbränslehantering AB.

Petersson J, Curtis P, Bockgård N, Simeonov A, Mattsson H, Gustafsson J, Stråhle A, 2009b. Site investigation SFR. Geological single-hole interpretation of KFR101, HFR101, HFR102 and HFR105. SKB P-09-34, Svensk Kärnbränslehantering AB.

Petersson J, Nissen J, Bockgård N, Simeonov A, Thunehed H, Döse C, Stråhle A, Winell S, 2009c. Site investigation SFR. Geological single-hole interpretation of KFR104 and KFR27. SKB P-09-35, Svensk Kärnbränslehantering AB.

Petersson J, Nissen J, Curtis P, Bockgård N, Öhman J, Mattsson H, Stråhle A, Winell S, 2009d. Site investigation SFR. Geological single-hole interpretation of KFR102A. SKB P-09-60, Svensk Kärnbränslehantering AB.

Petersson J, Nissen J, Curtis P, Bockgård N, Öhman J, Mattsson H, Stråhle A, Winell S, 2010. Site investigation SFR. Geological single-hole interpretation of KFR105. SKB P-10-06, Svensk Kärnbränslehantering AB.

Priest S D, 1993. Discontinuity analysis for rock engineering. New York: Chapman & Hall.

Rhén I, Follin S, Hermanson J, 2003. Hydrogeological Site Descriptive Model – a strategy for its development during Site Investigations. SKB R-03-08, Svensk Kärnbränslehantering AB.

Robin P-Y F, Jowett E C, 1986. Computerized density contouring and statistical evaluation of orientation data using counting circles and continuous weighting functions. Tectonophysics, 121, pp 207–223.

SKB, 2008a. Geovetenskapligt undersökningsprogram för utbyggnad av SFR. SKB R-08-67, Svensk Kärnbränslehantering AB (in Swedish).

SKB, 2008b. Site description of Forsmark at completion of the site investigation phase. SDM-Site Forsmark. SKB TR-08-05, Svensk Kärnbränslehantering AB.

Stephens M B, Fox A, La Pointe P, Simeonov A, Isaksson H, Hermanson J, Öhman J, 2007. Geology Forsmark. Site descriptive modelling Forsmark stage 2.2. SKB R-07-45, Svensk Kärnbränslehantering AB.

Svensson U, 2004. DarcyTools, Version 2.1. Verification and validation. SKB R-04-21, Svensk Kärnbränslehantering AB.

Svensson U, Ferry M, 2004. DarcyTools, Version 2.1. User's guide. SKB R-04-20, Svensk Kärnbränslehantering AB.

Svensson U, Kuylenstierna H-O, Ferry M, 2007. DarcyTools, Version 3.4. Concepts, methods, equations and demo simulations. SKB R-07-38, Svensk Kärnbränslehantering AB.

Terzaghi R D, 1965. Sources of error in joint surveys. Géotechnique, 15, pp 287–304.

Wang X, 2005. Stereological interpretation of rock fracture traces on borehole walls and other cylindrical surfaces. Ph. D. thesis. Virginia Polytechnic Institute and State University.

Yow J L, 1987. Technical Note: Blind zones in the acquisition of discontinuity orientation data, International Journal of Rock Mechanics and Mining Sciences & Geomechanics Abstracts, 24, pp 317–318.

Öhman J, 2010. Site investigation SFR. Hydrogeologic modelling of SFR v 0.1. Influence of the ridge on the flow fields for different target volumes. SKB R-09-43, Svensk Kärnbränslehantering AB.

Öhman J, Follin S, 2010. Site investigation SFR. Hydrogeological modelling of SFR. Data review and parameterisation of model version 0.1. SKB P-09-49, Svensk Kärnbränslehantering AB.

Öhman J, Sträng M, Moverare J, 2010. Site investigation SFR. PFL-f linking to Boremap data. KFR101, KFR102A, KFR102B, KFR103, KFR104, KFR105, KFR106 and KFR27. SKB P-10-01, Svensk Kärnbränslehantering AB.

Appendix A

Preliminary Hydro-DFN parameterisation v.0.2, submitted to SR-Site by 2009-11-27

This parameter table was prepared for SR-Site modelling purposes by the date 2009-11-27. By the date 2010-01-08, an error was detected in the parameterisation of the Shallow and Deep domains (marked by red in Table A-1). The source of the error was communicated and the corrected parameter values (Table A-1) were re-submitted to the SR-Site modelling team, by the date 2010-01-08.

Table A-1. Hydro-DFN model parameterisation, based on connectivity analysis.

Domain		Intensity [4]		Size		Orientation			Transmissivity ($T = a\ r^b$)	
	Set	$P_{32\ (r0,\ 169\ m)}$	$P_{32\ Tot}$	r_0	k_r	Tr	Pl	Fisher κ	a	b
Shallow										
> –60 m (RHB70)	EW	2.597	2.598	0.038	3.45	2.7	7.4	12.6	NA[2]	NA[2]
	NW	1.153	1.154	0.038	3.1	232.7	11.9	13.2	NA[2]	NA[2]
	NE	1.339	1.339	0.038	3.45	128.3	8.2	11.7	NA[2]	NA[2]
	HZ[5]	1.059	1.062	0.038	2.6	115.9	84.5	27.6	1.41E–7	1.43
	Gd[5]	1.865	1.871	0.038	2.79	232.2	85.1	6.5	2.11E–8	1.09
Repository										
–60 to –245[1] m	EW	1.407	1.407	0.038	3.45	5	12.7	8.5	6.00E–9	1.29
(RHB70)	NW	0.856	0.856	0.038	2.95	234	6	12.3	8.00E–9	1.13
	NE[3]	1.033	1.033	0.038	3.45	128.2	5.5	11.5	1.00E–8	1.25
	HZ	0.848	0.850	0.038	2.55	137	84.3	42.9	2.06E–9	1.85
	Gd	1.204	1.208	0.038	2.72	354.2	85.4	7.1	4.00E–9	1.05
Deep										
< –245[1] m	EW	0.918	0.918	0.038	3.45	2.5	19.6	9.7	NA[2]	NA[2]
(RHB70)	NW	0.867	0.867	0.038	3.1	233.3	7	14.9	NA[2]	NA[2]
	NE	1.023	1.023	0.038	3.45	304.7	0.1	11.2	NA[2]	NA[2]
	HZ[5]	0.595	0.596	0.038	2.75	127.7	80.9	27.9	1.34E–9	1.32
	Gd[5]	1.283	1.287	0.038	2.7	269.8	84.5	6.6	9.80E–10	0.93

[1] Approximate average borehole intercepts with ZFM871 (KFR102A and KFR27) based on SFR geologic model v.0.1

[2] Not evaluated because of scarce data. It is recommended that downstream modelling teams formulate their own strategy to extrapolate set-wise parameterisation from the repository level

[3] Based on exclusion of PFL No. 38 in KFR102A. The final SFR Geo model v. 1.0 is not complete, and thus the HRD of the hydro-DFN v .0.2 is strictly based on SHI interpretation. However, this PFL record is an outlier with respect to the complete data set, and therefore it is currently hypothesised that this PFL-record may be assigned to HCD in the final SFR Geo-model.

[4] The smallest modelled deterministic zones are on the order 300 m (SFR Geo. v.0.1), corresponding to a radius of 169 m. Stochastic fractures are therefore assumed to have a maximum radius of 169 m. Based on assumption of tectonic continuum, a total P_{32} (deterministic + stochastic features) is calculated for conversion to the DarcyTools intensity parameter.

[5] The maximum Terzaghi weight was set to about 25 in the updated SFR model. In the SDM, the weight was set to 7 (cf. R-07-48).

By 2009-11-27, the following erroneous values were reported to SR-Site:

Shallow domain, set HZ:	$a = 1.97\times10^{-8}$ m²/s,	b = 1.457
Shallow domain, set Gd:	$a = 3.70\times10^{-9}$ m²/s,	b = 1.16
Deep domain, set HZ:	$a = 1.36\times10^{-9}$ m²/s,	b = 1.45
Deep domain, set Gd:	$a = 2.20\times10^{-9}$ m²/s,	b = 0.90

Table A-2. Decisions taken by Sven Follin, 2009-11-27.

Domain		Transmissivity ($T = a\ r^b$)	
Shallow	**Set**	**a**	**b**
> –60 m (RHB70)	EW	6.00E–09	1.29
	NW	8.00E–09	1.13
	NE	1.00E–08	1.25
Deep	Set	a	b
< –245 (RHB70)	EW	6.00E–09	1.29
	NW	8.00E–09	1.13
	NE	1.00E–08	1.25

Appendix B

Excluded data: Sealed fractures, percussion boreholes, and KFM11A

The purpose of this Appendix is to briefly present some characteristics of data types that have been excluded from the parameterisation of the SFR hydro-DFN v.0.2. These excluded data types are Sealed fractures, which are assumed to be impervious, percussion borehole data which have lower confidence in data, and the cored borehole KFM11A which is located outside the Local SFR domain, and appears to be influenced by the Singö deformation zone.

Orientation patterns of Sealed and Open fractures

In the data analysed (KFR101, KFR102A, KFR102B, KFR103, KFR104, KFR105, and KFR27), three orthogonal fracture sets clearly dominate: sub-vertical NW- and EW-striking, and Gently dipping (or even sub-horizontal; Figure B-1). This is very similar to earlier observations made during the construction of SFR and Site Investigation Forsmark. There is a clear difference in orientation patterns between Open and Sealed fractures (Figure B-1). Sub-horizontal fractures are predominantly Open, while the subvertical NW- and NE-striking fractures are predominantly Sealed. There are several combined explanations for this, relating to the anisotropic stress regime, fracture genesis, and age; shallow horizontal fractures are younger, formed by glacial loading/unloading, while the subvertical fractures and gently dipping fractures relate to tectonic regimes during the later part of the Svecokarelian orogeny /Stephens et al. 2007/. Sheet joints are found down to –40 m RHB70 /Carlsson and Christiansson 2007/, but it appears likely that stress relief may also tend to open the horizontal subset of the pre-existing gently dipping set down to larger depths. The current stress regime ($\sigma_1 = \sigma_H$ at a bearing of 310°, and $\sigma_3 = \sigma_v$ in KFR27) tends to open horizontal fractures, and close NE-striking subvertical fractures. Over time, chemical weathering/precipitation processes tend to accentuate the anisotropic effect that the stress field has on the fracture network; flowing fractures (primarily horizontal, Open fractures) are subject to aggressive meteroric groundwater that dissolves fracture minerals such as calcite. On the other hand, dissolved constituents may precipitate as mineral filling in more stagnant water (for example in low transmissive subvertical fractures).

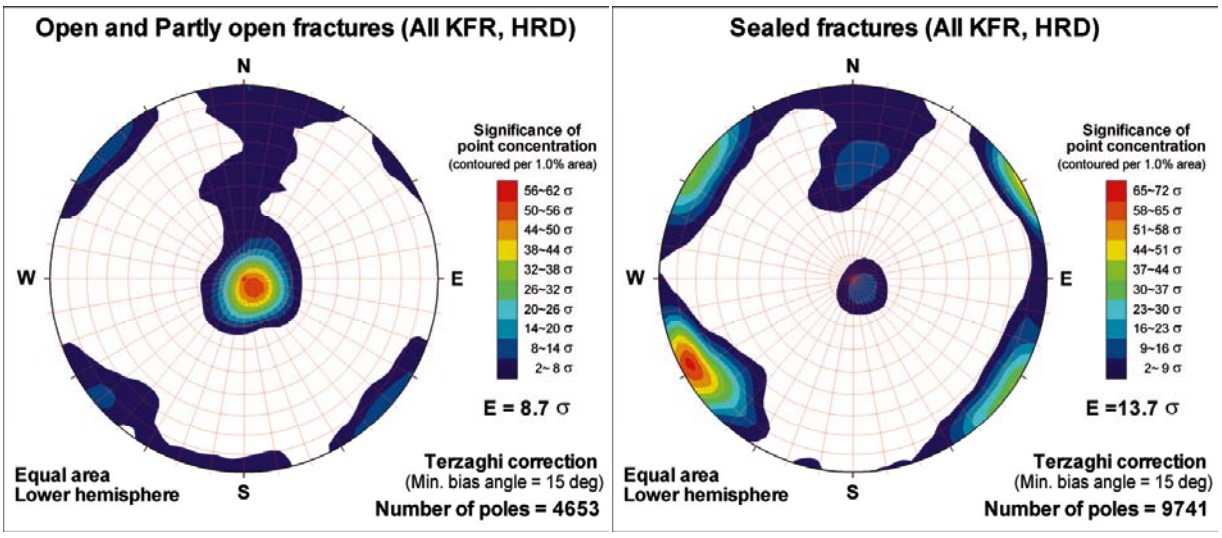

Figure B-1. *Kamb-contoured orientation of Open and Partly open versus Sealed fractures visible in BIPS cored boreholes (HRD).*

Percussion borehole data

Percussion borehole data are known to have a considerably lower confidence, both in mapped fractures and hydraulic data. The reason is that the fracture mapping in percussion boreholes relies on the resolution of BIPS imagery. Based on geologic mapping of *cored* boreholes it is known that a subset of the fracture population that has been confirmed as natural fractures (i.e. not borehole-induced fractures) in the core cannot be seen in BIPS, owing to image resolution. It is also known that in BIPS inspection, dark mineral infill in Sealed fractures is frequently mistaken for the aperture of Open fractures. To evaluate the reliability in percussion borehole data, they were evaluated and compared to the characteristics of the cored boreholes. If the percussion data have systematic deviating fracture characteristics, it is taken as an indication of measurement errors.

In the data from all cored boreholes included in this study (Figure 1-1), 27% of all fractures in HRD are mapped as Open or Partly open (in terms of Terzaghi weight sum), whereas the corresponding fraction is 44% in percussion-drilled boreholes. If the boreholes from Site Investigation Forsmark, HFM33–35 and KFM11A, are excluded, the corresponding fractions are 28%, respectively, 39%. Based on similar observations, percussion borehole data were excluded in the derivation of the geo-DFN in the Site Investigation Forsmark /Fox et al. 2007/.

Furthermore, the fractures interpreted as Open and Partly open in percussion data (HFR101–105) have an orientation pattern which is similar to the Sealed fractures in cored boreholes (predominantly subvertical NW-striking; Figure B-2), whereas the Open and Partly open fractures in core data

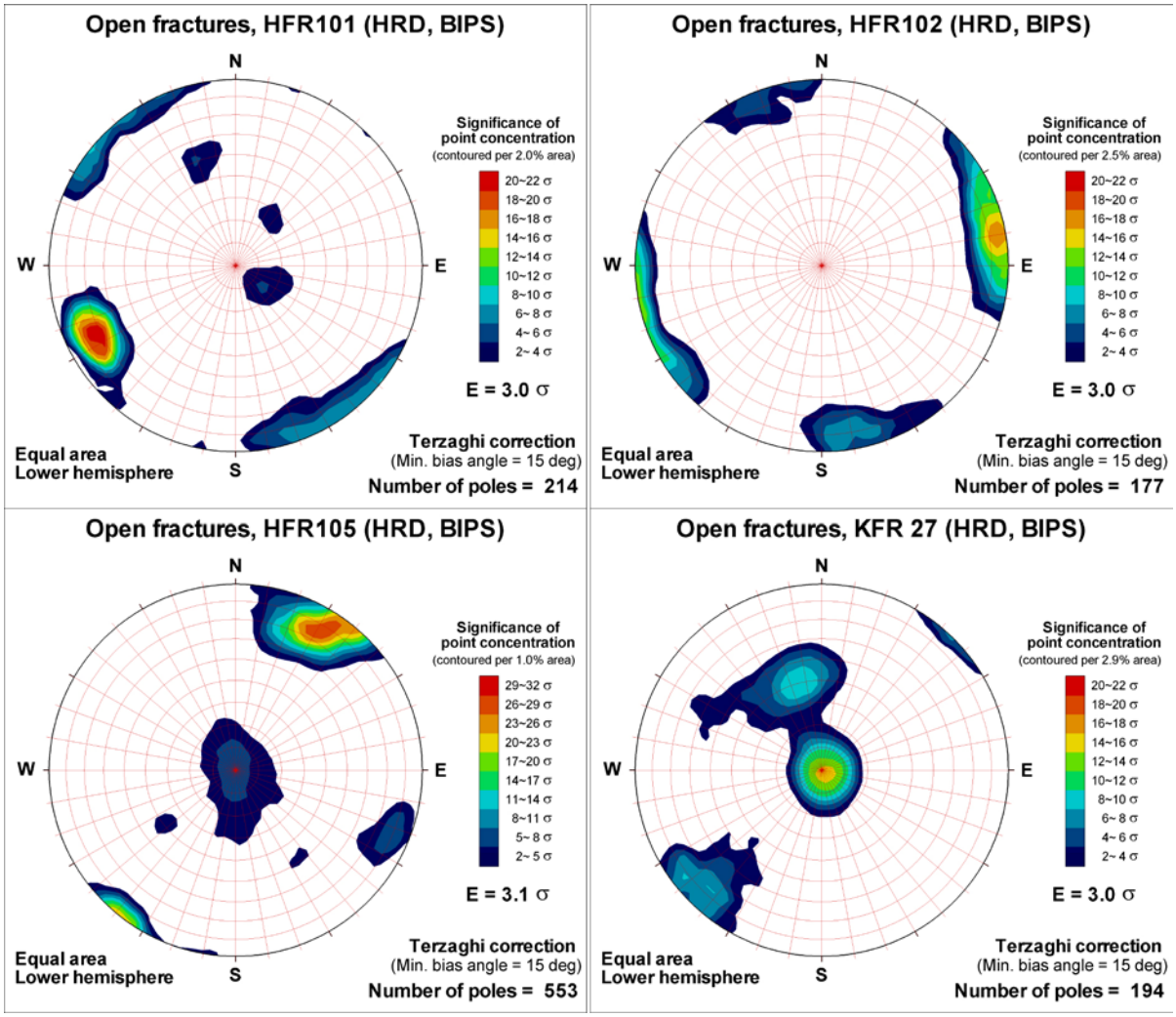

Figure B-2. *Kamb-contoured orientation of Open and Partly open fractures visible in BIPS percussion boreholes (HRD). Only the upper part of KFR27 is included, where core is missing.*

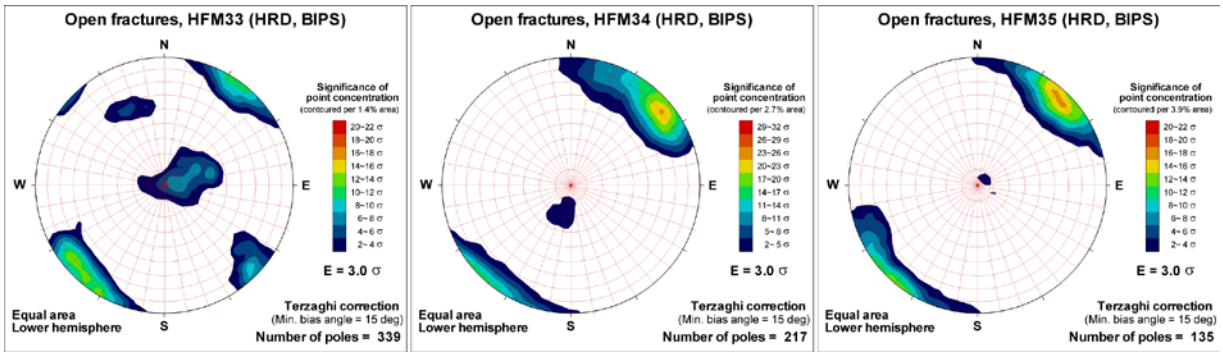

Figure B-3. *Kamb-contoured orientation of Open and Partly open fractures in HRD from Site Investigation Forsmark boreholes; the percussion boreholes HFM33–35.*

are predominantly sub-horizontal (cf Figure B-1). It is difficult to clearly state the extent to which this deviating orientation pattern reflects accidental inclusion of Sealed fractures, or the possible influence from the Singö zone. At least HFR105 is likely to be under influence of WNW-oriented structures (see lineaments in Figure 1-1). It should be noted that the same subvertical NW-striking pattern is observed in KFM11A and HFM33–35. Although the HRD definition is currently highly uncertain in this region (see below), an alternative interpretation is that the fracture characteristics in the South-western part of the Regional SFR domain (the surroundings around the Singö zone) should be represented by a separate fracture domain with different characteristics from that in the vicinity of SFR (see Section 3.1.3).

KFM11A

The classification of HRD in the SFR hydrogeological model v.0.2 relies on Single Hole Interpretation of possible zones, as currently there does not exist an updated geological model for the data set KFR101–105, KFR27, and KFM11A. The HRD definition is particularly uncertain for KFM11A. At depth, it has a 579 m long intercept, DZ1, which is associated to Singö deformation zone. Above DZ1, four WNW-oriented deformation zones are expected to intersect KFM11A, based on interpretation of lineaments in SFR geologic model v.0.1 (ZFMWNW2496, ZFMWNW0813, ZFMWNW3259, and ZFMWNW0804; /Curtis et al. 2009/). These potential intercepts are supported by hydraulic anomalies that are observed in the vicinity of intercepts between lineament extrapolations and KFM11A, although the geometrical match was not perfect /Öhman and Follin 2010/. The intercepts of these zones are currently under review and are expected to be modified in the final SFR Geologic model v 1.0. Therefore, the HRD definition in KFM11A is currently unclear.

Below, deviating characteristics of Open and Partly open fractures in excluded boreholes are presented with Kamb-contoured stereoplots.

Orientation deviations in KFM11A

There are only two dominating sets of Open and Partly open fractures in KFM11A, a horizontal set and a WNW-striking set. The PFL-f transmissivity is exceptionally high and is entirely dominated by the horizontal set. The definition of HRD is based on Single Hole Interpretation, which is highly uncertain in KFM11A (Section 2.2.1). KFM11A has a 579 m long PDZ intercept (defined in the SHI as DZ1) which is associated to the Singö zone (ZFMWNW0001) and its splays. Even after exclusion of the DZ1 the Open and Partly open fractures seem to be under influence of the Singö zone (Figure B-4). Visual inspection of HFM33–35 (above) strongly supports this observation. Based on the data at hand, the HRD rockmass in the vicinity of ZFMWNW0001 exhibits deviating characteristics and should be treated as a separate fracture domain. The SFR v.0.2 hydro-DFN primarily targets the local characteristics of the SFR investigation site, and therefore KFM11A is excluded from further analysis.

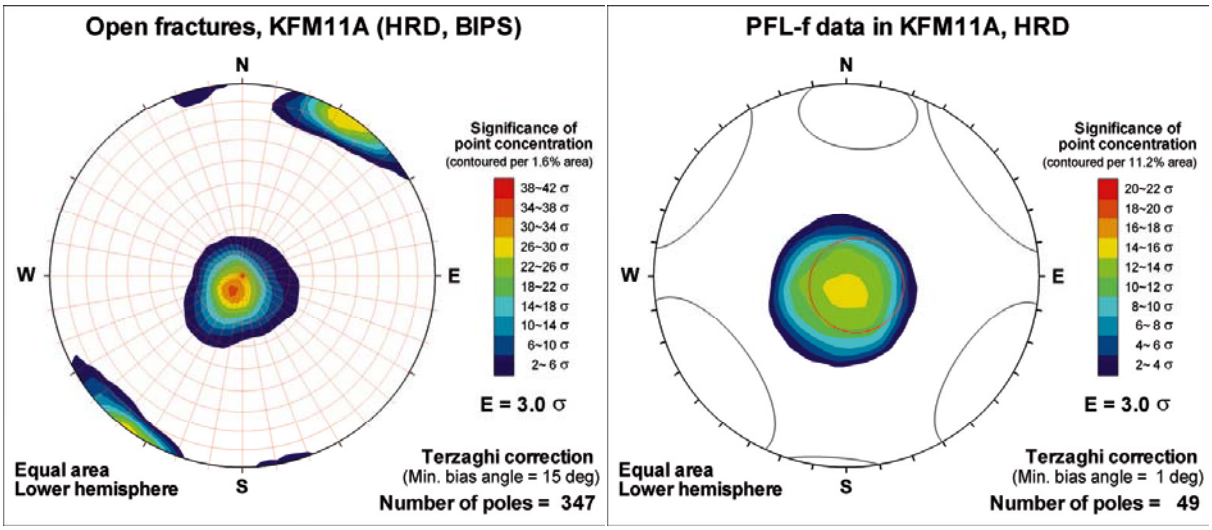

Figure B-4. *Kamb-contoured orientation of Open and Partly open fractures visible in BIPS (left) and PFL-f data (right) in KFM11A (HRD). For reference, the fracture set hard sectors identified in the SFR data set (Figure 3-2) are shown as circles.*

Analysis of PFL-f data

This appendix presents an overview of the hydraulic data set obtained from differential Posiva Flow Logging (PFL). The appendix also describes considerations made and decisions taken regarding PFL-f data. In the current study it was decided to parameterise the DFN using the connectivity analysis method (Section 2.1), a method where PFL-f data has a key role. A central assumption in this method is that the evaluated transmissivity for PFL-f records are assumed to reflect fracture transmissivities explicitly.

The PFL device (Figure C-1) is developed to detect *continuously flowing fractures*, i.e. flow paths that are connected to a positive hydraulic boundary. Therefore, PFL-f measurements are based on several days of pumping (c. one week), after which the flow regime is assumed to have reached radial steady-state. As the borehole is a line sink, the risk of short circuiting fracture flow is negligible, although problems with the rubber disks may arise if there are large cavities in the borehole wall, or if the bypassing flow from below is large (Figure C-1). The advantage of the bypass pipe is that the PFL method avoids measuring cumulative flow, which makes the method less sensitive to large flows at the bottom of the hole.

After an initial overlapping/sequential PFL flow logging with 5 m sections under natural flow conditions, detected flow anomalies are re-examined with the PFL Difference Flow logging (Posiva Flow Log/Difference Flow Method) under pumped conditions. In this Difference Flow logging method, flow is generally measured over a 1 m section, which is sequentially moved in steps of 0.1 m. Based on these measurements discrete inflows are identified (referred to as PFL-f data) and the *apparent* transmissivity is evaluated for each discrete feature /see details in Hurmerinta and Väisäsvaara 2009a, b, Kristiansson and Väisäsvaara 2008, Pekkanen et al. 2008/. Thus, the detected discrete inflows at 0.1 m resolution are assumed to reflect individual fractures, and evaluated *apparent* PFL-f transmissivities are then coupled to mapped geological fractures (Figure C-2).

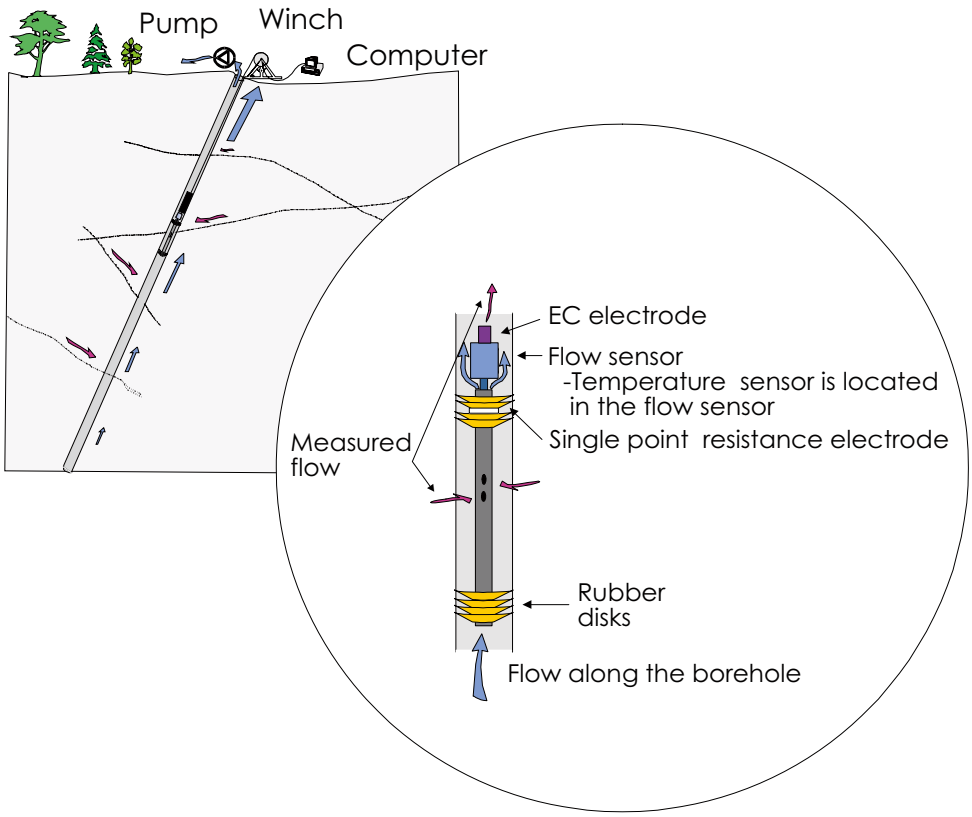

Figure C-1. *Schematic illustration of the PFL device. Taken from /Hurmerinta and Väisäsvaara 2009a/.*

PFL-f coupling to Boremap

The PFL-f data are linked to discrete Boremap features (Open and Partly open fractures, and crush zones), as described in /Öhman et al. 2010/. The length measurements in PFL-f logging are corrected by synchronization to borehole reference marks. Altogether, the uncertainty in length measurements has been estimated to ±0.2 m /Hurmerinta and Väisäsvaara 2009a/. A discrete Boremap feature also has a certain extension along the borehole, depending on its α-angle (and aperture), which is generally in the range 0.0 to 0.2 m. A Boremap feature is therefore expected have at least part of its borehole cross-sectional area inside the geometric window of ±0.2 m, in order to be a likely candidate for a given PFL-f record (Figure C-2).

The linking is a desktop study, which involves a joint judgment of, primarily, three aspects:

1) Visual inspection of BIPS imagery of the borehole in the vicinity of each PFL-f record.
2) Geometric match between PFL-f record and nearby Boremap features.
3) Confidence in the geologic interpretation of Open and Partly open fractures.

Table A1-34. KFR102A. Interpretation of PFL measurements and BOREMAP data

PFL-f No. 34, Adjusted borehole length, L_A = **188.4** m, T ≤ **2.6E-6** m^2/s, PFL confidence = **CERTAIN**

Boremap data							BIPS Image
Possible PFL-f features	*Adjusted secup (m)*	*Orientation (Strike/Dip)*	*Fract interpret*	*Frac. interp. confidence*	*PFL-anom. confidence*	*Aperture (mm)*	Corresponding Recorded secup in Boremap = **188.03** m Single hole interpretation = **RU3**
a[1]	**188.28**	**181/ 2**	**Open**	**Probable**	**1**	**0.5**	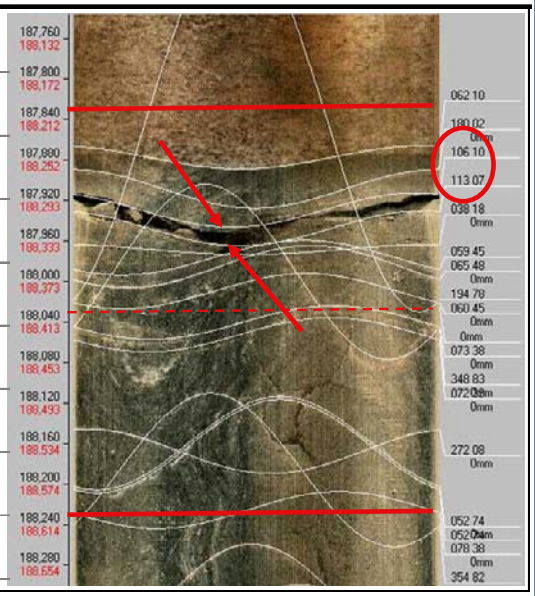
b[1]	**188.30**	**109/ 9**	**Crush zone**			**18**	
c	188.34	38/18	Open	Possible	1	0.5	

Comments: Crush zone

Best choice: **b**

Footnotes: 1) Closest, highest ranked open/partly open fracture, 2) This fracture can also be associated to an adjacent PFL-f No

Figure C-2. *Example of a PFL-f transmissivity record coupled to a Boremap feature (red arrows). The borehole length uncertainty ±0.2 m is indicated by red lines. Three possible candidates are identified, and a crush zone (candidate b) is selected to be the Best Choice.*

The selected Boremap feature is referred to as the Best Choice for a PFL-f record. In most cases, the three judgment aspects indicate the same Boremap feature; the confidence for these couplings is considered be higher, relatively to other couplings. Note that "confidence" is used as a relative term, as the couplings have not been confirmed by analysis of the core. In other cases, the judgment is more difficult, which result in a lower confidence linking. Three examples are given:

- Judgment aspects are incoherent: e.g. the candidate suggested from visual inspection of BIPS is mapped with low geologic confidence, or even as a sealed fracture.
- Lack of candidate features: e.g. the best candidate is far from the PFL-f anomaly (> 0.2 m), and mapped with low geologic confidence, or even as a sealed fracture.
- Indeterminate judgment criteria: Several equally likely candidates are found and it is impossible to conclude a single Best Choice.

In the situation where several equally likely candidates are found, all Boremap features are referred to as Alternative Best Choices. In the end, one of the Alternative Best Choices had to be reported as the Best Choice in /Öhman et al. 2010/. If the visual inspection in BIPS suggests one Alternative Best Choice as more likely than the others, it was taken as the Best Choice with a Certain linking confidence. Otherwise, the Alternative Best Choice closest to the PFL-f length measurement was selected, with an Uncertain linking confidence. For the hydro-DFN modelling purposes, the category with Alternative Best Choices and Uncertain linking was re-assessed.

Re-assessment of Uncertain Alternative Best Choices

There are 78 PFL-f data in HRD for which Alternative Best Choices exist and where the manual coupling was indecisive. It was decided to re-assess these from a hydro-DFN modelling perspective. The intention is to base the Best Choice on general observations on fracture characteristics, rather than simply the closest geometric match in Boremap.

Three different cases are considered:

1. Representative orientation. If Alternative Best Choices have similar orientation, the decision of Best Choice is assumed to have a negligible impact on DFN parameterisation. The criterion for this was that no Alternative Best Choices may deviate more than 25° in terms of solid angle from the finally decided Best Choice. It was found that 37 PFL-f records conformed to this criterion and the Best Choice was taken as the most representative feature orientation.
2. Use of local information. The approach is to select the Best Choice based on the orientation of its adjacent PFL-f linking. The criterion for this was that the ambient PFL-f must have a Certain linking, and that the decided Best Choice must deviate less than 30° in terms of solid angle from its closest PFL-f Certain orientation. It was found that 33 PFL-f records conformed to this criterion and the Best Choice was taken as the Alternative Best Choice closest to its neighbouring Certain PFL-f.
3. Use of the global information. In situations that do not conform to cases 1 or 2, it is assumed likely that, the PFL-f orientation should follow to the global DFN orientation model. The criterion here is simply that cases 1 and 2 fail. For the remaining 8 PFL-f records the Best Choice was taken as the Alternative Best Choice closest to either of the fracture set mean poles.

Case 1, the representative orientation method, conforms rather well to the established PFL-f orientations, although a cluster of vertical fractures with a strike of approximately 110° can be noted (Figure C-3a). As can be expected case 2, the application of local information also conforms well to the established PFL-f orientations. The changes in overall orientation pattern of PFL-f data, after implementation of cases 1 and 2, seem negligible (compare Kamb contours of Figure C-3a and b).

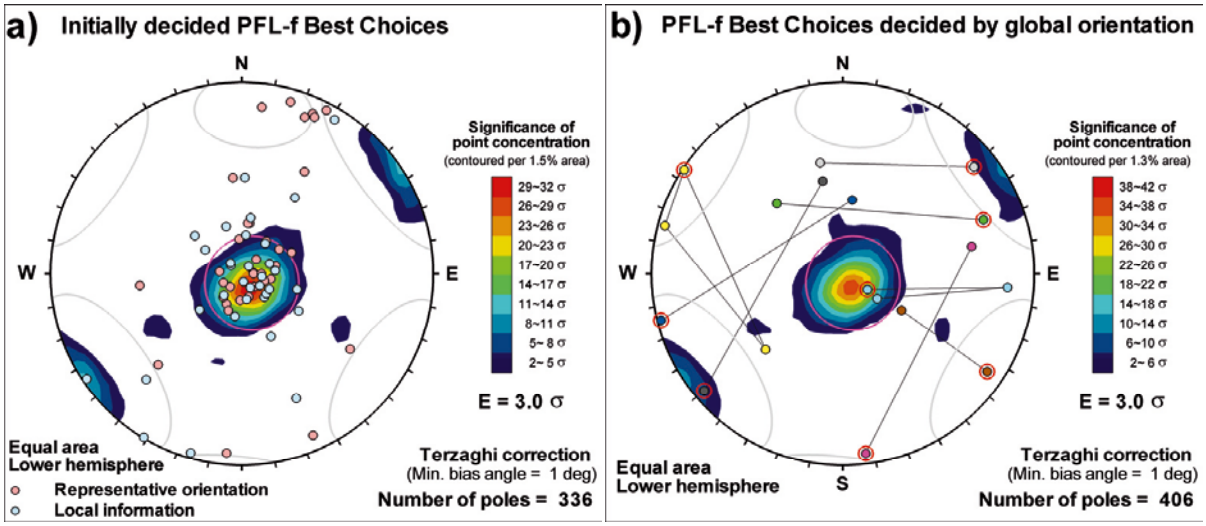

Figure C-3. *Decided Best Choice for PFL-f records where the selection between possible alternatives in manual Boremap linking was difficult; a) decision made by representative orientation and local information, and b) use of global information. Resulting Best Choices shown as poles in a), and as red circles in b), while the established PFL-f orientations are shown Kamb contours. The hard-sectors defined by visual inspection of Figure 3-2 are shown for reference, as these were used to select Best Choice in b).*

Theoretical and practical detection limit

In the hydro-DFN calibration of connected fractures, it is important to consider that the PFL-f data is truncated, not only by the detection limit of the measurement device, but also by the local noise level. It is often possible to detect the existence of flow anomalies below the measurement limit, although the evaluation of transmissivity below the limit is uncertain. Furthermore, low-transmissive flowing features may appear only as noise in relation to high inflow of nearby high transmissivity features. Flow is only registered if it exceeds the noise level by a factor of 10. In other words, low-transmissive features may be severely underrepresented in the presence of highly transmissive features. The implication of detection-limit truncation, and the potential underrepresentation of low transmissivity PFL-f records causes uncertainty in:

1) the estimation of connected fracture intensity (particularly for low-transmissive sets EW and NW),
2) the general shape of the transmissivity distributions, which causes uncertainty in the estimation of the relation between transmissivity and fracture size.

The theoretical detection limit for the PFL flow logging is 30 mL/h, which corresponds to a transmissivity of 8.33×10^{-10} m^2/s for a drawdown of 10 m /Pekkanen et al. 2008/. However, depending on the drawdown applied during the test, the detection limit differs in terms of transmissivity from borehole to borehole. For example in KFR105 it is as low as 7.7×10^{-11} m^2/s. Also, in some cases the applied drawdown has not been consistent for all sections of a borehole. Now, the practical detection limit of PFL-f interpretation depends on the noise level, which varies depending on local inflow. For example, in KFR27 the noise level varied between 30 mL/h and 2,000 mL/h /Hurmerinta and Väisäsvaara 2009a/. The most common practical detection limit is 2×10^{-9} m^2/s (Figure C-4). Consequently, some high transmissivity data are classified as uncertain, whereas vice-versa, some low transmissivities classed as certain (Figure C-4). It is therefore difficult to define an overall cut-off detection limit, T_{lim}.

The intensity calibration of the hydro-DFN therefore requires compensation for the variability in detection limits. It is practical to apply a common cut-off threshold in transmissivity for all boreholes in order to allow combining PFL-f data into a single data set. The PFL-f intensity below this cut-off can then be extrapolated, for example by means of statistical distributions /e.g. Follin et al. 2005/. In /Follin et al. 2007b/, the cut-off is specified as c. 1.0×10^{-9} m^2/s for the nearby Site Investigation Forsmark. In the work by /Follin et al. 2008/, the cut-off level was set to 4×10^{-10} m^2/s, which was

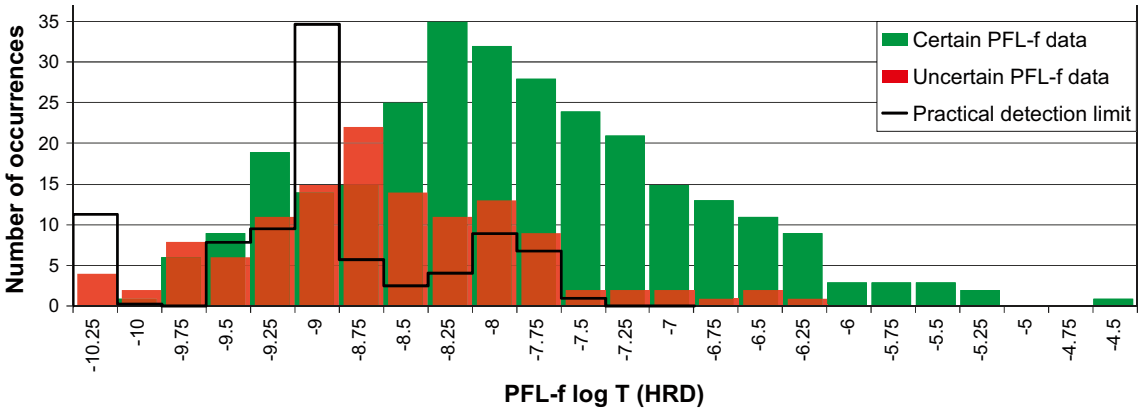

Figure C-4. *Transmissivity distribution of the PFL-f data set inside HRD. The practical detection limit varies with local noise level in inflow data (black line; normalised in terms of frequency).*

based on the lowest recorded value. The lowest measured transmissivity in the different boreholes of the present data set ranges from 10^{-8} m²/s in KFR103, to 7.7×10^{-11} m²/s in KFR105 (see Figure C-5). However, this common cut-off level must be cautiously selected with respect to the current data set. A high cut-off value reduces the number of available data, which induces uncertainty owing to small sample size. On the other hand, a low cut-off value includes a larger proportion of uncertain PFL-f records, a sub-population which is likely to be underrepresented owing to the noise level in the vicinity of high transmissivity PFL-f data, as discussed above.

It was decided to assume a general cut-off limit, $T_{lim} = 2.5\times10^{-9}$ m²/s (or log T = –8.6). This value is somewhat lower than the smallest record in KFR103 (note that, for example in KFR101, transmissivities below T_{lim} have been measured in PDZ, but these are excluded in Figure C-5). The selected T_{lim} is also just above the mode in practical detection limit (Figure C-4), which implies that the practical detection limit heavily censors the distribution below T_{lim}.

Missing transmissivity values

There are 6 PFL-f records in the HRD, for which transmissivity values could not be evaluated (Table C-1). The reason for this is technical measurement difficulties. For PFL-f data in the upper part of KFR27 where core is missing (PFL-f numbers 2, 3, and 9), the reference measurements at *in situ* conditions were unavailable. For PFL-f numbers 15 and 16 in KFR27, the applied drawdown

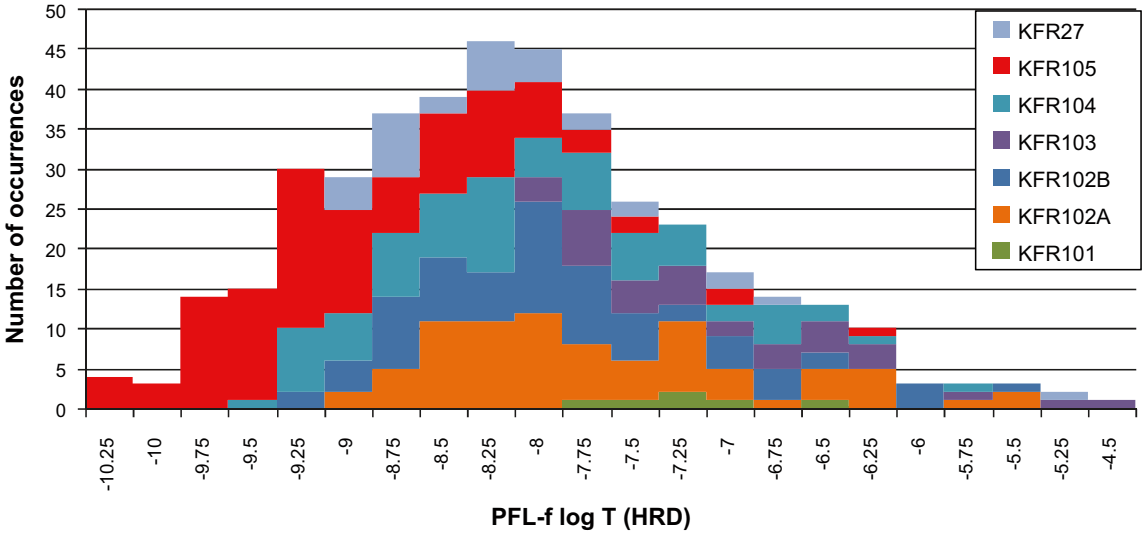

Figure C-5. *Stacked transmissivity distribution of the PFL-f data set inside HRD per borehole.*

failed to reverse the flow field, and the flow into the bedrock was higher during pumped conditions. This is abnormal and suggests that the flowing fractures have been altered during the test /Pekkanen et al. 2008/. However, the actual flows measured are below the median for KFR27. For PFL-f number 88 in KFR104 conditions were non-stationary, owing to a pump failure /Hurmerinta and Väisäsvaara 2009a/. These values were assumed a transmissivity value of 6.9×10^{-9} m^2/s (Table C-1). This value was chosen in order to have a minimum impact on the total PFL-f population, and corresponds to the median value of the entire PFL-f population in HRD. One alternative could have been to apply a higher value for the PFL-f data at elevations around –100 m RHB70, and a lower value for the PFL-f data at elevations around –230 m RHB70.

Table C-1. Assumed transmissivity for PFL-f records.

Borehole	Length, L_A (m)	PFL-f number	Boremap link confidence	PFL confidence	Assumed transmissivity	Elevation (m, RHB70)
KFR27	101.70	2	UNCERTAIN	CERTAIN	6.9×10^{-9} m^2/s	–98.85
KFR27	105.60	3	CERTAIN	CERTAIN	6.9×10^{-9} m^2/s	–102.64
KFR27	121.10	9	CERTAIN	CERTAIN	6.9×10^{-9} m^2/s	–118.47
KFR27	231.00	15	CERTAIN	CERTAIN	6.9×10^{-9} m^2/s	–227.87
KFR27	234.10	16	CERTAIN	CERTAIN	6.9×10^{-9} m^2/s	–230.99
KFR104	293.60	88	CERTAIN	UNCERTAIN	6.9×10^{-9} m^2/s	–230.44

Measurement scale and exclusion of data

The borehole interval 240 to 438 m length in KFR104 was only measured over a 5-m section, which was moved in steps of 0.5 m. The PFLs in the interval 99.3 to 135 m in KFR27 were interpreted with a 0.1 m resolution, but only have reference measurements at the 0.5 m resolution. Furthermore, no core is available above 147.49 m in KFR27. This coarser resolution makes the correlation to Boremap more uncertain, as a registered PFL-f record, could potentially have resolved 5 different discrete inflows, had the 0.1 m resolution been used. However, as transmissivity is evaluated from the inflow over a section, the accuracy in the actual transmissivity values are expected to be on the same order as the 0.1 resolution PFL-f data. It should be noted that the missing transmissivity in PFL-f numbers 2, 3, and 9 in KFR27 (Table C-1) are due to lack of reference *in situ* conditions, whereas in PFL-f number 88 in KFR104 it is due to pump failure. Altogether, there are 8 PFL-f in HRD that are measured at the 0.5 m resolution (of which 4 are listed in Table C-1), and 406 PFL-f data in HRD measured by the 0.1 m scale.

At the onset of this analysis, it was considered if all the 0.5 resolution PFL-f data should be excluded from the hydro-DFN, with consideration to confidence and support scale. During the course of this analysis, it was decided to exclude PFL-f data above 143 m length in KFR27, but to retain the coarsely resolved PFL-f data from KFR104 in the calibration of the hydro-DFN. There are several reasons for excluding the PFL-f records number 2, 3, and 9 in KFR27: 1) all records lack transmissivity evaluation, 2) it is suspected that these PFL-f records reflect a possible deformation zone (Figure C-12), and 3) this section of KFR27 is excluded the corresponding analysis of Open and Partly open fractures, as its core is missing. On the other hand, the motive for including data from the lower part of KFR104 is that it provides valuable information for depths where data are scarce. At these depths data exists only from KFR102A and KFR27 (see Figure 2-3). KFR102A indicates a low frequency, or even absence, of PFL-f data in HRD, whereas in KFR27 both the frequency and transmissivity is considerably higher, but mainly in the vicinity of possible deformation zones (cf. Figure C-1 and Figure C-12). KFR104 is relatively unaffected by deformation zones at depth and also has a low PFL-f frequency. As HRD data at depth are scarce and divergent, KFR104 may therefore contribute substantially to the general characterization of its hydraulic properties.

The data from KFR102A at depth, shows that no PFL-f records were discovered in regions where anomalies had not already been indicated by the initial logging (sequential 5-m scale measurements) /Hurmerinta and Väisäsvaara 2009b/. On the other hand, in areas where the initial logging did indicate anomalies, the 0.1-m resolution PFL-f interpretation could resolve several features. Relating these observations to KFR104, implies that inclusion of the long borehole sections without recorded anomalies is valid, and that for sections with anomalies the total transmissivity value is correct, but it

may possibly reflect more features than can be inferred by the 0.5-m resolution PFL-f interpretation. Theoretically, each interpreted PFL-f record at the 0.5-m resolution, could have been resolved into 5 discrete features, had the 0.1-m resolution been used. The likelihood of such a clustered scenario must be put in context of the general low PFL-f frequency in KFR104: there are altogether 5 registered PFL-f records at the 0.5 m resolution over a borehole length of 161.4 m (possible deformation zones excluded).

The general impression is that neither the Boremap correlation, nor the PFL confidence (i.e. confidence in existence) in KFR104 has a notably lower confidence than the overall PFL-f data set. However, it is difficult to draw the line between which alternative is preferable with respect to model confidence: including lower confidence data, which possibly may deteriorate results, or excluding such data and thereby reducing the sample size and spatial coverage, which in turn may increase uncertainty.

Below, the available PFL-f raw data are presented on a borehole-to-borehole basis, including data associated to leaking casing, PFL-f records without transmissivity values, and PFL-f records that could not be coupled to Boremap features /Öhman et al. 2010/. Furthermore, in the Boremap coupling to PFL-f data /Öhman et al. 2010/, a few PFL-f records were linked to the same Boremap feature; these are shown as separate features in Figure C-6 to Figure C-12, although in the DFN parameterisation their transmissivity was added and they were treated as one flowing feature.

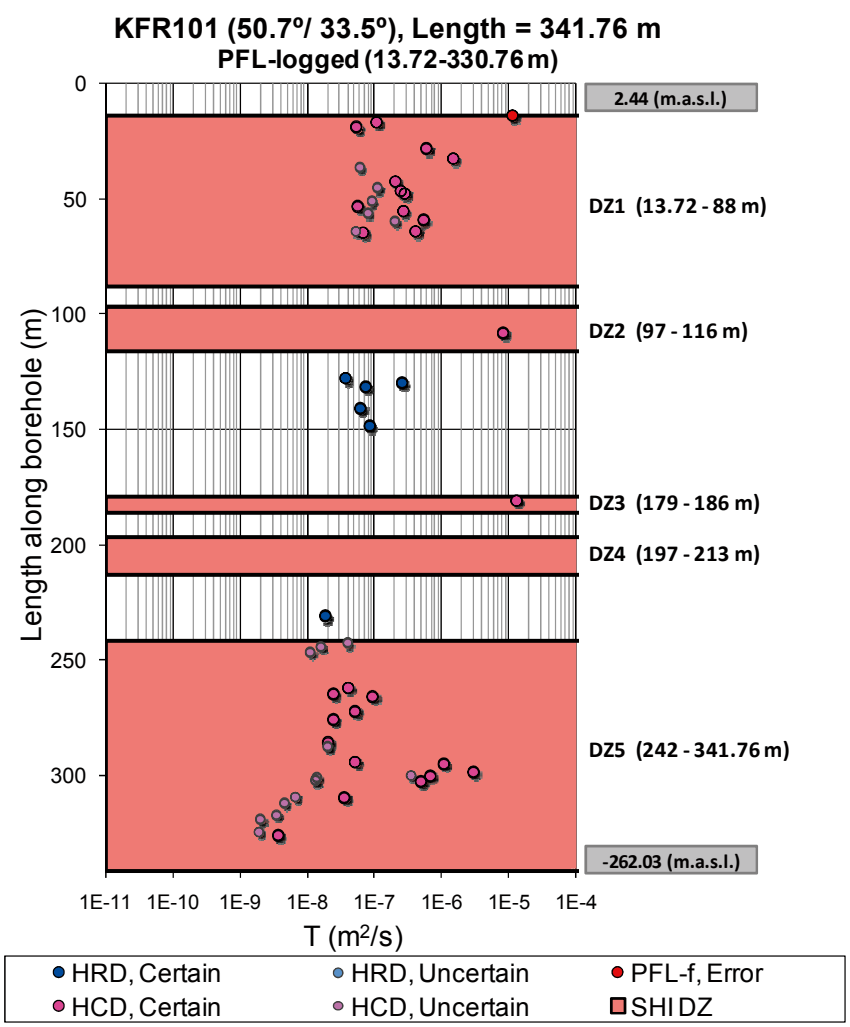

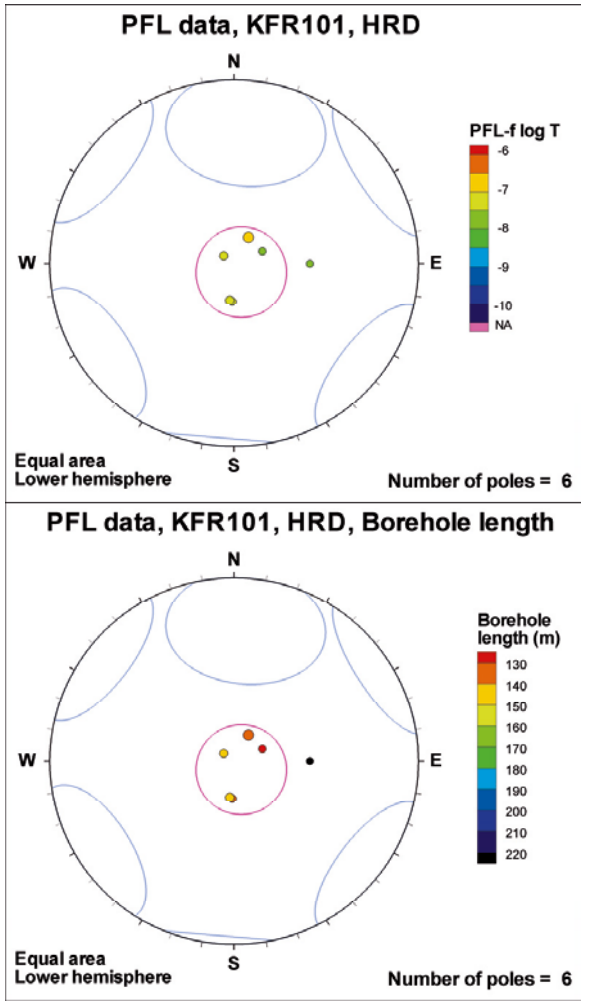

Figure C-6. HRD definitions according to SHI combined with PFL-f transmissivity in KFR101. PFL-f orientations coloured by transmissivity, respectively, borehole length, shown for reference.

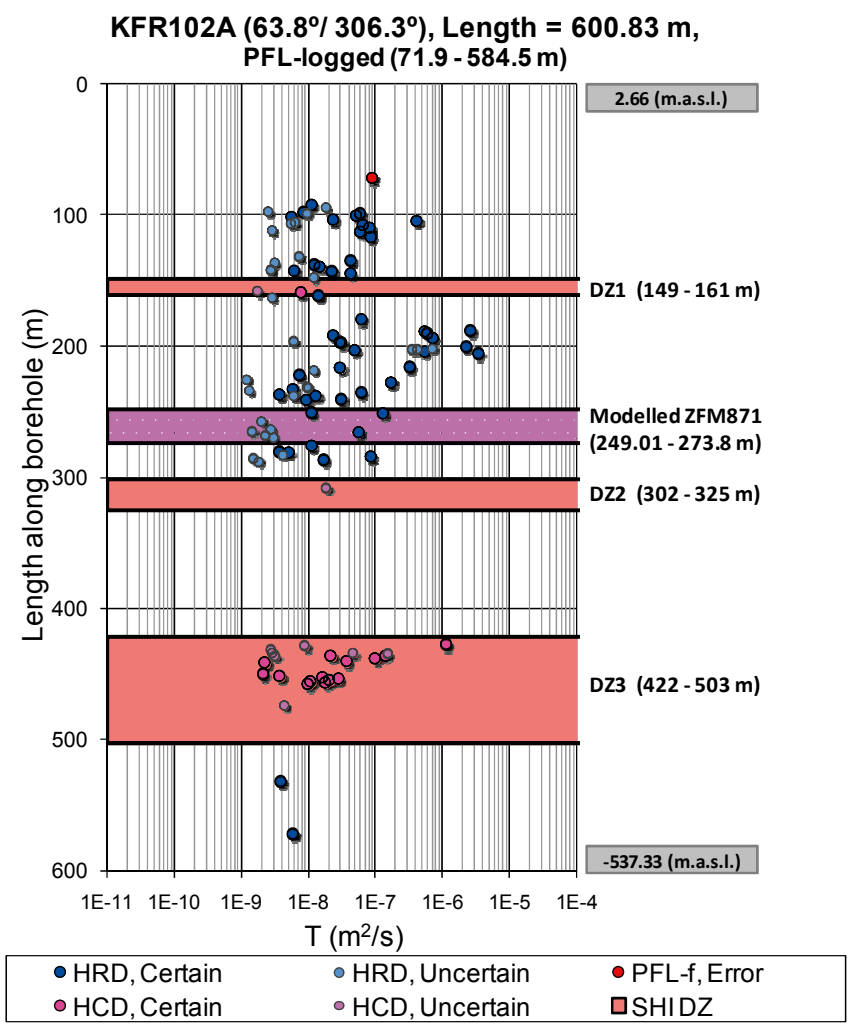

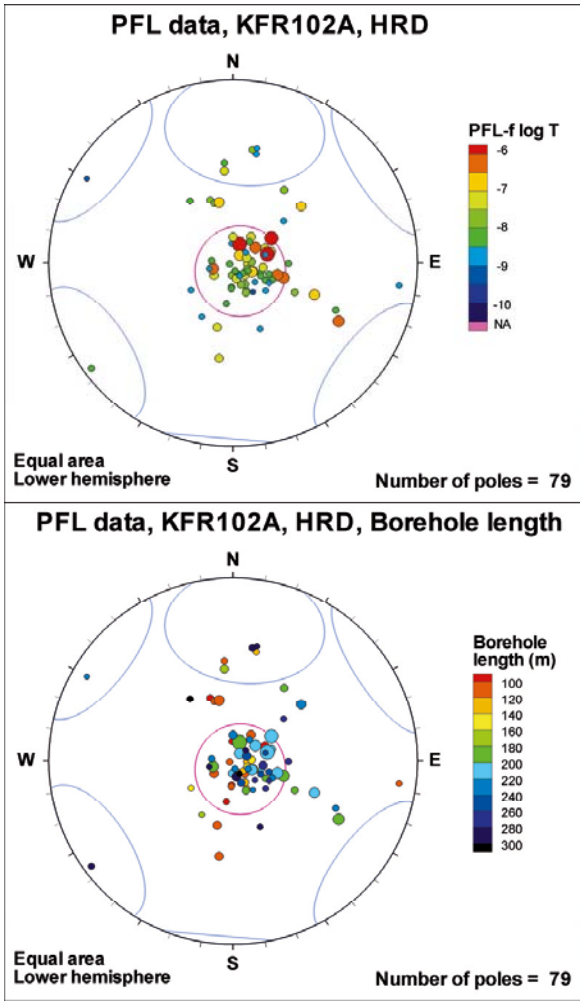

Figure C-7. *HRD definitions according to SHI combined with PFL-f transmissivity in KFR102A. PFL-f orientations coloured by transmissivity, respectively, borehole length, shown for reference. In the Geological model v.0.1, ZFM871 (formerly known as zonH2) is geometrically intercepted between 249.01 and 273.8 m borehole length. The model intercept does not match a mapped possible deformation zone.*

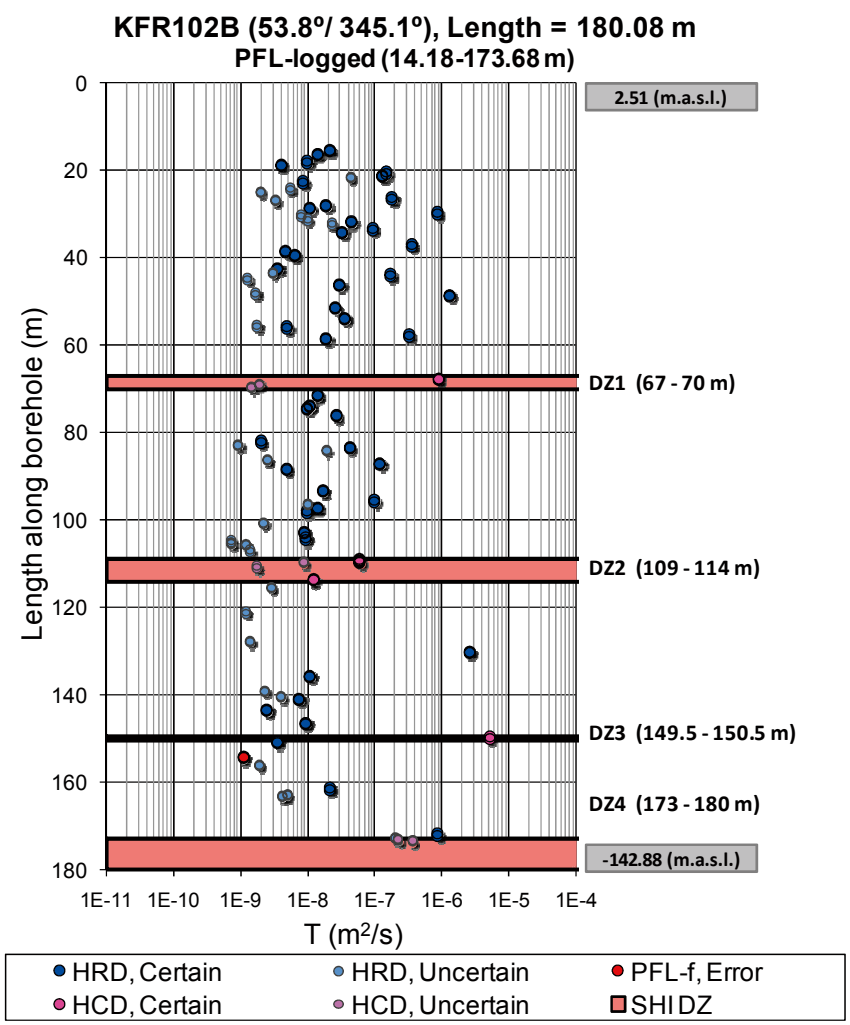

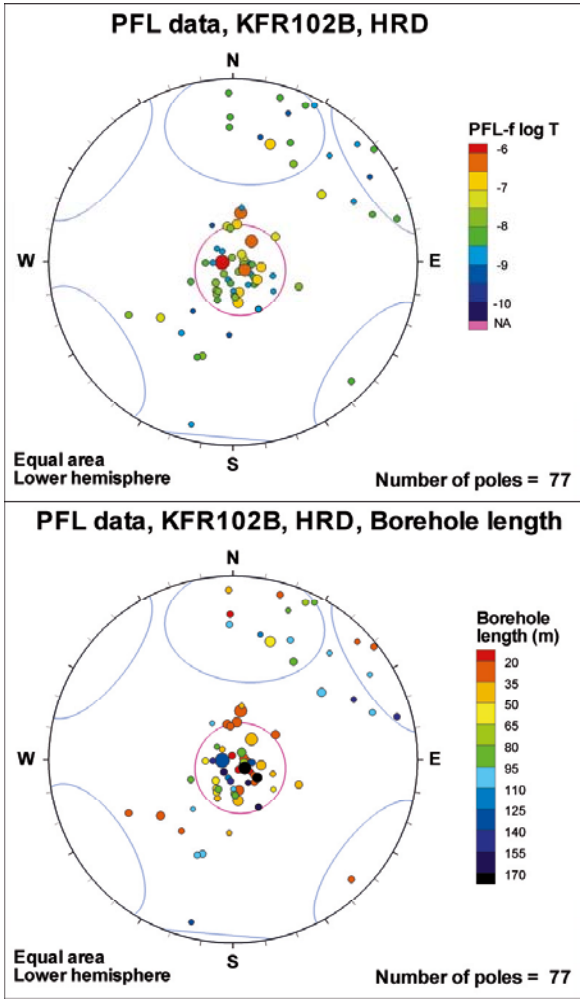

Figure C-8. HRD definitions according to SHI combined with PFL-f transmissivity in KFR102B. PFL-f orientations coloured by transmissivity, respectively, borehole length, shown for reference.

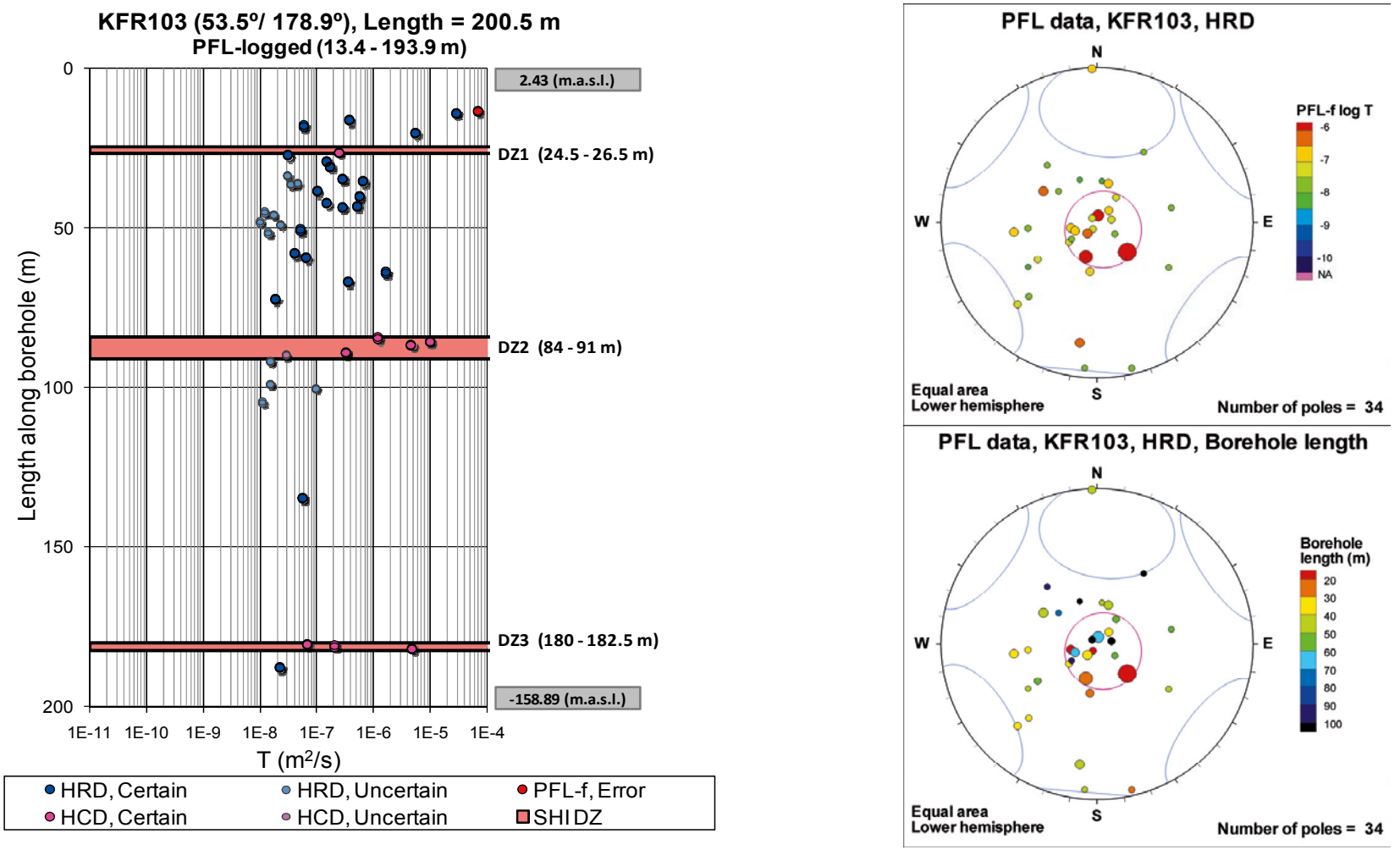

Figure C-9. HRD definitions according to SHI combined with PFL-f transmissivity in KFR103. PFL-f orientations coloured by transmissivity, respectively, borehole length, shown for reference.

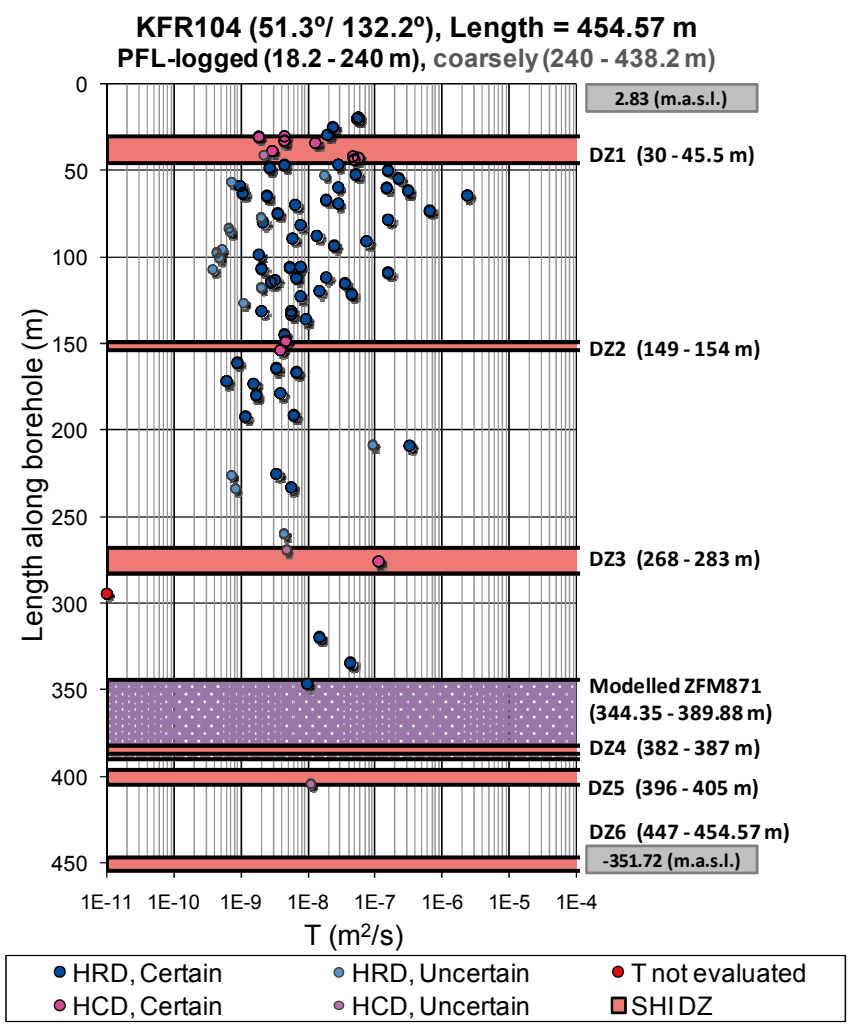

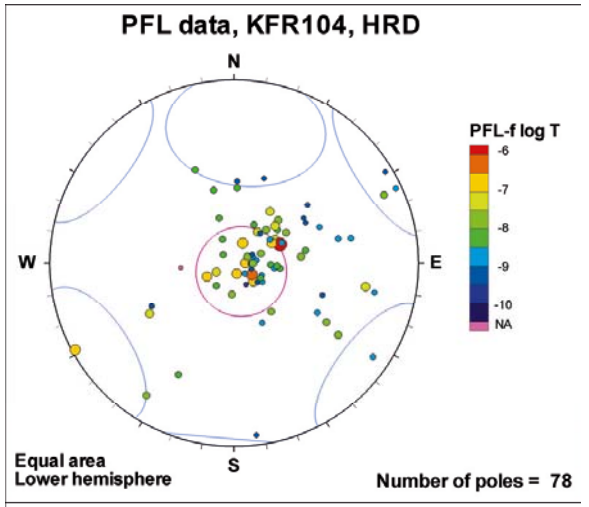

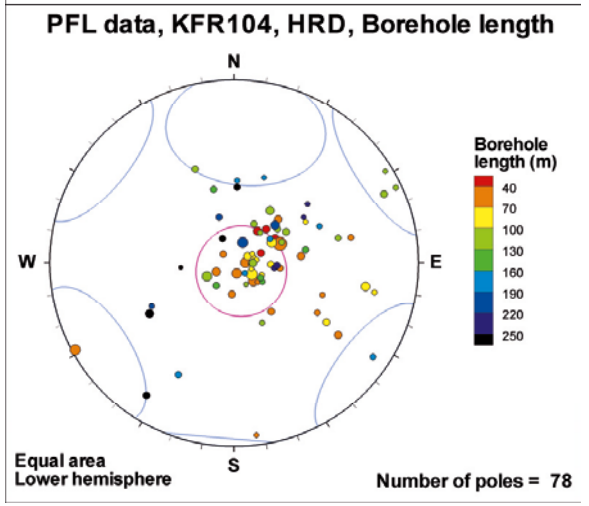

Figure C-10. *HRD definitions according to SHI combined with PFL-f transmissivity in KFR104. PFL-f orientations coloured by transmissivity, respectively, borehole length, shown for reference. In the Geological model v.0.1, ZFM871 (formerly known as zonH2) is geometrically intercepted between 344.35 and 389.88 m borehole length. Part of the model intercept matches the mapped possible deformation zone DZ4.*

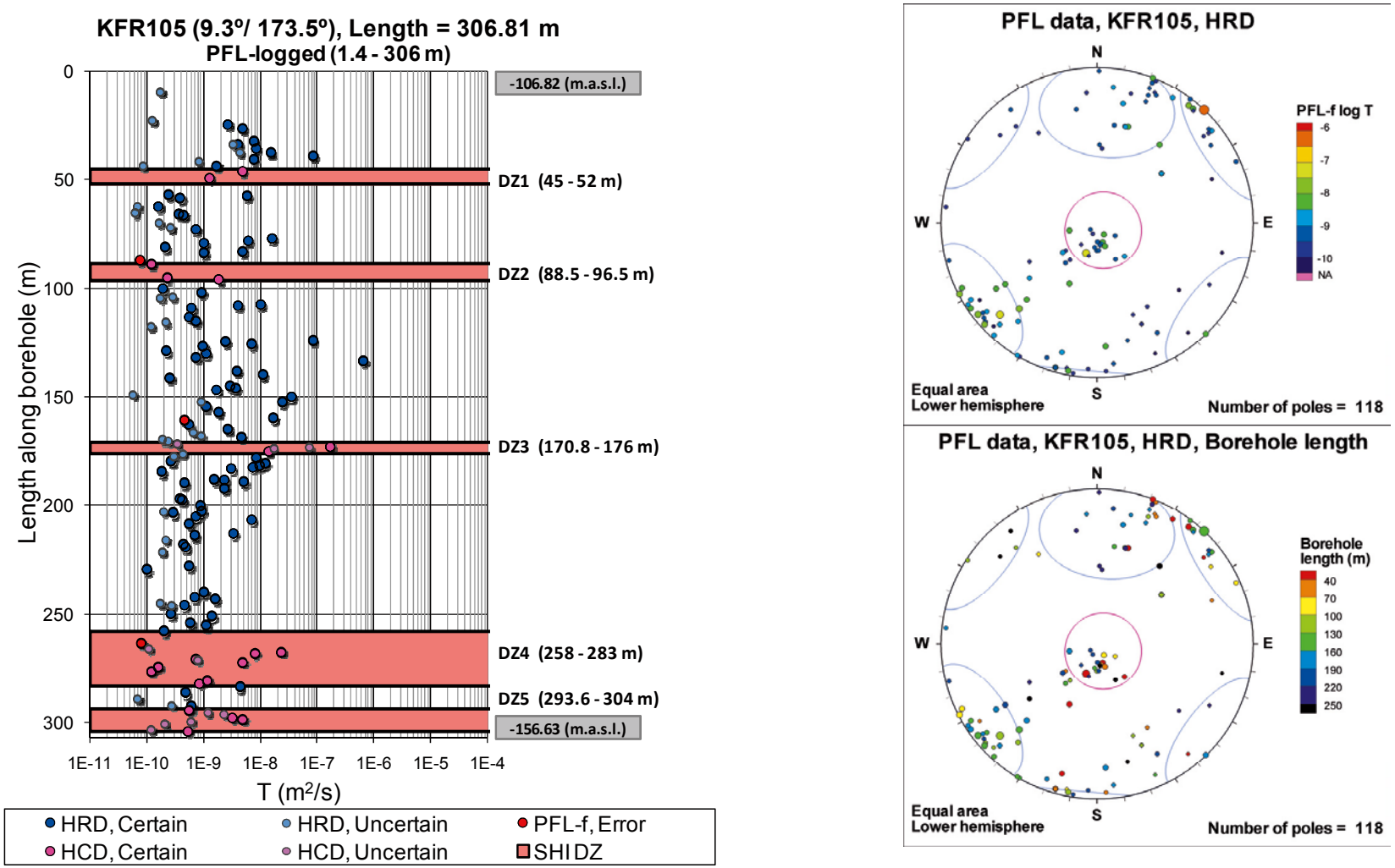

Figure C-11. *HRD definitions according to SHI combined with PFL-f transmissivity in KFR105. PFL-f orientations coloured by transmissivity, respectively, borehole length, shown for reference.*

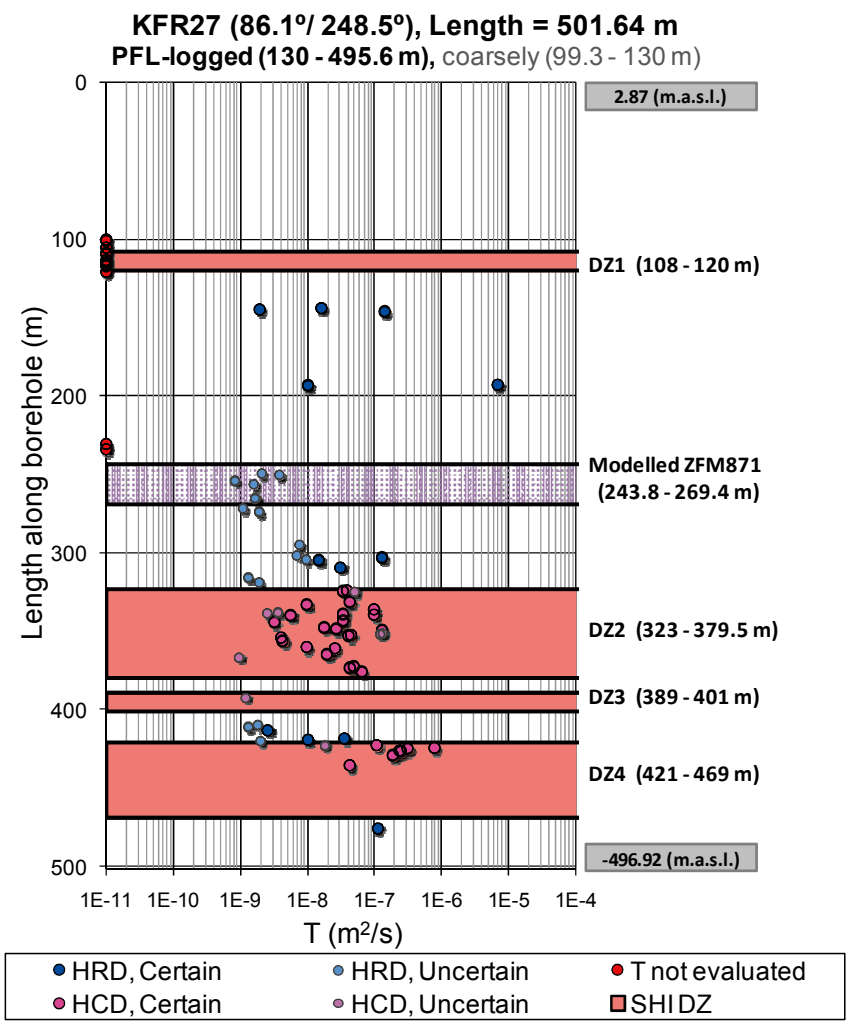

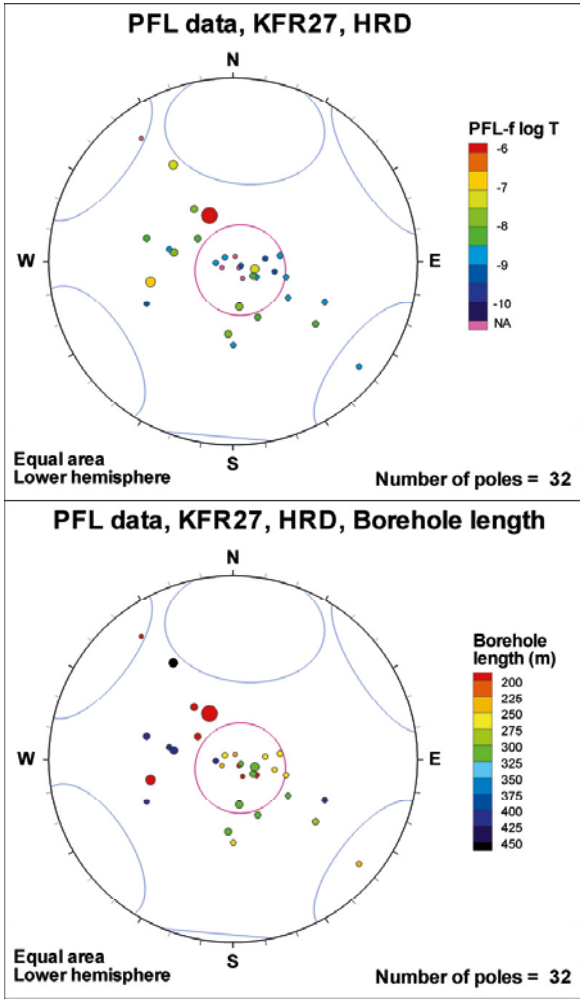

Figure C-12. *HRD definitions according to SHI combined with PFL-f transmissivity in KFR27. PFL-f orientations coloured by transmissivity, respectively, borehole length, shown for reference.*

Appendix D

Hydraulic observations during the site investigations for the extension of SFR

By Niclas Bockgård, Golder Associates AB.

This appendix summaries some observations during the first part of the site investigation for the extension of SFR and includes investigations and activities in the boreholes HFR101, HFR102, HFR105, KFR101, KFR102A, KFR102B, KFR103, KFR104 and KFR105. These are interesting observations that have not been accounted for, deterministically, in the current model version.

Hydraulic interferences

The hydraulic interferences observed during the investigations are summarized in Table D-1. The borehole sections KFR27 (193–198 m) and KFR102A (207 m), corresponding to an elevation interval –169 to 190 m RHB70, have also been identified as anomalously high transmissive (Figure 3-10).

Table D-1. Hydraulic interferences observed during the site investigations for the extension of SFR before the drilling of the two boreholes HFR106 and KFR106. Only clear responses are included in the table (marked with grey shading).

Disturbance (borehole section/activity)	Observation (borehole section)													
	HFR102:1 (28–55 m)	KFR02:4 (43–80 m)*	KFR04:1–3 (28–101 m)*	KFR05:2 (80–96)*	KFR7B:1 (9–21 m)*	KFR13:1–3 (4–77 m)*	KFR55:3 (22–39 m)*	KFR27:2 (47–109 m)	KFR101:1 (280–342 m)	KFR101:2 (91–279 m)	KFR102A:7–8 (0–184 m)	KFR102B:1–2 (128–180 m)	KFR103:2 (79–177 m)	KFR104:2 (98–332 m)
HFR101, Pumping														
KFR27 193–198 m, Drilling														
KFR102A 207 m, Drilling														
KFR102A c. 280 m, Drilling														
KFR105 133 m, Drilling														

* Boreholes drilled during the construction of SFR. Sections covering deformation zone ZFM871 (zone H2).

The occurrence of sheet joints and sub-horizontal zones

A key question for the site investigations has been to elucidate the occurrence of transmissive sheet joints and sub-horizontal zones in the candidate area for the SFR extension /SKB 2008a/. The hydrogeological investigations show no structures with the extremely high transmissivity, in the order of 10^{-4}–10^{-3} m^2/s, that in some cases have been observed in the uppermost c. 150 m of the bedrock in other parts of the Forsmark area /SKB 2008b/. However, a number of individual flow anomalies with transmissivities above 1×10^{-5} m^2/s have been observed above –150 m (RHB 70), see Table D-2.

Table D-2. Flow anomalies with T > 1.1×10–5 m²/s located above the altitude –150 m (RHB 70).

Borehole	Approx. altitude (m, RHB 70)	Transmissivity (m²/s)	Reference
HFR105	–108	1.1×10^{-5}	Jönsson et al. 2008
KFR101	–9	1.1×10^{-5}	Pekkanen et al. 2008
KFR101	–143	1.3×10^{-5}	Pekkanen et al. 2008
KFR103	–9	2.8×10^{-5}	Kristiansson and Väisäsvaara 2008

Appendix E

Identification of Pole Clusters and Soft-Sector Assignment

Fracture sets are assumed to follow the Univariate Fisher distribution, defined by a mean pole (trend and plunge) and a concentration parameter, Fisher κ. The Fisher distribution of different sets will overlap each other to various degrees. In sectors of high Fisher distribution overlap, it was decided that set-assignment of PFL-f data should not only be based on geometry alone, but also with respect to transmissivity (see below). This is based on the assumption that the transmissivity of PFL-f sets should be as homogenous as possible. For example, consider two PFL-f data with the same orientation, which by geometry can be assigned to two sets with equal probability; in this case the PFL-f with higher transmissivity is assigned to the set with higher transmissivity in general, while the lower transmissivity PFL-f recorded is assigned to the other set. This procedure is necessary in order to preserve the hydraulic contrast between sets, while preserving the geometric expectation value of the Fisher distribution.

There are several numerical methods to identify and parameterize orientation clusters within a fracture population, see /Munier 2004/ and references therein. The fracture assignment in this analysis relies on a mix of visual inspection and a quantitative clustering algorithm. As a first step, the identification of fracture sets is made by visual inspection of contoured plots of cluster significance /Kamb 1959/ and /Robin and Jowett 1986/. These initial hard sectors were defined by a mean pole and a confining hard-sector solid angle (see Figure E-1). In a second step, these hard sectors are transferred into probability-fields for set membership, using a Univariate Fisher-distributed soft-sectoring of data through a numerical algorithm (explained below). In the third step the set-belonging of PFL-f data is re-weighted by transmissivity. In the final step, fracture set parameterisation is calculated from the soft sectored data.

The decision to separate the orientation analysis into one manual and one numerical step was based on the following factors:

- A manual cluster identification based on visual judgment was preferred, as it allowed modellers to apply their hydrogeological understanding and consideration of local hydrogeological conditions to the analysis.
- A soft sector division is difficult (if even possible) to do by hand; therefore clusters are initially approximated in terms of hard sectors (manually), and then “transferred” into soft sectors (numerically), after which Fisher parameterization can be calculated.

The procedure to compute fracture orientation sets can be subdivided into the following five steps:

1. Fracture orientations were visualized using Kamb-contoured plots of cluster significance.
2. Fracture sets were identified by visual inspection and approximated manually. In this initial step, each cluster was approximated by a Fisher-type hard sector.
3. Fracture poles are calculated for the lower hemisphere, and all poles falling inside a hard sector are used to calculate the mean pole and Fisher κ for the hard-sectored cluster, (eqs. (E-1) to (E-3)).
4. Soft sectors (i.e. continuous probability functions for orientation-based fracture assignment to sets) are calculated for each cluster, (eq. (E-6)) based on the parameterization in step 3.
5. Fracture poles are again calculated for the lower hemisphere, and poles are stochastically re-assigned according to soft sector probabilities. Finally, the mean pole and Fisher κ are calculated for the soft-sectored clusters.

Fisher Distribution Parameterization Based on Pole Clusters

The mean orientation of a cluster of fracture poles was calculated using the eigenvector method /Davis 2002/, while the concentration of clusters is calculated by the resultant vector method /Priest 1993, after others/. Clusters are first approximately defined by hard sectors (Step 3, above) and then transformed into corresponding soft sectors (Step 5, above) as shown in Figure E-1. Fracture poles have been corrected for sampling bias using Terzaghi weights /Terzaghi 1965/; the sum of Terzaghi weights were used instead of actual fracture pole counts.

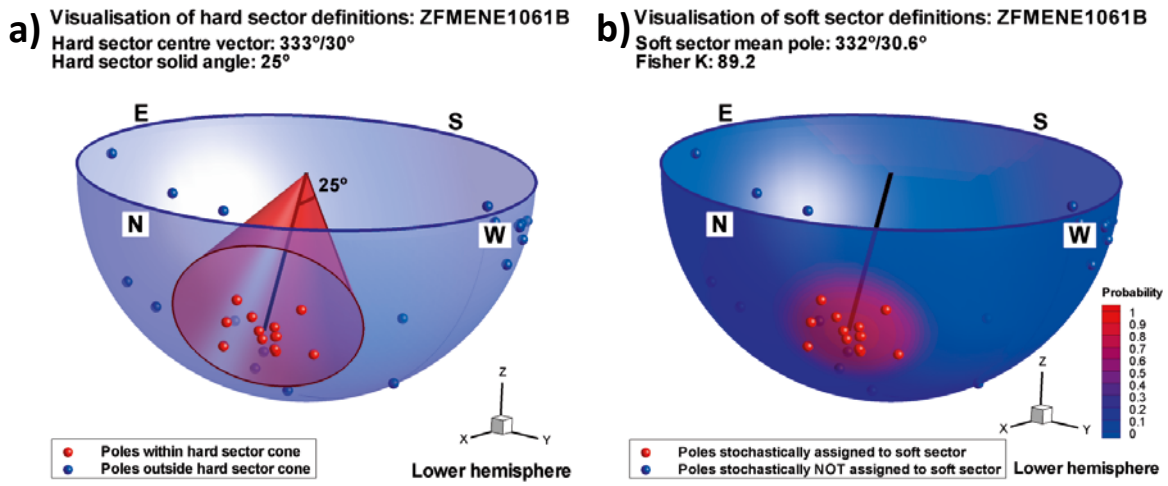

Figure E-1. *Visualization of principles used; a) a manually hard-sector defined set is transformed into b) a soft sectoring probability field, figure taken from /Stephens et al. 2007/. Note that, for example, the soft sector P=0.5 is defined by the characteristics of the fractures inside the hard sector, and does not necessarily coincide with the initial hard sector solid angle (25°).*

The orientation of each fracture i in a fracture cluster can be characterized by its fracture pole $\boldsymbol{n}_i$ (a unit-length vector normal to the fracture plane). This fracture pole is defined by its three vector co-ordinates so that $[\boldsymbol{n}_i] = [n_{ix}, n_{iy}, n_{iz}]^T$. For the calculation of the mean pole, a symmetric matrix $\mathbf{T}_j$ is defined for a set of N_j fractures of cluster j by:

$$\mathbf{T}_j = \sum_{i=1}^{N_j} w_i \left(\mathbf{n}_i \times \mathbf{n}_i^T\right) \qquad \text{(E-1)}$$

where w_i is the Terzaghi weight of each fracture i, and is equal to 1/sin (max(α, 1°)). Here, α is the angle between the borehole and the fracture plane. The minimum bias angle is used to avoid artificially large weights for fracture planes sub-parallel to the borehole orientation. The cluster mean pole orientation is obtained from the eigenvector ($\mathbf{e}_j$) associated to the largest eigenvalue (λ_j) in the eigenvalue solution /Davis 2002/:

$$\mathbf{T}_j \mathbf{e}_j = \lambda_j \mathbf{e}_j \qquad \text{(E-2)}$$

The maximum resultant vector $\mathbf{V}_j$, for the set of N_j poles in cluster j, is then used to calculate the Fisher concentration parameter (κ) of the cluster:

$$\mathbf{V}_j = \sum_{i=1}^{N_j} w_i \, \mathbf{n}_i \qquad \text{(E-3)}$$

It should be noted that it is possible to calculate two fracture poles with opposite directions from a fracture plane. Which one of these fracture-pole directions are used to define fracture orientation is generally irrelevant. However, in the calculation of the resultant vector, eq. (E-3), each fracture-pole direction must be chosen so as to maximize the resultant vector length (i.e. the fracture poles must have the same general direction; see Figure E-2). Otherwise, the resultant vector will not reflect the overall orientation of the fracture cluster, see also /Holmén and Outters 2002/. In this particular case, the maximum resultant is ensured by selecting $\mathbf{n}_i$ such that the scalar product, $\mathbf{n}_i \cdot \mathbf{e}_j$, is not less than zero (i.e. $\mathbf{V}_j$ and $\mathbf{e}_j$ are parallel).

The Fisher concentration in orientation, κ_j, /Fisher 1953/ for the cluster j is then approximated from the resultant vector by:

$$\kappa_j \approx \frac{W_j}{W_j - |\mathbf{V}_j|}, \qquad W_j = \sum_{i=1}^{N_j} w_i \qquad \text{(E-4)}$$

if $\kappa > 5$ (note that $\kappa < 5$ reflects a cluster with a very large spread in orientation). W_j is the Terzaghi-compensated fracture count of cluster j. The univariate Fisher distribution defines the probability density function symmetrically around its cluster mean pole, according to:

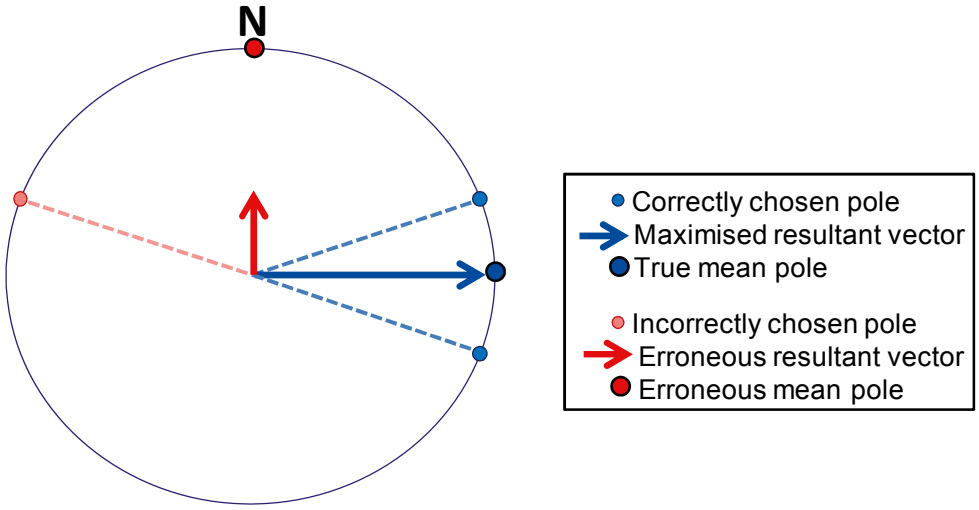

Figure E-2. *Conceptual figure of mean pole calculation for two vertical fractures (trend = 70°, respectively, 110°); a) the correctly calculated mean pole has a trend of 90°, and b) if poles are incorrectly chosen (red dashed line) and fail to maximize the resultant vector length, both its orientation and magnitude are unrepresentative of the cluster (i.e. erroneous mean pole and Fisher κ).*

$$f_j(\varphi_{ij},\theta)=\frac{\kappa_j \sin\varphi_{ij}\, e^{\kappa_j \cos\varphi_{ij}}}{2\pi\left(e^{\kappa_j}-1\right)},\qquad \varphi_{ij}=\arccos\left|\mathbf{n}_i\ \mathbf{e}_j\right| \tag{E-5}$$

where φ_{ij} is the solid angle between a fracture pole n_i and the cluster mean pole, e_j, and θ is the circumferential angle. The expected value of cluster j, in terms of Terzaghi-compensated fracture count E[X_j], at some orientation (φ_{ij}, θ_{ij}), is calculated by an infinitesimal integration of eq. (E-6), scaled by W_j.

In order to enable a comparison of the expectation value of all clusters for a given orientation, this integration area (dφ, $d\theta$) must be constant (i.e. independent of φ_{ij}). This is achieved by setting dθ = 1/(2 π sin φ_{ij}). Thus, the probability P for a given fracture i to belong to cluster j can be calculated from the expected value for cluster j, relative to the total expected value of all clusters:

$$P(x_i=X_j)=\frac{E[X_j]}{\sum_j E[X_j]}=\frac{W_j\, f_j(\varphi_{ij},\theta_{ij})/\sin\varphi_{ij}}{\sum_j W_j f_j(\varphi_{ij},\theta_{ij})/\sin\varphi_{ij}} \tag{E-6}$$

Transmissivity-based assignment of PFL-f data

Transmissivity is found to be anisotropic, i.e. varies with orientation. This partly depends on its orientation versus the stress-field, but probably also because of different geological characteristics of the set (e.g. fracture size). The fracture sets are derived by means of a soft-sector approach, which partly overlap (discussed above and implemented in Section 3.2.2; main report). Now, if PFL-f data are set-assigned based on orientation alone, it may include transmissivity values that are unrepresentative of the overall set characteristics at these overlapping regions. In order to maintain the fracture set characteristics, the set-assignment takes transmissivity into account in regions of soft-sector overlap.

Preliminary analysis reveals high transmissivity values are more frequent for low dip angles (Figure 3-5). The largest transmissivity (10^{-6} m^2/s) generally has a dip lower than 30°, and intermediate transmissivity (10^{-7} m^2/s) generally has a dip lower than 50–60° (with the exception of set NW). Thus, a transmissivity-based set-assignment is performed to reassign PFL-f data at geometrical soft-sector overlaps, between:

1) The Gently dipping and the sub-vertical sets (in the dip range between 40° and 50°).
2) The sub-horizontal set and the Gently dipping set (in the dip range between 0° and 30°).

Gently dipping and sub-vertical sets

In general, the gently dipping set has higher transmissivity in comparison to the sub-verticals. In the dip range between 40° and 50°, there is a soft-sector overlap between the gently dipping set and the sub-vertical sets EW, NW, and NE (Figure 3-15). It was therefore decided to set-assign PFL-f data based on transmissivity in this region. As a first step, all PFL-f data were binned by log transmissivity and set of belonging, according to the five-set probability fields (Section 3.2.2). In this calculation, data within the overlap range were excluded, in order to exclude unrepresentative hydraulic characteristics of a set (i.e. data with dips between 40° and 50° were excluded). The transmissivity binned PFL-f data was Terzaghi-weighted and calculated as relative frequency of occurrence, such that the sum of each transmissivity class equals unity (i.e. sum of columns in Table E-1 is equal to 1.0). This set-wise statistics was assumed to be valid also for the overlapping range. The relative Terzaghi-weighted frequency of occurrence of each transmissivity bin and set (Table E-1) was taken as the probability for any given PFL-f record with a certain transmissivity value to belong to respective set. Care was taken, so as not to allow PFL-f data to move from the Gently dipping set to an unlikely sub-vertical set (i.e. has small probability according to the Fisher distribution). The transmissivity-based probabilities for the Gently dipping set are larger for high transmissivity values in comparison between soft-sector probabilities (Table E-1) and lower for low transmissivity. In effect, the highest 6 PFL-f records (with transmissivities in log T bins –8 and –7.5) were moved from the subvertical sets to the Gently dipping set. However, most PFL-f data in the dip range between 40° and 50° did not change set.

Table E-1. Transmissivity-based probability of set-assignment at 40° < dip < 50°.

Log T	–10	–9.5	–9	–8.5	–8	–7.5	–7	–6.5	–6	–5.5	–4.5	Geometric P[1)]
EW	0.09	0.23	0.09	0.07	0.08	0.03	0.05	0.03	0	0	0	0.16
NW	0.35	0.29	0.23	0.22	0.25	0.06	0.08	0.33	0	0	0	0.05
NE	0.28	0.09	0.10	0.09	0.03	0	0.03	0	0	0	0	0.1
Gd and Hz	0.28	0.39	0.57	0.62	0.65	0.91	0.85	0.64	1	1	1	0.69

[1)] Average of soft sector probabilities for the PFL-f data in the dip range between 40° and 50°.

Gently dipping and the sub-horizontal sets

The horizontal set is in its entity (approximate dip range between 0° and 30°) overlapped by the Gently dipping set (Figure 3-15). The horizontal set dominates in the dip range between 0° and 20°. The larges transmissivity values (larger than 10^{-6} m^2/s) exist in the range 0° and 30° (Figure 3-5). At the onset of this analysis two PFL-f records were manually assigned to the horizontal set: PFL numbers 44 in KFR102A and 16 in KFR103. These two records have transmissivities of 5×10^{-7} m^2/s at dip 39° and 32°, respectively, which is considered unusually high at these high dips. The remaining PFL-f data were distributed between the two overlapping sets, similarly as done, above.

The transmissivity distribution of the Gently dipping set was estimated by binning its transmissivity values in the dip range between 30° and 60° (excluding the two records manually assigned to the horizontal set). The frequency of observations of all bins was normalised, such that the sum equals 1. This was taken as the global transmissivity distribution of the Gently dipping set, and assumed to be valid also in the dip range between 0° and 30° (Step 1 in Table E-2). The transmissivity in the dip range 0° to 30° (where Gd and Hz coexist) is larger than it is in the dip range 30° to 60° (where only Gd exists; pink area in Figure E-3a). This *deviating transmissivity statistics* is assumed to reflect the presence of set Hz, and is therefore used to discriminate between sets Gd and Hz in the range of overlap, i.e. dip 0° to 30°. Thus, transmissivity was binned in dip ranges 0° to 10°, 10° to 20°, and 20° to 30°, and normalised by the expectation value for set Gd (Step 2 in Table E-2). The difference in statistics between steps 1 and 2 is assumed to reflect the contribution of the horizontal set. This is visualised in Figure E-3b, d, f. In the third step, the transmissivity-based probability for assignment to the horizontal set was calculated by subtracting the values in step 2 from the reference data for set Gd, and normalising by the values from step 2 (Step 3 in Table E-2). The PFL-f data are then randomly assigned according to the probability values in step 3. The transmissivity distribution of set Gd has been more or less preserved (Figure E-3c), whereas the deviating statistics in the overlapping sector (predominantly high transmissivity) has been assigned to the horizontal set (Figure E-3e).

Table E-2. Transmissivity-based probability of set-assignment.

Set and dip interval	Bin (logarithmic transmissivity m²/s) –10	–9.5	–9	–8.5	–8	–7.5	–7	–6.5	–6	–5.5	–4	–4.5
Step 1) Reference statistics for Gd, estimated from non-overlapping dip range												
Gd, Dip [30 … 60]	0.02	0.07	0.17	0.22	0.3	0.15	0.04	0.02	0	0	0	0
Step 2) Binned transmissivity in overlapping range, normalized by the expectation of set Gd												
Gd and Hz, Dip [0…10]	0	0.33	0.53	1.07	0.93	0.73	0.53	0.4	0.13	0.13	0	0
Gd and Hz, Dip [10…20]	0.05	0.13	0.43	0.38	0.55	0.38	0.33	0.13	0.03	0.05	0	0
Gd and Hz, Dip [20…30]	0.05	0.05	0.18	0.3	0.25	0.23	0.05	0.1	0.08	0.03	0	0.03
Step 3) Back-calculated transmissivity-based probability for assignment to the horizontal set												
Hz, Dip [0…10]	0	0.8	0.67	0.8	0.67	0.79	0.92	0.95	1	1	0	0
Hz, Dip [10…20]	0.57	0.48	0.59	0.42	0.45	0.59	0.87	0.83	1	1	0	0
Hz, Dip [20…30]	0.57	0	0.01	0.28	0	0.32	0.13	0.78	1	1	0	1
Step 4) Final results, after random assignment to back-calculated probability values												
Hz, Dip [0…30]	0.02	0.05	0.1	0.18	0.17	0.15	0.15	0.1	0.05	0.04	0	0.01
Gd, Dip [0…30]	0.02	0.07	0.21	0.21	0.27	0.17	0.03	0.02	0	0	0	0

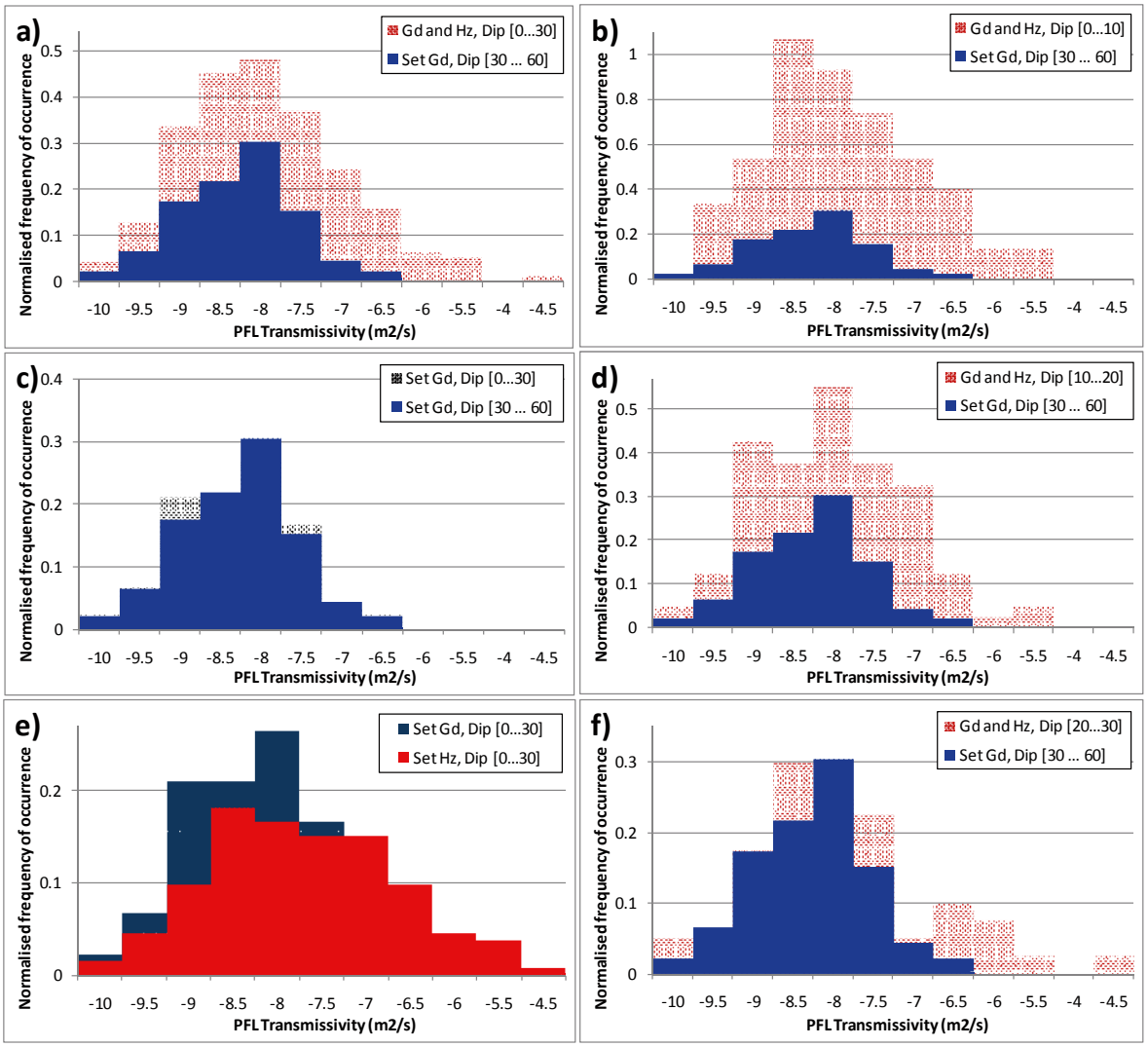

Figure E-3. *PFL-f transmissivity data for Gently dipping and Horizontal sets in HRD binned by transmissivity in different dip ranges. Reference statistics of the transmissivity distribution of set Gd, calculated in the dip range 30° to 60° are shown in blue. The excessive transmissivity frequency in the overlapping range is assumed to belong to the horizontal set, shown in red. The histograms are translucent to illustrate the overlap between populations.*

Appendix F

Constraining calibration criterion for $P_{32,COF}$

This appendix examines if a reasonable calibration criteria, $P_{32, COF}$, can be defined for the connectivity analysis (Sections 2.2.11 and 2.3). The bounds established in eq. (2-6) renders an ensemble of non-unique solutions of different combinations of $P_{32, COF}$ and k_r (see Table F-1). The lack of a well-defined conditioning target, $P_{32, COF}$, in combination with the unknown size distribution parameter, k_r, implies a major source of uncertainty in the hydro-DFN. In theory, this ensemble of possible solutions could perhaps be evaluated by inverse modelling, and the range of estimated parameter values would then demonstrate the uncertainty in the estimation of $P_{32, COF}$ and k_r. However, such a rigorous uncertainty analysis would be rather time consuming to perform and its benefit is considered to be relatively small, as the equifinality of $P_{32, COF}$ and k_r is already known to be large. This hydro-DFN is based on the methodology developed during Site Investigation Forsmark /Follin et al. 2005, 2007b/ for the purpose of practical implementation in downstream modelling. The model requisites are that its parameterisation should be realistic, with respect to previous understanding of the SFR and Site Investigation Forsmark domains, and that it honours borehole data.

Table F-1. Notation used in the main report.

Notation	Explanation
$P_{32, [Type]}$	The three-dimensional fracture intensity [m^2/m^3], for a [type] specified in the subscript.
Open	Open and Partly open fractures, as defined in Boremap data.
COF	Connected Open Fractures (i.e. Open and partly open fractures) that are connected to a hydraulic boundary (e.g. transmissive deformation zones, or the sea floor).
PFL	A Boremap feature (e.g. Open or Partly open fracture, or a crush zone) coupled to a specific capacity measured with the Posiva Flow Logging-device. The measured specific capacity is censored by a practical detection limit, T_{lim}.
T_{lim}	An assumed detection limit for the Posiva Flow Logging-device, $Q/s \geq 2.5\times10^{-9}$ m^2/s.
k_r	Power-law scaling exponent, determining the proportion between small and large fractures. The parameter has a strong influence on the connectivity of the fracture system. It is a relatively uncertain parameter, as it cannot be directly measured from borehole data, and is therefore estimated by means of a connectivity analysis.

From a practical aspect, the DFN calibration requires that $P_{32, COF}$ is tighter constrained than the theoretical bounds in eq. (2-6). Different possibilities in extrapolating $P_{32, COF}$ from the subset of PFL-f data above detection limit have been considered by /Follin et al. 2005/. KFR105 has an exceptionally low detection limit (Section 2.2.4) and thus has a large population of PFL-f data below the common transmissivity cut-off, T_{lim}. KFR105 is therefore used to test possible methods of extrapolating $P_{32, COF}$.

It is examined if $P_{32, COF}$ can be estimated by:

1) parameterisation of PFL-f transmissivity above T_{lim}, followed by an

2) extrapolation of the transmissivity below T_{lim}.

Power-law and log-normal distributions are considered. This strategy requires continuity in the transmissivity distributions: the subset of data below T_{lim} must follow the same distribution as the data above T_{lim}. The validity in this approach can be investigated by means of DFN-simulation. Fracture size and transmissivity have been assumed to be correlated (Section 2.2.9). Now, if a perfect correlation is assumed between fracture size and transmissivity, the size pattern of Connected Open Fractures (Figure F-1) should fairly well resemble its transmissivity pattern. Although this pattern varies significantly depending on DFN parameterization, it is clear that large fractures (high transmissivity) tend to be similar to its parent distribution of Open fractures, while shorter fractures (low transmissivity) are less likely to be connected, and therefore deviate from its parent distribution. These DFN realizations imply that, if the correlation between fracture size and transmissivity indeed is perfect, neither the power-law nor the log-normal distributions may be appropriate for estimating $P_{32, COF}$. However, in reality this perfect 1:1 correlation between size and transmissivity is unrealistic; the assumption is made for practical reasons (Section 2.2.9). Therefore the extrapolation methods were explored in a tentative manner.

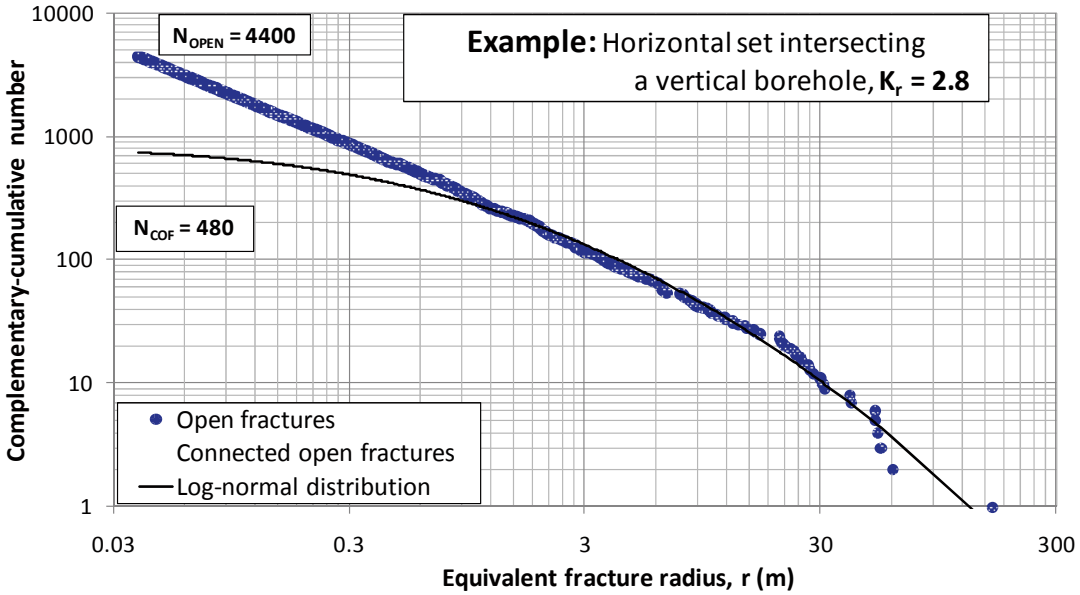

Figure F-1. *Example of the typical relation between the size distributions of Open, respectively, Connected Open Fractures shown in a Complementary cumulative number plot. The size pattern of Connected fractures depends not only on the size distribution, k_r, but also on the parameterisation of other fracture sets.*

Evaluation from data

In KFR105, the PFL-f data above T_{lim} constitutes 6% of the Open and Partly open fractures (sum of Terzaghi weights). The entire PFL-f data set, including uncertain data and transmissivity below T_{lim}, is 17% of the intensity of Open and Partly open fractures in KFR105. As most PFL-f data below T_{lim} are uncertain interpretations, $P_{32, COF}$ may be lower than 17% of $P_{32, Open}$. On the other hand, low transmissivity PFL-f data may be underrepresented owing to the noise level in the vicinity of high inflows (Section 2.2.4). Therefore $P_{32, COF}$ may well be higher than 17% of $P_{32, Open}$. If uncertain data are included, only one third of the PFL-f data in KRF105 has transmissivity above T_{lim}. This indicates that $P_{32, COF}$ should exceed $P_{32, PFL}$ above T_{lim} by at least a factor of 3.

Power-law extrapolation

Two obstacles can be identified in power-law extrapolation:

1) The power-law distribution is difficult to apply. The lower integration bound is unknown, but must be assumed in order to define the cumulative power-law distribution. The estimation of $P_{32, COF}$ is extremely sensitive to the assumed lower integration bound.
2) The power-law distribution may be inappropriate for connected fractures. Short fractures are less likely to be connected; if the parent population of Open and Partly open fractures are assumed to be power-law distributed, its subpopulation of connected fractures can therefore be expected to deviate from the parent population (Figure F-1).

For demonstration of the sensitivity in this approach, different values for the lowest transmissivity of the shortest connected fracture were explored. One possibility is setting the lower bound to 10^{-10} m^2/s, as this corresponds to the lowest certain PFL-f record. A power-law distribution was fitted to the subset of PFL-f data above T_{lim} in KFR105. The intensity of connected fractures (sum of Terzaghi weights) in the range between the assumed lower bound and T_{lim} (e.g. transmissivity between 10^{-10} and 2.5×10^{-9} m^2/s) can then be estimated by extrapolation (Figure F-2). A lower integration bound of 1.0×10^{-10} m^2/s corresponds to 100% Open fractures being connected, while a small increase in the lower bound to 2.0×10^{-10} m^2/s reduces $P_{32, COF}$ to 50% of $P_{32, Open}$. Power-law extrapolation from the PFL-f data above T_{lim} seems to be inappropriate (with consideration to the discussion above), and it would seem unlikely that 100% of the Open fractures indeed are connected, particularly if r_{min} is set equal to borehole radius.

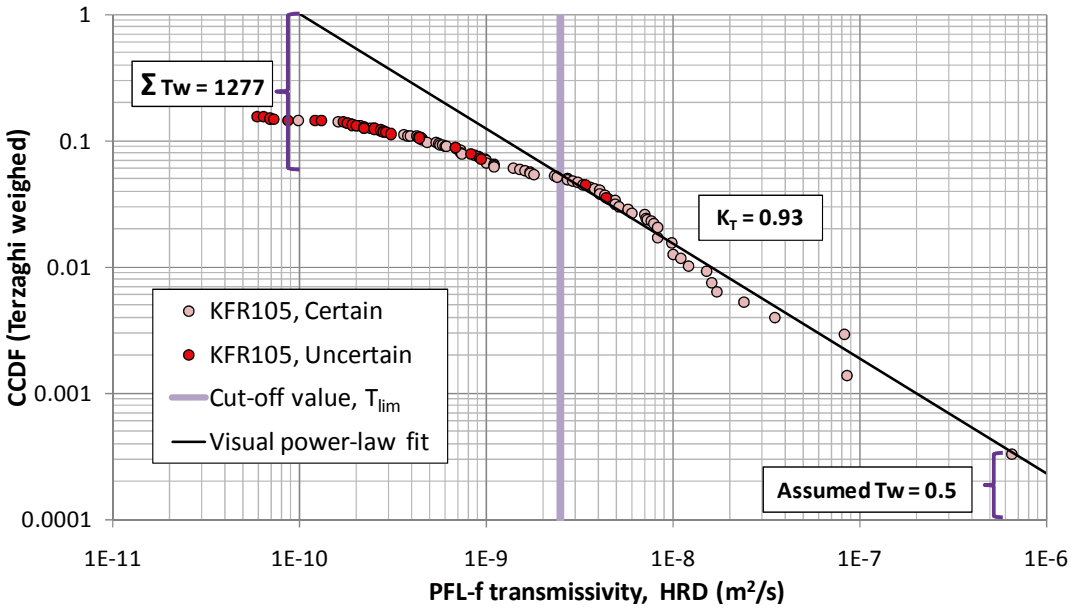

Figure F-2. *Complementary cumulative probability distribution of PFL-f transmissivity in KFR105 visually fitted to the upper tail of data, and extrapolated down to an assumed lower bound of 10^{-10} m^2/s.*

However, a similarity in pattern can be observed between Figure F-2 and Figure F-1. Breakpoints can be identified in both distributions, which divide the data into two subpopulations. The size pattern of Connected Open Fractures starts to deviate from its parent power-law relation of Open fractures below a radius of 20 m (Figure F-1). A similar breakpoint can be observed in PFL-f transmissivity at approximately 5×10^{-9} m^2/s (Figure F-2). One possible interpretation for the transmissivity breakpoint is underrepresentation of low PFL-f transmissivity (Section 2.2.4). However, the similarity in pattern between Figure F-1 and Figure F-2 suggests that if the lower tail of $P_{32,\,COF}$ is to be extrapolated by a power-law, it is more appropriate to fit the power-law relation to data below its breakpoint. Therefore, an alternative power-law was fit to PFL-f transmissivity within the interval between 4×10^{-10} and 4×10^{-9} m^2/s (Figure F-3). In this case, the lower integration bound of 1.0×10^{-10} m^2/s suggests that 21% of $P_{32,\,Open}$ are connected, or that $P_{32,\,PFL}$ above T_{lim} is 27% of $P_{32,\,COF}$. A lower bound to 2.0×10^{-10} m^2/s would suggest that 16% of $P_{32,\,Open}$ are connected, or that $P_{32,\,PFL}$ above T_{lim} is 37% of $P_{32,\,COF}$. This second approach appears more reasonable, and indicates that $P_{32,\,COF}$ should exceed $P_{32,\,PFL}$ above T_{lim} by a factor of 3–4. The drawback of this method is that there are generally few PFL-f data available below the breakpoint in other boreholes, which makes the method less applicable.

Log-normal extrapolation

Extrapolation with a log-normal distribution does not require a lower bound of the distribution. Therefore, the possibility in fitting PFL-f transmissivity in KFR105 to log-normal distributions was also examined. Two cases are compared: 1) the fit is made to transmissivity exceeding T_{lim}, and 2) the fit is made to the upper tail, $T > 10^{-8}$ m^2/s (Figure F-4). The intensity of Connected Open Fractures $P_{32,\,COF}$ can then back-calculated from the cumulative log-normal distributions. Using T_{lim} as cut-off value to estimate $P_{32,\,COF}$ renders that 19% of $P_{32,\,Open}$ are connected, or that $P_{32,\,PFL}$ above T_{lim} equals 30% of $P_{32,\,COF}$. It can be noted that although the distribution is fit to data above T_{lim}, the agreement is good over the interval below the break-point, 4×10^{-10} and 4×10^{-9} m^2/s (Figure F-4).

Using the higher cut-off value, 10^{-8} m^2/s, to estimate $P_{32,\,COF}$ would suggest that 23% of $P_{32,\,Open}$ are connected, or that $P_{32,\,PFL}$ above T_{lim} is 25% of $P_{32,\,COF}$. It appears that extrapolation with the log-normal approach is less sensitive to which part the transmissivity interval is available for fitting. However, the two fitted cases also demonstrate the non-uniqueness with fitting the upper tail of data to log-normal distributions; the second case would suggest that half of the population of Connected Open Fractures has a transmissivity lower than 10^{-10} m^2/s, values that are of little practical interest for the hydro-DFN. The log-normal extrapolation of PFL-f transmissivity suggests that $P_{32,\,COF}$ should exceed $P_{32,\,PFL}$ above T_{lim} by a factor of approximately 3–4.

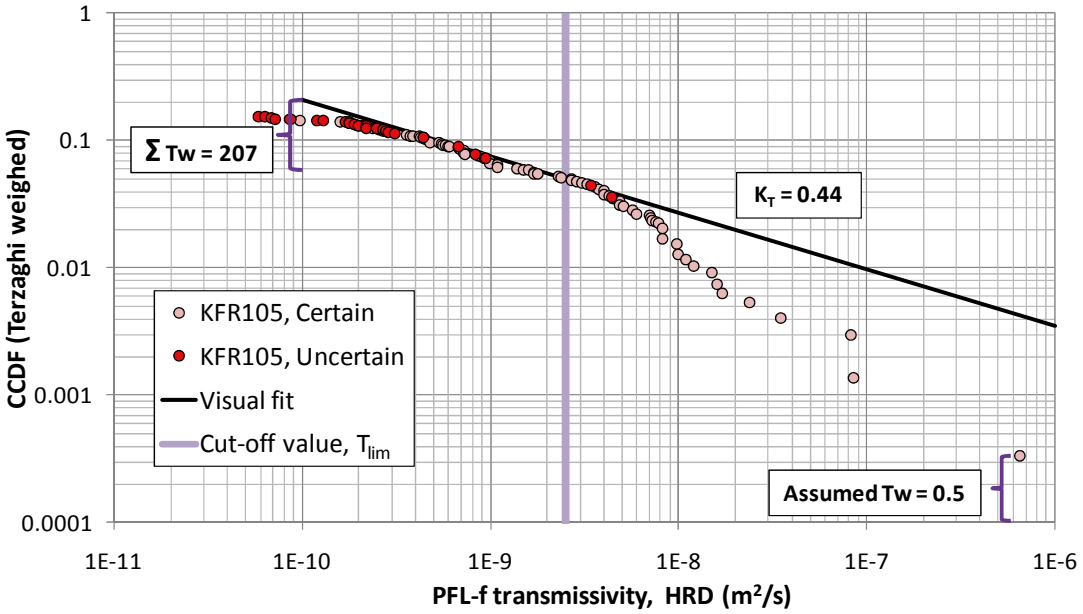

Figure F-3. *Complementary cumulative probability distribution of PFL-f transmissivity in KFR105 visually fitted to an interval of transmissivity between 4×10^{-10} and 4×10^{-9} m²/s, and extrapolated down to an assumed lower bound of 10^{-10} m²/s.*

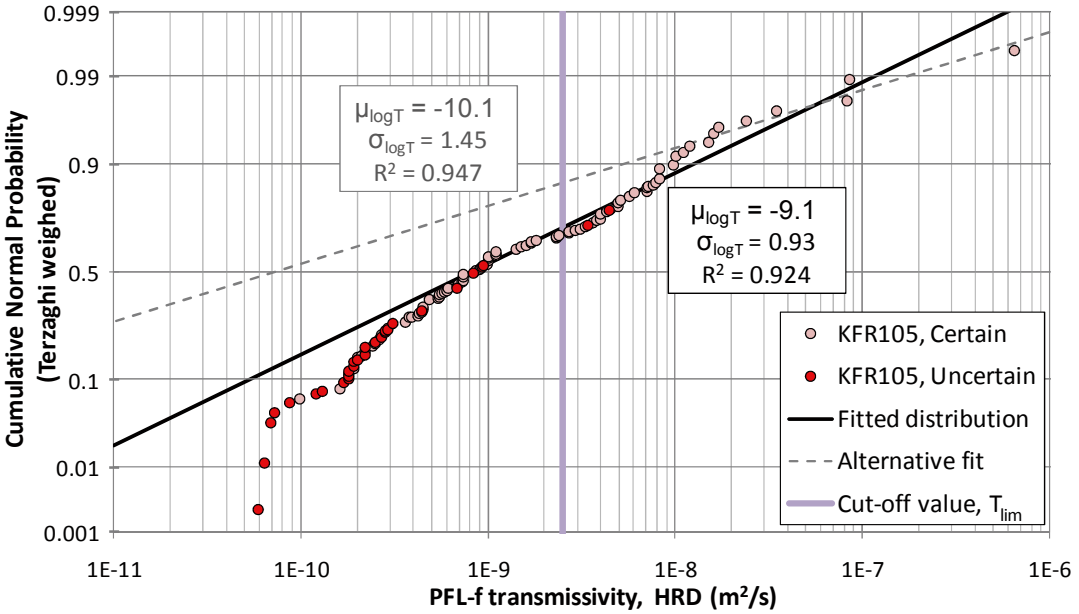

Figure F-4. *Lognormal distribution of PFL-f transmissivity in KFR105 fitted to the subset of data above T_{lim}. An alternative fit is shown for the upper tail of PFL-f data, with transmissivity exceeding 10^{-8} m²/s.*

Defining calibration criterion

As a comparison, simulations for the comparatively sparsely fractured rock in Site Investigation Forsmark indicated that 13% of the Open fractures are connected, and that 41% of these Connected fractures were above the transmissivity threshold applied /Follin et al. 2005/. In major part of the SFR data set, the HRD above ZFM871, the ratio between measured PFL-f and mapped Open and Partly open fractures is equal to 11 (excluding compensation of detection limits and variability between fracture sets). Thus, with compensation for detection limit, the overall ratio between $P_{32,\,Open}$ and $P_{32,\,COF}$ in SFR must be lower than 11, and thus implying that the connectivity in SFR is higher than that in Site Investigation Forsmark. However, note that the SFR data set represents shallower depths than the Forsmark data, where cored boreholes were generally cased down to –100 m RHB70.

Based on the observations made above, it appears that the estimated $P_{32,\,COF}$ exceeds $P_{32,\,PFL}$ above T_{lim} by a factor of approximately 3–4. It must be pointed out that this analysis has only been made for KFR105 and without consideration to variability between fracture sets. It can therefore not be concluded that the observations should hold general for all boreholes, at different depths, and for different fracture sets.

Nevertheless, the calibration of k_r, requires a defined matching criterion for $P_{32,\,COF}$. As a tentative calibration target it was therefore decided that $P_{32,\,COF}$ shall exceed $P_{32,\,PFL}$ by a factor ranging from 2 to 4. During the later stage of calibrations it was found difficult match this criterion for vertical sets in the shallow bedrock (Section 3.4).

Appendix G

DFN evaluation by means of flow simulations

The purpose of this appendix is to critically evaluate how the DFN, which was parameterised by means of the geometrical connectivity analysis, performs within a DFN flow simulation framework. Emphasis is placed in finding methodological inconsistencies that should be avoided in the final SFR v.1.0 hydrogeological model.

G.1 Inconsistency in intensity calibration of $P_{32,COF}$ and $P_{32,PFL}$

An inconsistency has been identified in the way $P_{32,\,COF}$ is conditioned to $P_{32,PFL}$. Simulated networks of Connected Open Fractures are Poissonian clusters (Section 2.2.8). This implies that in a connected fracture network, there is a locally higher expected intensity in the vicinity of a fracture that is intercepted by a borehole (e.g. Figure G-1). The PFL-f data do not reflect flowing fractures explicitly, but rather borehole sections (0.1 m) with an apparent transmissivity above practical detection limit. In practise, it is even unrealistic to expect that two neighbouring inflows less than 0.2 m apart can be resolved as two separate PFL-f records. The distribution of distance to the nearest PFL-f record is shown in Figure G-1. There are altogether 3 instances (of 608) where the separation distance is 0.2 m, and 11 instances separated 0.3 m. Outside the possible deformation zones defined in SHI (i.e. HRD), there are no PFL-f records with separation distance 0.2 m, and only 3 records separated 0.3 m. The most common separation distance range from 0.5 to 2 m (Figure G-1).

In the PFL-f interpretation of PFL-f data, all features within 0.1 m (or effectively 0.2 m) are regarded as Alternative Best Choices, of which finally only one is selected as "the flowing feature". In other words, according to the PFL-f methodology, the fracture count in PFL-f data over a 0.1 m bin can never exceed 1. Based on Figure G-1, it never exceeds 1 even over a 0.2 m bin in the SFR data set. In reality, the intensity of Open Certain fractures is exceptionally high within the 0.1 m bin of PFL-f records (referred to as "PFL_conf 1"), as compared to the neighbouring 0.1 m sections (referred to as "PFL_conf 2") and the background level (referred to as "Uniform expectation") as shown in Figure G-2.

In the connectivity analysis, no respect was paid to the 0.1 (or 0.2 m) resolution. To consistently relate the connectivity analysis to PFL-f data, its output should be converted into effective values over a certain bin size (0.2 m). In other words, all Connected fractures falling into a 0.2 m bin should be re-interpreted as only one feature (and its transmissivity should be summed). As demonstration, 50 realisations of the connectivity analysis were re-analysed in bin-sizes of 0.2 m and 0.3 m. The number of fractures per borehole interval bin is shown as fraction of total fracture count (Figure G-3). If the fracture count over each bin is constrained from exceeding 1, the total fracture count is reduced by 16% for a bin size of 0.2 m, or 27% for a bin size of 0.3m.

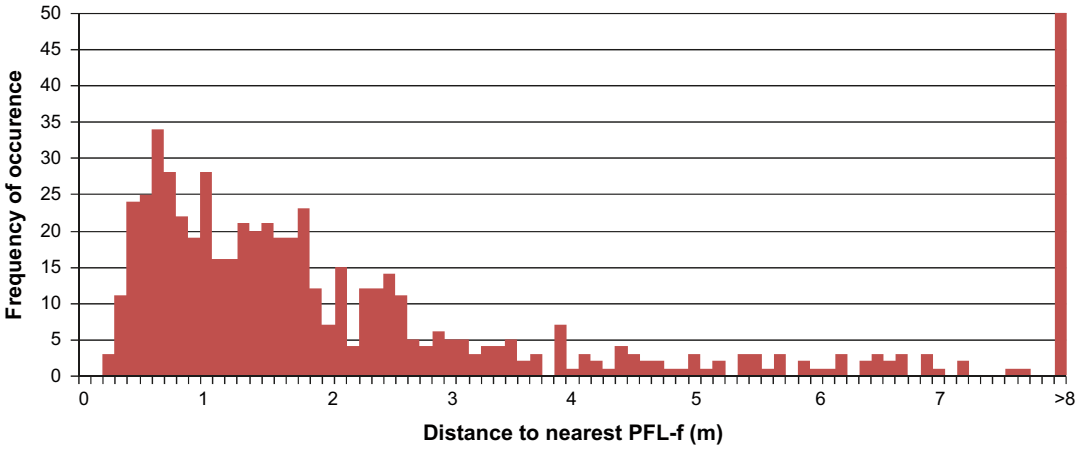

Figure G-1. *Distribution of separation distance to the nearest PFL-f record*

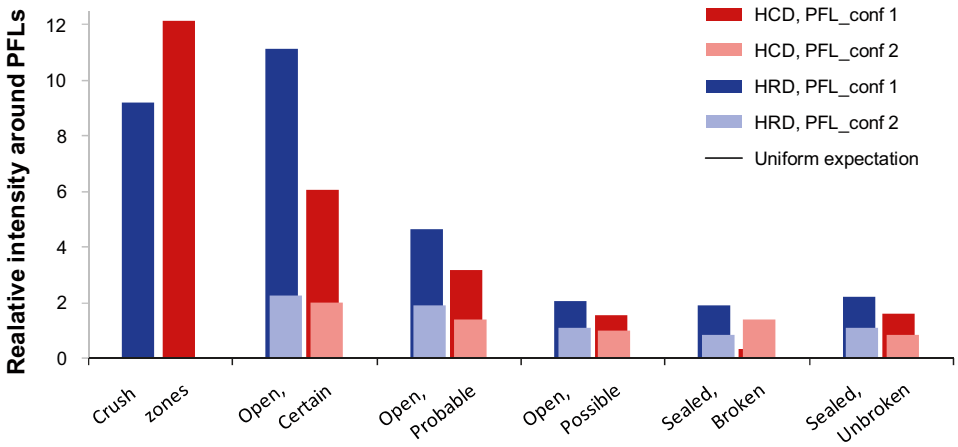

Figure G-2. *Fracture intensity in the vicinity of PFL-f records related to fracture intensity outside the geometric window of a PFL-f anomaly. Taken from /Öhman et al. 2010/.*

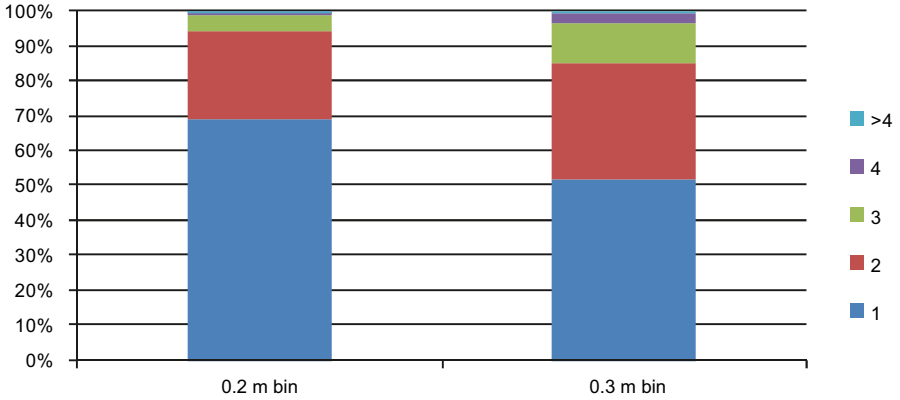

Figure G-3. *Number of Connected fractures inside a borehole interval bins (from 50 realizations).*

G.2 Flow simulations and effects of hydraulic chokes.

The hydro-DFN parameterization of the SFR model v.0.2 was calibrated to PFL-f data using the simplified connectivity analysis. This calibration approach is based on geometry alone, using a vertical scan-line borehole (zero radius) to compute fracture intersections. The transmissivity of intersected fractures of the Connected DFN was assumed to be directly related to evaluated PFL-f transmissivity data (i.e. without further consideration to upstream hydraulic bottlenecks). In other words, intersected fractures are assumed to be well-connected to a positive hydraulic flow boundary of constant head. However, in a sparsely fractured rock it is likely that borehole inflow is not only limited by the fracture intersecting a borehole, but also to the transmissivity of upstream fractures. Therefore flow simulations were performed with both DarcyTools and FracMan to evaluate the applicability of the geometric connectivity analysis. Ten realisations were studied, and the output from the connectivity analysis was compared to results of flow simulations, in terms of back-calculated interval transmissivity. Note that the flow simulations were *not* compared directly to PFL-f data, but only to output from the connectivity analysis.

There are three reasons for this:

1) This study is intended to evaluate the applicability of the connectivity analysis method; it is *not* intended to be a comprehensive model validation.
2) Only ten realisations are studied. Figure J-1 demonstrates that at least 50 realisations are required to attain stable expectation values.

3) The hydro-DFN was calibrated to PFL-f data in terms of set-wise, Terzaghi-weighted borehole intensity. It is not trivial to back-trace discrete fractures from simulated borehole inflow, in order to assess Terzaghi-weights and fracture set (particularly from DarcyTools, as discussed below). For example, there can be several fracture intersections over a short borehole interval.

It should also be pointed out that the findings made in this Appendix may relate to model setup (e.g. meshing, domain boundaries, truncation of low-transmissive features, etc). More realistic model setups may improve results, and therefore the results presented here should not be taken as definite evidence, but indicative of the effects of hydraulic chokes (Figure 2-1).

Methodology: borehole inflow evaluation

1. Fracture realisations of Open fractures were generated, according to the hydro-DFN parameterisation (Table 3-4, main report). The translation from a fracture network to ECPM in DarcyTools is based on volumetric intersection between fractures and grid cells /Svensson et al. 2007/, and therefore fractures must have a physical thickness. This thickness was set to a small value to avoid enhancing the connectivity (1 mm).
2. All fractures with transmissivity < 10^{-9} m^2/s were removed (see discussion below).
3. Isolated fractures were removed with the approximate DarcyTools algorithm <sortisol>.
4. The Connected fracture networks (step 3) were analysed in three different ways:
   a) vertical scan-line sampling (zero radius). The sampled fracture transmissivity is referred to as "connectivity analysis", and used as reference data for comparison to flow simulations,
   b) exported to FracMan, where all 1 mm apertures were collapsed into 2D-planes. The fracture networks were converted into finite-element meshes (using the modules MeshMaster and EdMesh). Borehole inflow was solved with MAFIC and can be directly compared to the connectivity analysis,
   c) imported to DarcyTools. DFN transmissivity was translated into ECPM grids, where zero-conductivity cells were removed. The meshes were successively refined with focus to resolve upstream hydraulic bottle-necks. Borehole inflow was solved with DarcyTools (Migal).
5. Simulated borehole inflow (steps 4b and 4c) is related to borehole interval transmissivity at different bin sizes, eq. (G-2), and compared to that of the connectivity analysis, step 4a, eq. (G-1). The results are summarized in Figure G-10, and the details are shown in Figure G-14 through Figure G-33.

The simulated flow in DarcyTools cannot always be linked back to a discrete feature, since the fracture network has been converted into ECPM with a vertical resolution of 0.1 m (Table G-2). Also, the flow simulations involve a fracture radius (r_0 = 0.038 m), where the intercepts non-perpendicular fractures will spread over a certain borehole interval (i.e. in contrast to the Connectivity scan line which produces a distinct interception point). Over this interval, there may be several fracture intersections (i.e. Poissonian clusters). This makes it difficult to compare transmissivity on the basis of discrete fractures. Furthermore, as discussed in Appendix G-1, it is probably more correct to perform transmissivity comparisons in terms of interval transmissivity for complete consistency to original PFL-f data.

The interval transmissivity from the connectivity analysis was calculated as the sum of n intercepted fractures T_f over each given interval:

$$T_i = \sum_n T_f^n \qquad \text{(G-1)}$$

The interval transmissivity from the flow simulations was back-calculated by Dupuits formula, assuming of cylindrical and steady state flow:

$$T_i = \frac{Q}{s2\pi}\ln\left(\frac{R}{r_0}\right) \approx \frac{Q}{s}, \qquad \text{(G-2)}$$

where s is drawdown (m), Q is borehole inflow (m^3/s), r_0 is borehole radius (m), and R is the radius of influence (m). In the PFL-f interpretation of transmissivity, the quotient R/r_0 was assumed to be

equal to 500 /e.g. Pekkanen et al. 2008/, independently of T, which reduces eq. (G-2) to $T \approx Q/s$. However, in sparsely fractured rock, it is unrealistic to assume cylindrical flow and constant radius of influence (independent of transmissivity and fracture size; see Figure 2-1).

Discretisation of borehole radius in FracMan

FracMan features the option between linear and quadratic flow equations. In this study, *linear* equations are chosen, as it allows a larger mesh (i.e. larger number of fractures); however, it also requires a more careful element discretisation at locations with non-linear gradient of drawdown (d^2s/dr^2). The gradient is expected to be non-linear at converging and diverging flow field locations. Obviously, this is expected to occur in the borehole near-field, but also to varying degrees at the hydraulic chokes. To evaluate this, two aspects are considered in the borehole discretisation of flow simulations (see Table G-1):

- discretisation (element size) and
- borehole representation (single node or all nodes at or within borehole radius).

A single fracture with a transmissivity of $T_{input} = 1.0\times10^{-5}$ m^2/s is studied. The fracture has full connectivity to the hydraulic bounds (H = 0 m, at z = 0 m, |x| = 50 m, |y| = 50 m), and intersects the borehole perpendicularly. A drawdown of –10 m is applied to the borehole and specific capacity, Q/s, is simulated using linear finite elements. The expected specific capacity can also be calculated analytically from fracture transmissivity by Dupuits formula, assuming of cylindrical and steady state flow, eq. (G-2). R is set to 50 m (model domain) and r_0 is 0.038 m, which results in an analytical value of $\mathbf{8.748\times10^{-6}}$ m^2/s. Simulated test cases are compared to this analytical value in terms of a Q/s-ratio (see Table G-1).

For illustration, three meshing examples – with resulting head fields – are shown in Figure G-4. The results presented in Table G-1 are also plotted as a function of discretised element length (Figure G-5).

Table G-1. Borehole discretisation test cases for FracMan.

Case	Borehole representation	Element size (m)	T_{input} (m^2/s)	Simulated Q/s (m^2/s)	Q/s-ratio [simulation/analytical]
1	single node	0.1	1.0×10^{-5}	7.75×10^{-6}	88.62%
2	single node	0.05	1.0×10^{-5}	7.08×10^{-6}	80.96%
3	single node	0.038	1.0×10^{-5}	6.84×10^{-6}	78.14%
4	single node	0.005	1.0×10^{-5}	4.92×10^{-6}	56.26%
5	All nodes r ≤ 0.038 m	0.005	1.0×10^{-5}	8.75×10^{-6}	100.03%

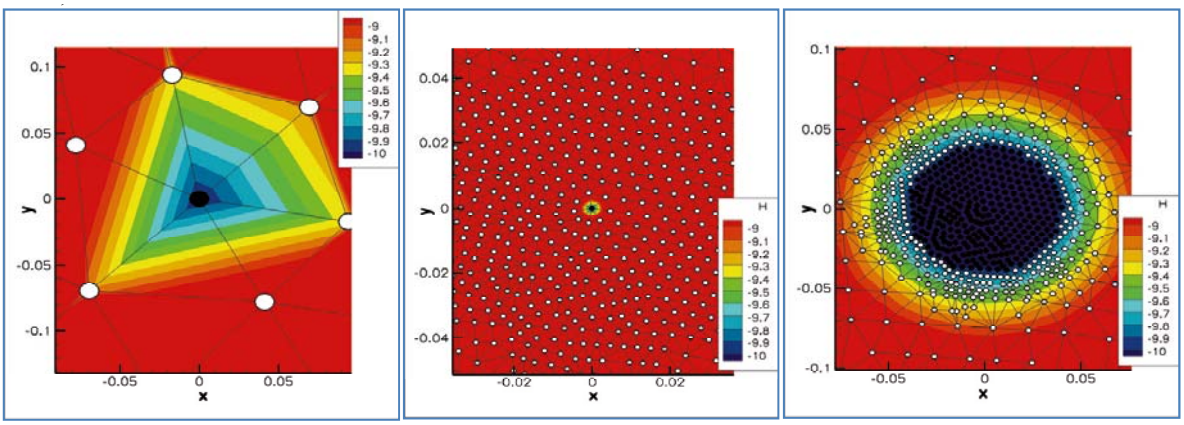

Figure G-4. *Close-up on borehole discretisation: Case 1 (left), Case 4 (middle), and Case 5 (right). Fracture nodes are white, while borehole nodes are black. Calculated head shown in colour scale (covers only 1 m drawdown). Note that the solved gradients are "fairly similar" in Cases 1 and 5, although Case 1 does not resolve the non-linear gradient in the vicinity of the borehole.*

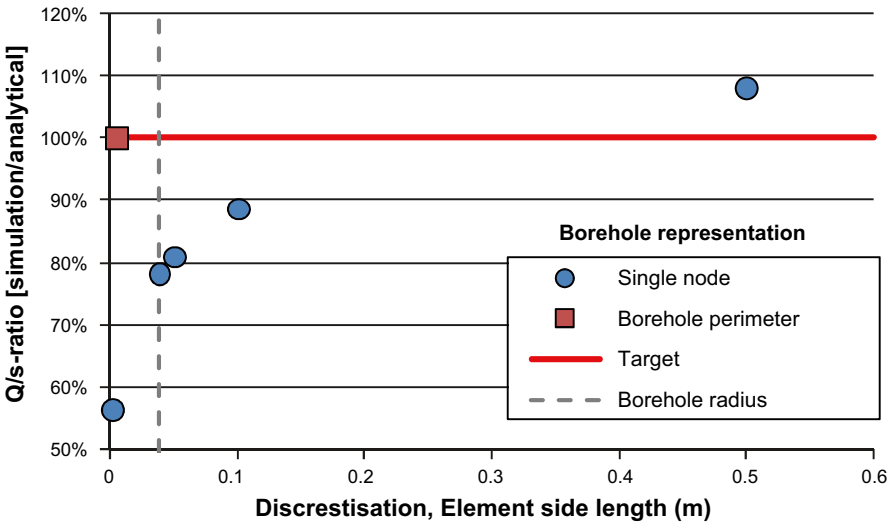

Figure G-5. *Ratio between simulated Q/s and analytical Q/s as a function of element side length (Target = 100%). Borehole radius 0.038 m shown with dashed line. The multiple node borehole representation is only made with a fine discretisation (0.0005 m).*

In cases 1 and 2, the borehole is represented by a single boundary node; the only difference is the discretisation element size. Cases 4 and 5 have identical meshes; the only difference is what nodes are defined as boundary nodes. Case 1 is only 11% off from the analytical value. However, Case 4 is 44% below the analytical value. Thus, the reason why Case 1 provides a better match is that its coarse discretisation does not resolve the resistance of the converging flow near the borehole node accurately. The inflow in Case 4 is choked by friction losses over the elements in contact with the borehole node, which is the result of convergent flow (note huge gradient over these elements).

When the hydraulic bound is expanded to borehole radius (Case 5) the simulation is only off by 0.03% (three correct digits). The reason is that the geometry is fairly well represented by the mesh (better than 0.5 cm precision). The change in gradient (d^2s/dr^2) is highest in the vicinity of the borehole perimeter (say, nearest 5 cm, or so), and therefore a fine geometric discretisation is likely to be important in this region. Consequently, it was decided to resolve the true borehole radius using a refined mesh in the vicinity of the borehole perimeter in flow simulations. The change in gradient is also expected to be large at hydraulic chokes. In this study no attempt was made to refine the discretisation at fracture intersections, and therefore the effects of hydraulic chokes may be somewhat overestimated. However, judging from Figure G-5, this negligence is assumed to be of secondary importance. More fractures are intersected if the true borehole radius is used, compared to if a scan-line (or single node) is used. This discrepancy is discussed in Appendix H. In the corresponding DaryTools simulations, the borehole is represented by a single cell (Figure G-8).

Meshing

The original fracture network is based on generation of Open fractures. Fractures were assigned an aperture of 1 mm in DarcyTools, but converted into 2D planes in FracMan. Fractures not connected to the hydraulic bounds (H = 0 m, at z = 0 m, |x| = 50 m, |y| = 50 m, see Figure 2-5) are removed by the DarcyTools command <sortisol> /Svensson and Ferry 2004/. A vertical borehole (L = 515 m, r = 0.038 m) is implemented at the centre of the domain, extending from –10 to –525 m RHB70 (i.e. covering the vertical extent of SFR core data). An impervious borehole casing is implemented between 0 and –10 m RHB70 to avoid short-circuiting flow. A 10 m drawdown (constant head) is prescribed to borehole cells/nodes.

Fractures with transmissivity lower than 10^{-9} m^2/s were excluded (the practical detection limit of PFL-f data, T_{lim}, has been assumed to be approximately 2.5×10^{-9} m^2/s). It may be expected that the discrepancy between geometrical connectivity analysis and flow simulations should be even larger

for low transmissive fractures (i.e. short fractures). Nevertheless, the focus of this evaluation was on fractures with transmissivity larger than 10^{-9} m^2/s. There are three reasons for this:

- Significant reduction of simulation time.
- Low transmissive fractures are of less importance in the final hydro-DFN (generally discarded in real model applications, due to ECPM conversion).
- PFL-f data below T_{lim} are more uncertain (see main report).

It is impossible to create identical model setups with the two different computational softwares. However, effort was made to setup the modelling geometries as similarly as possible, with emphasis to resolve fracture connectivity and the borehole radius. Note that in the FracMan mesh, floater elements are automatically removed (i.e. non-connected elements, which do not take part in the flow solution). The DT cell sizes decreases gradually from (1x1x1) m^3 at the domain boundaries down to ($0.067 \times 0.067 \times 0.1$) m^3 closer to the borehole. The minimum cell size was chosen to represent the borehole cross-sectional area with a single cell (i.e. the borehole cannot be resolved by the cell size normally applied in regional-scale modelling, c. 10 m). Cells with negligible conductivity (lower than 10^{-18} m/s) are excluded from the computational mesh. Cells with conductivity lower than 10^{-12} m/s are assumed to have little effect on the flow solution and set equal to 10^{-12} m/s (three orders of magnitude lower than the minimum transmissivity of 1 mm wide fractures). The final mesh typically contains 2-4 million cells. The element length in the FracMan meshes ranges from meter-scale at hydraulic boundaries and down below cm-scale in the vicinity of the borehole (resulting in typically 400,000 elements). More details on the mesh generation for the two models are specified in Table G-2 and Table G-3. Cylinder objects surrounding the vertical borehole, with some radius r, were used in the grid refinement. Note that the grids are adapted to the fracture geometry of the connected realisations in both setups. Note also that the values in Table G-2 and Table G-3 are maximum values; the actual cell/element sizes may well be smaller.

Table G-2. Sequential mesh generation in DarcyTools, adapted to ECPM conductivity. $K_{cell} < 10^{-18}$ m/s are excluded at the end of each iteration. Isotropic cell cutting, Δx = Δy.

Mesh iteration	Whole domain	Cylinder 1	Cylinder 2	Cylinder 3
1	Δx = Δz = 8 m	r = 10 m, Δx = Δz = 4 m blur 1	r = 1.7 m, Δx = Δz = 1 m blur 1	r = 0.35 m, Δx = 0.067 m, Δz = 0.1 m blur 3
2	Δx = Δz = 4 m	r = 20 m, Δx = Δz = 1 m blur 2	r = 2.5 m, Δx = Δz = 0.5 m blur 2	Same as above
3	Δx = Δz = 1 m	r = 10 m, Δx = Δz = 0.5 m blur 2	r = 1.7 m, Δx = 0.137 m, Δz = 0.1 m blur 2	Same as above
4	No refinement, $K_{cell} < 10^{-18}$ m/s are excluded, [$10^{-18} \le K_{cell} < 10^{-12}$ m/s] set to $K_{cell} = 10^{-12}$ m/s			

Table G-3. Sequential mesh generation in FracMan (element side length, ΔL).

Mesh iteration	Whole domain	Cylinder 1	Cylinder 2	Cylinder 3
1. MeshMaster	ΔL = 10 m	r = 7 m, ΔL = 1.5 m		
2. Edmesh		r = 1 m, ΔL = 0.1 m	r = 0.2 m, ΔL = 0.05 m	r = 0.1 m, ΔL = 0.025 m
3. MAFIC	Automatic floater removal (i.e. elements disconnected from the flow solution)			

In the FracMan mesh, the DFN connectivity (i.e. fracture intersections) is accurately reproduced automatically, independent of user-specified element size. Therefore a coarser discretisation can be used further away from the borehole in FracMan with little effect on the flow solution. The refinement in the vicinity of the borehole is intended to improve the resolution of the borehole perimeter and the non-linear head gradient resulting from the converging flow regime. The resulting borehole circumference (0.24 m) is generally resolved by c. 25 elements, with a typical side length of 1 cm (see Figure G-8).

Examples of meshes for one realisation are shown in Figure G-6, Figure G-7, and Figure G-8. The full vertical extent of one realisation is shown in Figure G-6d. However, it is difficult to demonstrate the details on connectivity and flow for the full vertical extent, and therefore the figures have been zoomed and fractures outside the region of interest have been clipped.

The discrepancy in the modelling setup is largest in the immediate vicinity of the simulated borehole (Figure G-8). The coarse representation of borehole radius in DarcyTools is compensated by increasing the conductivity in the cell-walls to the borehole by a factor of 3.2, a value that has been used previously in similar DarcyTools applications.

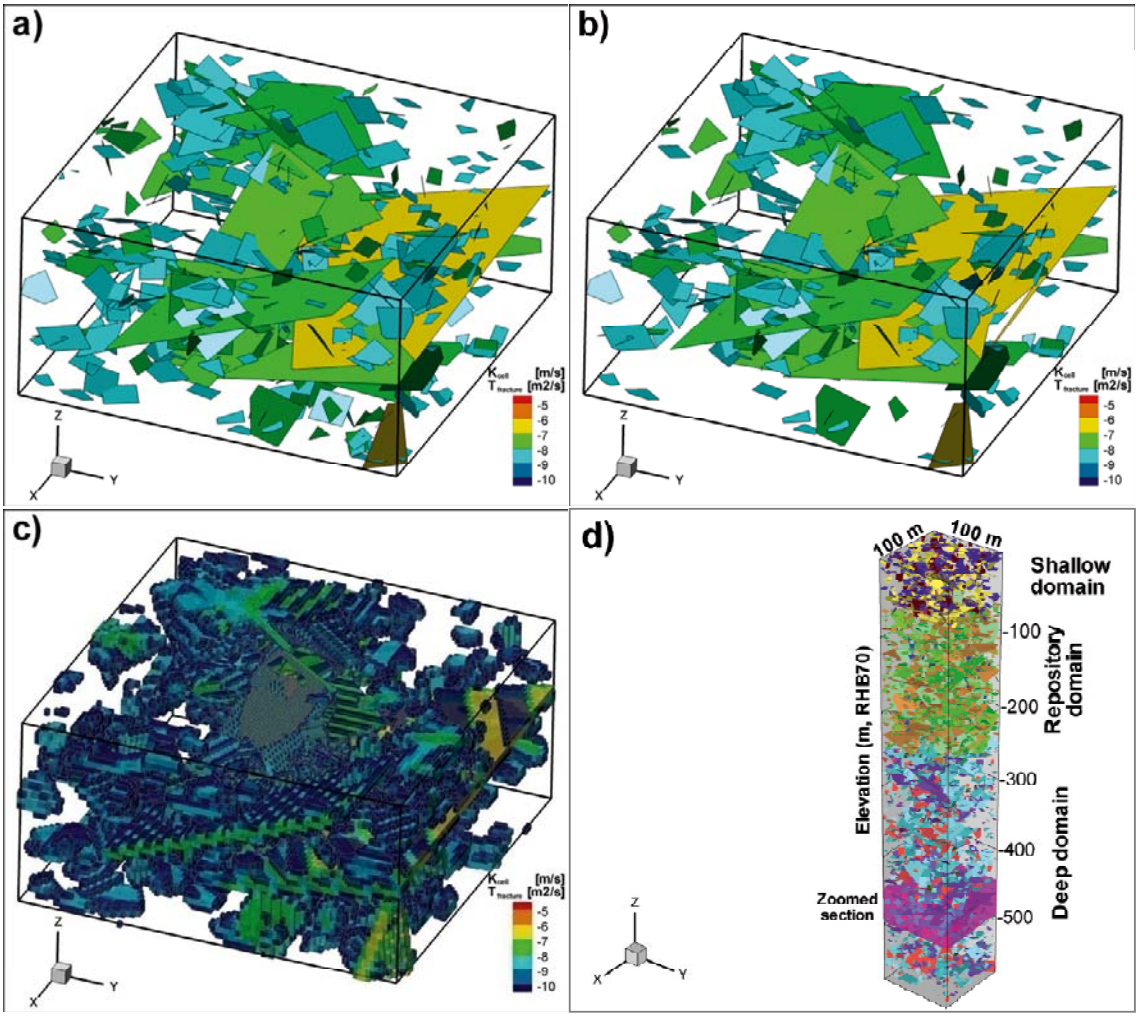

Figure G-6. *Connected fracture network in a zoomed-in sub-region of the flow domain (–445 to –495 m RHB70); a) generated fractures, b) computational mesh in FracMan, c) computational mesh in DarcyTools, and d) the entire fracture generation domain, used both in the connectivity analysis and the flow simulations. A simulated vertical borehole is located in the middle of the domain. For visibility, the fractures extending outside the domain have been clipped.*

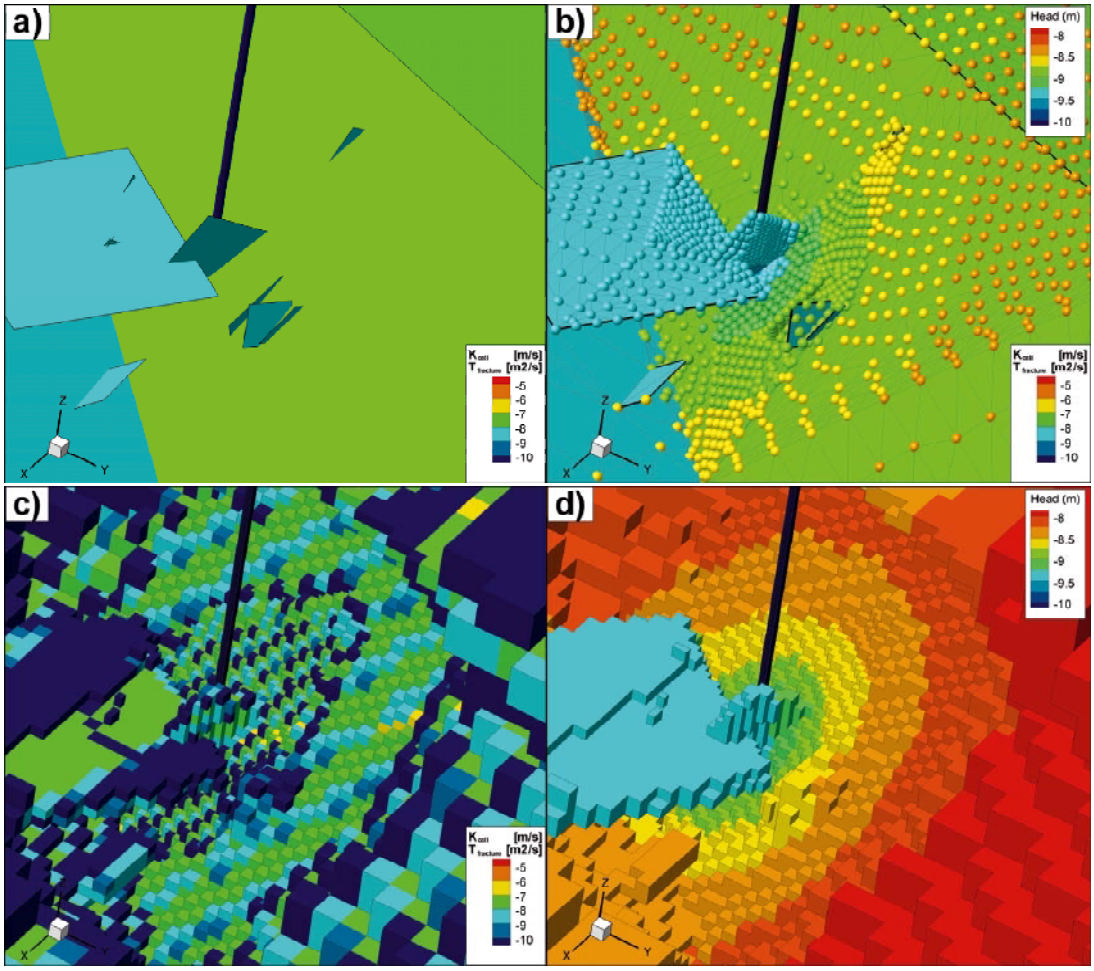

Figure G-7. *Discretisation and solved head-field within an approximate 2 m radius around the simulated borehole (black cylinder); a) the input DFN, b) FracMan mesh with element transmissivity and nodal head values, c) DacyTools mesh with cell-wall conductivity and c) cell-centre head values. Note that although conductivity and transmissivity are different entities they are shown with the same colour scale. The striped pattern in the DarcyTools conductivity field is the result of volume-fractional contribution from intersecting fractures that are non-parallel to the Cartesian grid.*

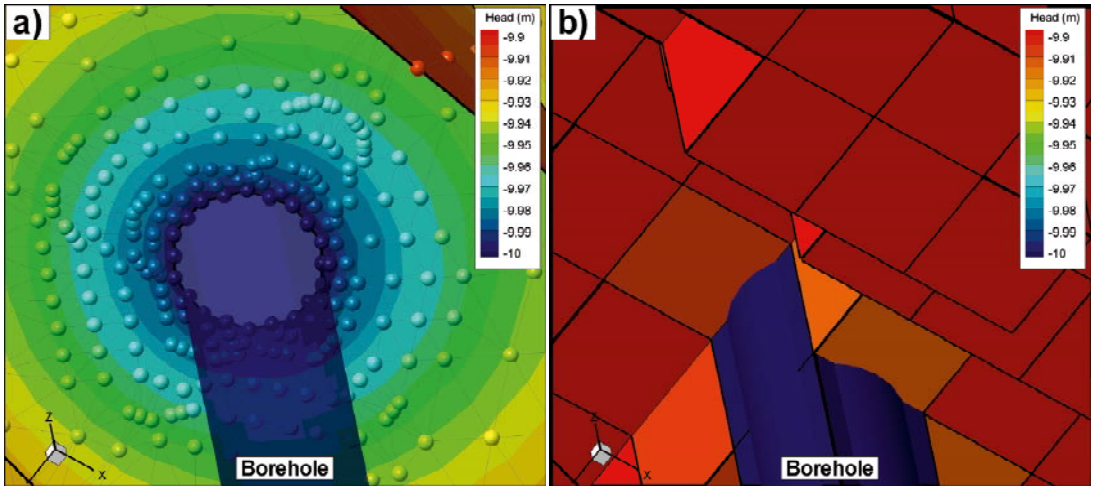

Figure G-8. *Discretisation of borehole radius and simulated head field in the immediate vicinity of the simulated borehole (a 0.1 m radius around the borehole is shown); a) FracMan and b) DarcyTools. In DarcyTools, the coarse representation of borehole radius is compensated by increasing the conductivity in the cell-walls to the borehole by a factor of 3.2. Note that the colour scale covers only a 0.1 m drawdown.*

Representativeness of 10 truncated realisations

The truncation of transmissivity below 10^{-9} m^2/s infallibly reduces the geometric connectivity of the fracture network. Consequently, the simulated P_{32COF} above T_{lim} (2.5×10^{-9} m^2/s) decreases and does not fully honour PFL-f data (see comparison in Figure G-9). This effect is only visible in the Shallow domain, which may be expected, as the connectivity in the Shallow domain to a higher degree depends on vertical (low transmissive) fractures connecting to the hydraulic boundary at the ground surface. It is likely that the truncation has less impact on actual flow, as connecting low-transmissivity fractures are likely to act as hydraulic bottlenecks. This notion is supported by Figure G-10a, b and Figure G-11a, as the discrepancy between the connectivity analysis and the flow-simulations is also largest in the Shallow domain.

Most likely, more than 10 realisations are probably needed to establish the significance of excluding low transmissive features from the connectivity analysis.

Evaluation in terms of discrete fracture inflow

Simulated borehole inflow in FracMan can be evaluated for discrete fractures. For each fracture intersecting the borehole, a ratio can be calculated between the back-calculated transmissivity, eq. (G-2), and its parameterised input value. A ratio of 100% implies that the parameterised input reproduces borehole inflow (i.e. consistent to PFL-f data), while a low ratio indicates the borehole inflow is choked by hydraulic bottle necks. On average, this ratio is equal to 17% for all 10 realisations, but it appears to vary with depth domain, fracture set, and input transmissivity (i.e. size), as shown in Figure G-11. The lower back-calculated transmissivity in the Shallow domain (Figure G-11a) is because the DFN connectivity depends, to a comparatively larger extent, on low-transmissive features connecting to the ground surface. The difference between sets (Figure G-11b) probably depends to a higher degree in differences in size, than on orientation (c.f. Figure G-11c). The proportion of choked fracture transmissivity (red colour) versus non-choked transmissivity (blue) is shown per depth domain and fracture set (Figure G-12), respectively, input transmissivity (Figure G-13).

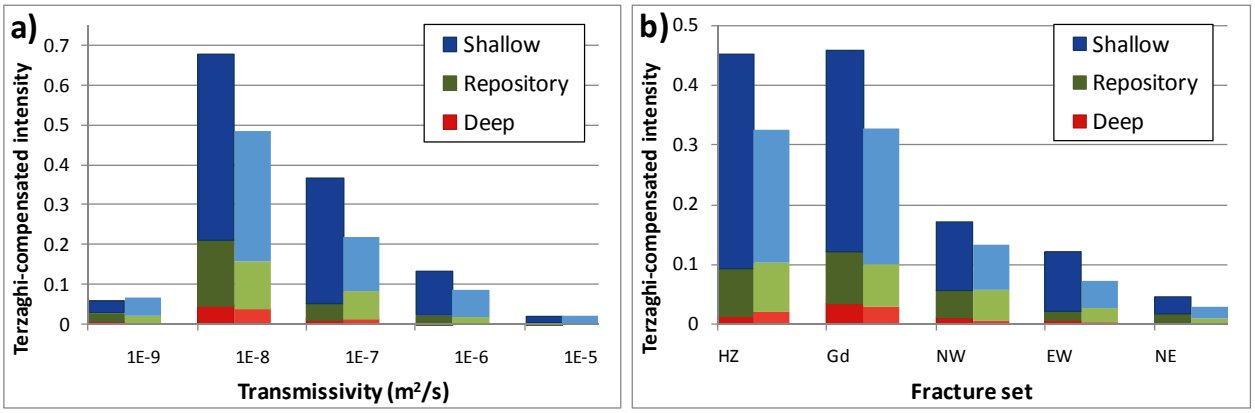

Figure G-9. *Terzaghi-compensated intensity of PFL-f data (dark colours) compared to output from 10 truncated realisations of the connectivity analysis (pale colours), in terms of a) transmissivity and b) set of belonging. Note that no borehole length binning has been applied for the connectivity analysis output.*

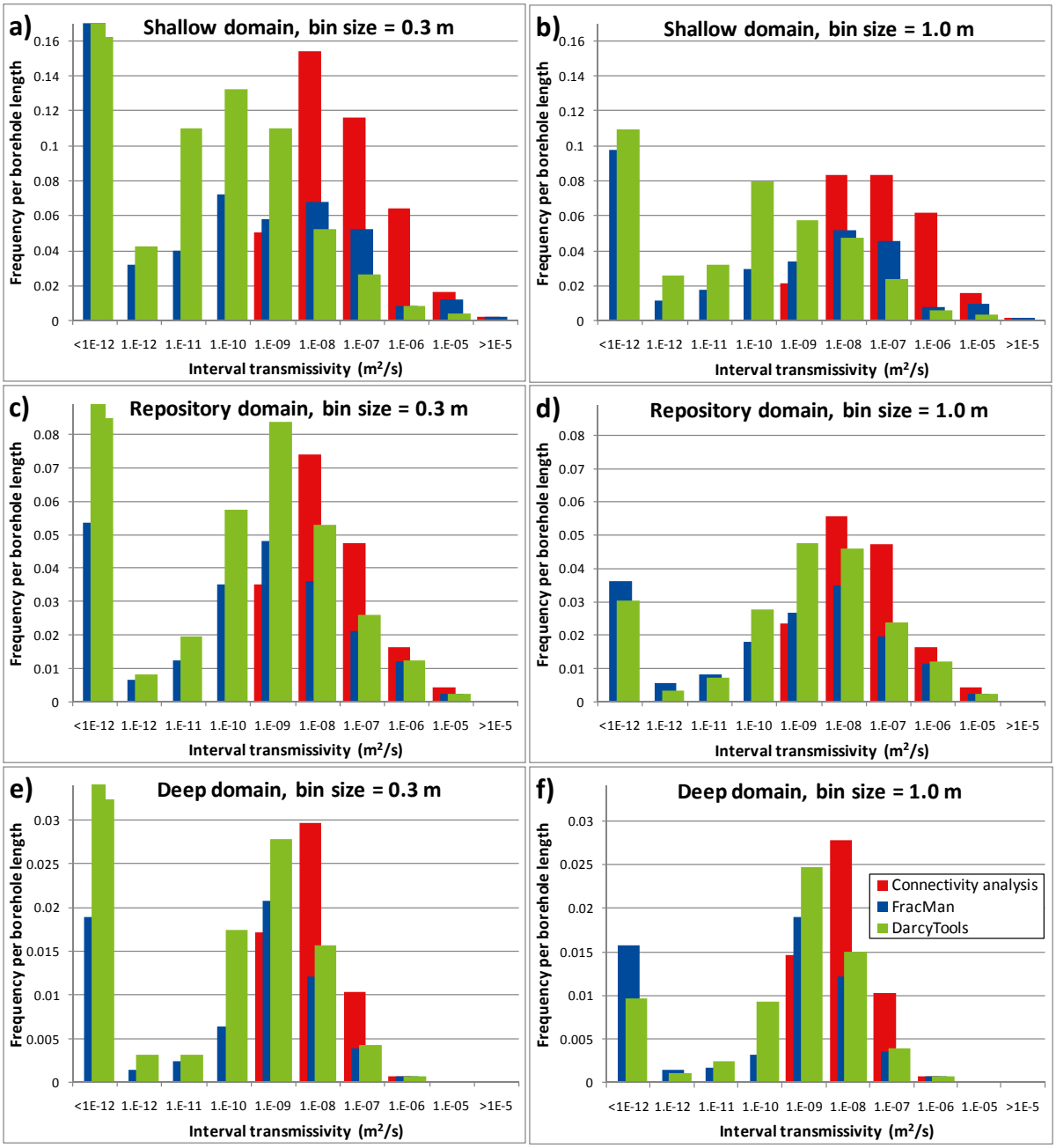

Figure G-10. *Interval transmissivity distributions compared for the three depth domains and different bin-sizes. The category "<1E–12" reflects non-zero transmissivity bins lower than $10^{-12.5}$ m²/s.*

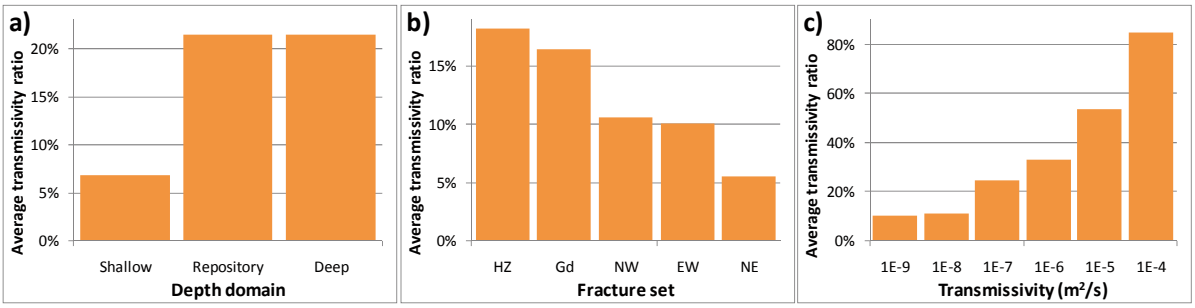

Figure G-11. *Average ratio between parameterised and back-calculated transmissivity from FracMan simulations; a) per domain, b) per fracture set, and c) as a function of input transmissivity.*

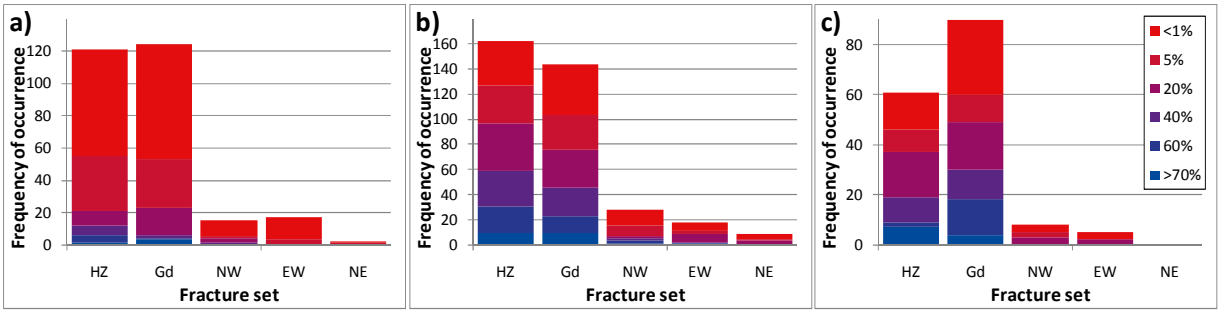

Figure G-12. *Ratio between parameterised and back-calculated transmissivity from FracMan simulations per fracture set; a) Shallow domain, b) Repository domain, and c) Deep domain. Red colour signifies inflow choked by hydraulic bottlenecks.*

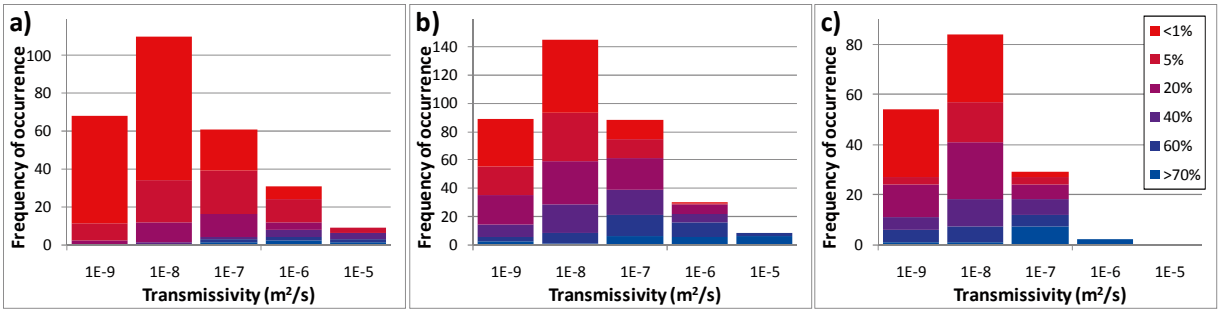

Figure G-13. *Ratio between parameterised and back-calculated transmissivity from FracMan simulations as a function of input transmissivity; a) Shallow domain, b) Repository domain, and c) Deep domain. Red colour signifies inflow choked by hydraulic bottlenecks.*

Conclusions

In summary, both the DFN simulations (FracMan) and fine-discretised continuum simulations (DarcyTools) shows the effects of hydraulic chokes. This must be accounted for when PFL-f data are applied in DFN parameterisation. A couple of methodological inconsistencies could be identified:

1) A PFL-f record is a borehole section where *apparent transmissivity* (interpreted transmissivity) exceeds the practical detection limit; it may well reflect the total inflow of several fractures. This spatial resolution of PFL-f data was not properly accounted for in the connectivity analysis. By definition, the number of PFL-records over a 0.1 m borehole section cannot exceed 1, whereas there may be several simulated fractures over the same interval. Consequently, the model will underestimate the true intensity. Recommendation: simulation results must also be binned over borehole sections, before comparison to PFL-f data.

2) In the connectivity analysis, the apparent PFL-f transmissivity was assumed to reflect the explicit transmissivity of the fractures intercepted by the borehole. This assumption relies on cylindrical flow regime that is well-connected to the hydraulic bounds. This assumption is inconsistent, due to presence of upstream hydraulic bottle-necks (Figure 2-1; Appendix G.2). Consequently, the geometry-based calibration approach does not guarantee that PFL-f data is honoured in terms of flow within a DFN modelling framework.

3) Hydraulic chokes seem to constitute large component of the variability in the *apparent transmissivity* of PFL-f data. The longer the flow path is to the nearest head boundary, the more likely it is to be subject to hydraulic chokes. Thus, the borehole location with respect to surrounding deformation zones may contribute to the observed spatial trends in PFL-f variability. Consequently, the model setup must be improved with real deformation zone geometry and real borehole locations, in order to gain better insight into the correlation between distance to hydraulic bounds and *apparent* PFL transmissivity.

4) The discretisation of the true borehole radius proved to have minor impact on flow simulations.

Detailed binned results, ΔL = 0.3 m

The assigned transmissivity is compared to "simulated transmissivity" (in reality, Q/s), as binned into borehole sections (**ΔL = 0.3 m**), are shown for ten realisations in Figure G-14 to Figure G-23. The assigned fracture transmissivity, as sampled by a vertical scan-line, is referred to as "connectivity analysis" (red bars) is compared to "simulated transmissivity", back-calculated borehole inflow from a) FracMan (blue bars), respectively, b) DarcyTools (green bars). Note that the plotted bars are overlapping in the figures. Therefore, *any visible red indicates that the back-calculated transmissivity from flow simulations is lower than that geometrically sampled in the connectivity analysis.*

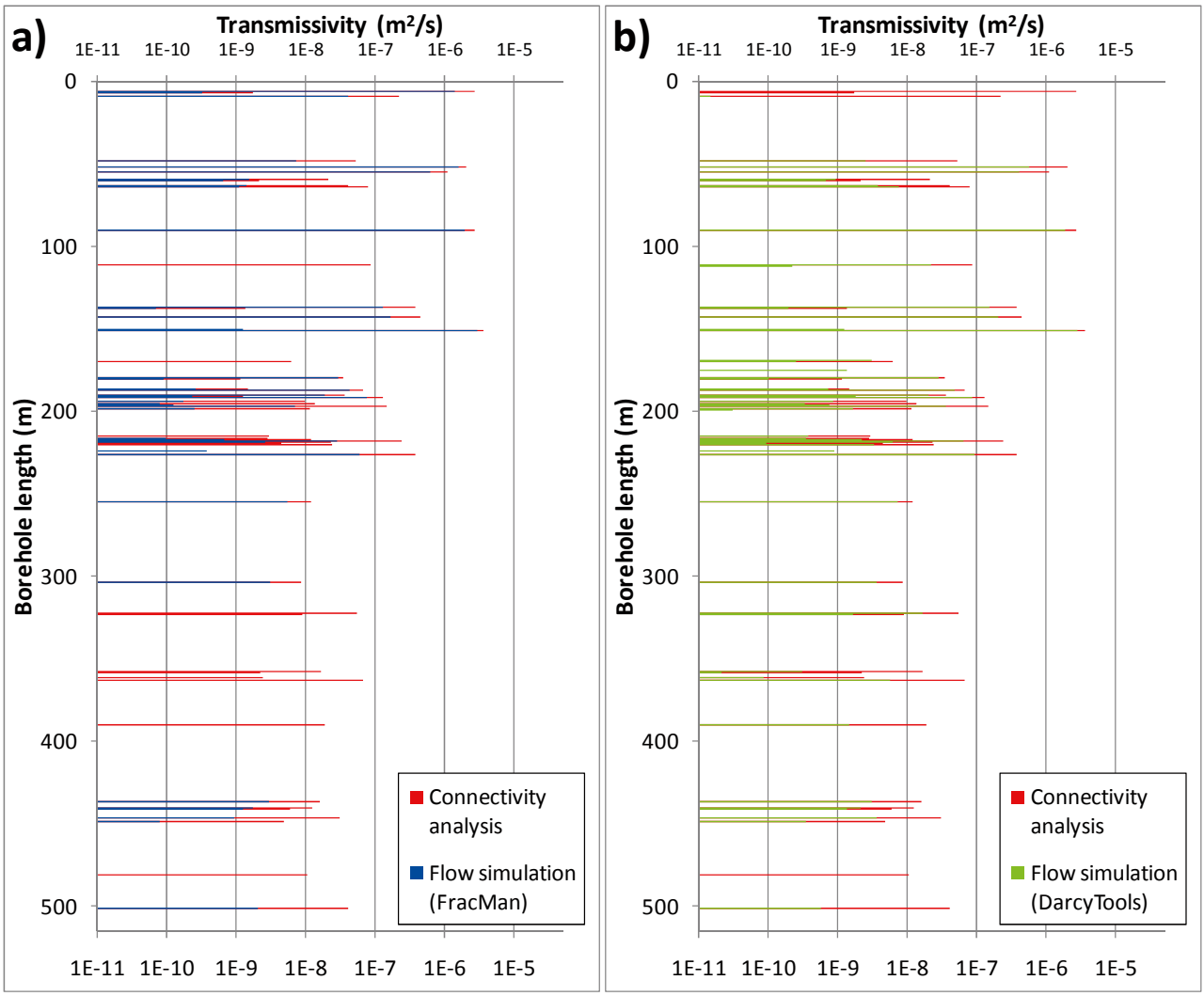

Figure G-14. *Realisation 1, ΔL = 0.3 m.*

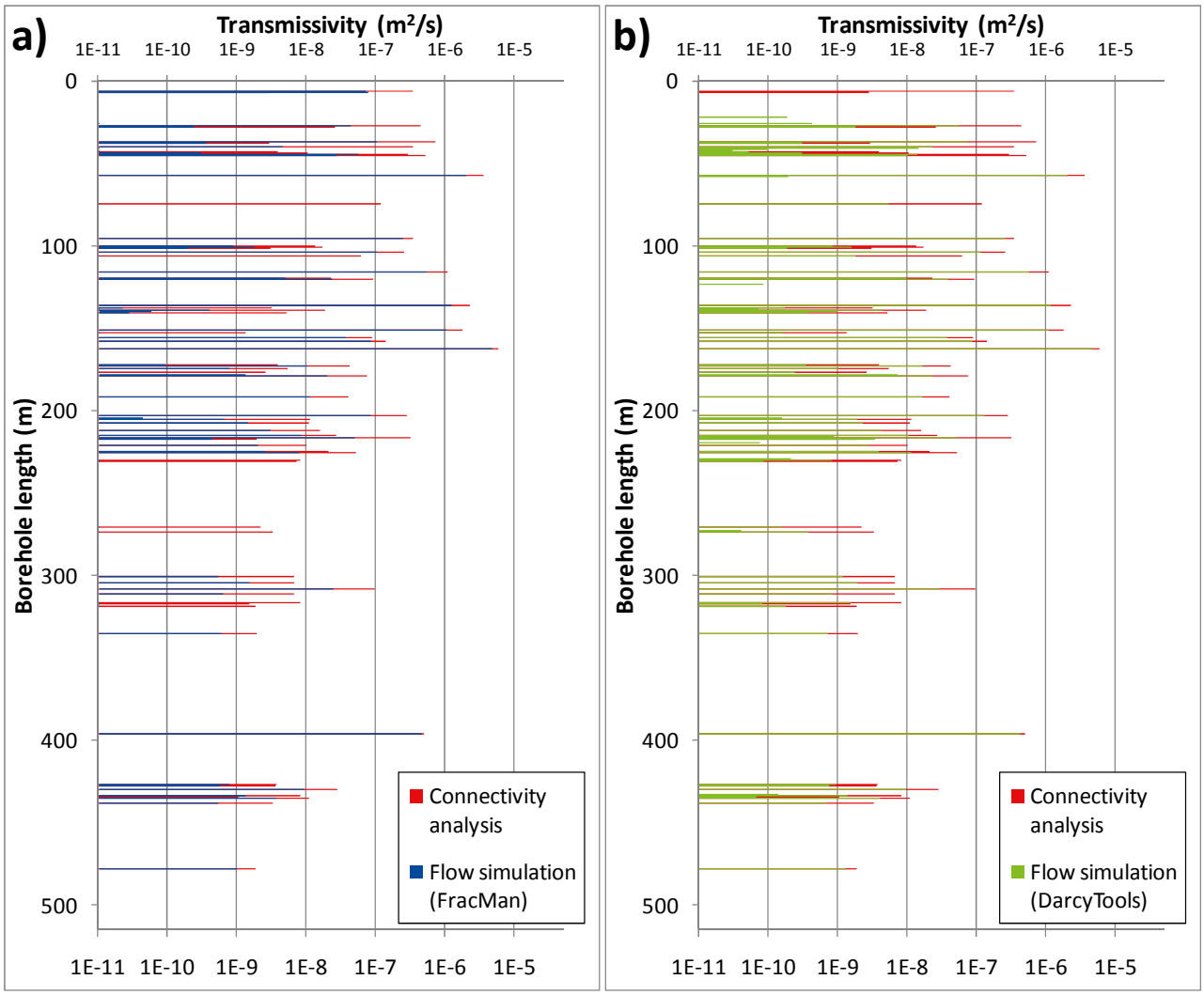

Figure G-15. *Realisation 2, ΔL = 0.3 m.*

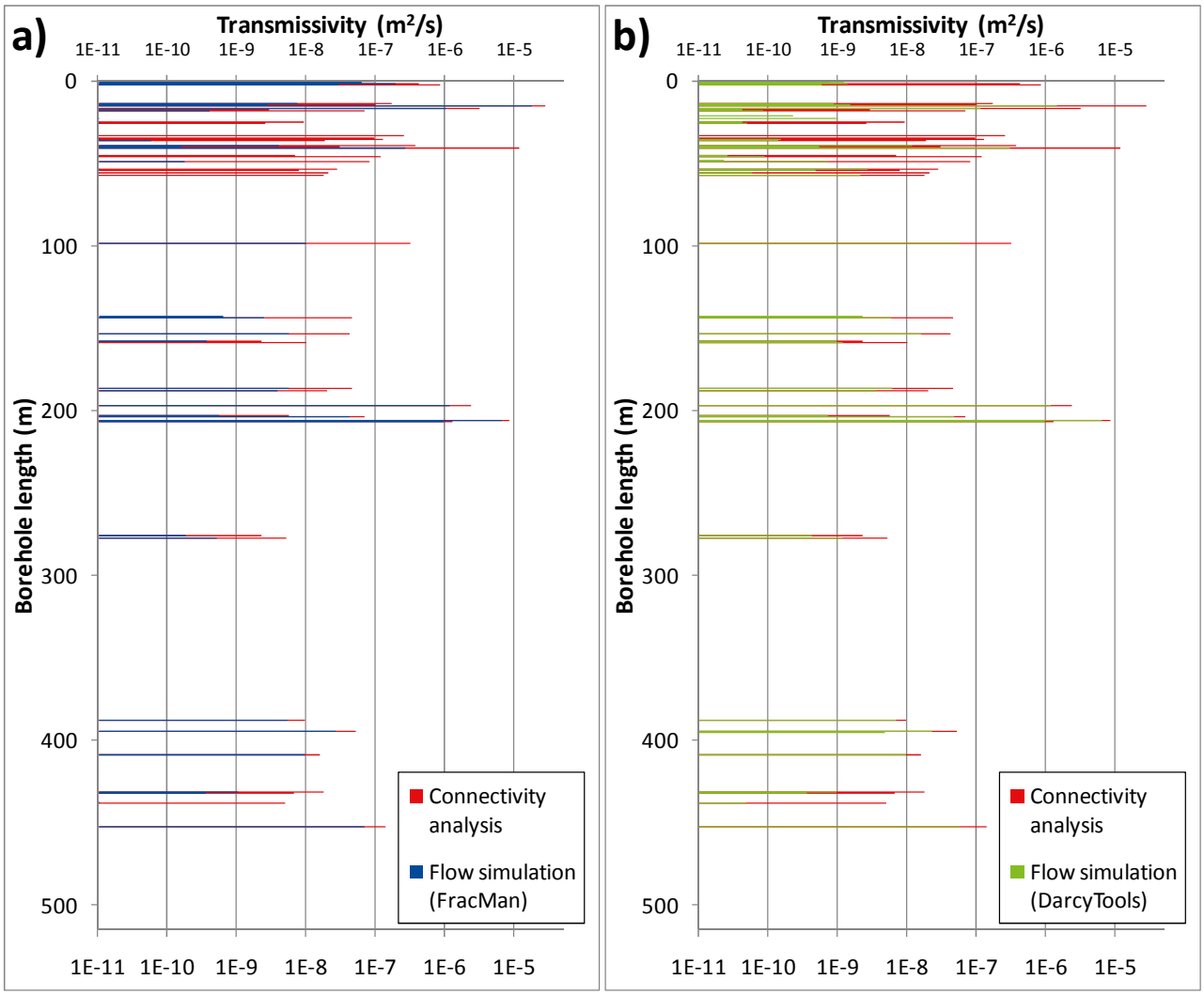

Figure G-16. *Realisation 3, ΔL = 0.3 m.*

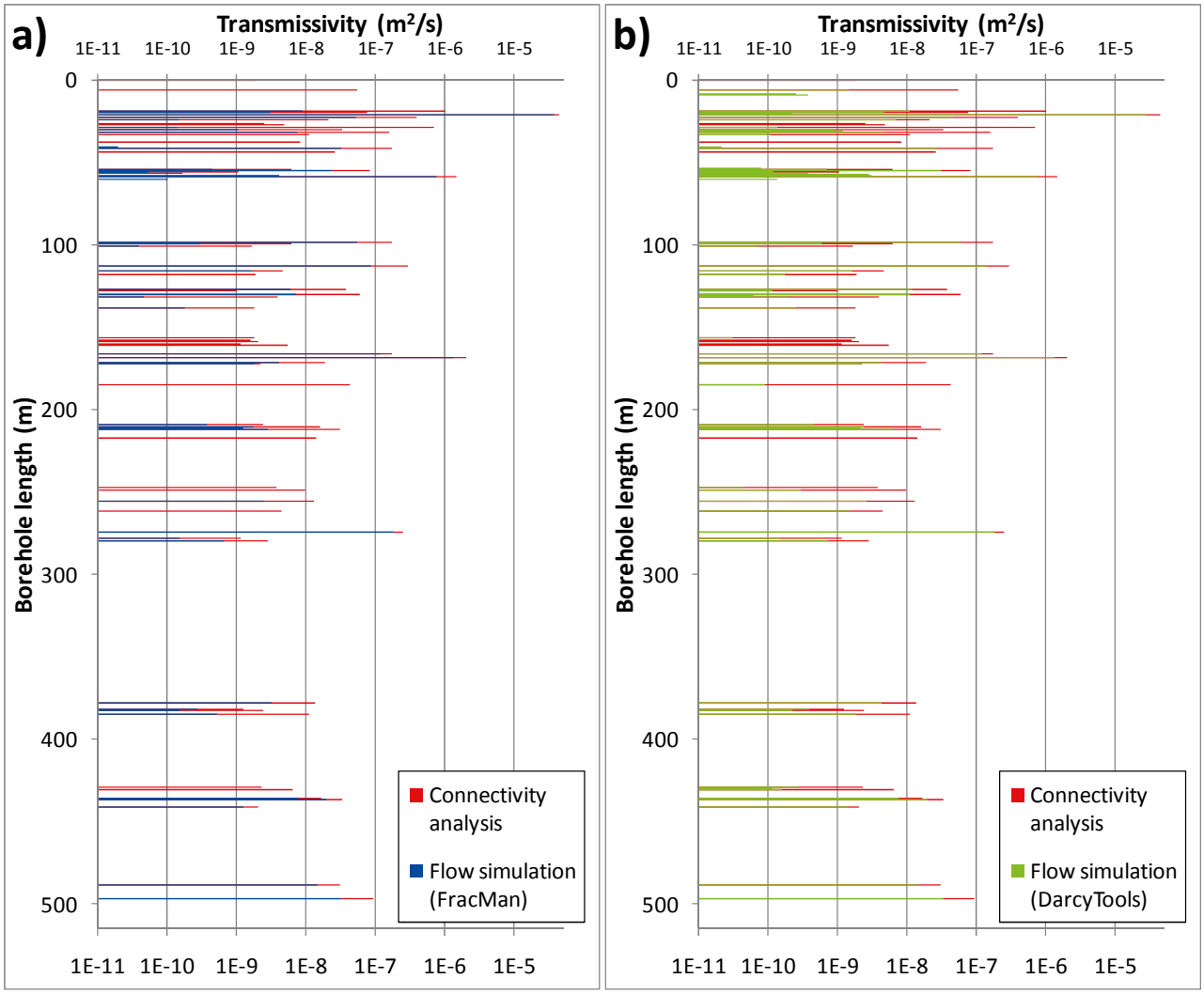

Figure G-17. *Realisation 4, ΔL = 0.3 m.*

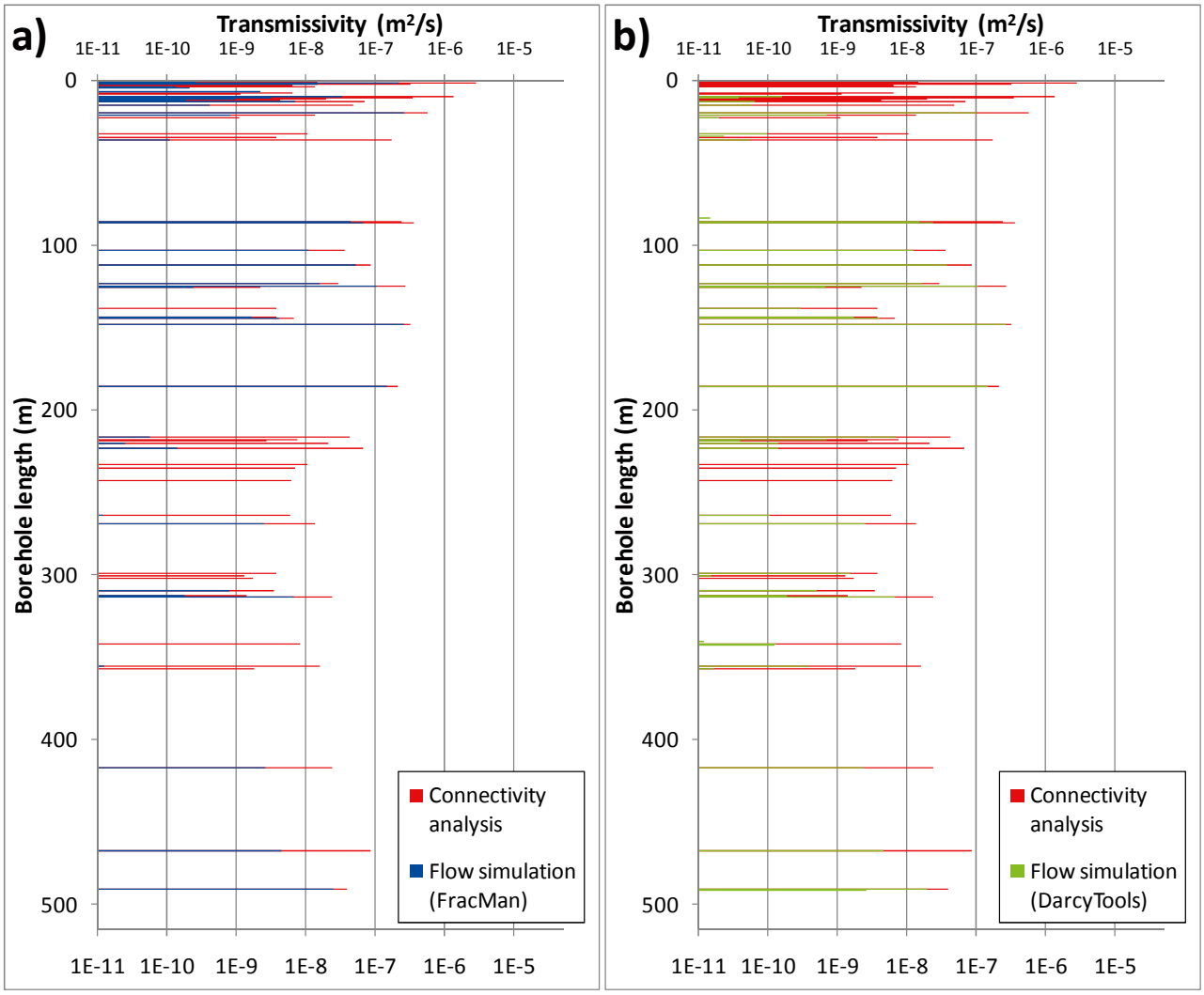

Figure G-18. *Realisation 5, ΔL = 0.3 m.*

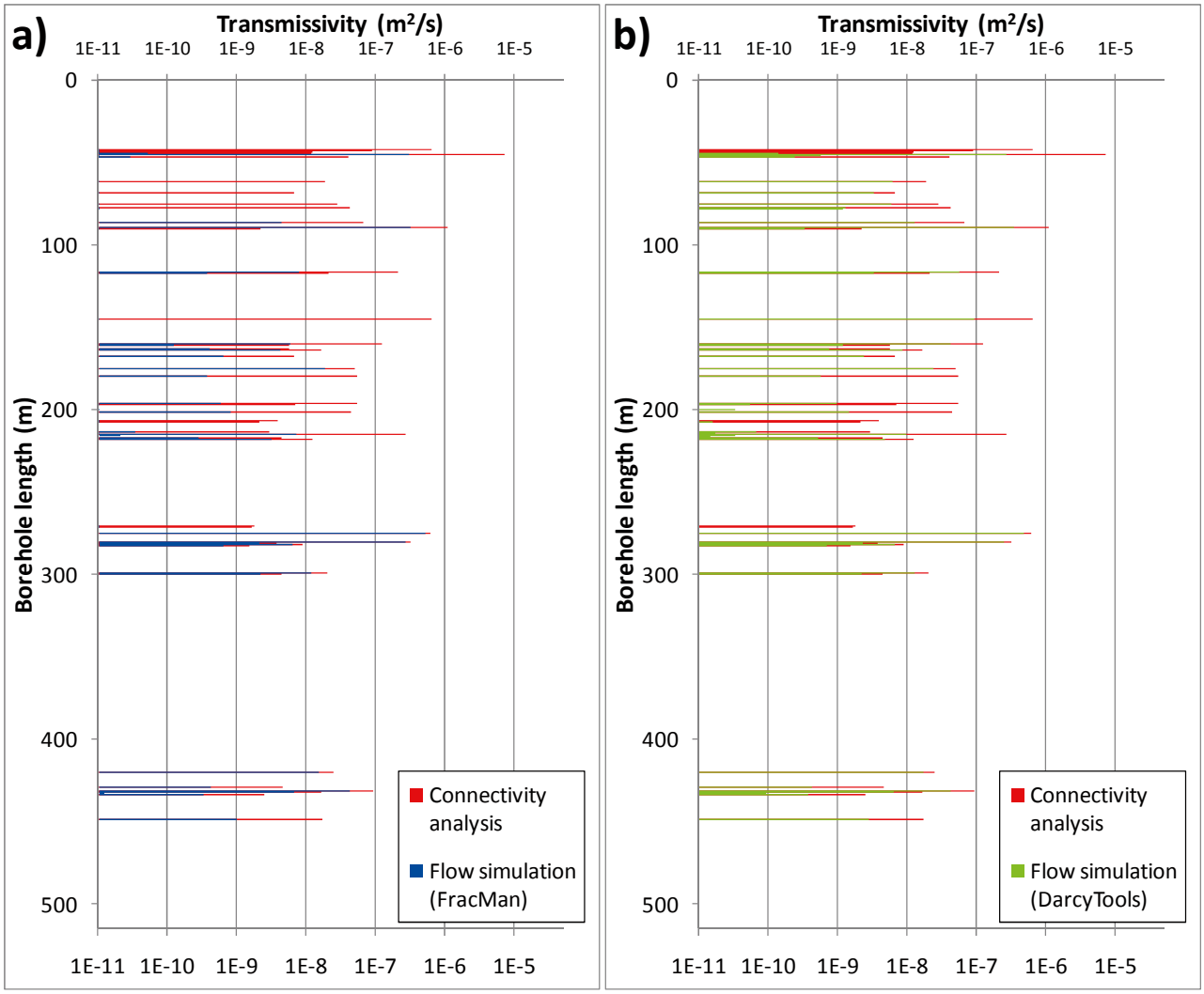

Figure G-19. *Realisation 6, ΔL = 0.3 m.*

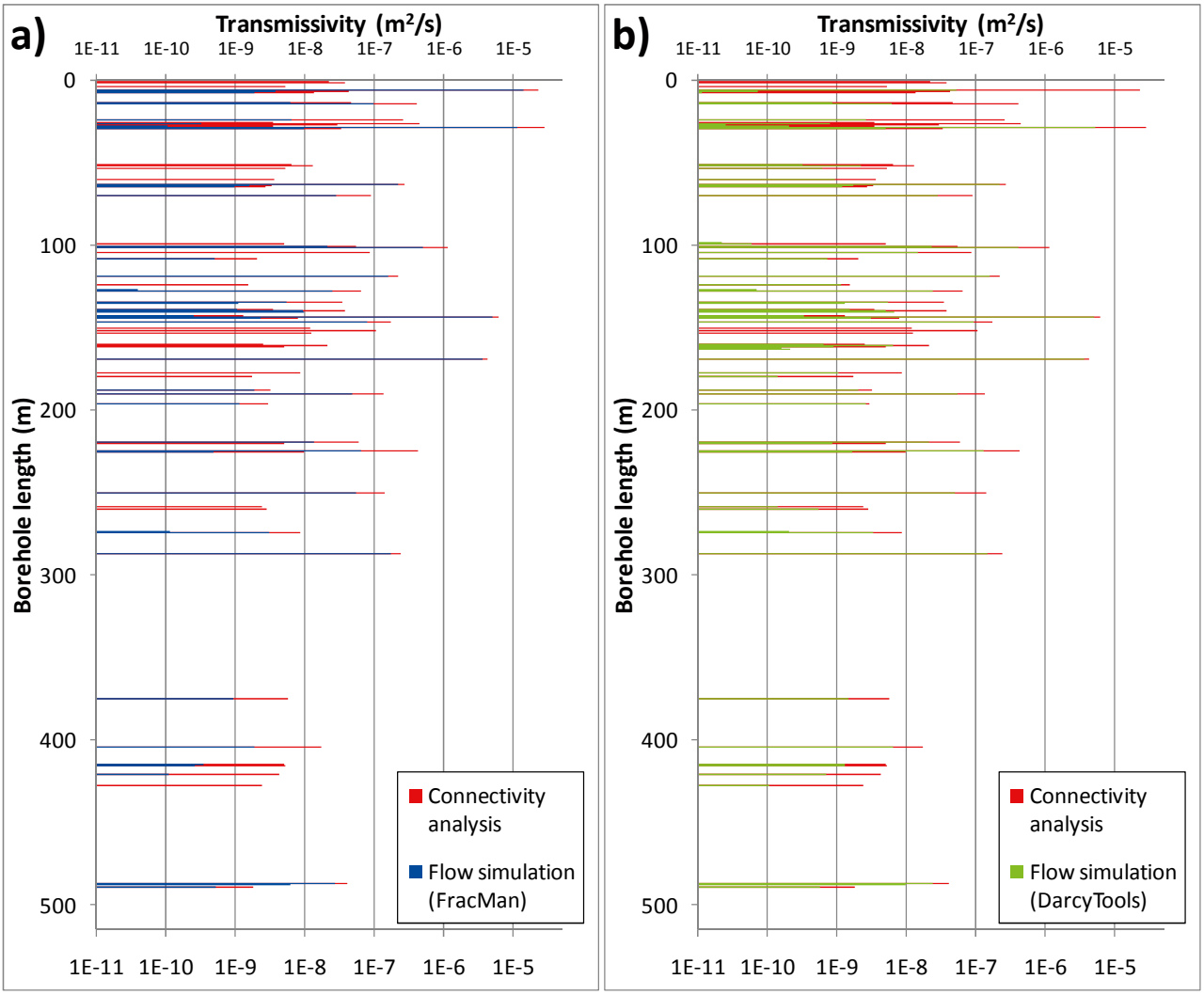

Figure G-20. *Realisation 7, ΔL = 0.3 m.*

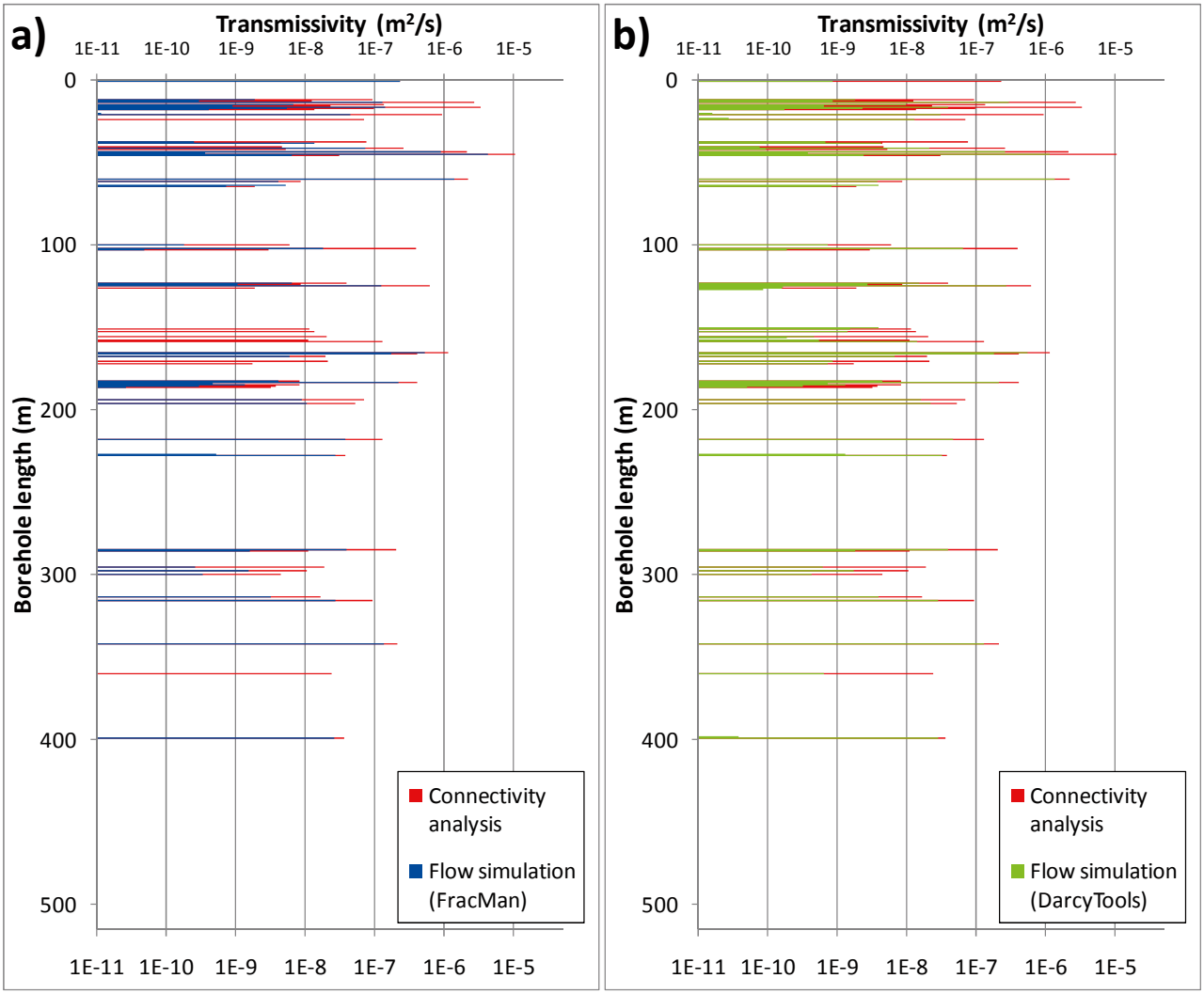

Figure G-21. *Realisation 8, ΔL = 0.3 m.*

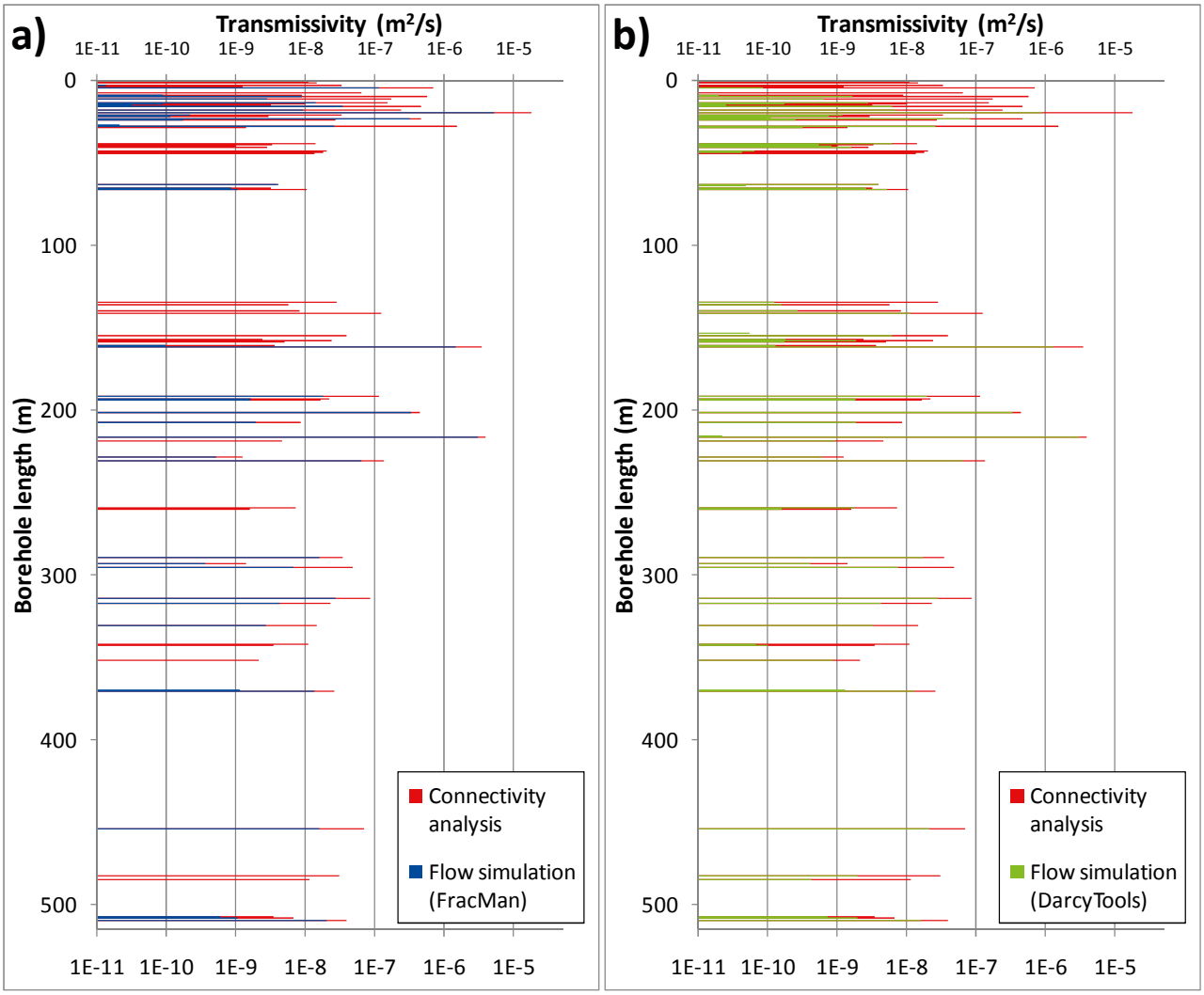

Figure G-22. *Realisation 9, ΔL = 0.3 m.*

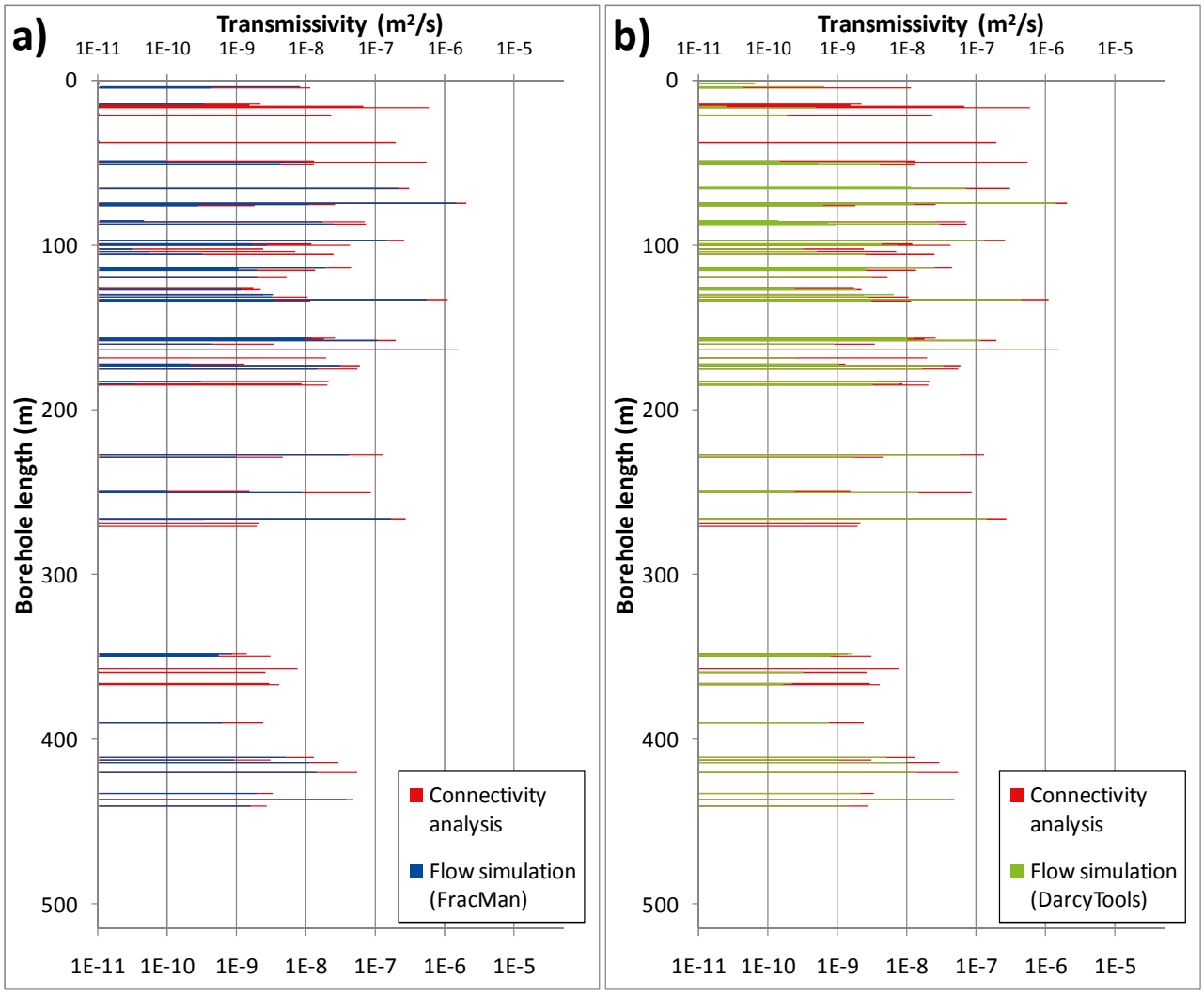

Figure G-23. *Realisation 10, ΔL = 0.3 m.*

Detailed results, ΔL = 1.0 m

The assigned transmissivity is compared to "simulated transmissivity" (in reality, Q/s), as binned into borehole sections (**ΔL = 1.0 m**), are shown for ten realisations in Figure G-24 to Figure G-33. The assigned fracture transmissivity, as sampled by a vertical scan-line, is referred to as "connectivity analysis" (red bars) is compared to "simulated transmissivity", back-calculated borehole inflow from a) FracMan (blue bars), respectively, b) DarcyTools (green bars). Note that the plotted bars are overlapping in the figures. Therefore, *any visible red indicates that the back-calculated transmissivity from flow simulations is lower than that geometrically sampled in the connectivity analysis.*

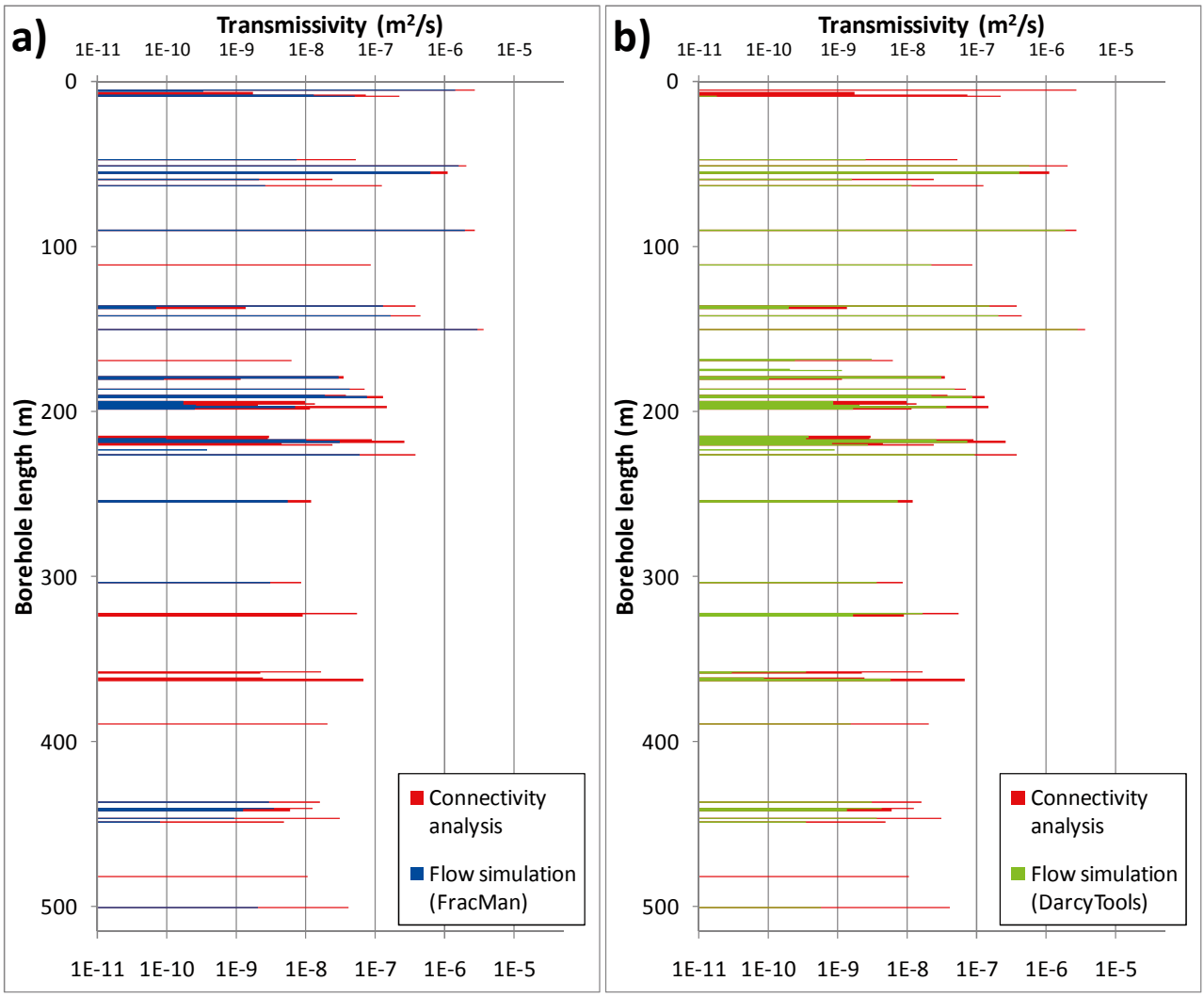

Figure G-24. *Realisation 1, ΔL = 1.0 m.*

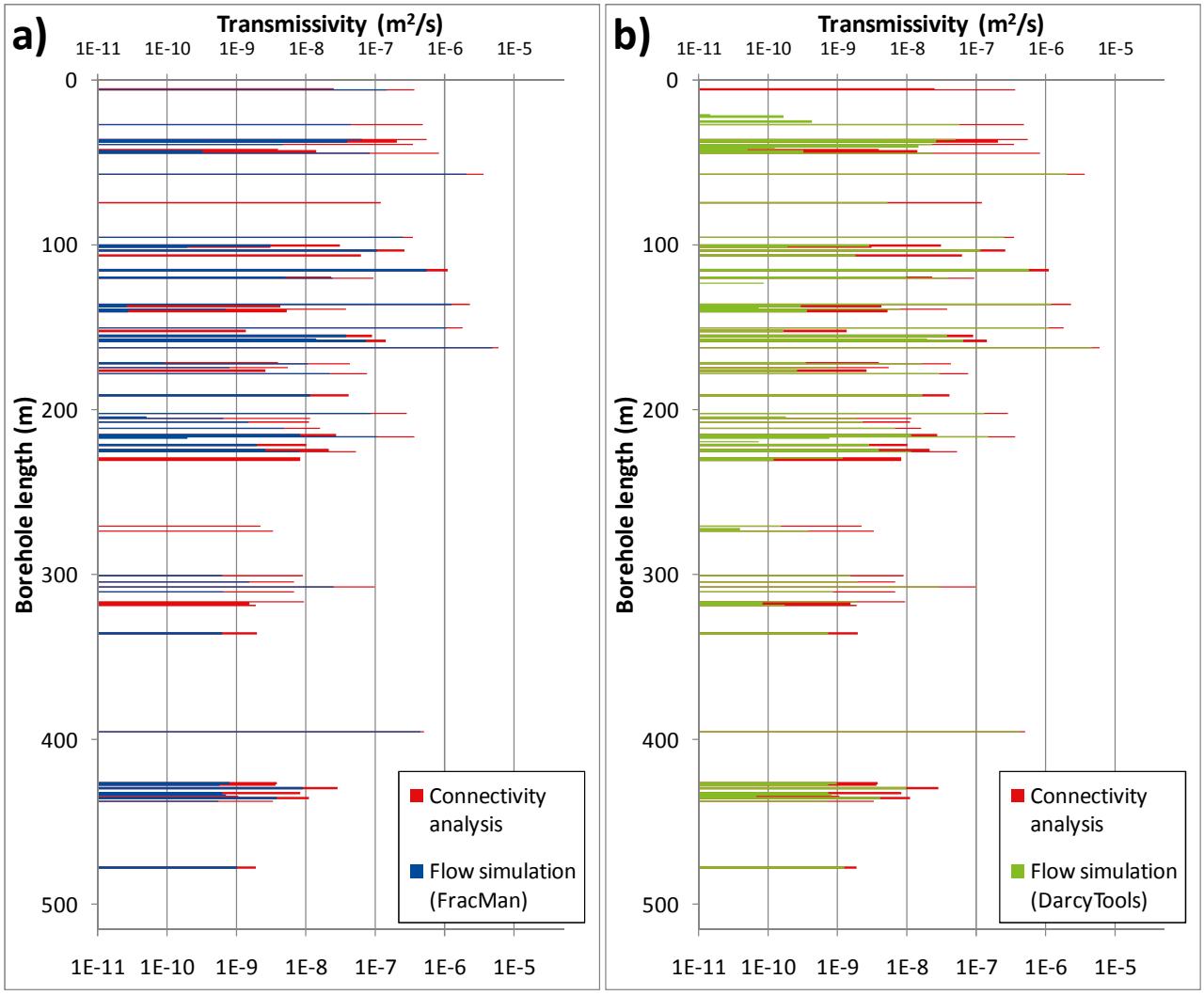

Figure G-25. *Realisation 2, ΔL = 1.0 m.*

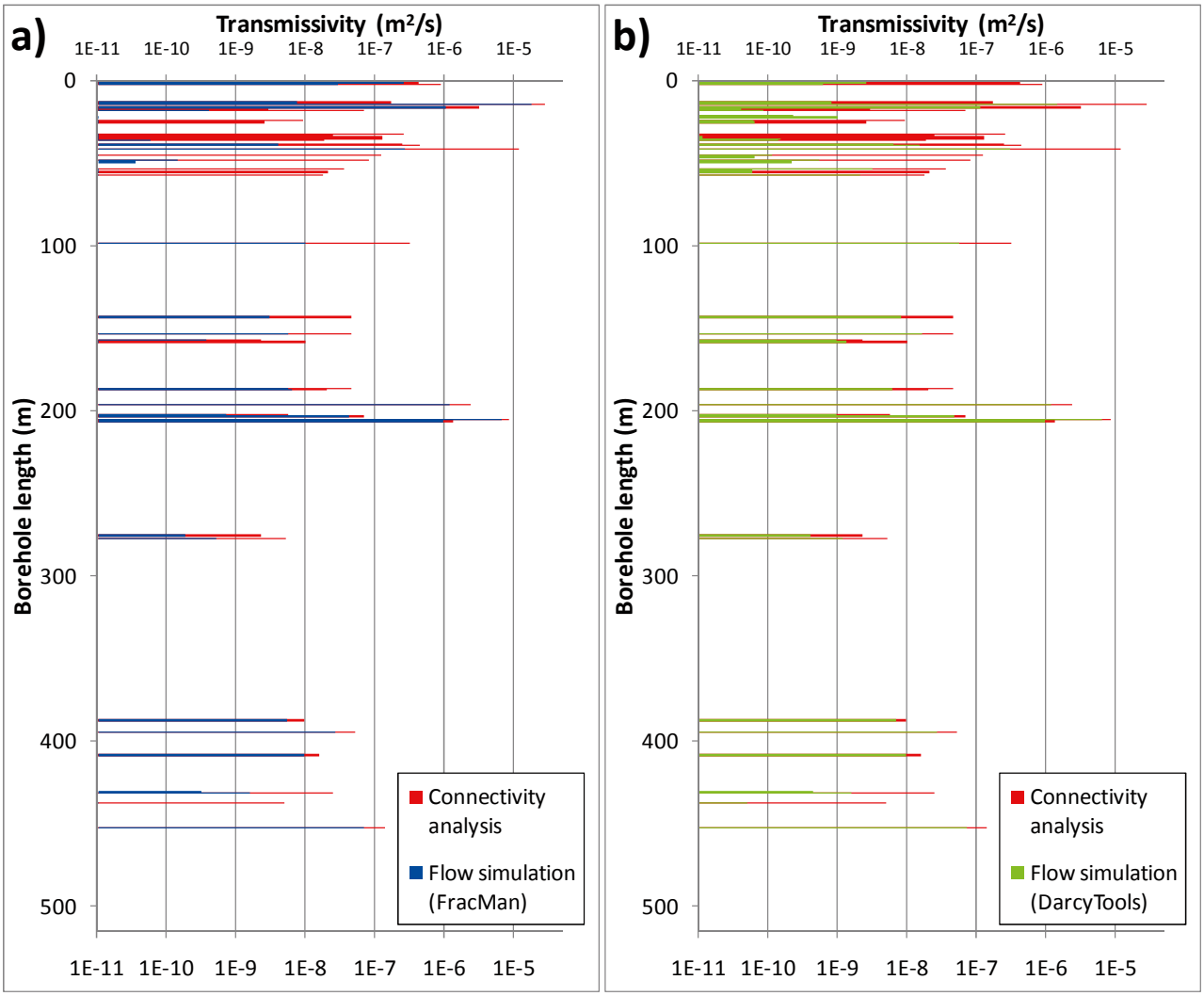

Figure G-26. *Realisation 3, ΔL = 1.0 m.*

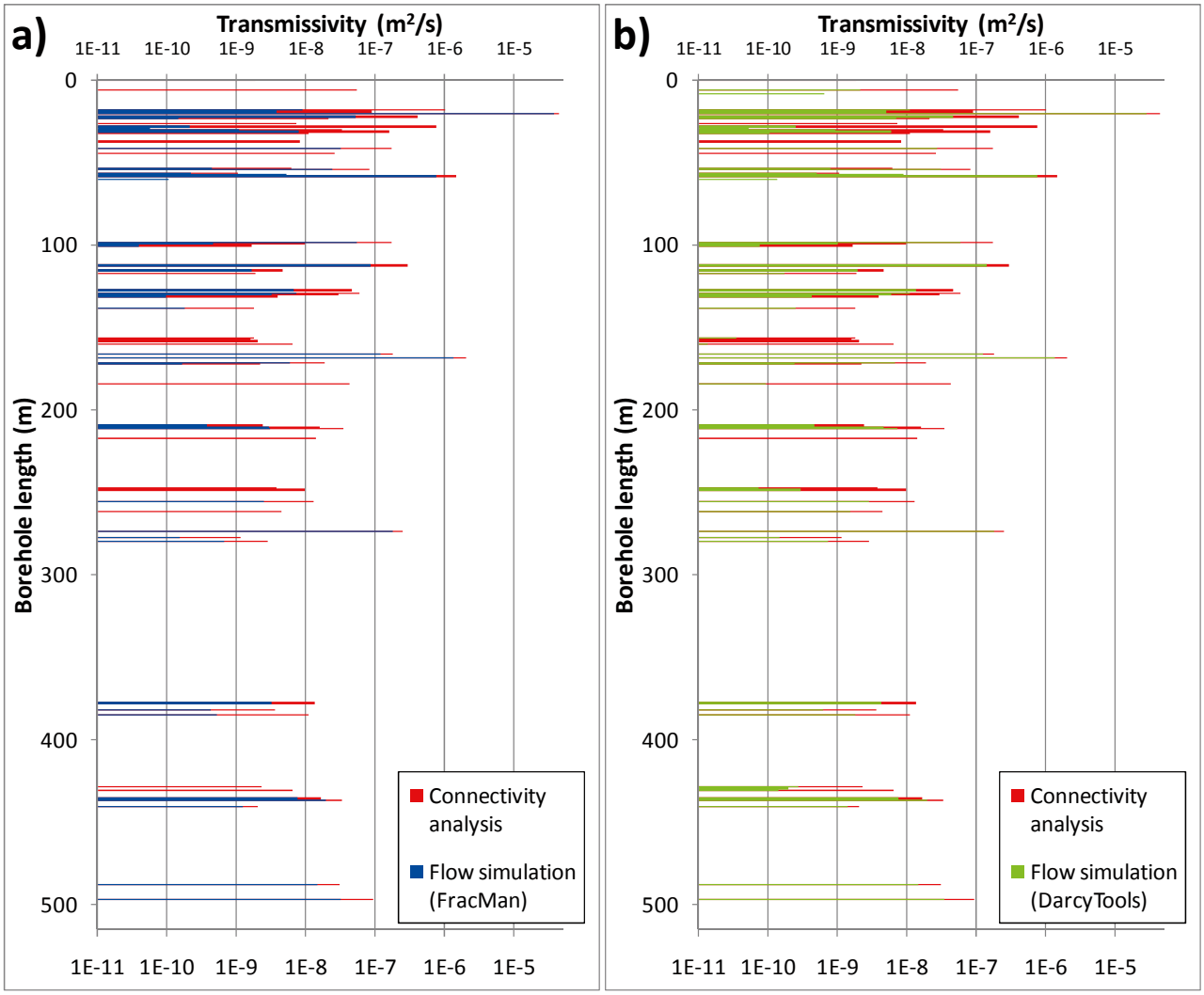

Figure G-27. *Realisation 4, ΔL = 1.0 m.*

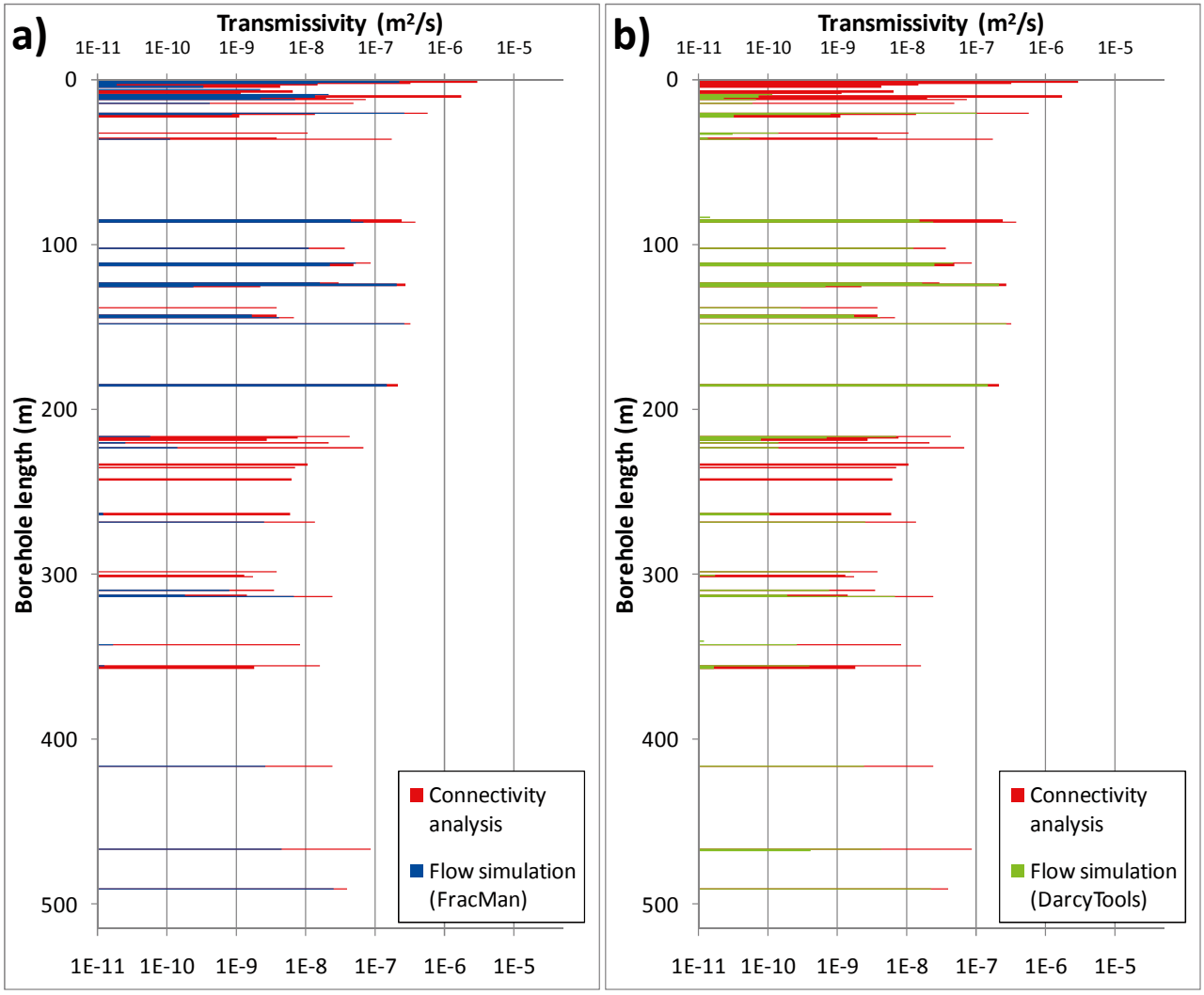

Figure G-28. *Realisation 5, ΔL = 1.0 m.*

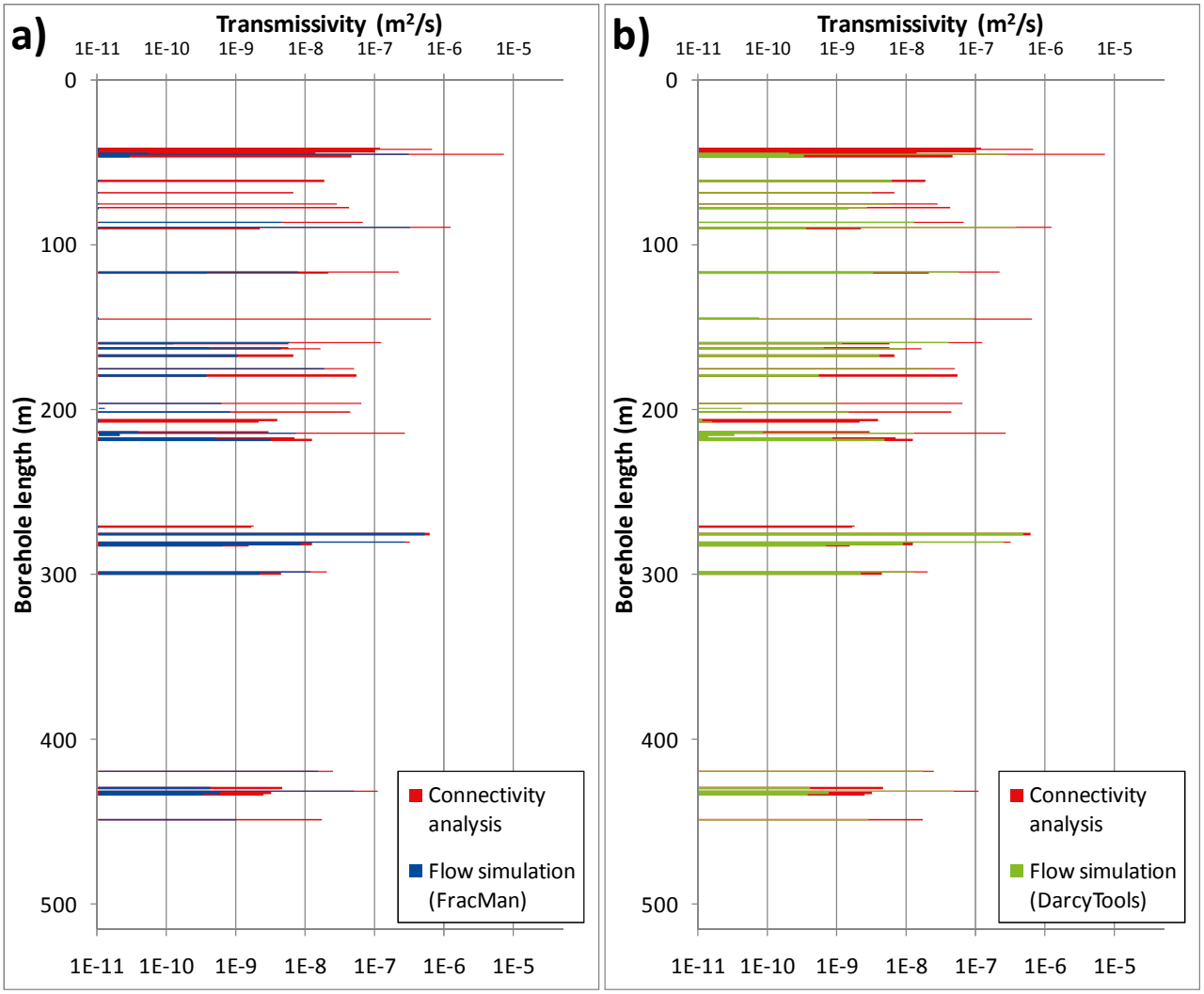

Figure G-29. *Realisation 6, ΔL = 1.0 m.*

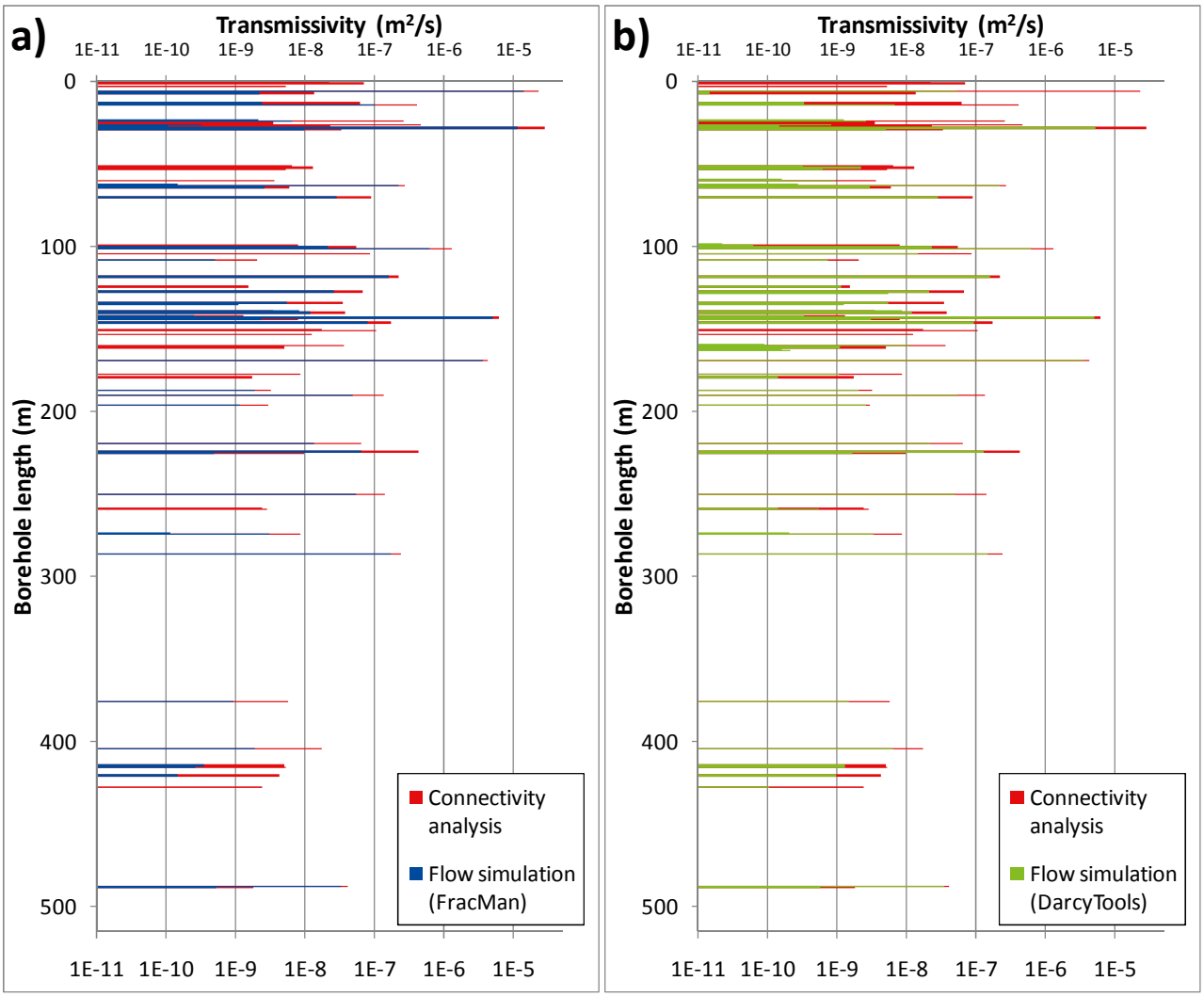

Figure G-30. *Realisation 7, ΔL = 1.0 m.*

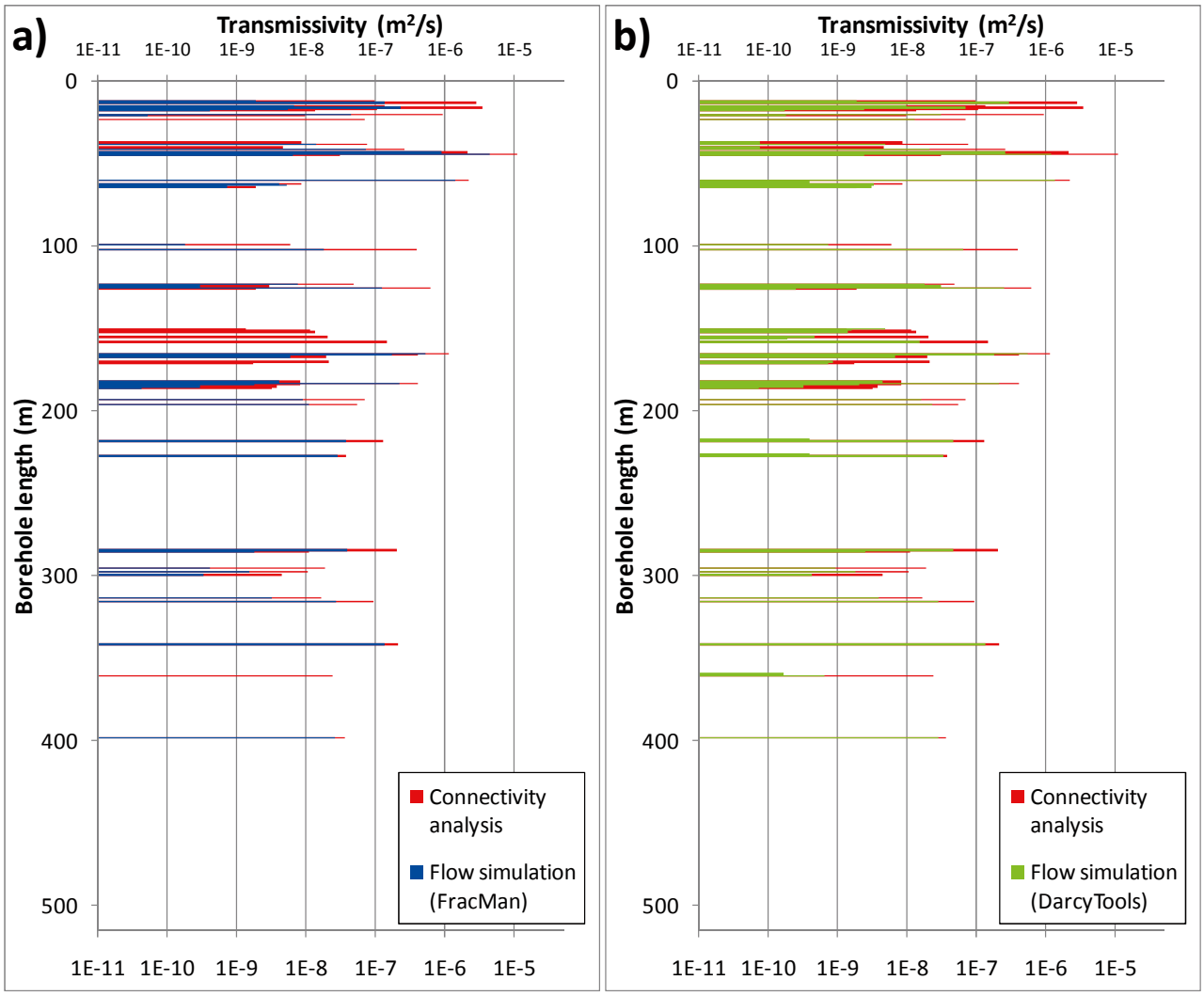

Figure G-31. *Realisation 8, ΔL = 1.0 m.*

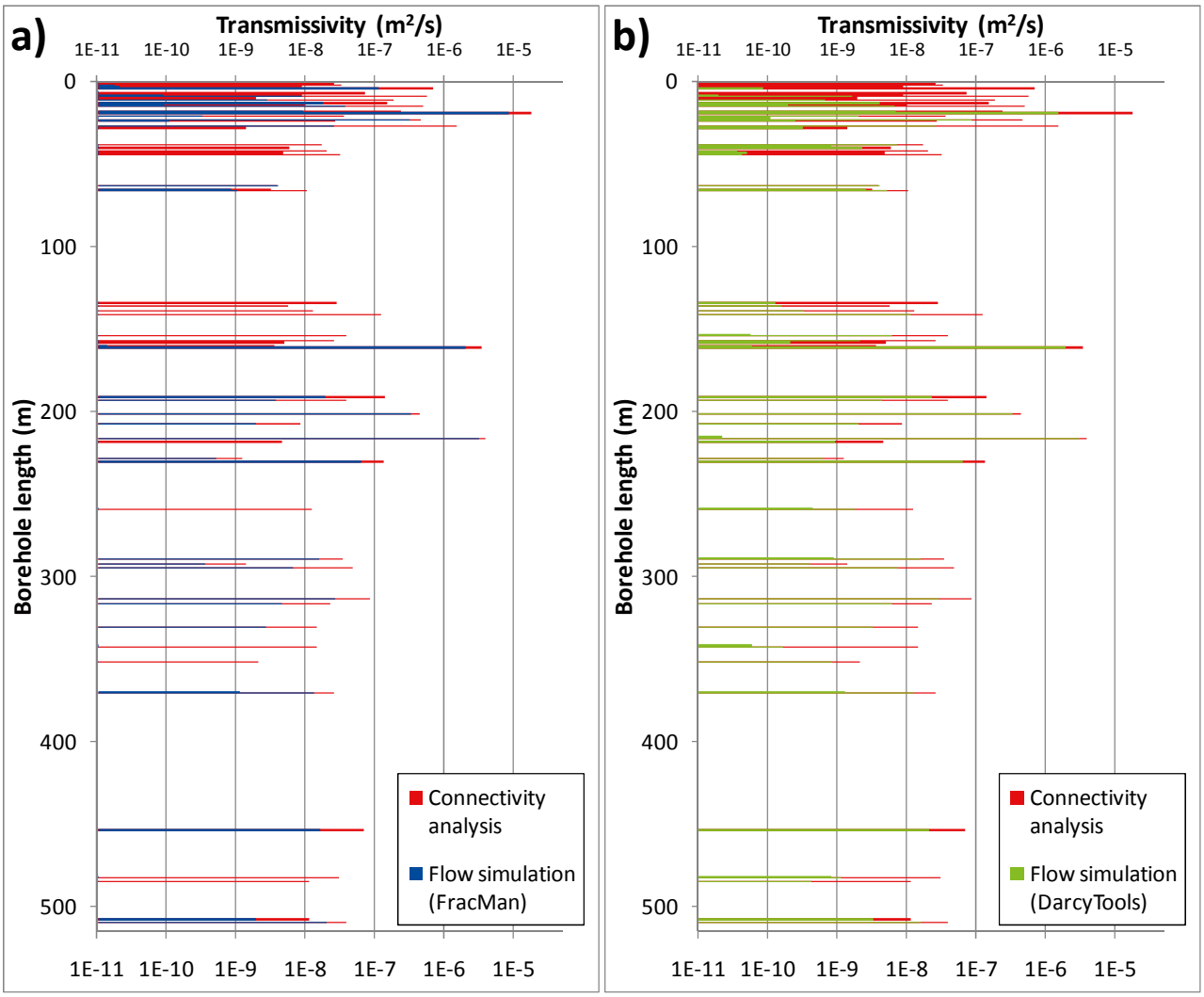

Figure G-32. *Realisation 9, ΔL = 1.0 m.*

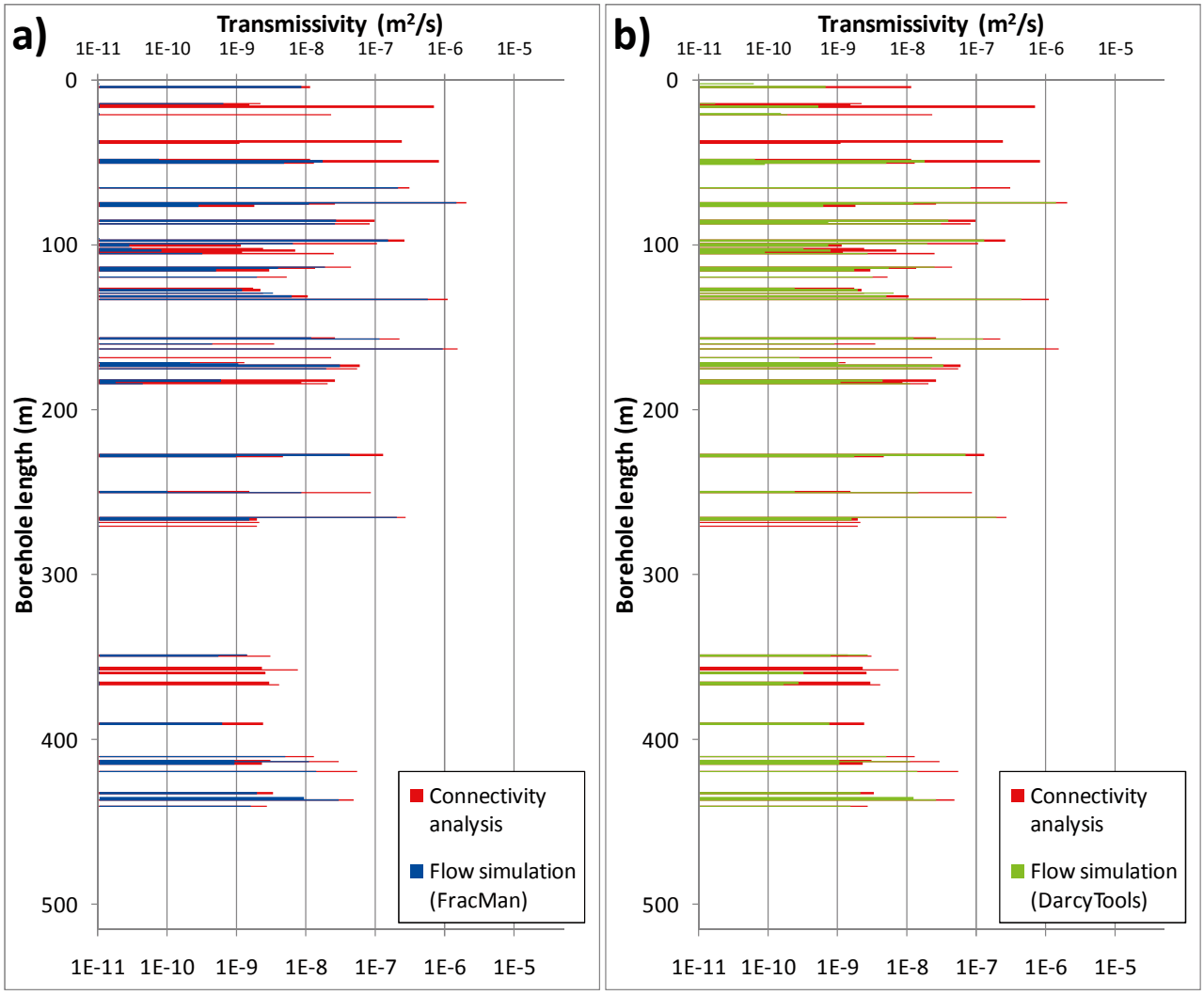

Figure G-33. *Realisation 10, ΔL = 1.0 m.*

Appendix H

Estimation of fracture size, based on mapped intersection type

A borehole with true radius (r_w = 0.038 m) was applied in flow simulations (Appendix G.2), while a scan-line (zero radius) had been used to sample fracture frequency during the underlying calibration process (connectivity analysis; main report, Section 2.3). The sampled fracture intensity indicated surprisingly different results, depending on if the borehole is represented by its true radius, or zero-radius (scan-line). This effect is accentuated for sub-vertical fracture sets (Table H-1), which is a geometrical effect relating to the simulated borehole being vertical (Figure H-2).

Table H-1. Observed differences in fracture intercepts in flow simulations.

Fracture set	Scanline	r_w = 0.038 m	Fractures not intersected by central axis
EW	266	1,140	77%
NE	82	396	79%
NW	277	1,525	82%
Gd	786	1,207	35%
HZ	441	627	30%

The motivation of using a scan-line during the calibration stage is that the vast majority of Open fractures mapped in Boremap, do not only intersect the borehole wall, but also the central axis of the borehole. On average, the parameter "CENTRUM_COVERED = 1" is approximately 99% in the SFR data set of Open fractures. Consequently, it seems reasonable to assume that the applied borehole radius in modelling should have little significance on sampled fracture frequency. In other words, the simulated fraction of fractures not intersected by the central axis (Table H-1) is expected to be approximately 1%. Two explanations are considered:

1) The Boremap data (parameter "CENTRUM_COVERED") has low confidence.
2) The assumed minimum fracture radius, $r_0 = r_w$ = 0.038 m, is unrealistic.

Hypothesis: Relation between intersection type and fracture size

An analytical relation between fracture size, alpha (the solid angle between the fracture plane and the intersecting borehole), and intersection-type probability is considered. This applies, given the fact that the fracture is beforehand known to be intersected, at least by the borehole wall (*a priori* assumption). In other words, it applies directly to Boremap data and borehole-sampled fractures in DFN modelling. The hypothetical situation where a small fracture is located inside the borehole cylinder without actually intersecting the central axis or the borehole wall is not considered. The reason for this is that such data are not included in the studied data set, as it could never have been mapped Boremap, in the first place. Basic assumptions are that fractures are **squares** of **equal size**, all with the side-length L (note that a similar expression can be derived for circular fractures). This side length is proportional to the probability of intersection-types A and B (Figure H-1). Here, type A refers to a situation where the fracture intersects the borehole wall, *but not* its central axis, while in type B *both* the borehole wall and its central axis are intersected.

The exposed sampling area for type A intercepts, where the *borehole central axis is **not** intersected*, is independent on α and is shown in purple and green colour in Figure H-1. The exposed area for type B, where the *borehole central axis **is** intersected*, does depend on α and is shown in blue colour in Figure H-1. Thus the probability for a type A intersection can be calculated by relating its area are to the total exposed sampling area:

$$P(A) = \frac{\pi r_w^2 + 2Lr_w\left(1+\sin\alpha\right)}{\pi r_w^2 + 2Lr_w\left(1+\sin\alpha\right) + L^2\sin\alpha} \qquad \text{(H-1)}$$

for any given side length, L, borehole radius, r_w, and alpha angle, α. Vice-versa the constant side length, L, can also be solved from a given probability.

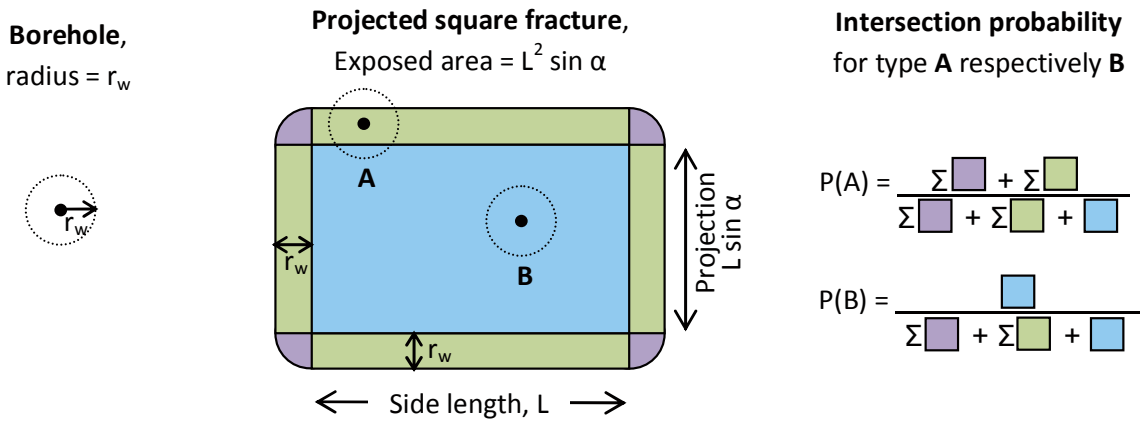

Figure H-1. *Exposed sampling areas for intercepts of type A (not covering borehole central axis) and B (covering borehole central axis), depending on α. These areas can be related directly to the probability of a fracture intersection being of type A, respectively, B.*

Data analysis Confidence in Boremap data

There are few mapped data with the parameter value "CENTRUM_COVERED = 0" (i.e. type A; altogether 54 of 5,502). This implies that this data may be sensitive to the possibility that a number of fractures – that in reality does not intersect the borehole central axis – have accidentally been erroneously mapped. Therefore data are analysed in detail, and a sensitivity case is presented. On the other hand, if these data in fact are unreliable, there is little motivation for using a scan-line in the calibration process. Approximately 4% of the Sealed fractures do not intersect the borehole central axis.

Borehole centre coverage data was analysed for Open fractures in HRD and found to have an obvious dependency to α (Figure H-2). This is a reassuring finding, which is geometrically consistent. A fracture sub-parallel to the borehole has a longer trace in the borehole wall, and is therefore more likely to terminate without reaching the central axis. The data are compared to the expected intersection probability, which is estimated from the analytical function, eq. (H-1), (here assuming a constant L = 3.8 m). For high alpha angles, the data has exceptionally low fraction of incomplete intersections (Type A), suggesting larger sizes.

Possibly, a vertical trend exists in intersection type, with shorter fractures at shallow depths and longer fractures at depth (Figure H-3). However, below –300 m RHB70 data are scarce (see Figure 2-3, main report).

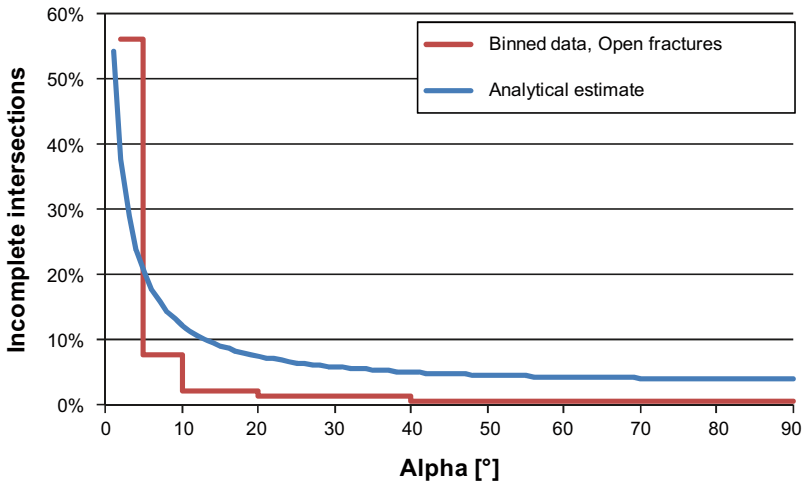

Figure H-2. *Binned fraction of incomplete intersections as a function of alpha. Analytical estimate is based on a constant fracture size of 3.8 m. Incomplete intersections refer to fractures intersecting the borehole wall, but not the central axis (type A in Figure H-1).*

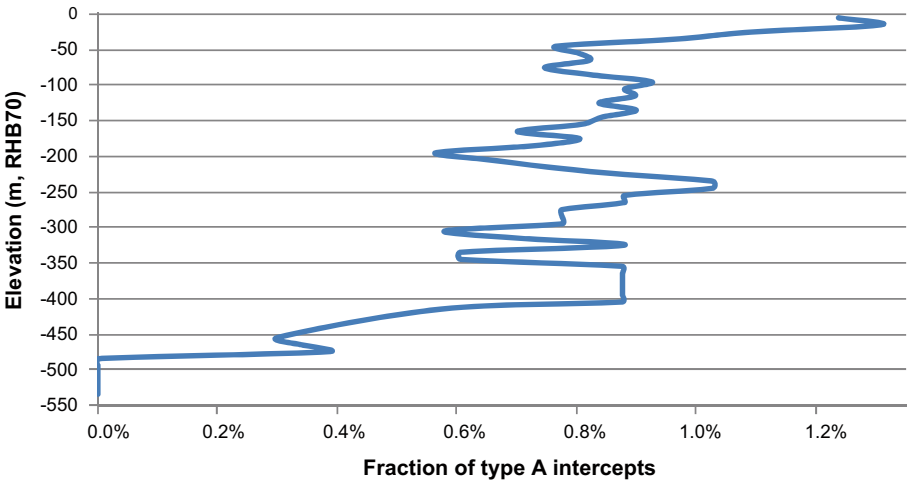

Figure H-3. *Moving average of the fraction of type A intercepts (borehole central axis not covered) with depth.*

Estimating set wise fracture size from intersection types

The analytical function, eq. (H-1), was then applied to estimate a representative constant fracture size (i.e. assuming all fractures equally large). It is not clear how this constant fracture size relates to a power-law distribution, but owing to the highly non-linear nature of a power-law distribution, it is expected to be fairly close to the minimum fracture size, r_0 (as, in terms of frequency, a power-law population is overwhelmingly dominated by the subpopulation close to its lower bound).

The fracture sets have clearly different fractions of type A intercepts (Table H-2), particularly set Hz (which is also associated to exceptionally large PFL-f transmissivity). Again, the sub-horizontal borehole KFR105 provides an unique opportunity to reveal if this exceptional statistics of Hz (Table H-2) relates sampling bias or the actual characteristics of set Hz. In fact, there are no intersects of type A for set Hz in KFR105, in spite of its low bias angle α (Table H-3). In this comparison it should be noted that the sample size is small, and that the overall fraction of type A intercepts is generally low (perhaps because no shallow data are included).

As a sensitivity case, the fraction of type-A intercepts were multiplied by a factor of 5 (considering the possibility that the parameter "CENTRUM_COVERED" has somehow systematically neglected type A intercepts (green values). The estimated size is consequently reduced by a factor of 5, from meter-scale down to decimetre-scale. Nevertheless this analysis suggests that fracture sizes are considerably larger than the currently assumed: $r_0 = r_w = 0.038$ m. A reasonable conclusion from this analysis is that the fraction of type A intercepts must be very high, if r_0 indeed is equal to $r_w = 0.038$ m.

Table H-2. Estimating representative size of fracture sets.

Set	Average α [°]	Fraction type A	Estimated size, r (m)	Fraction type A	Estimated size, r (m)
EW	47	4.6%	2.1	22.9%	0.4
NE	41	3.8%	2.8	18.8%	0.5
NW	32	6.1%	1.3	30.3%	0.2
Gd	56	2.8%	3.3	14.0%	0.6
Hz	59	0.4%	24.1	1.9%	4.8

Table H-2. Fraction of intersection type A in KFR105.

Set	No. data	No. type A	Fraction type A	Average Tw	Equivalent α [°]
EW	372	1	0.3%	1.2	55
NE	178	1	0.6%	1.5	42
NW	160	3	1.9%	2.0	30
Gd	61	1	1.6%	2.3	26
Hz	28	0	0.0%	2.9	20

Conclusions

This appendix suggests an inconsistency between mapped intercept types in Boremap and fracture size used in modelling. The analysis suggests that r_0 is larger than what has been assumed in the calibration. Some confidence-building trends can be noticed in the dataset. The mapped intercept types follow the expected trend in alpha (Figure H-2) and indicate that the horizontal set is not only particularly transmissive, but also are considerably larger. Also, sealed fractures have a higher frequency of intersection type A, suggesting that they are shorter than Open fractures, which also seems realistic.

On the other hand, the estimated values in Table H-2 are highly dependent on a high confidence in the geologic mapping of fractures. Obviously, tiny fractures with partial borehole intercepts must be much more difficult to detect during the geologic mapping and thereby possibly causing an unintentional, systematic underrepresentation of tiny fractures (i.e. a bias in the mapped data set). Thus, the estimated sizes relate to the *mapped* fracture system, which may be a biased subset of the *real* fracture system. According to observations made in the core, the bias in Open fractures at SFR is judged to be small or even negligible. In the end, it is difficult to assess the practical limitations in the core mapping, particularly with consideration to the conceptual simplification made in the distinction between Open and Sealed fractures. Fracture size is a highly uncertain parameter, and must be viewed in the context of the conceptual definition of what mapped, respectively, modelled fractures represent.

Sensitivity cases for Forsmark have shown that results where r_0 is set equal to borehole radius are more coherent with PFL-f data, e.g. Section 11.4 in /Follin et al. 2007a/, than if $r_0 = 0.282$ m (conditioned to outcrops) is applied. However, the analysis is made to data from a different domain and at greater depths. Also, the study is also provides indications, rather than indisputable evidence, owing to the dilemma of equifinality, discussed in Appendix F.

This study is inconclusive and can therefore *not* provide recommended values for modelling applications. The analysis suggests that r_0 may be larger than what has been assumed in this report. The most interesting finding in this appendix is that *horizontal fractures* are not only more transmissive, relatively to other sets, but may also be considerably larger in size. This notion could perhaps be related to glacial loading/unloading processes.

Appendix I

Vertical trends in orientation and intensity of Open fractures

Borehole data histograms are useful for examining possible vertical trends in orientation and intensity of Open fractures by visual inspection. Prior to the definition of sets, the borehole data can be binned by strike, dip and elevation and visualised in terms of fracture intensity (Figure I-1 and Figure I-2). Percussion data are also visualised, but not included in the analysis. The intensity ratio between steep and gently dipping Open fractures was analysed as a function of elevation and compared between boreholes (Figure I-1). For a consistent representation, the intensity was compensated by sin φ, see eq. (E-6), which corresponds to the equal-area projection of stereograms. The ratios were calculated such that the sum of binned intensity at each elevation within a borehole equals to 1.

The general impression is that fracture dip is rather distinctly divided into sub-horizontal fractures (dip 0°–20°) and sub-vertical fractures (dip 70°–90°). This pattern is relatively constant with depth. In the shallow rock the intensity of sub-horizontal and sub-vertical fractures is equally strong. The horizontal Open fractures dominate over elevations –60 to –300 m RHB70. The horizontal domination is exceptionally strong in KFR102A. A few exceptions can be noted. In KFR102B and KFR103 the sub-vertical fractures seem to dominate down to –100 m RHB70, after which the horizontal fractures dominate. The sub-vertical fractures also dominate in KFR105 and in KFR101below –120 m RHB70. Note that horizontal fractures are subject to sampling bias in the sub-horizontal borehole KFR105; which is incompletely compensated by Terzaghi-weighting in the blind sampling region (Figure 3-1).

In the deeper rock, below –300 m RHB70, the sub-vertical fractures tend to dominate. However, at these depths cored borehole data are only available from KFR102A and KFR27 (also KFR104). There are a few records without fracture intensity (shown as black). In most cases this is an artefact of excluding PDZ data (e.g. the result if only little HRD core length remains within an elevation bin).

A similar study was done in terms of strike intensity with elevation (Figure I-2). This was targeted towards variability in the sub-vertical fracture sets, and therefore all Open fractures with a dip less than 45° was excluded. The reason for doing so is that otherwise the dominating horizontal fractures are likely to mask the patterns in strike for vertical fractures. Theoretically, the strike is arbitrary for a horizontal fracture and with respect to measurement uncertainty even a small error, in terms of solid angle, translates into a large uncertainty in strike for any fracture in the dip range 0°–10°. In order to simplify the plots, the sub-vertical sets were assumed to be symmetrical in terms of dip; therefore strikes in the range 180° to 359° were subtracted by 180°, and then superimposed onto the strike range 0° to 180°. More simply put: the right-hand rule was disregarded and a fracture oriented (181°/89°) was included in the same intensity bin as a fracture oriented (1°/89°). Furthermore, Figure I-2 shows binned fracture intensity, calculated as sum of Terzaghi weights per available core length within each elevation bin (not expressed as relative ratios).

In the upper bedrock, elevation interval 0 to –60 m RHB70, core data are only available from boreholes KFR102B, KFR103, and KFR104. Set EW is the dominant sub-vertical set in KFR102B and KFR103 (Figure 3-2c and d). Over the same elevation interval, KFR104 exhibits a scattered pattern (Figure I-1). Consequently, set EW dominates in the combined intensity histogram (Figure I-2, lower row) down to an elevation of –50 m RHB70. Set EW continues to dominate KFR102B until the end of the borehole. Set EW is also strong in KFR102A over an elevation range –170 to –200 m RHB70 (Figure I-2), but with a deviating dip ranging 50° to 60° (Figure I-1 and Figure 3-2b). In KFR104, set EW is virtually absent over its entire length. Set EW is also found KFR27 at elevations –370 to –400 m RHB70.

Set NW is the dominating sub-vertical set over the elevation range –50 to –350 m RHB70 (see combined intensity histogram in Figure I-2, lower row). It is the dominating sub-vertical set in most boreholes, with the exception of KFR102B and KFR102A. The set NE is strong over the entire extent of KFR102A, although it also has a strong presence of set NW. Set NW is the clearly dominating sub-vertical set in both KFR104 and in KFR105. Over the elevation range –120 to 160 m RHB70 in KFR104, set NW even dominates over the horizontal set (Figure I-1 and Figure I-2). With the exception of KFR102A, set NE appears to be a scattered set at elevations above –300 m RHB70. Below –350 m RHB70, data are scarce, but it appears that set NE dominates.

In summary, the observed orientation distributions in Figure 3-2, which is dominated by Hz and NW, appear to be relatively constant with depth, particularly over the elevation range –80 to –350 m RHB70. At shallower depths 0 to –60 m RHB70 the sub-vertical sets are instead dominated by set EW, mainly based on data from KFR102B and KFR103 (drilled in different orientations from the same starting location; Figure 1-1). Data are also scarce for depths below –350 m (only available from KFR102A and KFR27), although it seems that set NE dominates over Hz at greater depths. Figure I-1

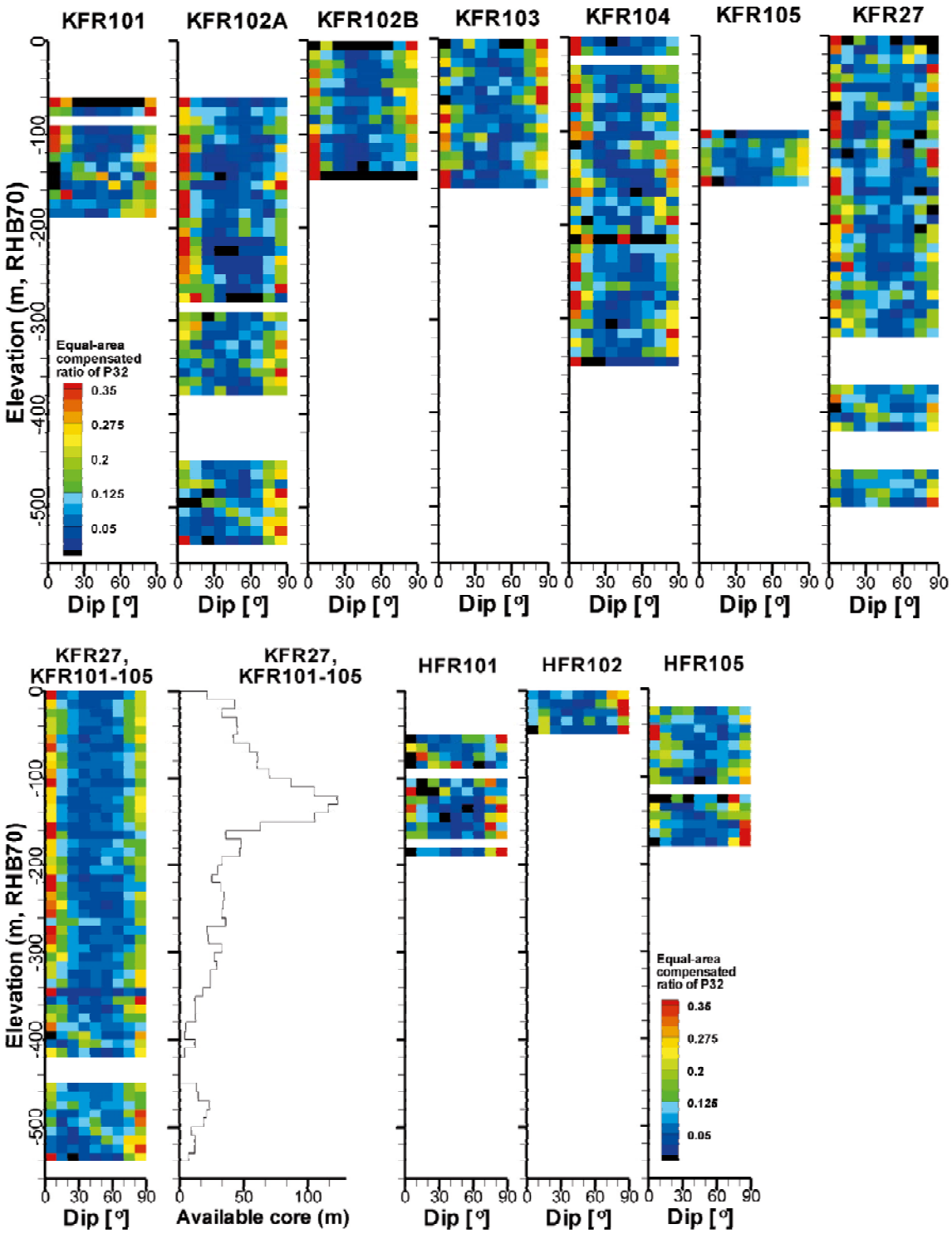

Figure I-1. *Intensity of Open and Partly open fractures in HRD binned by elevation and dip; top row: individual cored boreholes, bottom row: combined core data, total core length available in HRD, and individual percussion boreholes. Dip bin-size was 10°, and the intensity was compensated by the jacobian, sin φ in eq. (E-6).*

and Figure I-2 do not only show the variability in intensity of fracture orientations with depth and between boreholes, but also illustrates the discontinuity in data after the removal of PDZ. This fact complicates the inference of observed deviating fracture patterns. However, at this modelling stage, the general impression is that the suggested fracture sets can be assumed global for application to the entire data set. If the orientation model is assumed to be global, the observed variability must be interpreted as heterogeneity in fracture set intensity (in contrast to a locally rotated orientation model).

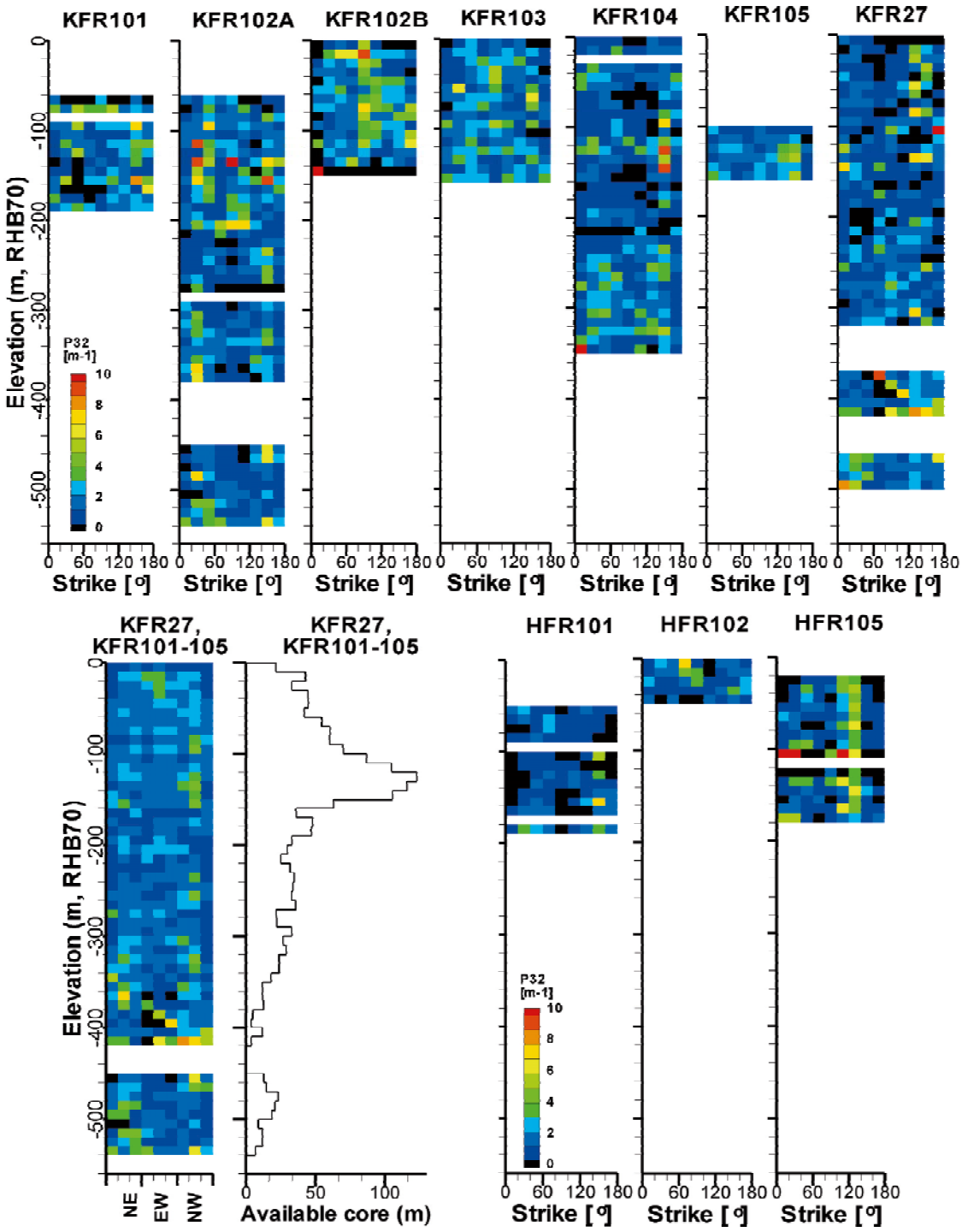

Figure I-2. *Intensity of steep Open and Partly open fractures in HRD binned by elevation and strike; top row: Individual cored boreholes and bottom row: combined core data, total core length available in HRD, and individual percussion boreholes. Strike bin-size was 20°, and strikes >180° were superimposed onto the range 0° to 180°. Fractures with dip <45° were excluded.*

Appendix J

DFN calibration

J.1 Number of realisation

The calibration between size and intensity was performed for each depth domain separately, as described in Section 2.3. First, the number of realisations required to attain stable simulation results must be determined. Results indicate that 50 realisations must be used in the calibration stage. For a successively increased number of realisations, the intensity of Open fractures and Connected Open Fractures, as seen by a vertical borehole, is examined. The cumulative average intensity of simulated $P_{32,\,Open}$ and $P_{32,\,COF}$ was calculated as a cumulative average with increasing number of realisations (Figure J-1a and b). For Open fractures, the cumulative average intensity could be expressed relative to its expectation value, $P_{32,\,Open}$ in borehole data. For Connected fractures, the expectation value is unknown, as $P_{32,\,COF}$ is a fitting parameter unavailable in data (Section 2.2.11). Therefore the convergence in simulated values of $P_{32,\,COF}$ is related to its final average for 100 simulations (Figure J-1b). This means that it cannot be concluded if the expectation value has been reached within these 100 realisations, or not. It should also be noted that, even if simulated explorations has reached stability in terms of fracture intensity, it does not guarantee stability in the simulated size distributions.

The general impression is that the average simulated borehole exploration stabilises after 30 to 50 realisations and that calculated values are within ± 5% of data. NW is the most variable set (Figure J-1a). The reason is a combination of relatively low fracture intensity, a low sampling bias angle (implying large Terzaghi-weights), and a high Fisher concentration κ (a low κ has an averaging effect on sampling bias). However, the visual impression is that the simulated values are relatively stable after 50 realisations (even though the Open fractures of set NW has not stabilised). Based on these observations, it was decided to use 50 realisations in the calibration process.

J.2 Connectivity analysis, Calibrating k_r

The fitted scaling exponent was calibrated by trial and error with the target to achieve an intensity of Connected Open Fractures, *as seen by a vertical borehole*, in the range 2 to 4 times larger than the intensity of PFL-f data above T_{lim}. For sets Gd and Hz, the fitted kr is within the range 2.55 to 2.79 (Table J-1), while it is generally above 3.0 for the sub-vertical sets. This is in line with observations from Site Investigation Forsmark, see Section 2.2.10 /Follin et al. 2007b/. For the set NW, k_r was calibrated to 2.95–3.1, although its ratio $P_{32,\,COF}/P_{32,\,PFL}$ exceeded the calibration target for the Shallow and Deep domains. Additional test cases with higher k_r for set NW were explored; these did not improve the results for NW, but instead deteriorated the calibration for sets Hz and Gd.

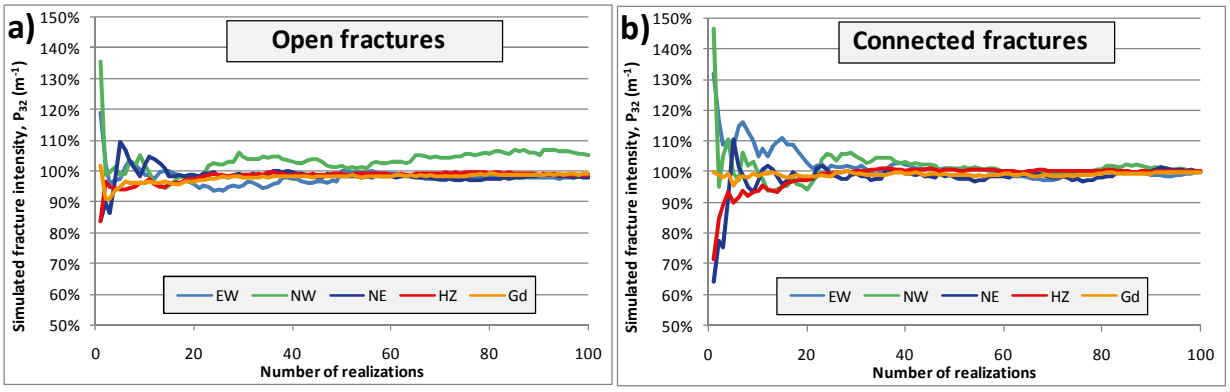

Figure J-1. *Convergence of simulated borehole exploration with number of realisations; a) initial fracture network of Open and Partly open fractures relative to data, and b) connected fracture network, after the removal of isolated fractures, related to the final value after 100 realisations.*

Table J-1. Calibration of kr based on connectivity analysis.

Domain	Evaluation of Connected fracture network	Fracture set				
		EW	NW	NE	HZ	Gd
Shallow domain	Fitted scaling exponent, k_r	3.45	3.1	3.45	2.6	2.79
	Simulated $P_{32, COF}$	1.36	0.79	0.70	0.72	1.16
	Reference data, $P_{32, PFL}$ ($T > T_{lim}$)	0.10	0.11	0.03	0.36	0.34
	Simulated ratio ($P_{32, COF}/P_{32, PFL}$)	13.8	6.9	24.8	2.0	3.4
	Simulated fraction ($P_{32, COF}/P_{32, Open}$)	55%	82%	59%	73%	70%
Repository domain	Fitted scaling exponent, k_r	3.45	2.95	3.45	2.55	2.72
	Simulated $P_{32, COF}$	0.17	0.16	0.14	0.22	0.26
	Reference data, $P_{32, PFL}$ ($T > T_{lim}$)	0.02	0.04	0.02	0.08	0.09
	Simulated ratio ($P_{32, COF}/P_{32, PFL}$)	11.3	3.5	8.1	2.7	3.0
	Simulated fraction ($P_{32, COF}/P_{32, Open}$)	14%	20%	15%	28%	24%
Deep domain	Fitted scaling exponent, k_r	3.45	3.1	3.45	2.75	2.7
	Simulated $P_{32, COF}$	0.07	0.06	0.05	0.05	0.12
	Reference data, $P_{32, PFL}$ ($T > T_{lim}$)	0.01	0.01	0.00	0.01	0.03
	Simulated ratio ($P_{32, COF}/P_{32, PFL}$)	9.8	4.9	NA	4.0	3.6
	Simulated fraction ($P_{32, COF}/P_{32, Open}$)	8%	7%	5%	10%	11%

For sets EW and NE, the calibration target could not be met, even for high values of k_r. The scaling exponent k_r was not allowed to exceed 3.45, as higher values were considered unrealistic and were not found to further improve the connectivity analysis. In fact, it may argued that the $P_{32, COF}/P_{32, PFL}$-ratio should be larger for fracture sets with low k_r, as in the presence of a well-connected Hz/Gd network it may have a relatively large population of short fractures with transmissivity below T_{lim}, which nevertheless are Connected. Fine-tuning the size-transmissivity relations demonstrate that the hydro-DFN is still capable of honouring PFL-f data (see Section 4.1.3). The connectivity is high in the Shallow domain (around 70%) and low in the Deep domain (around 10%).

J.2.1 Connectivity analysis, hydraulic parameterisation

Once the scaling exponents k_r had been established in the connectivity analysis (Table J-1), the empirical relations between transmissivity and fracture radius could be defined according to the methodology described in Section 2.3.3. The hydraulic parameterisation is made by conditioning the Connected fracture network to PFL-f data above T_{lim}. Most PFL-f data are available for set-wise conditioning in the Repository domain (Figure J-2; note that most come from KFR105). The Shallow domain is strongly dominated by sets Hz and Gd, and it is suspected that their high transmissivity may have masked the presence of sets EW, NE, and NW. It was found difficult to derive a realistic transmissivity relation for the sub-vertical sets; instead it is suggested that it is extrapolated from the Repository domain. In the Deep domain the available data is scarce (note the difference in y-axes; Figure J-2). Nevertheless, a hydraulic conditioning to sets Hz and Gd was pursued, while it was considered better to extrapolate the hydraulic parameterisation of sub-vertical sets from the Repository domain.

For each fracture set, the complementary cumulative size distribution of Connected fractures was matched, percentile-by-percentile, to the complementary cumulative transmissivity distribution of PFL-f data above T_{lim} (e.g. Figure 2-6). In this matching, the excessive simulated Connected fracture intensity (i.e. $P_{32, COF}$–$P_{32, PFL}$ [$T > T_{lim}$]) was assumed to reflect transmissivity below T_{lim}. As a result, each PFL-f anomaly is associated to a fracture radius. The relation between PFL-f transmissivity and its associated radius can then be approximated by an empirical relation, eq. (2-4). Both root-mean-square fits and visual fits were considered for the determination of the coefficients *a* and *b* (e.g. Figure J-3). In general, it was decided to rely on visual fits, as it allows flexibility in defining the endpoints of the fitted interval. More precisely, a visual fit allows conditioning the relation to the PFL-f intensity at T_{lim}, and the option to exclude possibly deviating data in the upper tail of PFL-f data. The results are summarized in Section 3.4, main report.

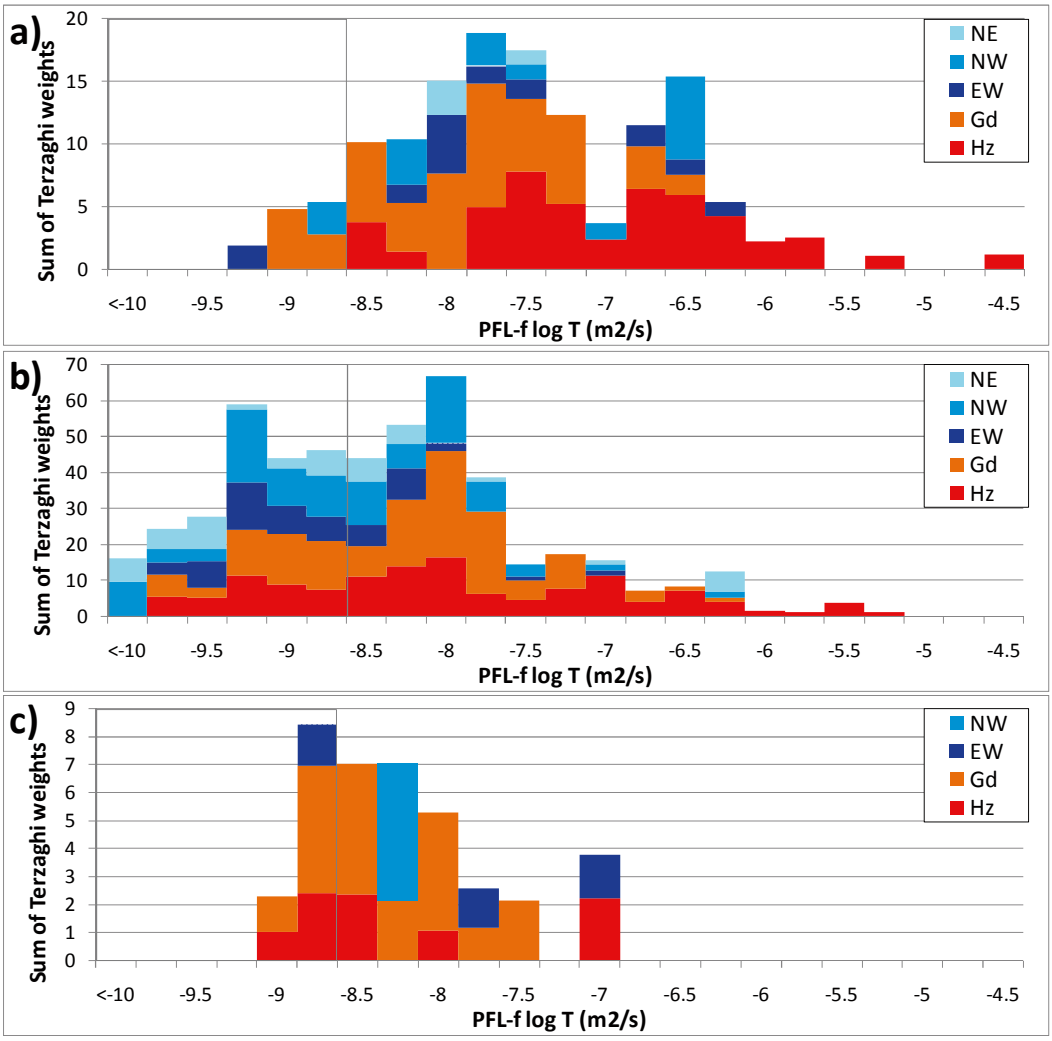

Figure J-2. *Stacked histograms of PFL-f data in HRD per depth domain, showing the available data for hydraulic conditioning of Connected fracture networks. Data below cut-off limit shown with grey area.*

Repository domain

The determination of the coefficients *a* and *b* is shown in Figure J-3). The logarithmic cross plots between simulated radius of Connected fractures and PFL-f transmissivity has a fairly linear appearance for sets Hz, Gd, and NW (Figure J-3a–c). This implies that the breakpoints in the transmissivity distributions (e.g. Figure F-2), respectively, radius distributions (e.g. Figure F-1) have coincided well in terms of percentiles. The cross plots for sets NE and EW has a less linear appearance, which signifies that shape of the data do not follow the empirical relation, eq. (2-4). This makes the determination of the coefficients *a* and *b* more difficult. The established transmissivity relations are applied to the Connected fracture network and compared to PFL-f data in Figure J-4. As can be expected, the simulated fracture transmissivity differs in shape to the PFL-f data for sets NE and EW.

It was found that the possible outlier, PFL No. 38 in KFR102A, has a drastic influence on the transmissivity relations (cf Figure J-3e and f). If this record is included the maximum transmissivity of set NE is 2×10^{-5} m^2/s for 50 realisations, while if it is excluded, the largest simulated transmissivity drops almost two orders of magnitude to 3×10^{-7} m^2/s (Figure J-4e and f).

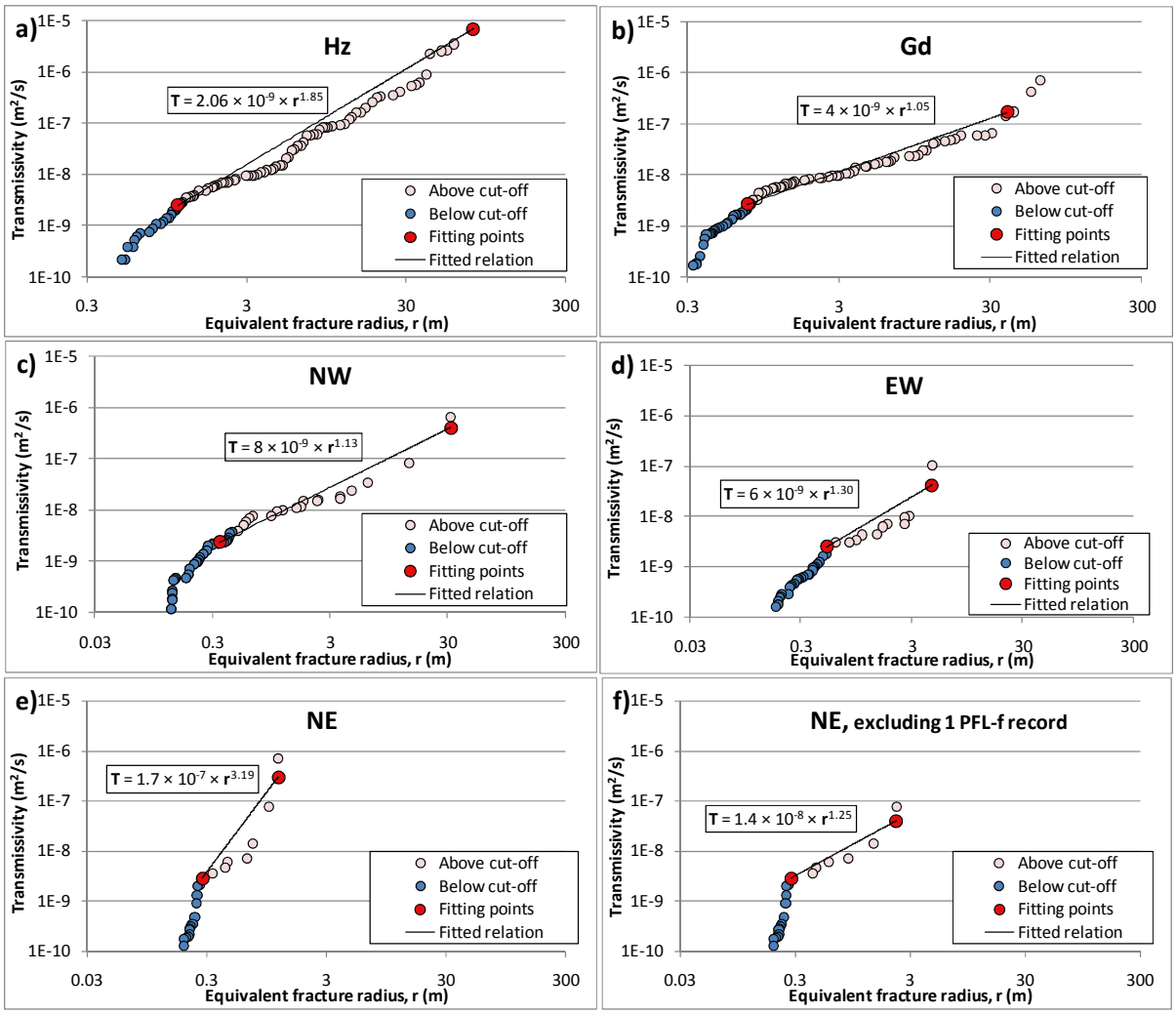

Figure J-3. *Fitted relations between simulated fracture radius of Connected fractures to transmissivity of PFL-f data in the Repository domain.*

Shallow and deep domains

The overall transmissivity in the shallow domain is at least one order higher than in the repository domain (Figure J-2a, b). There are also very few PFL-f records below T_{lim} in the Shallow domain. It is therefore possible that the practical detection limit of PFL-f data is higher in the Shallow domain in comparison to the deeper rock where transmissivity is lower. In fact, there appears to be a break-point in PFL-f intensity at an approximate transmissivity of 10^{-8} m²/s (Figure J-7). This break-point could possibly relate to the size distribution of connected fractures (Appendix F), but it may also indicate that the transmissivity cut-off, T_{lim}, should be locally increased to 10^{-8} m²/s for the Shallow domain.

More importantly, the exponential relation between PFL-f transmissivity and associated fracture radius exhibit a breakpoint at approximately 10^{-8} m²/s (i.e. its "linear range in log-log scale"; Figure J-6a, b). The PFL-f data below 10^{-8} m²/s in the Shallow domain were therefore assumed to be underrepresented, and the transmissivity relations were primarily fitted to PFL-f data above 10^{-8} m²/s (as opposed to the general cut-off at 2.5×10^{-9} m²/s). The implication of this decision is that the complementary cumulative transmissivity plots do not match at 2.5×10^{-9} m²/s (cf. Figure J-7a, b and Figure 2-6b), but at the selected lower fitting points (Figure J-6a and b).

In the Deep domain PFL-f data are scarce and the transmissivity is lower (i.e. a lower noise level for the PFL-f interpretation). It can therefore be argued that a lower cut-off could be applied in the Deep domain to improve the fitted transmissivity relations. Owing to the scarce data, all PFL-f records were included and the fit was made according to least sum of squares.

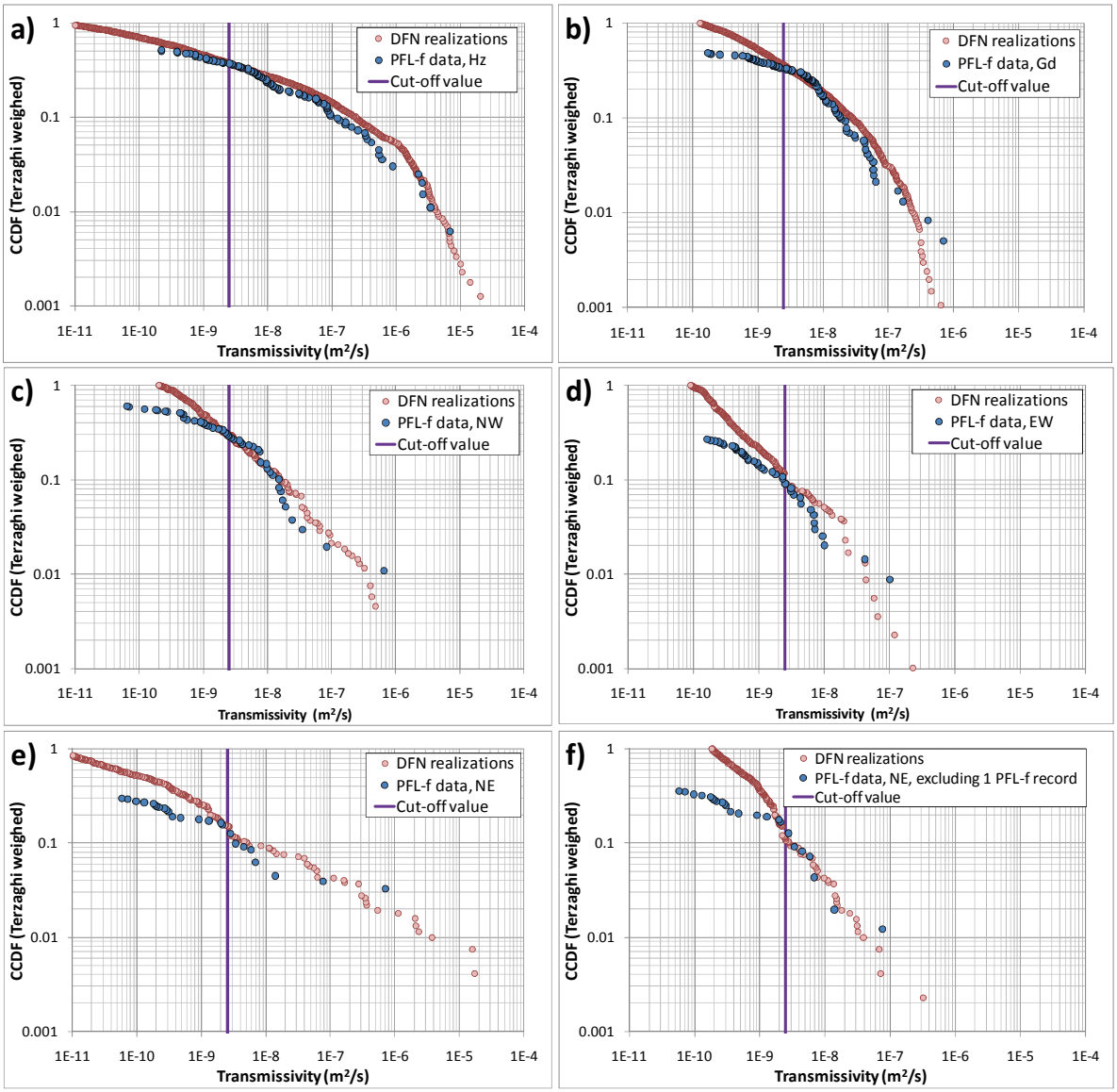

Figure J-4. *Transmissivity distribution of PFL-f data in the Repository domain compared to simulated Connected fracture transmissivity, using relations established in Figure J-3.*

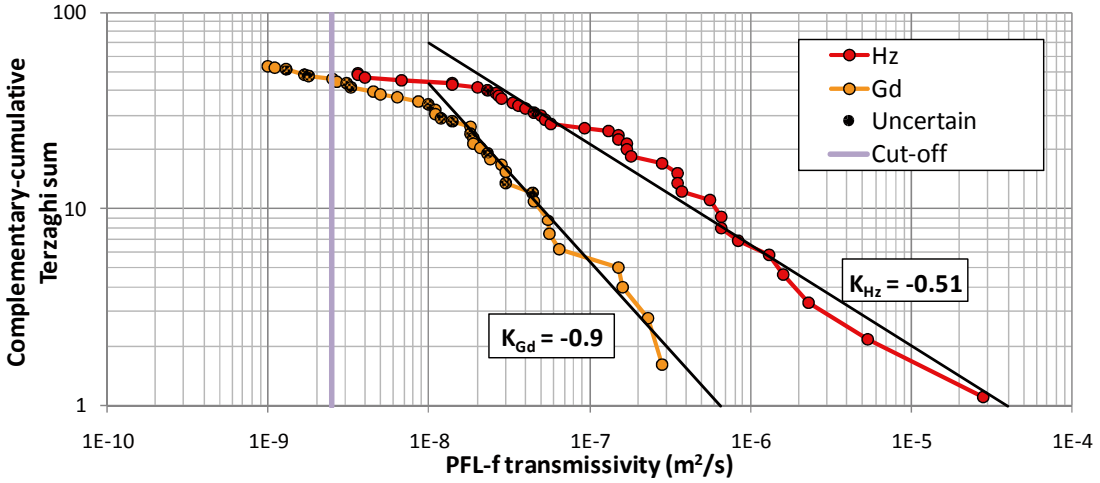

Figure J-5. *Complementary cumulative transmissivity distribution of PFL-f data in the Repository domain.*

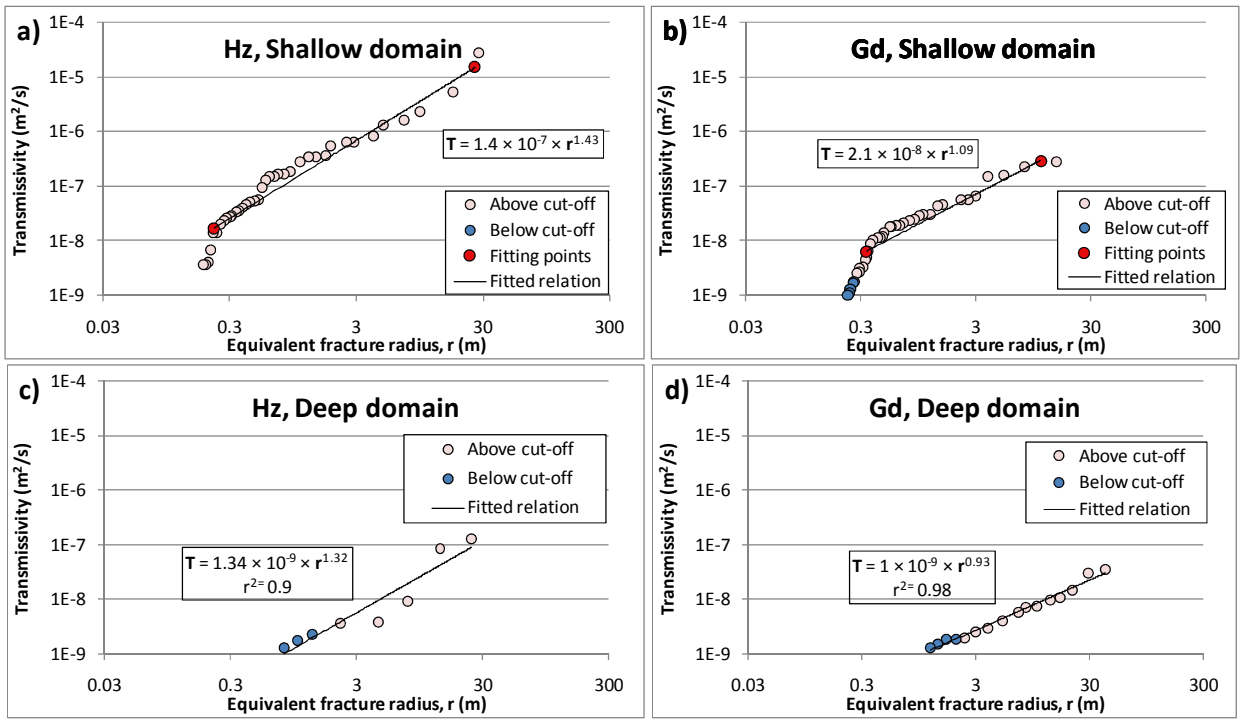

Figure J-6. *Fitted relations between simulated fracture radius of Connected fractures to transmissivity of PFL-f data in the Shallow, respectively, Deep domains.*

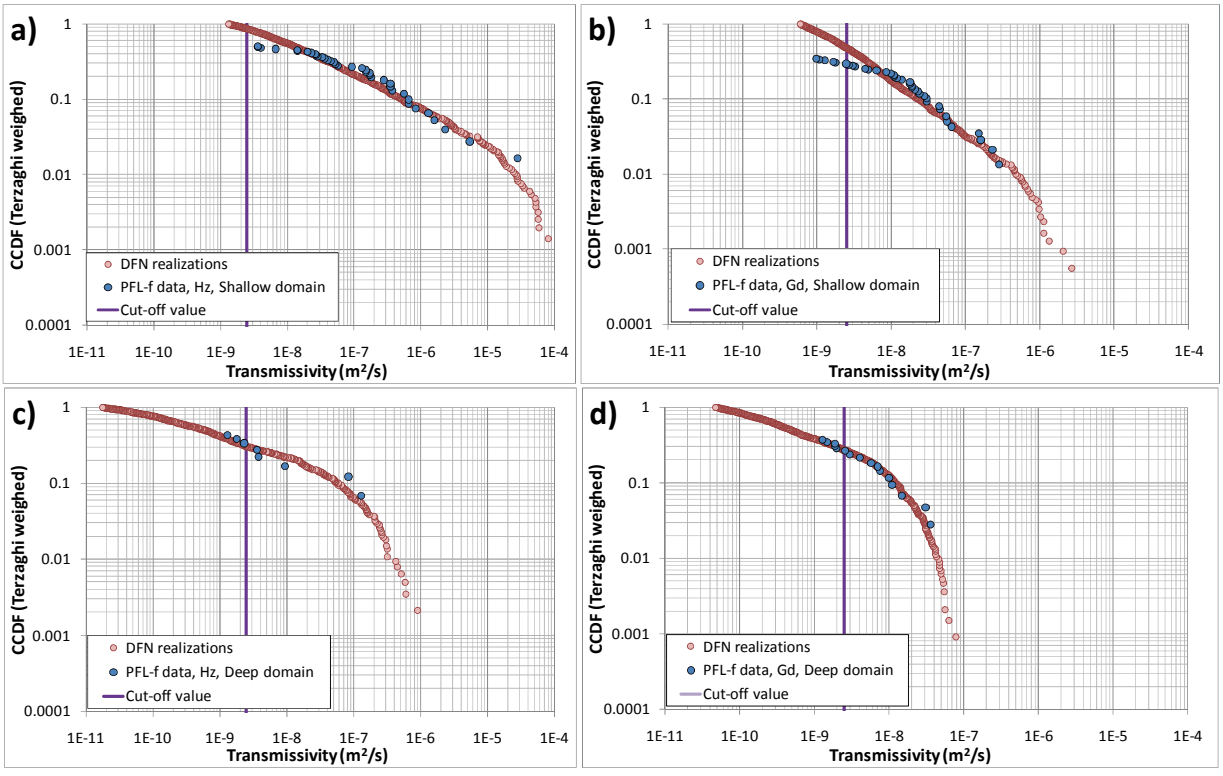

Figure J-7. *Transmissivity distribution of PFL-f data in the Shallow domain (a and b) and the Deep domain (c and d) compared to simulated Connected fracture transmissivity, using relations established in Figure J-6.*

J.3 Tectonic continuum, defining k_r

The calibration of k_r proves to be difficult for the vertical sets (NE and EW in particular, see above). The calibration criterion could not be met, although the scaling exponent was set to 3.45, which was considered as a maxim7um value (Section 2.2.10). A high k_r results in a strong dependency between size and transmissivity, which may result exceptional high maximum transmissivity for set NE unless the outlier PFL-f record in KFR102A is excluded (Figure J-4e). It should also be emphasised that the assumed calibration target of a ratio $P_{32,\,COF}/P_{32,\,PFL}$ within a range 2 to 4 is not indisputable. It was set up by practical necessity rather than based on solid evidence; instead it was based on the judgment of observations made in one borehole, in one domain and for all fracture sets combined (Appendix F). In other words, if fracture sets have different scaling exponents, the $P_{32,\,COF}/P_{32,\,PFL}$-ratio may well vary between sets. Furthermore, for a $k_r = 3.45$, the intensity of fractures with a radius larger than 30 m is negligible, which would imply that power-law scaling between small fractures and deformation zones does not apply (Figure J-8).

Therefore, an alternative approach is demonstrated, which is based on the assumption of Tectonic Continuum. This is only performed for the sub-vertical sets EW, NE, and NW, as the deformation zone model is primarily based on extrapolation of sub-vertical lineaments /Curtis et al. 2009/ and only contains two sub-horizontal zones. Furthermore, k_r for sets Hz and Gd could be calibrated satisfactorily according to the connectivity analysis method. The scaling exponent k_r is fit between the borehole intensity of Open fractures (more specifically $P_{32,\,Open+HCD}$) and that of modelled deterministic deformation zones, $P_{32,\,HCD}$. The $P_{32,\,HCD}$ was calculated for the SFR regional domain by the triangulated area of deformation zones in SFR Geologic model v0.1 divided by total model volume. The deformation zones were set-divided according to the probability fields of the global orientation model, shown in Figure 3-17. A lineament length of 1,000 m was used as cut-off and corresponds to a fracture radius of 564 m. As an example, the power-law fit between total intensity at borehole radius and deformation zone intensity at the cut-off of 564 m is shown for the repository domain in Figure J-8. The total intensity at borehole radius only decreases with a factor of 2, and the deformation zone intensity is assumed to be constant with depth. Consequently, the fit for the Shallow and Deep domains have a very similar appearance. The resulting k_r are specified in Table J-2.

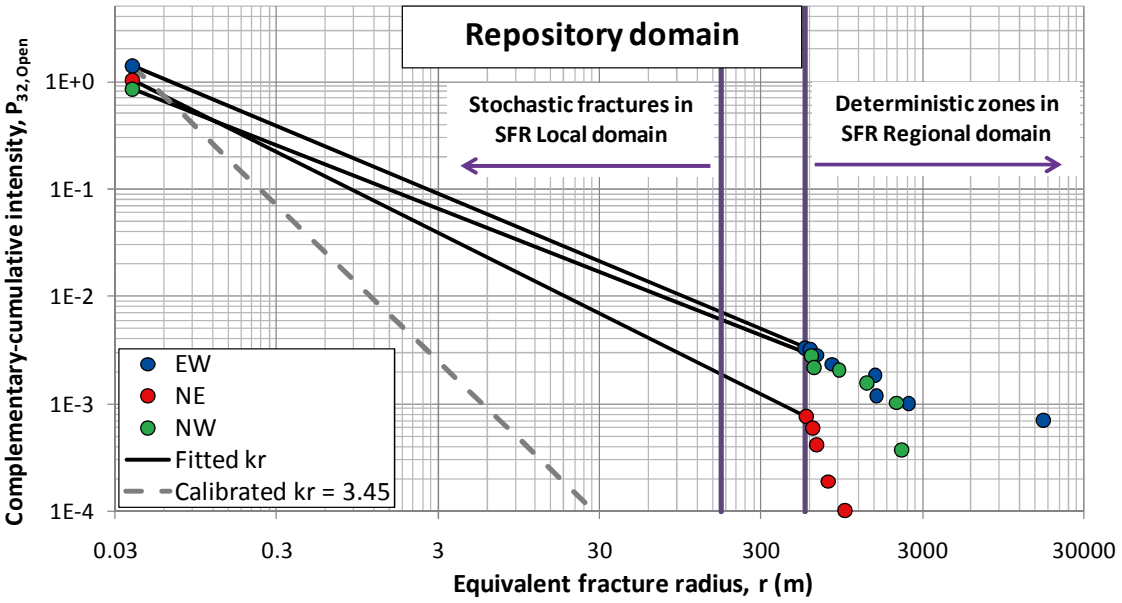

Figure J-8. *Using the assumption of Tectonic continuum to fit size distribution scaling exponent k_r between borehole intensity of Open fractures ($P_{32,\,Open\,+\,HCD}$) to the intensity of deformation zones, $P_{32,\,HCD}$.*

With this approach, set NE has the steepest slope and it would be even steeper if a larger cut-off radius for deformation zones would have been used (Figure J-8). It can also be noted that k_r decreases with depth (Table J-2), implying that it is the smallest fraction of fractures that decrease with depth. It can be noted the k_r for sub-vertical sets are generally in between the k_r for sets Hz and Gd, except in the Deep domain where sets NE and EW have lower k_r than set Hz. The reason for the increasing k_r at depth is that intensity at borehole radius ($P_{32, Open+HCD}$) decreases with depth, while the intensity of deformation zones, $P_{32, HCD}$, has been assumed to apply equally to all depth intervals. This may be an unrealistic assumption (i.e. a lineament with a length of 1,000m does not necessarily extend to a depth of 1,000 m). In reality the uncertainty in deformation zone intensity is large a depth.

Furthermore, Tectonic Continuum is a convenient modelling hypothesis in absence of intermediate-scale data, but there exists little evidence that borehole-scale fractures should follow the same size pattern as kilometre-scale deformation zones. It should therefore be emphasised that it cannot be concluded that Tectonic Continuum-based approach is an improvement to the calibration method; its purpose is to demonstrate that uncertainty in the characterisation of rock require different conceptual approaches, which render alternative possible solutions.

The results of simulated borehole exploration for 100 realisations for Tectonic Continuum based k_r are summarized in Table J-2. Small changes are noted in the connectivity of the Shallow domain: the calibration target is still met for sets Hz and Gd, and about 80% of the Open fractures are connected (Table J-2), whereas the corresponding fraction was 70% in the calibration method (Table J-1). This signifies that the connectivity analysis is not strongly dependent on k_r in the Shallow domain (at least for $k_r > 2.7$). In the Repository and Deep domains, the connectivity has increased drastically, from a range 5% to 28% (Table J-1) to a range of 44% to 61% (Table J-2). The simulated $P_{32, COF}$/$P_{32, PFL}$-ratio is very high for the sub-vertical sets. It can be noted that also sets Hz and Gd exceed the calibration target in $P_{32, COF}/P_{32, PFL}$-ratio for Repository and Deep domains. As demonstrated in Section 4.1.3, transmissivity relations can still be fine-tuned such that the simulated $P_{32, COF}$ ($T > T_{lim}$) honours PFL-f data. The results are summarized in Section 3.4, main report.

Table J-2. Simulated Connected fracture network, assuming Tectonic Continuum for sub-vertical fracture sets.

Domain	Evaluation of Connected fracture network	Fracture set				
		EW[1)]	NW[1)]	NE[1)]	Hz[2)]	Gd[2)]
Shallow domain	Fitted scaling exponent, k_r	2.694	2.778	2.626	2.6	2.79
	Simulated $P_{32, COF}$	1.91	0.97	1.13	0.84	1.4
	Reference data, $P_{32, PFL}$ ($T > T_{lim}$)	0.10	0.11	0.03	0.36	0.34
	Simulated ratio ($P_{32, COF}/P_{32, PFL}$)	19.5	8.5	39.7	2.3	4.1
	Simulated fraction ($P_{32, COF}/P_{32, Open}$)	74%	84%	84%	79%	75%
Repository domain	Fitted scaling exponent, k_r	2.63	2.752	2.596	2.55	2.72
	Simulated $P_{32, COF}$	0.8	0.52	0.54	0.51	0.66
	Reference data, $P_{32, PFL}$ ($T > T_{lim}$)	0.02	0.05	0.02	0.08	0.09
	Simulated ratio ($P_{32, COF}/P_{32, PFL}$)	46.7	11	31.5	6.3	7
	Simulated fraction ($P_{32, COF}/P_{32, Open}$)	57%	61%	53%	60%	55%
Deep domain	Fitted scaling exponent, k_r	2.585	2.75	2.597	2.75	2.7
	Simulated $P_{32, COF}$	0.48	0.46	0.46	0.26	0.6
	Reference data, $P_{32, PFL}$ ($T > T_{lim}$)	0.01	0.01	0.00	0.01	0.03
	Simulated ratio ($P_{32, COF}/P_{32, PFL}$)	68.1	39.7	NA	19.8	17.5
	Simulated fraction ($P_{32, COF}/P_{32, Open}$)	52%	53%	45%	44%	46%

[1)] Based on assumption of Tectonic Continuum. See example in Figure J-8.

[2)] Not based on Tectonic Continuum. Values taken from the intensity calibration of connected fractures, Section 3.4.

J.3.1 Tectonic continuum, hydraulic parameterisation

Repository domain

The fitted coefficients *a* and *b* for sets Hz and Gd are fairly similar to the results of the connectivity analysis (cf Figure J-9 and Table 3-4). This is expected since their size distribution of Open fractures was not changed. The persistence in transmissivity parameterisation is explained by the assumption that all excessive simulated Connected intensity (i.e. $P_{32,\,COF}$–$P_{32,\,PFL}$ [$T > T_{lim}$]; see Figure 2-6) is assumed to reflect transmissivity below T_{lim}. Based on this assumption, PFL-f data are always associated to the upper tail of the simulated size distribution; this upper tail is less dependent on k_r of the sub-vertical sets.

The fitted coefficient *a* of the sub-vertical sets is considerably lower in the Tectonic Continuum case (cf Figure J-9 and Table 3-4). The reason for this is that the lower k_r results in a Connected fracture network with larger fractures and higher intensity (Table J-2), and these large fractures must be associated with relatively lower transmissivity values in order to honour the PFL-f intensity above T_{lim}. The fitted exponents *b* are only modestly higher. This can be expected since the radius scaling exponent k_r has been decreased while the shape of the transmissivity distribution has been maintained (i.e. the same PFL-f data are used).

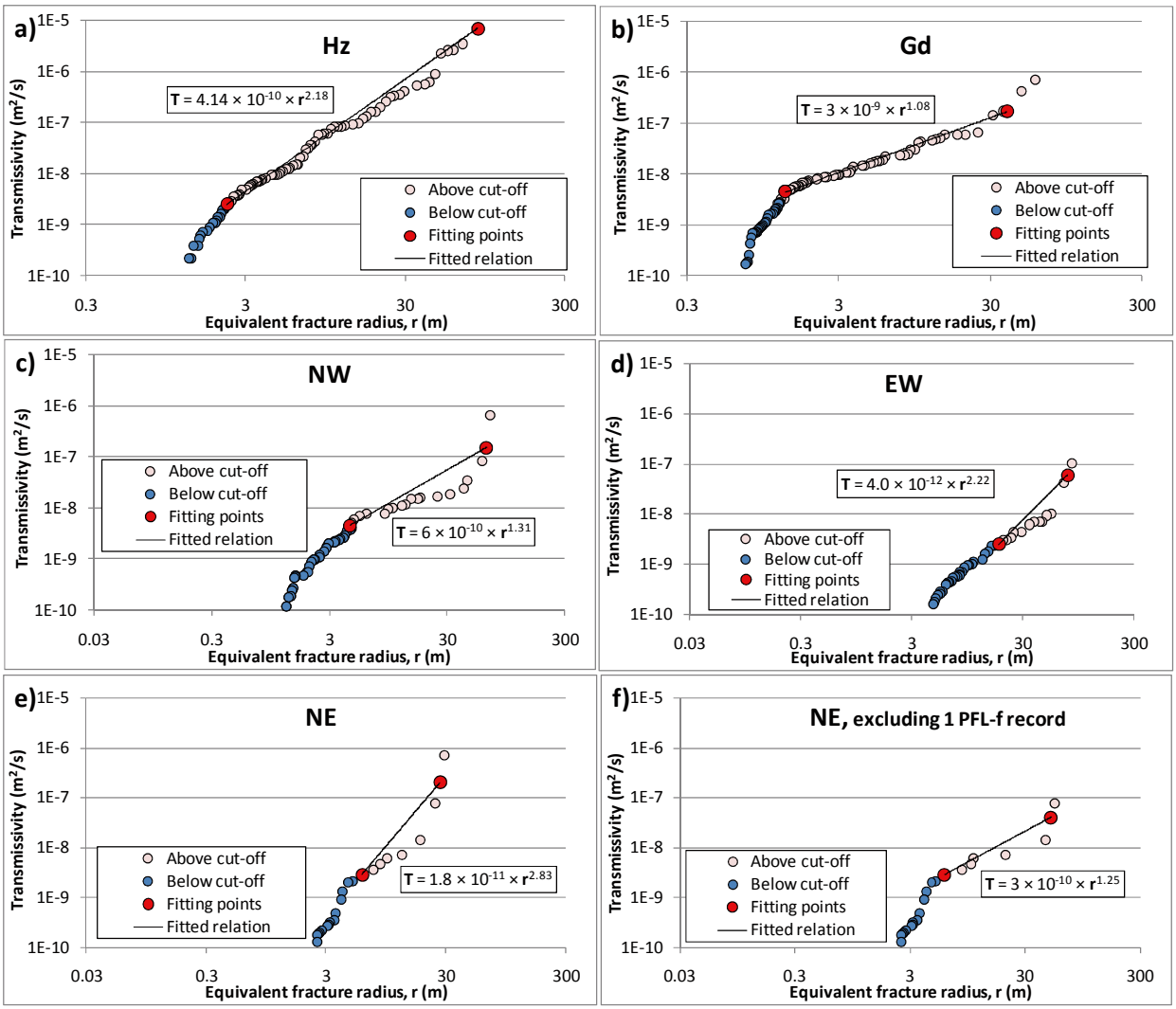

Figure J-9. *Fitted relations between simulated fracture radius of Connected fractures to transmissivity of PFL-f data in the Repository domain.*

The “linear appearance” in the log-log crossplots between radius and transmissivity (Figure J-9) is approximately similar to the patterns observed in Figure J-3. For set NW the distribution breakpoints are displaced, resulting in a “non-linear appearance”, which is difficult to fit. The fitted transmissivity relations are applied to the Connected fracture networks and compared to PFL-f data (Figure J-10). As can be expected, set NW provides the poorest agreement in shape to data.

Shallow and Deep domains

The transmissivity relations of sets Hz and Gd in the Shallow domain was fitted by least sum of squares (Figure J-11a, b); it can be noted that these fits are very similar to the corresponding manual fit in the connectivity analysis (Figure J-6a, b): both *a* and *b* are of similar magnitudes. Again, the Shallow domain does not appear to be very sensitive to changes in kr of the sub-vertical sets (which may be expected since it only resulted in minor changes in connectivity of the fracture network). The applied transmissivity relations are compared to PFL-f data in Figure J-12.

Also in the Deep domain, the estimated coefficients *a* and *b* for sets Hz and Gd are very similar to those established in the connectivity analysis, in spite of the drastic increase in simulated connectivity

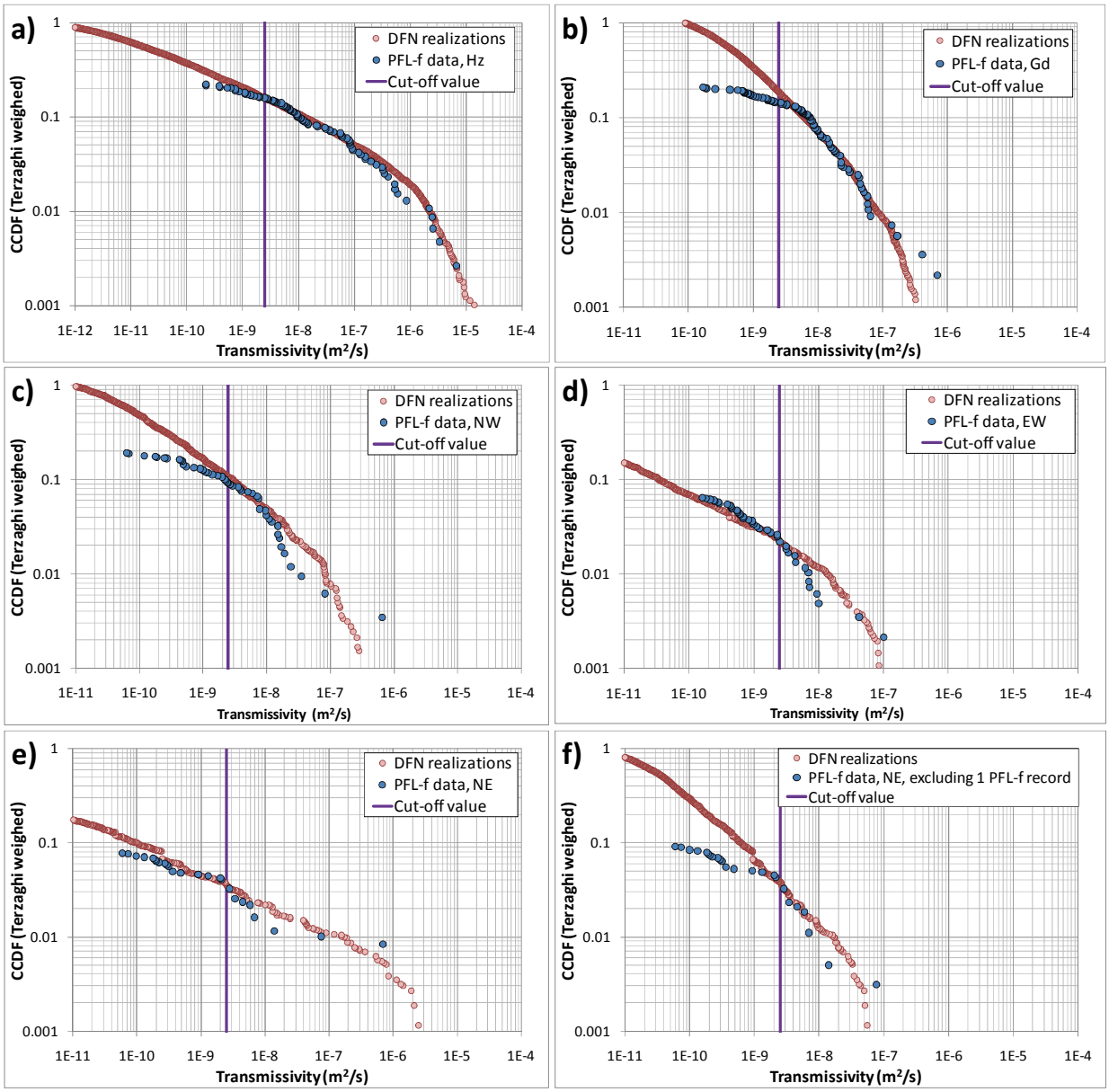

Figure J-10. *Transmissivity distribution of PFL-f data in the Repository domain compared to simulated Connected fracture transmissivity, using relations established in Figure J-9.*

(cf Table J-1 and Table J-2). In comparison to the Repository domain, the scarce PFL-f data in the Deep domain accentuates the percentile-matching even further towards the very few largest simulated fractures. A detailed inspection of the simulated size distributions of Connected fractures confirms that the applied changes in k_r for the sub-vertical sets almost exclusively enhances the connectivity of small fractures (i.e. with radii below the interval fitted to PFL-f data; (Figure J-11c, d).

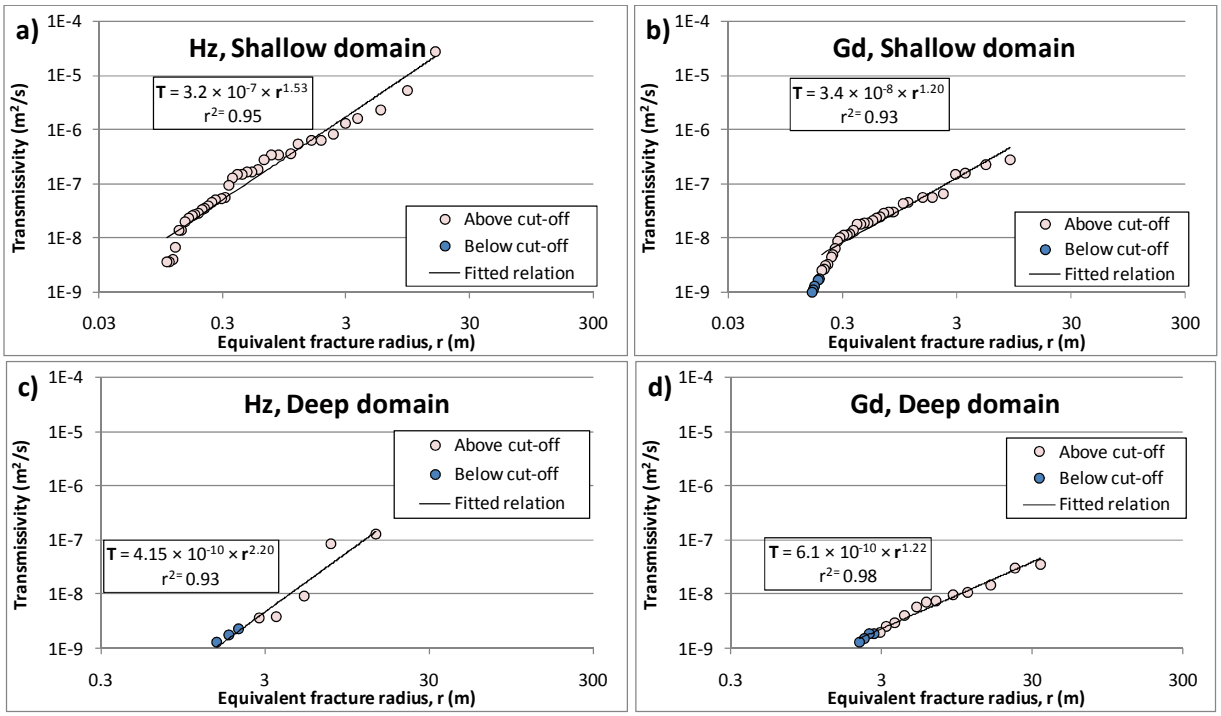

Figure J-11. *Fitted relations between simulated fracture radius of Connected fractures to transmissivity of PFL-f data in the Shallow, respectively, Deep domains.*

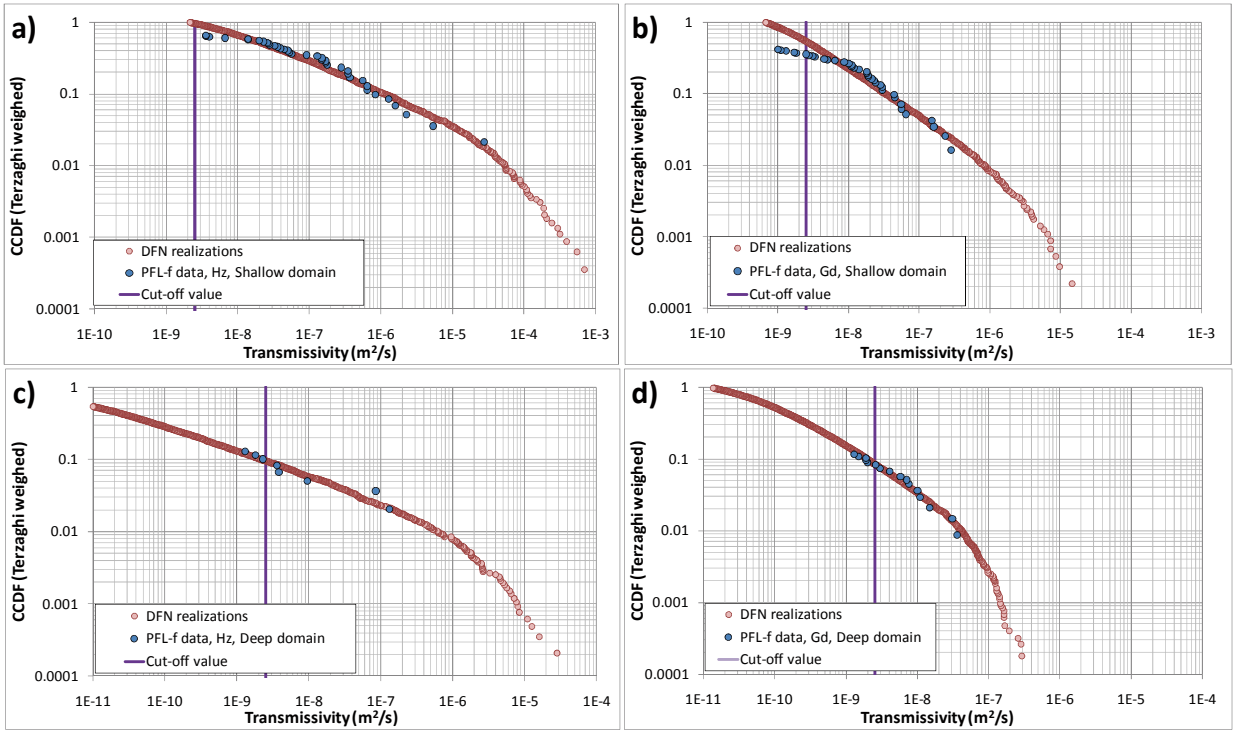

Figure J-12. *Transmissivity distribution of PFL-f data in the Shallow domain (a and b) and the Deep domain (c and d) compared to simulated Connected fracture transmissivity, using relations established in Figure J-11.*

Appendix K

Notation frequently used in this report

This report contains several acronyms, abbreviations, and parameter notations that are less commonly used outside SKB work. This appendix is intended to facilitate the readability of the report. Frequently used acronyms are listed in Table K-1 and frequently used parameter notation is listed in Table K-2.

Table K-1. Acronyms frequently used in the report.

Acronym	Stands for	Explanation
CCDF	Complementary Cumulative Density Function	Useful for plotting distributions
COF	Connected Open Fractures	A network Open and Partly open fractures that connects to a hydraulic boundary (e.g. transmissive deformation zones, or the sea floor)
DFN	Discrete Fracture Network	In DFN modelling fractures, and fracture flow, are typically resolved as a network of planar geologic features.
ECPM	Equivalent Continuous Porous Medium	A hydrogeological modelling concept, where the hydraulic properties of conductive fracture network is approximated by that of a porous medium. ECPM does not resolve explicit fracture flow, and hence is useful in large scale simulations.
GEHYCO	GEnerate HYdraulic COnductivity	A DarcyTools module used to translate a hydraulic DFN into an ECPM /Svensson et al. 2007/
HRD	Hydraulic Rock Domain	Hydraulic rockmass unit between deformation zones
HCD	Hydraulic Conductor Domain	Hydraulic unit representing deformation zones
NBT	Nedre ByggTunneln	A lower tunnel section in SFR
PFL	Posiva Flow Logging method	See Appendix C
PFL-f record	Discrete inflow detected by PFL	A Boremap feature coupled to a discrete borehole inflow and an evaluated apparent transmissivity (see Appendix C)
PDZ	Possible Deformation Zone	A borehole section that has geologically been interpreted as a possible deformation zone intercept
RHB70	Elevation reference system [m]	
RVS	Rock Visualization System	Geology modelling tool
SHI	Single Hole Interpretation	An established SKB method to geologically identify PDZ in borehole data
SFR	Slutförvar för kortlivat radioaktivt avfall	The existing disposal facility for short-lived radioactive waste
SKB	Svensk Kärnbränslehantering AB	The Swedish Nuclear Fuel and Waste Management Company
ZFMWNW805	Modelled deformation zone in RVS	Formerly known as SFR zone8
ZFM871	Modelled deformation zone in RVS	Formerly known as SFR zoneH2
ZFMWNW0001	Modelled deformation zone in RVS	Also known as Singö deformation zone

Table K-2. Notation frequently used in the report.

Notation	Explanation
α	Solid angle between the borehole and the fracture plane [°]
a	Fitting parameter for transmissivity of a fracture with 1.0 m radius
b	Fitting parameter for transmissivity, exponent by which transmissivity scales with radius
κ	Fisher concentration, defining the dispersion in fracture orientation
k_r	Power-law scaling exponent, determining the proportion between small and large fractures. The parameter has a strong influence on the connectivity of the fracture system. It is a relatively uncertain parameter, as it cannot be directly measured from borehole data, and is therefore estimated by means of a connectivity analysis.
$P_{10,\,[Type]}$	The one-dimensional fracture intensity [1/m], for a [type] specified in the subscript
$P_{32,\,[Type]}$	The three-dimensional fracture intensity [m^2/m^3], for a [type] specified in the subscript
[Open]	Open and Partly open fractures, as defined in Boremap data
[COF]	Connected Open Fractures (i.e. Open and partly open fractures) that are connected to a hydraulic boundary (e.g. transmissive deformation zones, or the sea floor)
[PFL]	A Boremap feature (e.g. Open or Partly open fracture, or a crush zone) coupled to a specific capacity measured with the Posiva Flow Logging-device. The measured specific capacity is censored by a practical detection limit, T_{lim}.
r_0	minimum fracture radius [m], assumed equal to borehole radius 0.038 m.
T_{lim}	An assumed detection limit for the Posiva Flow Logging-device, $Q/s \geq 2.5\times10^{-9}$ m^2/s.